LOW-TEMPERATURE PROTONATION STUDIES OF AN ELECTRON-POOR OSMIUM METHYL COMPLEX, AND MOLECULAR PRECURSORS FOR THE CONSTRUCTION OF GRAPHENE NANOSTRUCTUES WITH ATOMICALLY PRECISE EDGE STRUCTURES

BY

PETER J. SEMPSROTT

DISSERTATION

Submitted in partial fulfillment of the requirements
of the degree of Doctor of Philosophy in Chemistry
in the Graduate College of the
University of Illinois at Urbana-Champaign, 2018

Urbana, Illinois

Doctoral Committee:

Professor Gregory S. Girolami, Chair
Professor Joseph W. Lyding
Professor Catherine J. Murphy
Professor Thomas B. Rauchfuss

Abstract

Treatment of $Cl_2PCH_2Cl_2$ with CF_3SiMe_3 in the presence of CsF promotor gave the cesium salt $Cs[((CF_3)_2P)_2CH]$, which was converted to the electron-poor diphosphine $(CF_3)_2PCH_2P(CF_3)_2$ (dfmpm) by addition of ethereal hydrogen chloride. Treatment of $(C_5Me_5)_2Os_2Br_4$ with excess dfmpm in the presence of zinc dust in refluxing ethanol gave the piano stool osmium complex $(C_5Me_5)Os(dfmpm)Br$, which was converted to $(C_5Me_5)Os(dfmpm)Me$ in excellent yield by treatment with excess $ZnMe_2$ in refluxing toluene. The analogous ethyl complex $(C_5Me_5)Os(dfmpm)Et$ can also be prepared in a similar fashion, but with simultaneous formation of the hydrides $(C_5Me_5)Os(dfmpm)H$ and $(C_5Me_5)Os(\kappa^1\text{-}dfmpm)(C_2H_4)H$ by beta-hydrogen elimination.

Protonation of $(C_5Me_5)Os(dfmpm)Me$ with $(CF_3SO_2)_2NH$ at –110 °C in $CDCl_2F$ yielded the methane coordination complex $[(C_5Me_5)Os(dfmpm)CH_4][N(SO_2CF_3)_2]$. The analogous $^{13}CH_4$ complex exhibited a binomial quintet in the ^{13}C NMR with a coupling constant (127 Hz) almost identical to that of free methane (125 Hz). Kinetic analysis revealed that the enthalpy and entropy of activation for methane loss was $\Delta H^{\ddagger} = 14.9 \pm 1.5$ kcal mol^{-1} and $\Delta S^{\ddagger} = 12.3 \pm 8.8$ cal mol^{-1} K^{-1}, respectively, and the barrier for methane loss was $\Delta G^{\ddagger} = 12.8 \pm 0.1$ kcal/mol at –100 °C, which is in good agreement with previous DFT calculations. Treatment of $(C_5Me_5)Os(dfmpm)^{13}CH_3$ and $(C_5Me_5)Os(dfmpm)^{13}CHD_2$ with $(CF_3SO_2)_2NH$ and $(CF_3SO_2)_2ND$ at –110 °C in $CDCl_2F$ gave a mixture of the four methane complex isotopologs $[(C_5Me_5)Os(dfmpm)^{13}CH_4][N(SO_2CF_3)_2]$, $[(C_5Me_5)Os(dfmpm)^{13}CH_3D][N(SO_2CF_3)_2]$, $[(C_5Me_5)Os(dfmpm)^{13}CH_2D_2][N(SO_2CF_3)_2]$, and $[(C_5Me_5)Os(dfmpm)^{13}CHD_3][N(SO_2CF_3)_2]$ in one NMR tube, which permitted an isotopic perturbation of resonance (IPR) analysis. The IPR

data in conjunction with the DFT analysis indicated that methane is coordinated to osmium in a κ^1 fashion.

A reinvestigation of the protonation of the ruthenium complex $(C_5Me_5)Os(dmpm)Me$ resulted in rapid generation of free methane, even at low temperature.

Several oligophenylene derivatives were investigated as possible precursors for the surface-assisted synthesis of various graphene structures, including graphene sheets, graphene sheets with a regular pattern of holes, and graphene nanoribbons (GNRs). Criteria were specified for determining the likelihood that oligophenylene precursors would form the intended structures. Through this approach, 2,6-bis(2,5-dibromophenyl)biphenyl and 1,4-bis(2,6-dibromophenyl)benzene were identified as attractive candidates for the surface-assisted construction of graphene structures. Solution-based iterative cross-coupling (ICC) of anthracene derivatives was also investigated as an alternative strategy for the construction of GNRs. Synthetic routes and general fabrication methods that could lead to the construction of GNR-based electronic structures were suggested.

In initial attempts to synthesize the identified GNR precursor candidates, Suzuki coupling of 2,2′-diiodobiphenyl with (2,5-dibromophenyl)boronic acid failed to yield the desired 2,6-bis(2,5-dibromophenyl)biphenyl product. On the other hand, 1,4-bis(2,6-dibromophenyl)benzene was successfully prepared, although in low yield, by Suzuki coupling of 1,4-phenylenediboronic acid with 1,3-dibromo-2-iodobenzene; the latter compound was synthesized by treatment of 1,3-dibromobenzene with LDA, followed by addition of iodine.

Acknowledgments

There are many people who deserve my thanks for helping me reach this point. To my advisor Greg Girolami: thank you for taking a risk and giving me a second chance at grad school. Thanks also for training me to think like a scientist, and for all the delightful discussions (complicated NMR splitting patterns, methane coordination mode analysis, etc.). I consider myself fortunate to have had an advisor who is an excellent scientist and a caring person, as well as a first-rate teacher. I hope someday to communicate ideas as clearly as you do.

To my doctoral committee: thanks for your patience and for helping me stay on track. Thanks especially to Tom Rauchfuss for the profitable and enjoyable discussions on phosphines.

To Vera: thanks for being a fabulous hostess of great group parties (homemade cheesecake ice cream – seriously?), and also for occasionally coming out of retirement to rescue NMR disasters. Your stories from your own grad school days are always a blast!

To Girolami group members past and present: thank you for making graduate school a rewarding and enjoyable experience. Charity: I'm indebted to you for your superb computational studies. Dunbar: thanks for teaching me to respect chemicals just enough to survive. Jenny: thanks for getting me started on the methane project, and for hosting many grad student parties. Luke: thanks for teaching me to be a safe, conscientious, and productive chemist, and for the late-night philosophical conversations. Justin: thanks for the many interesting conversations, and for contributing some really good ideas to my research. Noel: thanks for being a friend, and for maintaining a positive attitude. Joe: thanks for having lots of good ideas, and for being a fellow organic-background student. Brian: thanks a million for all the help with the low-temperature NMR and other chemistry, and for being such a great friend. To Jean, Ruishen, and Nick: thanks for making important contributions to my thesis work and for being fun to work with. To all the

rest – Bellott, Mark, Ben, Tracey, Kristina, Sumeng, Kaili, Chelsea, and Atreyo: thanks for making graduate school a mostly pleasant experience. Thanks also to Adrian Radocea in the Lyding group for your patience in teaching me about materials science and for doing some great work on polyarene deposition.

I owe much thanks to the competent and helpful staff here at Illinois. Thanks to Danielle and Jeff in the X-ray lab; Rudi, Marie, and Beth in the microanalysis lab; Furong, Haijun, and Kevin in the mass spec lab; Donny, Dave, Rich, Amanda, and Andy in the glass shop; Jeff, Kyle, and Kyle in the electronics shop; and Hodge and Brad in the machine shop for delivering prompt results and/or keeping my equipment running smoothly. Special thanks to Vera, Dean, Jen, Lingyang, Ben, and John for enabling my custom setups and for tolerating late-night rescue phone calls. To the incredible secretaries in the IMP office – Beth, Connie, Theresa, Karen, and Stacy: somehow you manage to skillfully yet cheerfully manage a large group of quirky people (myself included). You're fabulous at what you do, and you're also fun to talk with. Thank you!

To my incredible family, what can I possibly say? Dad, Mom, David, Kevin, Lydia, and Michael (and Grandma and Grandpa too): thank you for always loving me and being there for me, for encouraging me through the ups and downs, and for taking an interest in conversations that were over your heads. Thanks for taking all those late-night phone calls, and for all the other sacrifices that are too numerous to mention. I love you all more than I can ever express.

To all my church friends in the Champaign-Urbana area (many of you are chemists!): thank you for being a great support group, and for caring so selflessly and patiently. Thanks especially to Jeremy, Eric, Bob, Paul (my late-night lab safety buddy!), Michael, Joe, Nick, Max, Ross, Giang, Nina, Zack, David, James, Jen, Beth Ann, Bethany, Shawn, Jacob, and Chad for encouraging me and holding me accountable. You guys are great!

Table of Contents

Chapter 1. **Exceptionally weak ligands for transition metal complexes: alkanes, highly fluorinated alkanes, and noble gas elements 1**

Chapter 2. **Development of improved syntheses of fluorinated methylenediphosphines 28**

Chapter 3. **Synthesis, characterization, and low-temperature protonation of an osmium methyl complex bearing a fluorinated diphosphine ligand 55**

Chapter 4. **Attempts to form a ruthenium methane complex and an osmium ethane complex, and suggestions for future progress 106**

Chapter 5. **Design of molecular precursors for the bottom-up construction of graphene nanostructures with atomically precise edge structures 131**

Appendix A. **Detailed description of the optimized procedure for low-temperature NMR characterization of osmium methane complexes 157**

Appendix B. **Full NMR spectra of all new compounds 162**

Chapter 1. Exceptionally weak ligands for transition metal complexes: alkanes, highly fluorinated alkanes, and noble gas elements

Introduction

In the vast array of known transition metal complexes, there are a small number in which at least one of the ligands can be considered as being bound exceptionally weakly. In the context of this thesis, an "exceptionally weak ligand" is a small molecule of low enough reactivity that it would not normally be thought of as a ligand at all: namely, an alkane, a highly fluorinated alkane, or a noble gas. There are no doubt a few other types of small molecules that fit the general description given here, but they will not be discussed in detail.

Transition metal complexes containing such exceptionally weak ligands are interesting for several reasons. First, they present an opportunity to gain greater insight into the nature of van der Waals bonding interactions. Second, such complexes, which we may call "coordinatively pseudounsaturated," are intermediates in many catalytic processes that take place at transition metal centers;[1] in past times such complexes would have been described as truly coordinatively unsaturated, when in fact the "vacant" coordination site is actually occupied by an exceptionally weak ligand. For example, such complexes are often present as important intermediates in the selective activation and functionalization of alkane C–H bonds,[2,3] which is a key step in the conversion of methane and other light alkanes (the principal components of natural gas) to more convenient and environmentally benign fuels[4,5] and other higher-value chemical products.[4]

The following are key factors that make alkanes, highly fluorinated alkanes, and noble gas elements such poor ligands for transition metals: (1) they have low polarizabilities, (2) their HOMOs (bonding and/or non-bonding) are low energy, making them poor donors, (3) their LUMOs are high energy, making them poor acceptors, and (4) their orbitals generally overlap

poorly with other binding partners. It should be noted, however, that because polarizability increases and the HOMO-LUMO gap decreases as one travels down a column in the periodic table, the binding enthalpy is larger for the heavier noble gases than for the lighter ones. To a lesser extent, alkanes and highly fluorinated alkanes also increase in polarizability with increasing molecular weight; thus, the binding enthalpies generally increase as the molecule becomes larger (although steric factors may sometimes counterbalance this preference).

Some of the key questions about transition metal complexes with exceptionally weak ligands are the following: how fast does coordination of the weak ligand occur upon generation of an available coordination site? What is the overall geometry of the complex? What is the strength of the metal-ligand interaction? How is the reactivity of the complex impacted by coordination of the weak ligand? How are the spectroscopic properties affected by coordination of the weak ligand? How are bonds to other ligands affected? Furthermore, in the cases of alkanes and highly fluorinated alkanes, what is the precise nature of the bonding between the metal and the weak ligand: which ligand atoms bond with the metal, how does the ligand geometry change, and how are the bonds in the ligand altered upon coordination?

Before continuing with a review of the literature on transition metal complexes with exceptionally weak ligands, we believe the issue of the nomenclature for coordination modes of alkanes and highly fluorinated alkanes needs fresh consideration. For a couple of decades, the nomenclature suggested by Hall and Perutz[1] has been the standard; it is indeed very descriptive, and it brought consistency to the literature that had been lacking to that point. Nevertheless, there are issues of incorrect usage of terminology and unnecessary complexity with this nomenclature that merit some adjustments. Figure 1.1 shows the current nomenclature (a), with the suggested revised nomenclature underneath (b). Not only does the revised nomenclature reduce the

complexity of designation, in that it does not require any specification of the atoms involved in order to fully define the coordination mode, but it also makes correct usage of the hapticity (η) and denticity (κ) designations, because hapticity refers to contiguous atoms only, whereas denticity is a more general designation that applies to non-contiguous atoms.[6] This thesis will therefore make use of the revised nomenclature, and it is suggested that subsequent literature do the same.

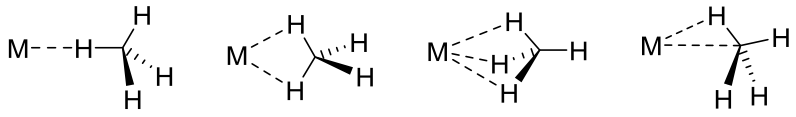

a	η^1	η^2–*H,H*	η^3–*H,H,H*	η^2–*C,H*
b	κ^1	κ^2	κ^3	η^2

Figure 1.1. The four possible coordination modes for bound methane (and for alkanes in general). Shown in **(a)** is the current nomenclature.[1] Shown in **(b)** is the suggested revision.

Early work: Short-lived complexes formed by photolysis of transition metal carbonyls

Group 6 complexes. Transition metal complexes containing coordinated alkanes, highly fluorinated alkanes, and noble gases were first identified in the 1970s by matrix isolation and solution experiments.[7-9] These experiments showed that it is not unusual for transition metals to interact even with solvents that typically are considered inert. In the groundbreaking matrix isolation studies by Perutz and Turner, metal carbonyls $M(CO)_6$ (M = Cr, Mo, W) were frozen in a host matrix consisting of one or more of the exceptionally weak ligands and photolyzed to produce $M(CO)_5$ fragments which then captured some of the host species. The adducts were studied by infrared and ultraviolet/visual spectroscopies, IR being sensitive to the metal coordination geometry and the identity of the coordinated ligand and UV/vis being sensitive

predominantly to the ligand identity. These analyses indicated that argon and tetrafluoromethane are similar to each other in coordinating strength, as are xenon and methane.[7,9-12] In the solution studies, the same metal carbonyls were subjected to laser flash photolysis at room temperature in cyclohexane and perfluoromethylcyclohexane solutions and examined by UV/vis spectroscopy. These studies revealed that cyclohexane lies between argon and xenon in coordinating strength, and perfluoromethylcyclohexane is comparable to neon. Additionally, the generated $Cr(CO)_5$-solvent adduct reacted with carbon monoxide to regenerate $Cr(CO)_6$ at a rate three orders of magnitude faster in perfluoromethylcyclohexane solution than in cyclohexane solution, consistent with the conclusion that perfluorocarbons coordinate more weakly than their hydrocarbon counterparts to metal centers.[13-15]

In the decades after these pioneering experiments, several important pieces of information regarding metal alkane complexes, particularly chromium complexes, were uncovered by solution studies. The binding enthalpy of the chromium-cyclohexane complex $Cr(CO)_5$(cyclohexane) was determined in cyclohexane solution by means of photoacoustic calorimetry, a method that involves measuring the acoustic wave generated by photochemically-induced thermal expansion of the solvent, from which the binding energy can be calculated.[16,17] The strength of the interaction was 13 kcal mol^{-1}.[18] Time-resolved IR (TRIR) studies following laser flash photolysis of $Cr(^{12}CO)_5(^{13}CO)$ in cyclohexane enabled estimation that the axial-equatorial CO–Cr–CO bond angle was 93° in the cyclohexane complex.[19,20] Sub-picosecond UV/vis and TRIR photolysis studies of $Cr(CO)_6$ in cyclohexane and methanol solutions gave somewhat conflicting results about the rate of solvent coordination: UV/vis work suggested that irradiation generated excited-state $Cr(CO)_6$, which underwent non-exponential photodissociation of CO, attaining a maximum yield of $Cr(CO)_5$ within 500 femtoseconds.[21,22] Generation of the

cyclohexane coordination product $Cr(CO)_5$(cyclohexane) apparently reached a maximum within the experimental time resolution of 800 femtoseconds,[23] whereas coordination of methanol occurred with a rise time of ~2 picoseconds (the slower coordination for methanol was thought to be due to slower solvent reorganization as a result of hydrogen bonding).[21,23] IR work, however, indicated that coordination of cyclohexane to $Cr(CO)_5$ took place over ~15 picoseconds in cyclohexane.[24,25] The discrepancy may be related to the generation of vibrationally excited species upon irradiation, which complicated spectroscopic analyses.[1,25]

A significant advance in understanding the stability of transition metal complexes of exceptionally weak ligands came from studies of the photodissociation of CO from chromium-arene carbonyl complexes in alkane solutions, followed by reformation of the starting material by reaction with carbon monoxide. The most important finding of these studies was that, for a given ligand set, the Gibbs free energy of activation (and thus the rate of reaction) depends far more on entropy than enthalpy.[26] Specifically, complexes with cyclic alkanes experience more severe entropic penalties in the transition state (and thus react more slowly with CO) than complexes with linear alkanes. Figure 1.2 shows the relation of the rate constant of reaction with CO to the enthalpy and entropy of activation.

An important qualifier to this conclusion is that the negative entropies of activation observed in this study suggest that the decomposition occurs through an associative rather than dissociative mechanism (with the possible exception of complexes containing the extremely bulky hexaethylbenzene auxiliary ligand). Therefore, the stabilities of these (arene)$Cr(CO)_2L$ complexes toward reaction with CO do not reflect the *coordinating ability* of exceptionally weak ligands, so much as they reflect the *favorability of the approach of CO* to the weak ligand complex. Instead, the Gibbs free energy of activation for ligand dissociation (if this can be

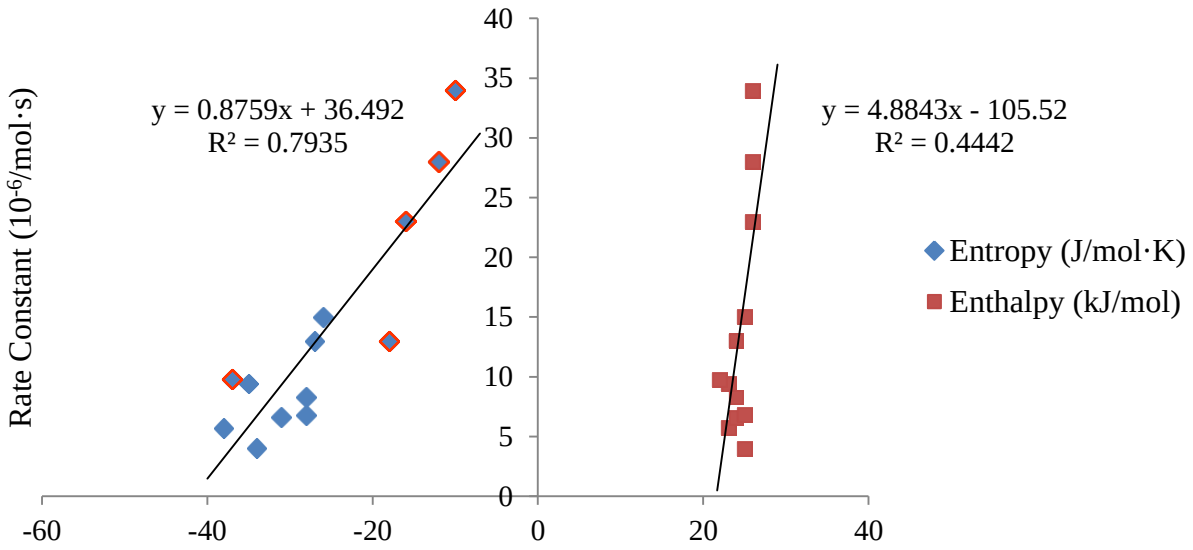

Figure 1.2. Dependence of the rate constant for the reaction of chromium alkane complexes with CO on the enthalpy (red squares) and entropy (blue diamonds) of activation. The R^2 values clearly show that the correlation is much better for the entropy of activation. The blue diamonds with orange outlines indicate the series of complexes containing the same auxiliary ligand set (specifically, with benzene as the arene), and thus differing only in the coordinated alkane.[26]

measured), as well as the Gibbs free energy of binding, relate more directly to and are better indicators of the coordinating strength of exceptionally weak ligands than the activation parameters for bimolecular (associative) substitution. This topic will be covered in greater detail below.

Gas-phase studies have also yielded useful information. Reactive species (such as transition metal fragments with open coordination sites) are likely to be longer-lived in the gas phase than in solution, provided that the conversion of the reactive species to product is not a unimolecular process, and there are no solvents to complicate spectroscopic results. Accordingly, $M(CO)_5$ species were unambiguously observed in gas phase studies (M is Cr or W), and their complexation with exceptionally weak ligands was investigated. The results confirmed the

UV/vis assignments previously made in the matrix studies; in the process, the number of tungsten-weak ligand complexes was greatly expanded.[27-33]

Group 7 complexes. Although early studies concentrated on the photolysis of homoleptic group 6 carbonyls in the presence of exceptionally weak ligands, a few other transition metal carbonyl complexes were subjected to the same conditions, and the resulting adducts interrogated. For example, photolysis of $Mn(CO)_5X$, where X is methyl or hydride, in low-temperature matrices of exceptionally weak ligands gave similar results to the group 6 work, except that the UV/vis maxima for the manganese complexes displayed greater sensitivity to the identity of the host matrix than seen for $Cr(CO)_6$.[34,35] Other heteroleptic group 7 carbonyls have also been studied, such as the manganese half-sandwich complexes $(C_5H_xR_{5-x})Mn(CO)_3$. For these compounds, the rate of the reaction between the solvent complex $(C_5H_xR_{5-x})Mn(CO)_2L$ and carbon monoxide depended on the steric bulk of the cyclopentadienyl group: bulkier groups led to faster reaction with CO, implying that the reaction occurs by a dissociative mechanism.[36-38]

Group 8 and group 9 complexes. Photolysis of iron pentacarbonyl in xenon and methane matrices also forms the analogous $Fe(CO)_4L$ complexes, but argon was apparently not a strong enough ligand and the iron tetracarbonyl remained in the triplet ground state as a coordinatively unsaturated species.[39-41] The complex $Ru(CO)_3(PMe_3)_2$, however, was able to coordinate argon, methane, and xenon when it was photolyzed in matrix isolation experiments, and the resulting solvent adducts exhibited large host-dependent shifts in the UV/vis maxima.[42]

TRIR experiments on Cp*, Bp*, and Tp* rhodium carbonyl complexes in liquid Kr or Xe, where Cp* is C_5Me_5, Bp* is $H_2B(3,5\text{-}Me_2\text{-pyrazolyl})_2$, and Tp* is $HB(3,5\text{-}Me_2\text{-pyrazolyl})_3$, showed the presence of the corresponding Kr or Xe complexes, although it appeared that the Tp*

rhodium carbonyl gave two different Xe complexes, differing only in the hapticity of the Tp* ligand (η^2 and η^3).[43-48]

Later work: longer-lived complexes formed by photolysis of transition metal carbonyls

Understandably, most of the complexes with exceptionally weak ligands mentioned so far are quite short-lived (lifetimes on the order of milliseconds to seconds at temperatures of ~140 K).[49,50] In the quest for longer-lived complexes having lifetimes of minutes to hours or longer at similar or higher temperatures, one must consider the possible decomposition pathways. For noble gas complexes, decomposition in the absence of a competing ligand would almost certainly occur via dissociation of the noble gas atom as a first step, whereas in the presence of a competing ligand, there is the additional possibility of an associative mechanism. For alkanes and highly fluorinated alkanes, loss of the weak ligand could also occur via associative or dissociative mechanisms, depending on the presence or absence of competing ligands (just as for noble gas ligands). However, another major pathway exists for alkanes and highly fluorinated alkanes, namely oxidative addition of a C–H or C–F bond to the metal.

For noble gas complexes, decreasing the electron richness of the metal center should generally stabilize the complex, primarily by inducing a stronger dipole in the noble gas element.[8] For transition metal complexes with alkanes and highly fluorinated alkanes, however, the electronic factors have to be more carefully balanced. The primary bonding interaction in σ-complexes (complexes containing a bonding interaction between an empty metal orbital and a ligand σ-bonding orbital) usually involves σ-donation into empty metal d-orbitals, but π-backbonding from a filled metal d-orbital into a σ* ligand orbital usually contributes as well, further strengthening the net bonding interaction.[4,51]

These principles lead to several periodic trends. For noble gas complexes with group 5 to group 7 transition metals, the metal-ligand bond strength increases (and the complexes become longer-lived) as one moves from first-row to second-and third-row metals, and from earlier to later metals;[8] the same dependence of metal-ligand bond strength on the identity of the metal is also seen for alkanes.[50] One caveat to this general trend is that for alkanes and their highly fluorinated analogues, strengthening the metal-ligand interaction ultimately leads to oxidative addition, resulting in "loss" of the metal-weak ligand bond in favor of two stronger bonds.

The tendency of increasing stability upon moving to later transition metals is primarily due to the decreasing energy of empty d-orbitals of σ symmetry on the metal, leading to stronger σ-donation from the weak ligand. However, this factor must be balanced, as previously mentioned, with the greater ability of earlier transition metals to engage in π-backbonding. The tendency of increasing stability upon moving to lower row transition metals is primarily due to increased diffuseness of the metal d-orbitals, leading to greater orbital overlap with the weak ligand orbitals, a factor which apparently outweighs the increased energy (and thus lower acceptor capacity) of empty d-orbitals of σ symmetry on the metal. Accordingly, longer-lived complexes of exceptionally weak ligands (lifetimes on the order of at least minutes at practical temperatures) are usually found only with second and third row transition metals.

Group 5 and group 6 complexes. A few longer-lived niobium and tantalum complexes with exceptionally weak ligands have been observed (lifetimes of tens to hundreds of microseconds at room temperature). $CpM(CO)_3L$, where M is Nb or Ta and L is *n*-C_7H_{16} or Xe, were studied as part a series of compounds establishing the periodic trends mentioned above.[49,50] Note that only the more strongly coordinating members of the exceptionally weak ligand family produced longer-lived complexes with niobium and tantalum.

Although the group 6 metals played a major role in early investigations into complexes with exceptionally weak ligands, they seem to be less ubiquitous in later work. Perhaps the early favoring of group 6 metals had to do with the fact that the group 6 carbonyls are readily available, stable, and easily handled, attributes which render the complexes ideal for use in photolysis experiments. In addition, the early methods of probing the properties of the complexes with weak ligands either involved short times scales or were performed at very low temperatures. Thus, the complexes did not need to be very stable to be investigated. Such methods are, of course, still available and useful today, but the use of longer-lived complexes provides greater opportunities to study them, and rhenium in particular seems to have gained preference over group 6 metals in this regard (see next section on group 7 complexes). Nevertheless, several group 6 complexes with longer lifetimes (tens to hundreds of microseconds at room temperature) have been studied. For $Cr(CO)_5L$ and $Mo(CO)_5L$, where L is Xe or *n*-C_7H_{16}, and $W(CO)_5L$, where L is CH_4, Xe, or *n*-C_7H_{16}, the general periodic trends noted above (longer lifetimes for more polarizable ligands and for second and third row metals complexes) were mostly followed.[50,52]

Group 7 complexes. A significantly greater number of group 7 complexes with longer lifetimes have been characterized in recent years, especially due to the work of Poliakoff and George and coworkers. Among the more striking results are the characterization of the two krypton complexes $CpRe(CO)_2Kr$ and $Cp^*Re(CO)_2Kr$, which have lifetimes of nearly 50 microseconds at room temperature.[53,54]

Among the other longer-lived group 7 complexes that were studied in the late 1990s and early 2000s, mostly by UV/vis and/or TRIR, are the following: $(C_5H_5)M(CO)_2Xe$, $(C_5Me_5)M(CO)_2Xe$, $(C_5Et_5)Mn(CO)_2Xe$, $(C_5H_5)Re(CO)_2(CH_4)$, $(C_5H_5)M(CO)_2(C_2H_6)$,

$(C_5H_5)M(CO)_2(n\text{-}C_7H_{16})$, and $(C_5H_5)M(CO)_2(cy\text{-}C_5H_{10})$, where M is Mn or Re. These complexes exhibited lifetimes from a few minutes at ~140 K ($(C_5Et_5)Mn(CO)_2Xe$ and $(C_5H_5)Mn(CO)_2(C_2H_6)$) to tens of minutes at the dry ice sublimation temperature of 195 K ($(C_5H_5)Re(CO)_2(n\text{-}C_7H_{16})$ and $(C_5H_5)Re(CO)_2(cy\text{-}C_5H_{10})$).[50,53,54]

Reactivity profiles for exceptionally weak ligands

One observation that emerged from the studies discussed so far is the reactivity series for exceptionally weak ligands (i.e., the relative coordinating ability of the ligands). Two different thermodynamic metrics are relevant to the stability of exceptionally weak ligands: the bond enthalpy and the Gibbs free energy of activation for dissociation of the weak ligand. Both metrics are measures of the strength of the bond between the transition metal and the weak ligand, and directly relate to the nature and extent of favorable orbital interactions (i.e., the fundamental chemical reason that the ligand associates with the metal).

One shortcoming of the bond enthalpy is that it does not directly translate to the thermodynamic or kinetic stability of the complex in question because it excludes entropic effects and the barrier to ligand loss. The drawback of the Gibbs free energy of activation is that it depends on the energy of both the activated state and the ground state, and therefore reveals less about the fundamental chemical nature of the ground state of transition metal complexes with exceptionally weak ligands. Therefore, it is desirable to construct both a series based on Gibbs free energies of activation (this can be termed a "reactivity series") *and* a series based on bond enthalpies (this can be termed a "BDE series").

An approximate initial understanding of the BDE series came from the UV/vis studies in the 1970s of the energy of the e to a_1 transition in $M(CO)_5L$ complexes, where M = Cr, Mo, W, and L = Ne, Ar, Kr, Xe, CH_4, and CF_4. This energy exhibits a strong blue shift as the

coordinating strength of the ligand increases. The BDE series thus elucidated was as follows: Ne < CF_4 < Ar < Kr < Xe < CH_4.[7,9] The UV/vis e to a_1 transition correlates well with the coordinating strength of exceptionally weak ligands, because the a_1 molecular orbital is primarily composed of the transition metal d_{z^2} orbital, which is driven higher in energy as the strength of binding to the weak ligand increases.[1] However, it has been noted that this particular transition also depends weakly on the axial-equatorial bond angle between the CO ligands,[55] which will change depending on the steric bulk of the weak ligand. Thus, the e to a_1 transition seems to be a good judge of the presence of a bonding interaction with a weak ligand, but it is not a perfectly reliable judge of the *precise* relative strength of that interaction, giving only a *general* relative indication of binding enthalpy.

Photoacoustic calorimetry provided bond enthalpy values for group 6 complexes with a few alkanes,[18,56] yielding the following BDE series: *n*-C_5H_{12} < *n*-C_7H_{16} < *i*-C_8H_{18} < *c*-C_6H_{12}. About the same time, gas-phase TRIR measurements of the equilibrium between $W(CO)_5$ and $W(CO)_5L$ (L = various noble gases, alkanes, and fluoroalkanes) as a function of temperature allowed determination of the binding enthalpies,[30,31] yielding the following BDE series: Ar < CH_2F_2 < Kr < C_2H_6 < C_3H_8 ≈ Xe < *i*-C_4H_{10} ≈ *c*-C_3H_6 ≈ *n*-C_4H_{10} < *c*-C_5H_{10} ≈ *n*-C_5H_{12} ≈ *n*-C_6H_{14} < CH_3F < *c*-C_6H_{12} < C_2H_5F.

Elucidating a reactivity series is a little more complicated than initial consideration might suggest. As mentioned previously, the concept of a reactivity series in this thesis is based on the Gibbs free energy of activation for dissociation of weak ligands from transition metals; however, most decomposition studies of transition metal complexes with exceptionally weak ligands have been carried out in the presence of competing ligands (most commonly CO). George and coworkers have demonstrated that, whereas the decomposition of transition metals complexes

with noble gas elements generally proceeds via a dissociative mechanism when exposed to CO, transition metal complexes with alkanes generally react with CO via an *associative* mechanism, rendering the resulting kinetic analysis invalid for determining a reactivity series containing alkanes.

This conclusion is confirmed by examination of an earlier decomposition study of Cr-alkane complexes in the presence of CO, which showed that there was very little variance in the enthalpy of activation,[26] even though the ground state bond enthalpies of the same alkanes with the $Cr(CO)_5$ fragment are substantially different.[18,56] It should be noted, however, that these studies involved an excess of CO, so it does not necessarily follow that the presence of a competing ligand in *any* quantity will result in decomposition of transition metal alkane complexes via an associative mechanism. Nevertheless, at this point a reactivity series can be definitively provided only for noble gas elements, as follows: Ar < Kr < Xe.[52] This is, of course, the expected order of stability, based on known periodic trends.

State of the art: NMR characterization of noble gas and alkane complexes

One of the most exciting and important advances in the past couple of decades is the use of nuclear magnetic resonance (NMR) spectroscopy to characterize transition metal complexes with exceptionally weak ligands. NMR is a much slower and less sensitive characterization method than UV/vis, IR, photoacoustic calorimetry, and mass spectrometry (the main methods used in early characterization), but it can provide extremely helpful and detailed information about the chemical environment of the atoms involved in bonds between transition metals and exceptionally weak ligands, which can be difficult or impossible to obtain by the other methods.

Ball and coworkers achieved the first successful NMR characterization with $CpRe(CO)_2$(cyclopentane), which was prepared by photolysis of $CpRe(CO)_3$ in neat

cyclopentane.[57] The *in situ* photolysis required the use of a fiber optic cable to deliver UV/vis irradiation into the solution in the NMR tube, and because the ^{1}H and ^{13}C resonances of the solvent would obscure the resonances of interest for the alkane complex, it was necessary to employ a solvent suppression pulse sequence.[58] Although the experimental requirements were fairly complicated, the results were worth the effort, as a definitive resonance for the protons of a bound methylene unit was observed, complete with proton-proton coupling from adjacent methylene protons and carbon-proton coupling from the bound methylene carbon (with ^{13}C labeling).[57]

Subsequently, Ball and coworkers expanded their NMR studies to include $Cp'Re(CO)_2L$, where $Cp' = C_5H_5$ or i-PrC_5H_4 and L = n-C_5H_{12} or c-C_6H_{12},[59,60] and $CpRe(CO)(PF_3)L$, where L = n-C_5H_{12}, c-C_5H_{10}, and c-C_6H_{12}.[61] Additionally, they performed the first NMR study of a noble gas complex, (i-PrC_5H_4)$Re(CO)(PF_3)(Xe)$, which included determination of the ^{129}Xe chemical shift.[62] The $Re(PF_3)$ complexes were the most stable complexes studied to that point, although the binding involved enough π-backbonding in the case of alkane ligands that an equilibrium between complexed alkane and oxidative addition to alkyl hydride was observed (the extent of oxidative addition varied substantially with the alkane ligand).[61,62] The PF_3 ligand also provided a convenient additional NMR handle. Duckett, George, Perutz, and coworkers also showed that replacement of the Cp ligands by tris(pyrazolyl)borate groups was compatible with the formation of alkane complexes amenable to NMR study, and indeed produced an extraordinarily stable cyclopentane complex.[63]

The study on (i-PrC_5H_4)$Re(CO)_2$(n-pentane) (there are three different isomers of bound pentane, involving binding through carbons 1, 2, or 3) used the concept of isotopic perturbation of resonance (IPR)[64-68] to conclusively demonstrate that coordination to the metal occurs through

only one C–H bond at a time (i.e., κ^1 or η^2 binding – IPR cannot distinguish between the two, because it indicates only the number of hydrogen atoms that bridge to the metal center), although equilibration between otherwise equivalent C–H bonds was rapid enough on the NMR timescale that only one average resonance was observed for the bound methyl or methylene group.[59] Figure 1.3 shows the ^{1}H NMR resonances for the three distinct isomers of bound pentane, as well as for the $^{13}CH_3$, $^{13}CH_2D$, and $^{13}CHD_2$ isotopologues of pentane bound through carbon 1. The authors also noted that there was a slight preference for binding of methylene groups over methyl groups,[59] which is the opposite of the preference typically observed for oxidation addition of alkanes to transition metal complexes,[69] and the opposite of the preference in the tungsten complex $(C_6Et_6)W(CO)_2$(*n*-pentane), although steric clashing with the hexaethylbenzene ligand appears to be a significant factor for the preference of methyl binding in the tungsten case.[70]

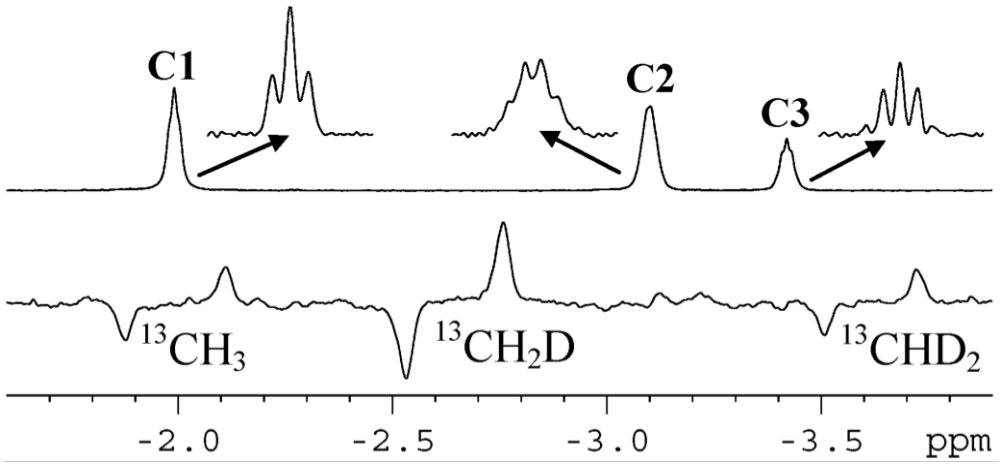

Figure 1.3. ^{1}H NMR spectra of the three isomers of (*i*PrC_5H_4)Re$(CO)_2$(*n*-pentane) (top), with the C1, C2, and C3 labels indicating the carbon through which pentane is bound, and the three isotopologues of pentane bound through carbon 1 (bottom), with the labels indicating the isotopic composition of the methyl group. Note the strong dependence of the methyl group's chemical shift on the number of deuterium atoms involved.[59]

One difficulty associated with the NMR studies mentioned so far was that the high energy UV light necessary for photoejection of CO is strongly absorbed by the metal complexes, so that the light could propagate through the solution only if low concentrations of analyte were employed, leading to poor signal to noise ratios. One improvement in this regard was the use of N_2 complexes as starting materials, because dissociation of N_2 can be induced in higher yields with lower energy UV irradiation, and N_2 is a poorer nucleophile than CO and thus less prone to subsequent reaction with the generated complexes with exceptionally weak ligands. Indeed, switching to N_2 as the labile ligand to generate an open site for the coordination of alkanes did result in simpler reaction setups (conventional glassware can be used with the lower energy UV light) and generation of higher concentrations of product.[71]

Another difficulty associated with the NMR studies previously described, which was not overcome by the use of N_2 as the labile ligand, was that the generation of transition metal complexes with exceptionally weak ligands required generation of the open coordination site in the presence of solvent quantities of the weak ligand. A couple of disadvantages of using the weak ligand as the solvent are as follows: 1) Except in the case of noble gases with very small natural abundances of NMR active nuclei (for argon, the only NMR active naturally occurring isotope, ^{39}Ar, has a natural abundance of about 10^{-12} %), the use of solvent quantities of the ligand results in extremely intense resonances relative to the resonances from the desired complex, necessitating solvent suppression techniques, and potential loss of information about many of the resonances from the weak ligand complex due to peak overlaps.[57] 2) The temperature limitations of standard NMR spectrometers preclude the use of krypton, methane, and possibly ethane, at least at atmospheric pressure, because these ligands are gases at the low temperature limit of the spectrometers. For the temperature limitation, an obvious solution is to

carry out the experiments at elevated pressures; however, this adds yet another level of complication to an already challenging experiment, and does nothing to address the excessively intense solvent resonance.

For methane (and in principle any alkane), there is another route which circumvents these limitations. This method – protonation of a transition metal alkyl – is similar to the method for the preparation of transition metal dihydrogen complexes introduced by Crabtree and coworkers[72,73] and later used by many others.[51] Preparing alkane complexes by treatment of a transition metal alkyl with an appropriate acid bypasses the need to generate a coordinatively unsaturated complex. This method, which was used by Gross and Girolami to prepare an osmium methyl/hydride that was in rapid equilibrium with its methane tautomer,[74] was later used by Brookhart and coworkers to generate the only transition metal methane complex that had been characterized before the work reported in this thesis.[75]

The metal alkyl protonation methodology has several advantages: 1) A much wider range of NMR solvents is available, allowing for selection on the basis of properties such as chemical inertness, solubilizing ability, liquid range, lack of interfering resonances, and inclusion of deuterium for locking purposes. Several useful choices exist, but $CDCl_2F$ has enjoyed the greatest popularity, especially since the report of an inexpensive and facile one-step synthesis from $CDCl_3$ by Siegel and Anet.[76] 2) Because no UV irradiation is necessary (and because more solubilizing solvents may be used), higher concentrations of alkane complexes can be generated, leading to clearer spectra that have the potential to reveal greater detail. 3) The protonation of an electrically neutral alkyl complex necessarily generates a cationic product, just as in the case of analogously generated dihydrogen complexes.[51] Cationic metals generally show enhanced σ-donation from the exceptionally weak ligands,[8] which in dihydrogen complexes tends to

strengthen the bonding to the metal center.[51] Additionally, cationic complexes will be less prone to oxidative addition of alkanes than corresponding neutral complexes, because π-backbonding is a major contributor to C–H bond cleavage, and molecular orbitals are lower in energy (and thus poorer donors) in a cationic complex than in the corresponding neutral complex.[51]

Brookhart's cationic rhodium methane complex was suggested via density functional theory (DFT) calculations to have a κ^1/η^2 coordination mode,[75] just as in the case of Ball's rhenium pentane complexes.[59] These results are in general agreement with other theoretical studies of transition metal alkane complexes.[77-80] Subsequently, Brookhart and coworkers extended their rhodium pincer chemistry to include an ethane complex that was characterized by NMR spectroscopy, supplemented with DFT calculations.[81]

Into the future: X-ray crystal structures of transition metal complexes with weak ligands

Although the first solid-state structure of a transition metal complex involving bonding interactions with an exceptionally weak ligand was obtained two decades ago (an iron porphyrin complex with *n*-heptane), it was the only such example until much more recently, and the binding was encouraged by the host-guest effect.[82] (Crystal structures of a series of uranium complexes with η^2-coordinated cyclic alkanes were reported almost 15 years ago, which are technically not transition metal complexes, but are obviously related and highly relevant to the topic at hand.[83] It has been noted that the metal-alkane distances were rather long, and host-guest interactions appear to be important in this case as well.[84])

About the same time, Seppelt and coworkers achieved crystallographic characterization of a remarkable gold xenon complex by reduction of AuF_3 with xenon in the presence of HF/SbF_5. The resulting complex ($[AuXe_4][Sb_2F_{11}]$, see the crystal structure of the cation in Figure 1.4) was stable in solution to 233 K, and up to room temperature with addition of

moderate added xenon pressure.[85] Interestingly, the strength of the gold-xenon bond is largely due to relativistic effects.[86] This complex still stands as the sole example of a crystallographically characterized transition metal-noble gas complex.

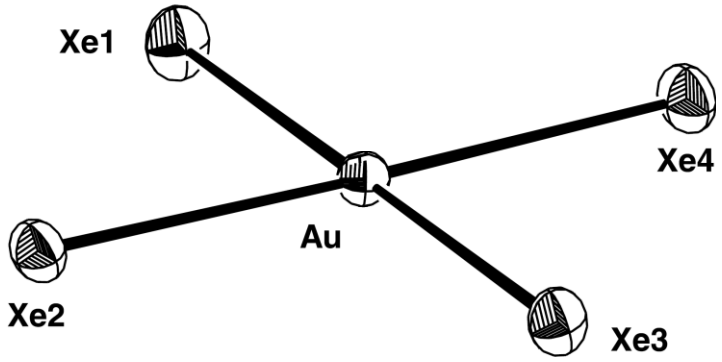

Figure 1.4. An ORTEP view of the X-ray crystal structure of the square planar $[AuXe_4]^+$ cation in the complex $[AuXe_4][Sb_2F_{11}]$.[85]

More recently, Weller and Macgregor and coworkers employed an ingenious method – a gas-solid reaction – to obtain the crystal structure of a rhodium norbornane complex. They treated single crystals of a rhodium norbornadiene cation with molecular hydrogen, and the rhodium complex catalyzed the hydrogenation of both double bonds in norbornadiene to afford coordinated norbornane. The reaction proceeded with minor enough structural changes to maintain the single crystal nature of the sample, allowing a solid-state structure of the alkane complex to be obtained. Although the coordinated norbornane was crystallographically disordered, the refined structure was sufficient to conclude that one C–H bond each from carbons 1 and 2 were coordinating, indicating double η^2 coordination.[87] Loss of the coordinated alkane was observed when the alkane complex was dissolved in $CDCl_2F$ at 163 K, indicating lower stability compared to rhodium methane and ethane complexes,[75,81,87] although the stability in the solid state is dependent on the steric bulk of the auxiliary diphosphine ligand.[87-89]

Exposure of a variant of the original norbornane complex containing a bulkier auxiliary diphosphine ligand (as well as exposure of the corresponding parent norbornadiene complex) to molecular deuterium gas (D_2), followed by treatment with molecular hydrogen gas, resulted in reversible C–H/C–D activation. The results showed that the C–H/C–D activation was selective for the *exo* face of the coordinated alkane, even though coordination to the rhodium center was through the *endo* face, in contrast to hydrogenation/deuteration of the parent diene, which occurred at the coordinated *endo* face.[90]

Very recently, Weller and Macgregor and coworkers extended their gas-solid methodology to observe a transition metal complex with a light linear alkane in the solid state. By treating a solid-state sample of a rhodium pentadiene complex with hydrogen gas, they obtained a single-crystal X-ray structure of a rhodium *n*-pentane complex, once again observing double η^2 coordination, in this case through carbons 2 and 4.[91] Figure 1.5 shows the crystal structure of the pentane-containing cation.

Although much progress has been made since the initial discovery of transition metal complexes with exceptionally weak ligands, the dearth of solid-state structures and related scarcity of complexes stable at or near room temperature remain important challenges. Additionally, the absence of experimentally determined structural data for complexes with the simplest alkane – methane – stands as a notable gap in knowledge, because methane is likely to suffer from steric constraints less than any other alkane, and thus can be expected to provide important information on intrinsic chemical preferences regarding the coordination mode of alkanes to transition metal complexes. Chapter 3 presents our addition to the field in this regard.

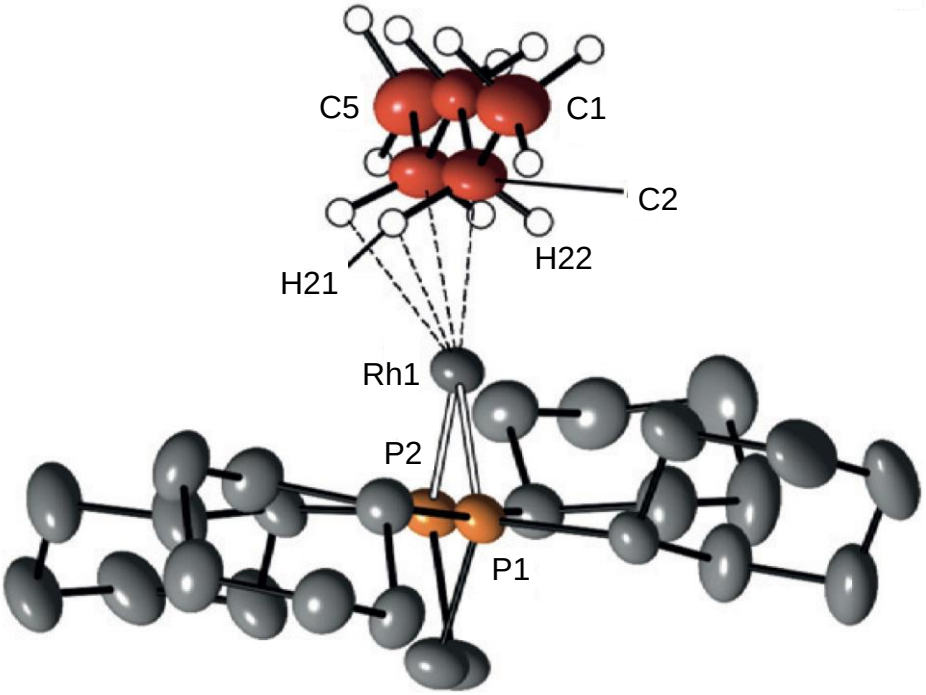

Figure 1.5. An ORTEP view of the cationic portion of the X-ray crystal structure of the rhodium pentane complex [Rh(dcpe)(pentane)][BAr^F_4], where Ar^F is 3,5-bis(trifluoromethyl)phenyl and dcpe is 1,2-bis(dicyclohexylphosphino)ethane.[91]

References

1. Hall, C.; Perutz, R. N. *Chem. Rev.* **1996**, *96*, 3125-3146.

2. Goldman, A. S.; Goldberg, K. I., *Organometallic C–H Bond Activation: An Introduction* In *Activation and Functionalization of C—H Bonds*; Goldberg, K. I., Goldman, A. S., Eds.; American Chemical Society: Washington, D.C., 2004; Vol. 885, p 1-43.

3. Sharma, A.; Hartwig, J. F. *Nature* **2015**, *517*, 600-604.

4. Crabtree, R. H. *J. Chem. Soc., Dalton Trans.* **2001**, 2437-2450.

5. Golisz, S. R.; Brent Gunnoe, T.; Goddard, W. A., III; Groves, J. T.; Periana, R. A. *Catal. Lett.* **2011**, *141*, 213-221.

6. Green, M. L. H.; Parkin, G., *The Covalent Bond Classification Method and Its Application to Compounds That Feature 3-Center 2-Electron Bonds* In *The Chemical Bond III*; Springer International Publishing: Switzerland, 2017; Vol. 171, p 79-140.
7. Perutz, R. N.; Turner, J. J. *Inorg. Chem.* **1975**, *14*, 262-270.
8. Grills, D. C.; George, M. W. *Adv. Inorg. Chem.* **2001**, *52*, 113-150.
9. Perutz, R. N.; Turner, J. J. *J. Am. Chem. Soc.* **1975**, *97*, 4791-4800.
10. Burdett, J. K.; Downs, A. J.; Gaskill, G. P.; Graham, M. A.; Turner, J. J.; Turner, R. F. *Inorg. Chem.* **1978**, *17*, 523-532.
11. Upmacis, R. K.; Gadd, G. E.; Poliakoff, M.; Simpson, M. B.; Turner, J. J.; Whyman, R.; Simpson, A. F. *J. Chem. Soc., Chem. Commun.* **1985**, 27-30.
12. Upmacis, R. K.; Poliakoff, M.; Turner, J. J. *J. Am. Chem. Soc.* **1986**, *108*, 3645-3651.
13. Kelly, J. M.; Hermann, H.; Von Gustorf, E. K. *J. Chem. Soc., Chem. Commun.* **1973**, 105-106.
14. Bonneau, R.; Kelly, J. M. *J. Am. Chem. Soc.* **1980**, *102*, 1220-1221.
15. Kelly, J. M.; Long, C.; Bonneau, R. *J. Phys. Chem.* **1983**, *87*, 3344-3349.
16. Braslavsky, S. E.; Heibel, G. E. *Chem. Rev.* **1992**, *92*, 1381-1410.
17. Borges dos Santos, R. M.; Lagoa, A. L. C.; Martinho Simoes, J. A. *J. Chem. Thermodyn.* **1999**, *31*, 1483-1510.
18. Morse, J. M.; Parker, G. H.; Burkey, T. J. *Organometallics* **1989**, *8*, 2471-2474.
19. Hermann, H.; Grevels, F. W.; Henne, A.; Schaffner, K. *J. Phys. Chem.* **1982**, *86*, 5151-5154.
20. Church, S. P.; Grevels, F. W.; Hermann, H.; Schaffner, K. *Inorg. Chem.* **1985**, *24*, 418-422.

21. Joly, A. G.; Nelson, K. A. *J. Phys. Chem.* **1989**, *93*, 2876-2878.

22. Xie, X.; Simon, J. D. *J. Am. Chem. Soc.* **1990**, *112*, 1130-1136.

23. Simon, J. D.; Xie, X. *J. Phys. Chem.* **1986**, *90*, 6751-6753.

24. Wang, Z.; Zhu, X.; Spears, K. G. *J. Am. Chem. Soc.* **1988**, *110*, 8695-8696.

25. Sprague, J. R.; Arrivo, S. M.; Spears, K. G. *J. Phys. Chem.* **1991**, *95*, 10528-10531.

26. Creaven, B. S.; George, M. W.; Ginzburg, A. G.; Hughes, C.; Kelly, J. M.; Long, C.; McGrath, I. M.; Pryce, M. T. *Organometallics* **1993**, *12*, 3127-3131.

27. Breckenridge, W. H.; Sinai, N. *J. Phys. Chem.* **1981**, *85*, 3557-3560.

28. Breckenridge, W. H.; Stewart, G. M. *J. Am. Chem. Soc.* **1986**, *108*, 364-367.

29. Ishikawa, Y.; Brown, C. E.; Hackett, P. A.; Rayner, D. M. *Chem. Phys. Lett.* **1988**, *150*, 506-510.

30. Brown, C. E.; Ishikawa, Y.; Hackett, P. A.; Rayner, D. M. *J. Am. Chem. Soc.* **1990**, *112*, 2530-2536.

31. Wells, J. R.; Weitz, E. *J. Am. Chem. Soc.* **1992**, *114*, 2783-2787.

32. Weiller, B. H. *J. Am. Chem. Soc.* **1992**, *114*, 10910-10915.

33. Wells, J. R.; House, P. G.; Weitz, E. *J. Phys. Chem.* **1994**, *98*, 8343-8351.

34. Church, S. P.; Poliakoff, M.; Timney, J. A.; Turner, J. J. *Inorg. Chem.* **1983**, *22*, 3259-3266.

35. Horton-Mastin, A.; Poliakoff, M.; Turner, J. J. *Organometallics* **1986**, *5*, 405-408.

36. Rest, A. J.; Sodeau, J. R.; Taylor, D. J. *J. Chem. Soc., Dalton Trans.* **1978**, 651-656.

37. Creaven, B. S.; Dixon, A. J.; Kelly, J. M.; Long, C.; Poliakoff, M. *Organometallics* **1987**, *6*, 2600-2605.

38. Johnson, F. P. A.; George, M. W.; Bagratashvili, V. N.; Vereshchagina, L. N.; Poliakoff, M. *Mendeleev Commun.* **1991**, 26-28.

39. Poliakoff, M.; Turner, J. J. *J. Chem. Soc., Dalton Trans.* **1974**, 2276-2285.

40. Poliakoff, M. *Chem. Soc. Rev.* **1978**, 527-540.

41. Poliakoff, M.; Weitz, E. *Acc. Chem. Res.* **1987**, *20*, 408-414.

42. Mawby, R. J.; Perutz, R. N.; Whittlesey, M. K. *Organometallics* **1995**, *14*, 3268-3274.

43. Weiller, B. H.; Wasserman, E. P.; Bergman, R. G.; Moore, C. B.; Pimentel, G. C. *J. Am. Chem. Soc.* **1989**, *111*, 8288-8290.

44. Weiller, B. H.; Wasserman, E. P.; Moore, C. B.; Bergman, R. G. *J. Am. Chem. Soc.* **1993**, *115*, 4326-4330.

45. Schultz, R. H.; Bengali, A. A.; Tauber, M. J.; Weiller, B. H.; Wasserman, E. P.; Kyle, K. R.; Moore, C. B.; Bergman, R. G. *J. Am. Chem. Soc.* **1994**, *116*, 7369-7377.

46. Bengali, A. A.; Schultz, R. H.; Moore, C. B.; Bergman, R. G. *J. Am. Chem. Soc.* **1994**, *116*, 9585-9589.

47. Bengali, A. A.; Arndtsen, B. A.; Burger, P. M.; Schultz, R. H.; Weiller, B. H.; Kyle, K. R.; Moore, C. B.; Bergman, R. G. *Pure Appl. Chem.* **1995**, *67*, 281-288.

48. Yeston, J. S.; McNamara, B. K.; Bergman, R. G.; Moore, C. B. *Organometallics* **2000**, *19*, 3442-3446.

49. Grills, D. C.; Childs, G. I.; George, M. W. *Chem. Commun.* **2000**, 1841-1842.

50. Childs, G. I.; Grills, D. C.; Sun, X. Z.; George, M. W. *Pure Appl. Chem.* **2001**, *73*, 443-447.

51. Kubas, G. J. *Metal Dihydrogen and σ-Bond Complexes: Structure, Theory, and Reactivity*; Kluwer Academic Publishers: New York, 2001.

52. Sun, X. Z.; George, M. W.; Kazarian, S. G.; Nikiforov, S. M.; Poliakoff, M. *J. Am. Chem. Soc.* **1996**, *118*, 10525-10532.

53. Sun, X.-Z.; Grills, D. C.; Nikiforov, S. M.; Poliakoff, M.; George, M. W. *J. Am. Chem. Soc.* **1997**, *119*, 7521-7525.

54. Grills, D. C.; Sun, X. Z.; Childs, G. I.; George, M. W. *J. Phys. Chem. A* **2000**, *104*, 4300-4307.

55. Burdett, J. K. *Inorg. Chem.* **1975**, *14*, 375-382.

56. Leu, G.-L.; Burkey, T. J. *J. Coord. Chem.* **1995**, *34*, 87-97.

57. Geftakis, S.; Ball, G. E. *J. Am. Chem. Soc.* **1998**, *120*, 9953-9954.

58. Piotto, M.; Saudek, V.; Sklenar, V. *J. Biomol. NMR* **1992**, *2*, 661-665.

59. Lawes, D. J.; Geftakis, S.; Ball, G. E. *J. Am. Chem. Soc.* **2005**, *127*, 4134-4135.

60. Lawes, D. J.; Darwish, T. A.; Clark, T.; Harper, J. B.; Ball, G. E. *Angew. Chem., Int. Ed.* **2006**, *45*, 4486-4490.

61. Ball, G. E.; Brookes, C. M.; Cowan, A. J.; Darwish, T. A.; George, M. W.; Kawanami, H. J.; Portius, P.; Rourke, J. *Proc. Natl. Acad. Sci. U.S.A.* **2007**, *104*, 6927-6932.

62. Ball, G. E.; Darwish, T. A.; Geftakis, S.; George, M. W.; Lawes, D. J.; Portius, P.; Rourke, J. P. *Proc. Natl. Acad. Sci. U.S.A.* **2005**, *102*, 1853-1858.

63. Duckett, S., B.; George, M. W.; Jina, O. S.; Matthews, S. L.; Perutz, R. N.; Sun, X.-Z.; Vuong, K. Q. *Chem. Commun.* **2009**, 1401-1403.

64. Saunders, M.; Jaffe, M. H.; Vogel, P. *J. Am. Chem. Soc.* **1971**, *93*, 2558-2559.

65. Saunders, M.; Kates, M. R. *J. Am. Chem. Soc.* **1977**, *99*, 8071-8072.

66. Saunders, M.; Kates, M. R.; Wiberg, K. B.; Pratt, W. *J. Am. Chem. Soc.* **1977**, *99*, 8072-8073.

67. Saunders, M.; Telkowski, L.; Kates, M. R. *J. Am. Chem. Soc.* **1977**, *99*, 8070-8071.

68. Calvert, R. B.; Shapley, J. R. *J. Am. Chem. Soc.* **1978**, *100*, 7726-7727.

69. Labinger, J. A.; Bercaw, J. E. *Nature* **2002**, *417*, 507-514.

70. Young, R. D.; Lawes, D. J.; Hill, A. F.; Ball, G. E. *J. Am. Chem. Soc.* **2012**, *134*, 8294-8297.

71. Calladine, J. A.; Torres, O.; Anstey, M.; Ball, G. E.; Bergman, R. G.; Curley, J.; Duckett, S. B.; George, M. W.; Gilson, A. I.; Lawes, D. J.; Perutz, R. N.; Sun, X.-Z.; Vollhardt, K. P. C. *Chem. Sci.* **2010**, *1*, 622-630.

72. Crabtree, R. H.; Lavin, M. *J. Chem. Soc., Chem. Commun.* **1985**, 794-795.

73. Crabtree, R. H.; Lavin, M.; Bonneviot, L. J. *J. Am. Chem. Soc.* **1986**, *108*, 4032-4037.

74. Gross, C. L.; Girolami, G. S. *J. Am. Chem. Soc.* **1998**, *120*, 6605-6606.

75. Bernskoetter, W. H.; Schauer, C. K.; Goldberg, K. I.; Brookhart, M. *Science* **2009**, *326*, 553-556.

76. Siegel, J. S.; Anet, F. A. L. *J. Org. Chem.* **1988**, *53*, 2629-2630.

77. Martin, R. L. *J. Am. Chem. Soc.* **1999**, *121*, 9459-9460.

78. Bergman, R. G.; Cundari, T. R.; Gillespie, A. M.; Gunnoe, T. B.; Harman, W. D.; Klinckman, T. R.; Temple, M. D.; White, D. P. *Organometallics* **2003**, *22*, 2331-2337.

79. Flener-Lovitt, C.; Woon, D. E.; Dunning, T. H.; Girolami, G. S. *J. Phys. Chem. A* **2010**, *114*, 1843-1851.

80. Chan, B.; Ball, G. E. *J. Chem. Theory Comput.* **2013**, *9*, 2199-2208.

81. Walter, M. D.; White, P. S.; Schauer, C. K.; Brookhart, M. *J. Am. Chem. Soc.* **2013**, *135*, 15933-15947.

82. Evans, D. R.; Drovetskaya, T.; Bau, R.; Reed, C. A.; Boyd, P. D. W. *J. Am. Chem. Soc.* **1997**, *119*, 3633-3634.

83. Castro-Rodriguez, I.; Nakai, H.; Gantzel, P.; Zakharov, L. N.; Rheingold, A. L.; Meyer, K. *J. Am. Chem. Soc.* **2003**, *125*, 15734-15735.

84. Weller, A. S.; Chadwick, F. M.; McKay, A. I., *Transition Metal Alkane-Sigma Complexes: Synthesis, Characterization, and Reactivity* In *Adv. Organomet. Chem.*; Perez, P. J., Ed. 2016; Vol. 66, p 223-276.

85. Seidel, S.; Seppelt, K. *Science* **2000**, *290*, 117-118.

86. Pyykko, P. *Science* **2000**, *290*, 64-65.

87. Pike, S. D.; Thompson, A. L.; Algarra, A. G.; Apperley, D. C.; Macgregor, S. A.; Weller, A. S. *Science* **2012**, *337*, 1648-1651.

88. Pike, S. D.; Chadwick, F. M.; Rees, N. H.; Scott, M. P.; Weller, A. S.; Kramer, T.; Macgregor, S. A. *J. Am. Chem. Soc.* **2015**, *137*, 820-833.

89. McKay, A. I.; Kramer, T.; Rees, N. H.; Thompson, A. L.; Christensen, K. E.; Macgregor, S. A.; Weller, A. S. *Organometallics* **2017**, *36*, 22-25.

90. Chadwick, F. M.; Kramer, T.; Gutmann, T.; Rees, N. H.; Thompson, A. L.; Edwards, A. J.; Buntkowsky, G.; Macgregor, S. A.; Weller, A. S. *J. Am. Chem. Soc.* **2016**, *138*, 13369-13378.

91. Chadwick, F. M.; Rees, N. H.; Weller, A. S.; Kramer, T.; Iannuzzi, M.; Macgregor, S. A. *Angew. Chem.* **2016**, *128*, 3741-3745.

Chapter 2. Development of an improved synthesis of fluorinated methylenediphosphines

Introduction

For many years, diphosphines have been popular and highly useful ligands for transition metal catalysts.[1-4] Diphosphines bind well to many transition metals, owing to their soft Lewis basicity, and their chelating nature provides increased binding stability and control over coordination geometry.[4] For these reasons, the judicious use of diphosphine ligands has, in some cases, led to marked improvements in catalyst stability and activity.[5-7] Because phosphines are stable against inversion, they can be made chiral, and as such are sometimes capable of promoting chiral transformations.[8] Use of chiral diphosphines often affords greater stereocontrol,[9-11] in part due to increased rigidity and enforcement of a particular conformation in the binding of a substrate to a catalyst, even when the chiral centers are located away from the phosphorus donor atoms.[12]

Whereas typical phosphines bear either alkyl or aryl groups, and thus tend to be good electron donors,[4] phosphines bearing perfluoroalkyl groups have significant Lewis acidic character.[13-15] In some cases, transition metal complexes with such phosphines show enhanced reactivity (and sometimes enhanced stability) relative to their unfluorinated counterparts.[14,15]

As part of our group's efforts to synthesize and characterize osmium methane complexes, computational analysis revealed that perfluoroalkyl diphosphines would likely be effective in stabilizing the methane adducts.[16] Specifically, electron-poor diphosphines would stabilize the Os^{II} methane adducts relative to the Os^{IV} methyl/hydride complexes, without introducing significant counterbalancing steric effects or decreasing the methane binding energies (see Chapter 3 for a more detailed discussion). In particular, methylenediphosphines (as opposed to diphosphines with longer backbones) have proven to be the most effective chelating ligands,

because they prevent the methyl/hydride complexes from isomerizing from a *cisoid* to a stable but uninteresting *transoid* seven-coordinate piano stool structure. We set our sights on synthesizing bis[bis(trifluoromethyl)phosphino]methane (dfmpm); this diphosphine best combines both the computationally-predicted ability to stabilize an Os^{II} methane complex, and experimental accessibility. The rest of this chapter details our efforts toward synthesizing this and other related diphosphines.

Results and Discussion

Improved synthesis of bis[bis(trifluoromethyl)phosphino]methane (dfmpm). Several decades ago, a modular synthetic route to diphosphines bearing perfluoroalkyl groups was reported.[17] However, this route suffered from several drawbacks, including use of organomercury reagents, multiple trap-to-trap distillations, and sealed tube reactions that would be – respectively – toxic, tedious, and hard to scale up. Therefore, we sought an alternative route. Tetrachloro methylenediphosphine, $Cl_2PCH_2PCl_2$, seemed to be an appropriate starting material, as judged from its known chemistry.[18,19] We have found that the published synthesis of this diphosphine, which uses aluminum, dichloromethane, and phosphorus trichloride,[18,20] is far from ideal but works well enough on a large scale for our purposes (although in our hands, only about half of the reported 30% yield was consistently achievable). Tetrachloro methylenediphosphine can also be obtained commercially, but is relatively expensive in 100 g quantities.

Trifluoromethylation reactions are often problematic: most CF_3-organometallic reagents rapidly decompose to difluorocarbene and metal-fluoride products. A significant exception to this tendency is the Ruppert-Prakash reagent (CF_3SiMe_3), which is remarkably resistant to this reaction for kinetic reasons.[20] Several authors have reported that $R_{3-n}PX_n$ phosphines (X = leaving group) can be successfully trifluoromethylated by treatment with the Ruppert-Prakash

reagent, usually in tandem with a fluoride promotor.[19,21-23] The transformation is particularly effective when phenoxide is the leaving group,[19] but has not been demonstrated with chloride as the leaving group. Indeed, we find that no reaction occurs upon treatment of tetrachloro methylenediphosphine with CF_3SiMe_3 in the presence of cesium fluoride. Fortunately, tetrachloro methylenediphosphine reacts readily with sodium phenoxide to afford nearly quantitative yields of tetraphenyl methylenediphosphonite, $(PhO)_2PCH_2P(OPh)_2$.[24,25] This phenoxylation reaction is more convenient than the alternative literature procedure (treatment with phenol in the presence of an amine)[18,25] because it avoids the separation issues associated with the partial solubility of the byproduct amine hydrochloride salt in ether.

Initial attempts to carry out the fluoride-promoted trifluoromethylation of tetraphenyl methylenediphosphonite to dfmpm yielded unexpected results. Although the literature recipe calls for catalytic amounts (0.1 equiv) of the promotor CsF,[19] in our hands the starting material $(PhO)_2PCH_2P(OPh)_2$ was not completely consumed under these conditions, and no desired product was obtained. We found, however, that addition of stoichiometric amounts of CsF (5 equiv along with 5 equiv of CF_3SiMe_3 per mol of $(PhO)_2PCH_2P(OPh)_2$) caused complete consumption of the starting material, as observed by ^{31}P NMR spectroscopy. A single product was formed; its expected $X_6AA'X'_6$ splitting patterns in the ^{19}F and ^{31}P NMR spectra indicated that both phosphorus atoms were in identical environments, and that both were attached to two CF_3 groups. The δ 18.5 ^{31}P NMR chemical shift of this product, however, was shifted downfield by ~25 ppm from the reported value[17] for dfmpm. Furthermore, the crude reaction product, a sticky dark red semi-solid, was non-volatile, despite the fact that the desired dfmpm diphosphine is a volatile liquid.

It should be noted that all trifluoromethylated diphosphines previously synthesized through the use of the Ruppert-Prakash reagent contained at least two carbon atoms in the backbone.[19,21-23] The significance of this point lies in the fact that, for a methylene diphosphine, the CH_2 group lies directly between *two* phosphorus atoms. When the latter undergo complete trifluoromethylation, the CH_2 protons become quite acidic, and this factor explains the unexpected behavior described above. The excess CsF/CF_3SiMe_3 reagent deprotonates the initially formed dfmpm product, yielding the cesium salt $Cs[(CF_3)_2PCHP(CF_3)_2]$. This deprotonation reaction, which irreversibly consumes the CsF promotor,[19] explains why incomplete conversion of starting material was observed when only a catalytic amount of the promotor was employed. When stoichiometric (larger) amounts of CsF are added, the trifluoromethylation proceeds to completion, but this cesium salt is the final product. The formation of this salt, which is the conjugate base of the desired dfmpm ligand, explains the presence of just one ^{31}P NMR signal with the expected splitting pattern, yet at the wrong chemical shift, as well as the inability to distill out any product.

Fortunately, we found that treatment of the Cs salt with ethereal hydrogen chloride cleanly reformed the desired diphosphine dfmpm, which could be separated from cesium chloride by filtration, and distilled from the mixture at 79-86 °C in low to moderate yield (~20%) as a clear and colorless liquid. The high volatility of dfmpm made it difficult to separate the diphosphine completely from the diethyl ether solvent by fractional distillation, and typical samples of distilled dfmpm contain ~5 mol% Et_2O; the presence of the ether, however, has no adverse effect in subsequent reaction steps. Scheme 2.1 shows the synthetic path to dfmpm. Although the yield is low, the main benefit of this preparative sequence is its ability to afford

multigram quantities of this diphosphine, versus milligram quantities for the previous literature route.[17]

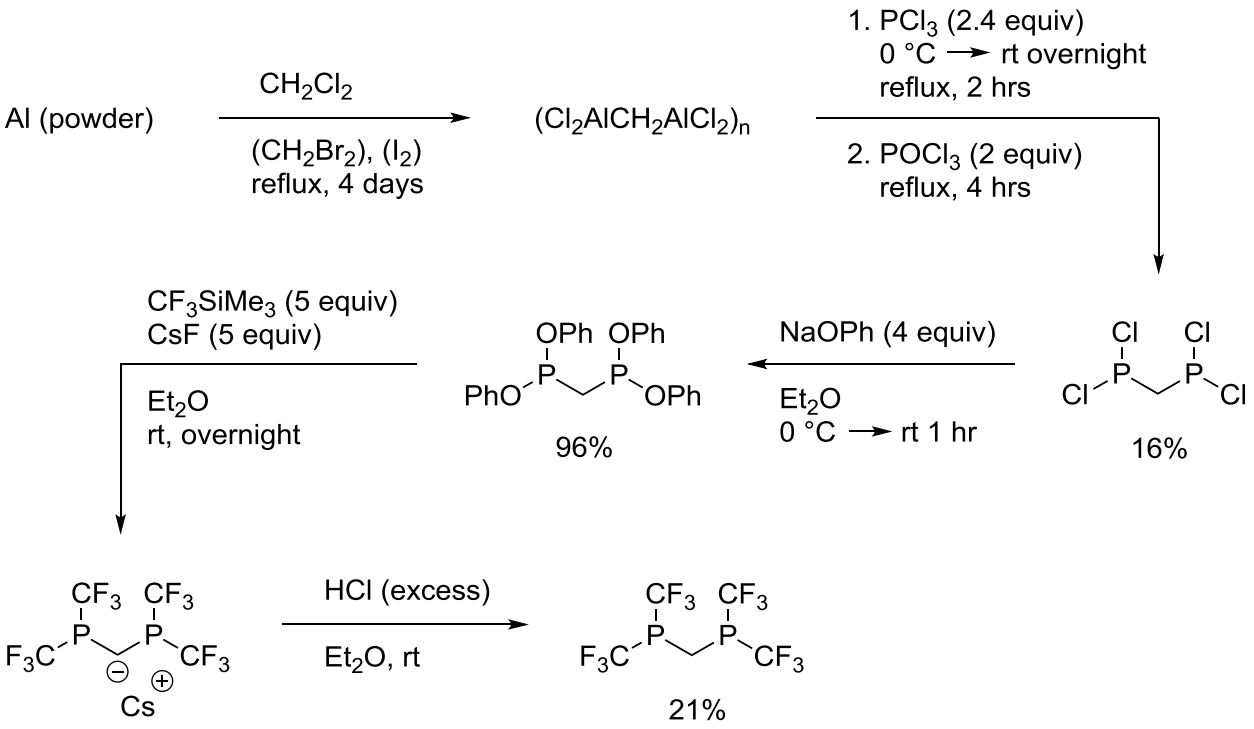

Scheme 2.1. Synthetic pathway for bis[bis(trifluoromethyl)phosphino]methane (dfmpm).

The presence of twelve fluorine nuclei in the dfmpm ligand has a profound impact on the NMR spectra, because the two phosphorus nuclei and twelve fluorine nuclei give rise to an $X_6AA'X'_6$ spin system. Such spin systems often exhibit strong second-order effects that can significantly affect the spectrum, depending on the magnitude of the $J_{AA'}$ coupling constant.[26,27] The current system illustrates this phenomenon well, as shown by the ^{19}F and ^{31}P NMR spectra of dfmpm and the cesium salt of its conjugate base (Figure 2.1). For each compound, there is only one resonance for each type of nucleus because both phosphorus nuclei and all twelve fluorine nuclei, respectively, are chemically equivalent (but not magnetically equivalent, giving rise to the second-order effects).

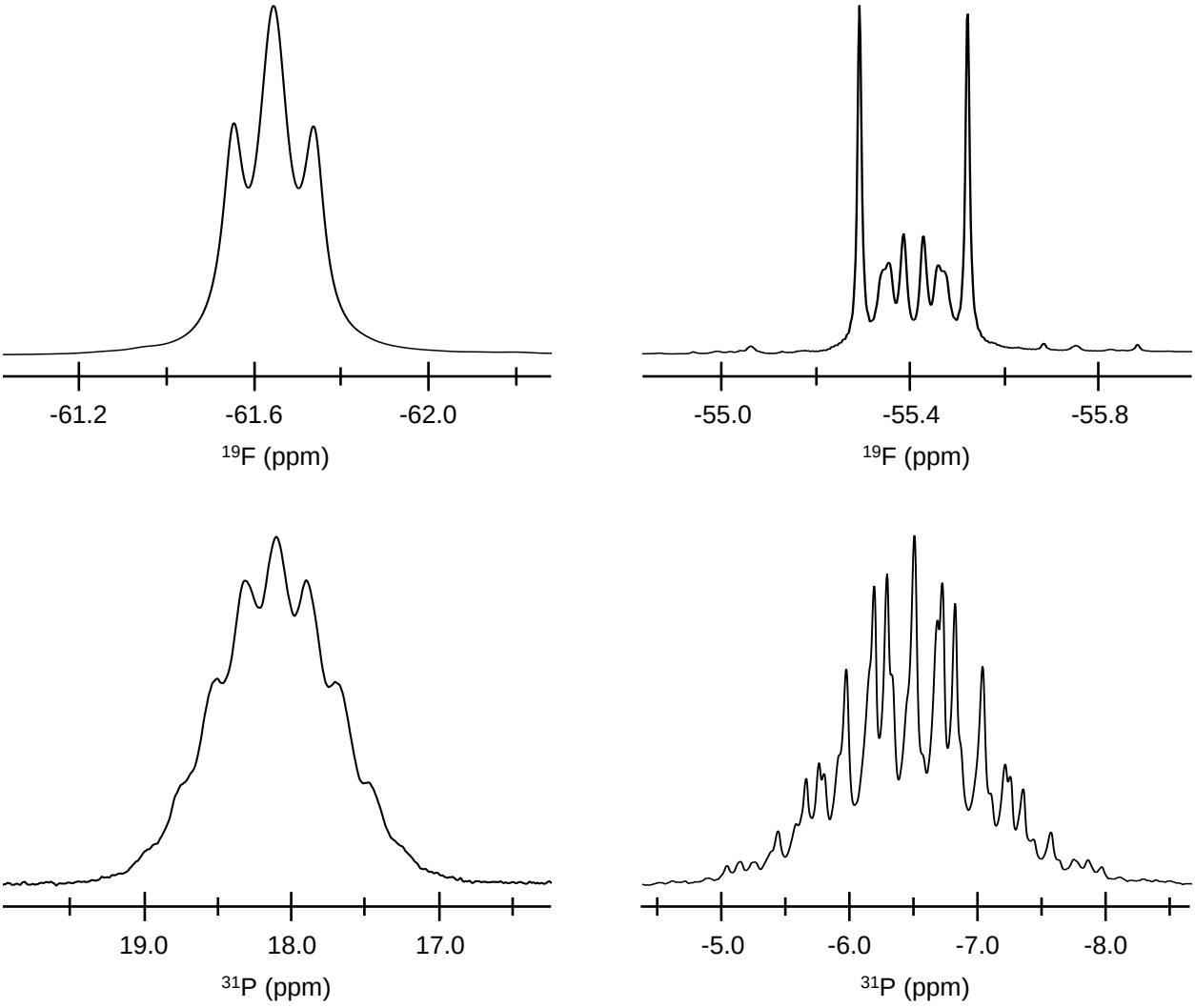

Figure 2.1. Selected regions of ^{19}F (top) and ^{31}P (bottom) NMR spectra of $Cs[(CF_3)_2PCHP(CF_3)_2]$ (left) and $(CF_3)_2PCH_2P(CF_3)_2$ (right) in C_6D_6.

The line shapes seen in Figure 2.1 indicate that the coupling constants in the neutral ligand and the cesium salt are not identical. In the $^{19}F\{^1H\}$ NMR spectrum, the cesium salt displays a "virtually coupled triplet" in which the P-P coupling constant must be relatively large. The virtual coupling results in a deceptively simple line shape in which the twelve fluorine nuclei appear to be coupling to two magnetically *equivalent* phosphorus nuclei, even though the latter are in fact magnetically *inequivalent*. For the neutral dfmpm ligand, on the other hand, the

P-P coupling constant must be relatively small, because its $^{19}F\{^{1}H\}$ NMR resonance is not a triplet, but rather has a characteristic "filled-in doublet" shape.

The X portion of $X_nAA'X'_n$ spin systems can often be analyzed to afford quantitative values for all the coupling constants.[27] Specifically, the X portion of the spectrum consists of $2n + 1$ pairs of lines placed symmetrically about ν_x; one of these pairs (called the N doublet) is the most intense and its two lines are separated by $|J_{AX} + J_{AX'}|$. The N doublet shows that $|J_{PF} + J_{PF'}|$ is 69 ± 1 Hz for the cesium salt of dfmpm, but $|J_{PF} + J_{PF'}|$ is 85.8 ± 0.2 Hz for neutral dfmpm. The positions and intensities of the other $2n$ pairs of lines depend only on the ratio $|J_{AA'}|/|J_{AX} - J_{AX'}|$ (assuming $J_{XX'}$ is 0 Hz, see below). If the separation between the two lines of the innermost pair is S_1 and the separation between the two lines of the next innermost pair is S_2, then the values of $|J_{AA'}|$ and $|J_{AX} - J_{AX'}|$ are given by the following:

$$\boldsymbol{|J_{AA'}| = |[(3S_1 + S_2)(S_1 - S_2)]/[2(3S_1 - S_2)]|}$$

$$\boldsymbol{|J_{AX} - J_{AX'}| = |[S_1S_2(S_1 + S_2)/(3S_1 - S_2)]^{1/2}|}$$

For neutral dfmpm, these pairs of lines are visible in the ^{19}F NMR spectrum, and the values of S_1 = 15.8 ± 0.2 Hz and S_2 = 38.9 ± 0.4 Hz show that $|J_{PP'}|$ is 117 ± 17 Hz and $|J_{PF} - J_{PF'}|$ is 63 ± 4 Hz. From these values and from the N doublet separation, we calculate that $|J_{PF}|$ is 74 ± 2 Hz, $|J_{PF'}|$ is 11 ± 2 Hz, and the value of the $|J_{PP'}|/|J_{PF} - J_{PF'}|$ ratio is 1.9. The $J_{AA'}$ coupling constant can also be computed more easily (and more accurately) as follows, provided that the ratio $|J_{AA'}|/|J_{AX} - J_{AX'}|$ is greater than 1: if one considers half of the bilaterally symmetric pattern, then $J_{AA'}$ is also given by the separation between the line nearest to the center of the pattern, and the first weak line on the outside of the N doublet.[27] From this measurement, we find that $|J_{PP'}|$ is 121 ± 1 Hz.

For $Cs[(CF_3)_2PCHP(CF_3)_2]$, the ^{19}F NMR spectrum is not well enough resolved to calculate the $|J_{AA'}|$ coupling constant in this way, but the large coalesced center line is clear

evidence that the ratio $|J_{PP'}|/|J_{PF} - J_{PF'}|$ is substantially larger in this compound than in the neutral diphosphine.[27,28] If we assume that the two-bond coupling constant $|J_{PF}|$ is about the same in the two compounds (which is equivalent to the assumption that deprotonation mostly affects electron density between the two phosphorus atoms), then we can simulate the line shapes only if $|J_{PP'}|$ is unrealistically large, ca. 900 Hz. If we assume instead that the four-bond coupling constant $|J_{PF'}|$ is about the same in the two compounds (which is reasonable because it should be small for both compounds), then from line shape simulations (Figure 2.2) we can estimate that $|J_{PP'}|$ is approximately 300 ± 50 Hz. Thus, deprotonation of the backbone CH_2 group causes a large increase in $J_{PP'}$. This effect has been seen previously: $J_{PP'}$ is 107 Hz for the unsymmetrical diphosphine $Me_2PCH_2PPh_2$, but increases upon deprotonation to 339 Hz for the corresponding unsymmetrical diphosphinomethanide.[29]

It is worth noting that the line widths of some of the peaks inside the N doublet in the ^{19}F spectrum of neutral dfmpm are greater than the widths of the N doublet lines. Different line widths for different transitions in an $X_nAA'X'_n$ spin system is a known phenomenon; there can be several different causes, including hindered internal rotation, non-zero values of $J_{XX'}$, differing relaxation times for different transitions, intermolecular exchange, and quadrupolar broadening.[30,31] In the case of dfmpm, the coupling constants calculated from the experimental ^{19}F spectrum failed to accurately reproduce the line shapes observed for the peaks inside the N doublet, regardless of the line width chosen. However, including a small but non-zero value of 0.94 Hz for $J_{FF'}$ resulted in a nearly perfect match between the experimental and simulated spectra (compare Figures 2.1 and 2.2).

Note that the 0.94 Hz $J_{FF'}$ coupling constant in dfmpm is between atoms separated by six bonds. Such long-range coupling has precedent;[32] in fact, a *ten-bond* J_{FF} coupling of 1.5 Hz has

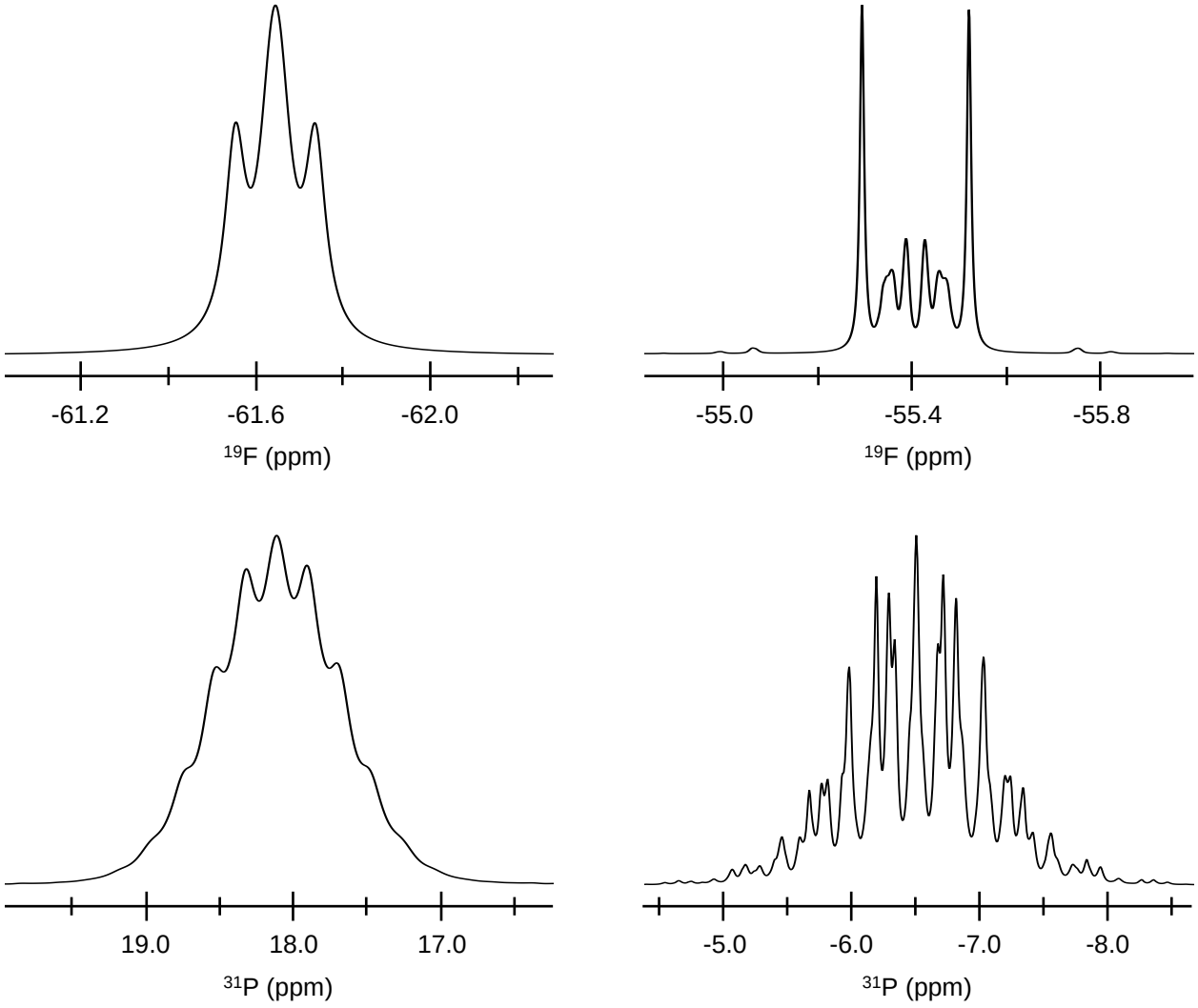

Figure 2.2. Simulated ^{19}F (top) and ^{31}P (bottom) NMR spectra of $Cs[(CF_3)_2PCHP(CF_3)_2]$ (left) and $(CF_3)_2PCH_2P(CF_3)_2$ (right). The parameters for dfmpm are 121 Hz, 74 Hz, 11 Hz, and 0.94 Hz for $J_{PP'}$, J_{PF}, $J_{PF'}$, and $J_{FF'}$, respectively, with 4 Hz and 7 Hz line widths for ^{19}F and ^{31}P spectra, respectively. Those for the cesium salt are 300 Hz, 58 Hz, 11 Hz, and 1 Hz for $J_{PP'}$, J_{PF}, $J_{PF'}$, and $J_{FF'}$, respectively, with 21.2 Hz and 30 Hz line widths for ^{19}F and ^{31}P spectra, respectively.

been seen between CF_3 groups in a sulfur diimide.[33] Theoretical treatments demonstrate that coupling between fluorine atoms separated by four or more bonds is mediated primarily by 'through space' coupling.[34-37] The results are a reminder that F–F coupling constants cannot be assumed to be zero solely because the two F atoms are separated by a large number of bonds.

Attempts to devise a more efficient and modular synthesis of dfmpm. In view of the inconvenience and low yield of the preparation of the tetrachloro methylenediphosphine precursor, we sought a higher-yielding and more modular route to this compound. Modular (symmetric) approaches for the formation of methylene diphosphines and their derivatives can be placed into one of two classes: reaction of a nucleophilic methylene (or substituted methylene) unit with an electrophilic phosphorus reagent, or reaction of an electrophilic methylene (or substituted methylene) unit with a nucleophilic phosphorus reagent.

Nucleophilic methylene/electrophilic phosphorus routes. For this approach, a dianionic methylene equivalent is needed. The reagents "Li_2CH_2" and "$MgCH_2$" (and their substituted analogs) are known, but their preparations are not particularly convenient.[38-41] (An improved preparation[42] of methylenebis(magnesium bromide) has recently come to our attention. This reagent merits our attention in future attempts to improve the synthesis of dfmpm and related methylenediphosphines.) Far more convenient to prepare is the methylenebis(iodozinc) reagent $CH_2(ZnI)_2$,[43,44] and we were able to repeat its preparation successfully. Unfortunately, reaction of this methylene dizinc reagent with several different P^{III} electrophiles (PCl_3, $P(OPh)_3$, $(PhO)_2PCl$,[45] $Me_2C(CH_2O)_2PCl$[46]) failed in all cases to produce the desired tetrachloro methylenediphosphine or the analogous diphosphonites. Only the reaction between methylenebis(iodozinc) and diphenylphosphorochloridite, $(PhO)_2PCl$, produced phosphorus resonances near that expected for tetraphenyl methylenediphosphonite (δ = 175-180), but the reaction was not clean: $[(PhO)_2P]_2CH_2$ could not be isolated from the reaction products, and the resulting mixture failed to react with Ruppert's reagent to form any dfmpm.

Attempts to couple CH_2I_2 and PCl_3 *in situ* using activated magnesium were unsuccessful, as were efforts to make methylene diphosphines from P_2I_4,[47] so the nucleophilic

methylene/electrophilic phosphorus routes were abandoned. No attempts were made to carry out the reaction of a methylene nucleophile with a P^V electrophile, because the products of such reactions are easily made by another route: coupling of a methylene electrophile with a P^V nucleophile (see below). Scheme 2.2 shows the various attempts to prepare dfmpm using a nucleophilic methylene unit.

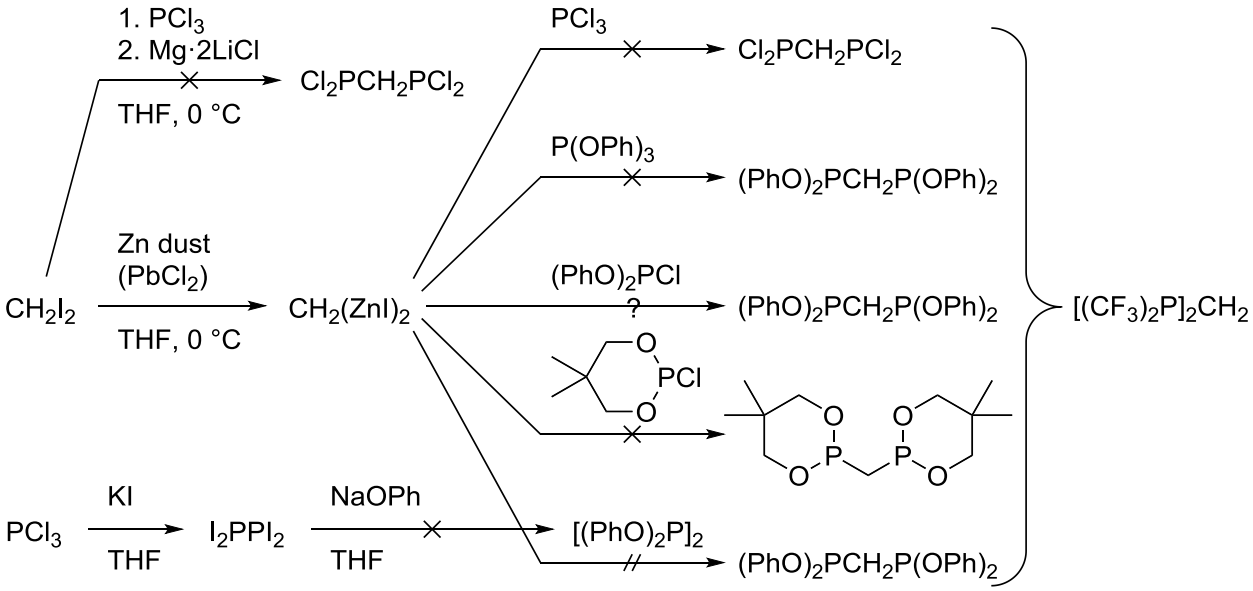

Scheme 2.2. Attempted nucleophilic methylene routes toward dfmpm. Crossed arrows (×) designate failed reactions, hashed (//) designates unattempted, and (?) designates unclear results.

Electrophilic methylene/nucleophilic phosphorus routes. We also explored an alternative approach to dfmpm, involving an electrophilic methylene synthon and nucleophilic phosphorus reagents. For this approach, dihalomethanes (excluding CH_2F_2) are obvious choices for the electrophile. Because the final target is a phosphine, direct reaction of dihalomethanes with a P^{III} nucleophile would be desirable; however, clean formation of a P^{III} metallate was problematic. PCl_3 is too unselective to metallate directly (Li, Na), and metalation of $P(OPh)_3$ failed even in refluxing tetrahydrofuran (Li, Na). Several PCl_3 surrogates in which two of the

reactive sites are blocked can be readily prepared, including the bis(phenoxy) compound $PCl(OPh)_2$,[45] the neopentyl glycolate $PCl[(OCH_2)_2CMe_2]$,[46] the 2,2′-biphenoxy compound $PCl(OC_6H_4C_6H_4O)$, and the *N*,*N*′-di*tert*butyl-1,3-propanediamide[48] compound PCl[N(*t*-Bu)$(CH_2)_3$N(*t*-Bu)], but neither direct metalation of these phosphorochloridites or diazaphosphorinanes, nor reduction to a phosphorus hydride followed by deprotonation (diazaphosphorinane only), afforded P^{III} metallates. Scheme 2.3 shows the various attempts to make dfmpm from an electrophilic methylene unit and these P^{III} nucleophiles.

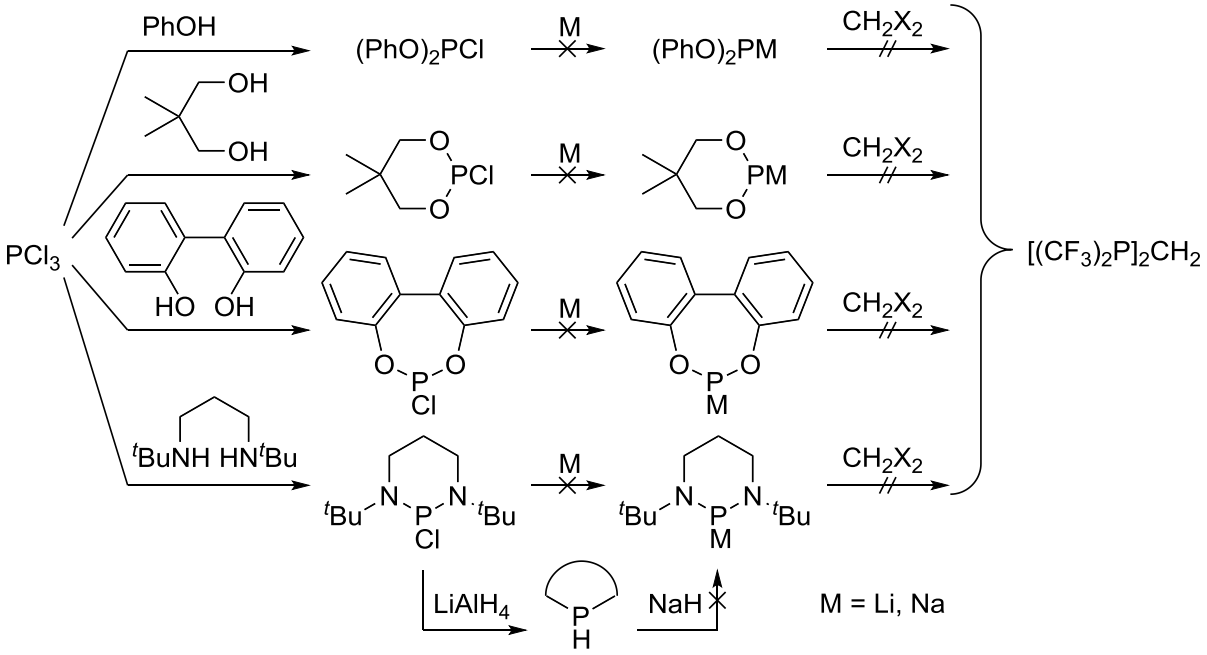

Scheme 2.3. Attempted electrophilic methylene routes toward dfmpm with P^{III} nucleophiles. Crossed arrows (×) designate failed reactions and hashes (//) designate unattempted reactions.

Formation of P^V nucleophiles is much simpler, because hydrogen atoms attached to P^V are much more acidic. Per a published procedure, diethyl phosphite was readily deprotonated with sodium hydride, and the resulting sodium salt $NaP(O)(OEt)_2$ reacted cleanly with dichloromethane in tetrahydrofuran to give tetraethyl methylenediphosphonate, $(EtO)_2P(O)CH_2P(O)(OEt)_2$, in decent yield.[49] The difficulty with this route lies in the subsequent

reduction of P^V to P^{III}. All efforts to effect such a conversion met with failure, in spite of the use of many different reductants ($LiAlH_4$, Et_3SiH, $(Me_3Si)_2$) and combinations of reductants ($CeCl_3/LiAlH_4$,[50] $ROTf/LiMH_4$,[51,52] $Mg/TiCl_4$,[53] Cl_3SiH/Et_3N,[54] $(HMe_2Si)_2O/Ti(O\text{-}i\text{-}Pr)_4$[55]) chosen for their mildness and selectivity. This result is not particularly surprising, because reductants capable of removing the phosphonate oxy group are even more likely to remove the more labile alkoxy or aryloxy groups.

In light of the relatively easy desulfurization of tertiary diphosphine disulfides to diphosphines[56] (which is a reductive process), we considered whether tetraethyl methylenebis(thiophosphonate), $(EtO)_2P(S)CH_2P(S)(OEt)_2$, could be desulfurized to afford tetraethyl methylenediphosphonite, $(EtO)_2PCH_2P(OEt)_2$, which could potentially be trifluoromethylated to give dfmpm. It is known that phosphorus pentasulfide and Lawesson's reagent (2,4-bis(4-methoxyphenyl)1,3,2,4-dithiadiphosphetane) convert diethyl phosphite to diethyl thiophosphite, $(EtO)_2P(S)H$, in good yield.[57] Unfortunately, although diethyl thiophosphite is readily deprotonated with sodium hydride, the resulting sodium salt $NaP(S)(OEt)_2$ failed to react with dihalomethanes (chloride or bromide) to give tetraethyl methylenedi(thiophosphonate). The problem may stem from the propensity of deprotonated thiophosphites to react via radical chemistry rather than via nucleophilic pathways.

We investigated a possible alternative route to $(EtO)_2P(S)CH_2P(S)(OEt)_2$ by sulfurization of tetraethyl methylenediphosphonate; the latter compound is easy to make, as described above. However, the sulfurization procedure that worked so well for diethyl phosphite completely failed for tetraethyl methylenediphosphonate. Scheme 2.4 shows the various attempts to prepare dfmpm using an electrophilic methylene unit and P^V nucleophiles ("reductant" refers to all the reagents and reagent combinations mentioned above).

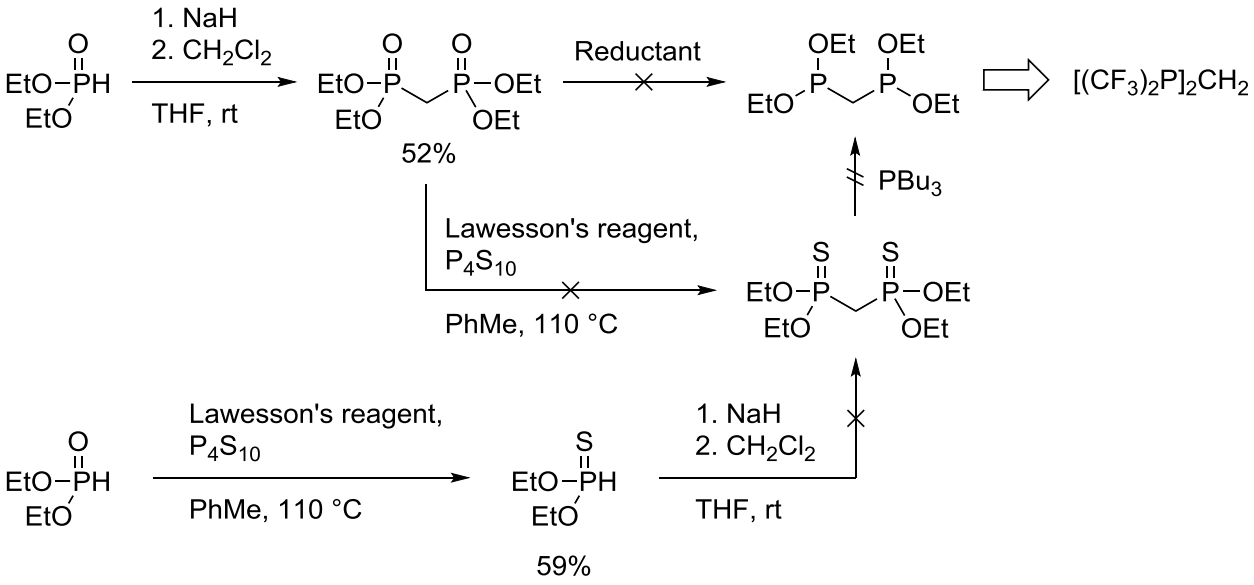

Scheme 2.4. Attempted electrophilic methylene routes to prepare dfmpm with P^V nucleophiles. Crossed arrows (×) designate failed reactions and hashes (//) designate unattempted reactions.

Although the direct reduction of diphosphonates to diphosphonites and the sulfurization/desulfurization routes both proved to be dead ends, there are other reported methods for the conversion of diphosphonates to tetrachloro diphosphines. One of these methods is reduction to a diphosphine followed by chlorination.[58-61] However, the $LiAlH_4$ reduction of methylenediphosphonates to methylenediphosphine ($H_2PCH_2PH_2$) proceeds in very poor yields, and the methylenediphosphine product is difficult to separate completely from the dibutyl ether that is used as the reaction solvent.[58] Although $LiAlH_4$ is commonly employed in the reduction of phosphonates to phosphines, a 1:1 mixture of $LiAlH_4$ and TMSCl is a milder reductant that often affords greater yields.[59]

Several chlorinating agents have been used to convert hydrophosphines $H_{3-n}PR_n$ to chlorophosphines $Cl_{3-n}PR_n$, where n is 1 or 2, most with rather poor results or inconvenient procedures.[60-70] Phosgene is one of these chlorinating agents, but it is highly toxic and requires very careful handling.[59] Recently it was reported that PCl_5 cleanly accomplishes the desired

conversion in common ethereal solvents; however, methylenediphosphine was not included in this study.[71] Scheme 2.5 shows a possible new synthetic route to dfmpm and derivatives, but we have not investigated this possibility.

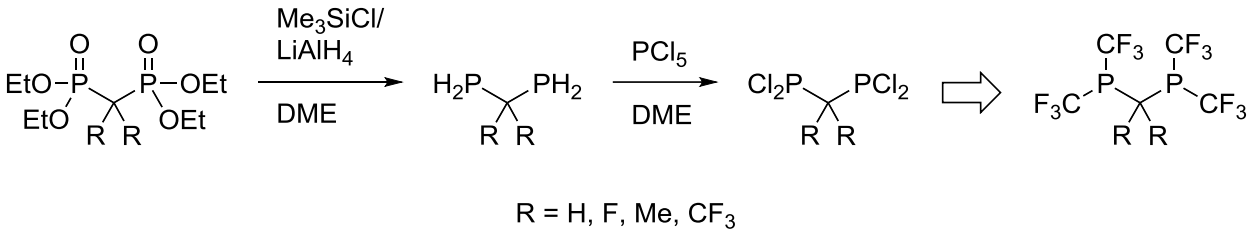

Scheme 2.5. Synthesis plan for the reduction/chlorination route to dfmpm and derivatives. The method for substitution with R groups is discussed in the text.

It should be noted that one advantage of methylenediphosphonates is that they lend themselves to facile derivatization via deprotonation of the methylene backbone, followed by treatment with various electrophiles.[72] In light of the series of diphosphines we wished to utilize, we investigated whether tetraethyl 2,2-propylenediphosphonate and tetraethyl 1,1-difluoro-methylenediphosphonate could be prepared by one-pot treatment of tetraethyl methylene-diphosphonate with 2 equiv. of sodium hydride in tetrahydrofuran, followed by addition of 2 equiv. of methyl iodide[73] or *N*-fluorobenzenesulfonimide,[74] respectively. We found that formation of tetraethyl 2,2-propylenediphosphonate occurs without major issues, except that care is needed (ice bath and slow addition rate) to avoid a runaway exotherm during the methylation step. The tetraethyl 2,2-propylenediphosphonate product was isolated by removal of solvent under vacuum. The resulting product can be purified by vacuum distillation, but the crude product is sufficiently clean to be used for subsequent chemical reactions. A similar preparation of this compound has been described.[75]

Fluorination was less straightforward. Because *N*-fluorobenzenesulfonimide is likely to react with excess sodium hydride, the fluorination was first attempted stepwise. The monofluorination reaction appeared by ^{19}F and ^{31}P NMR to proceed well, but aqueous workup returned only starting (unfluorinated) diphosphonate. Depending on the nature of the decomposition during aqueous workup, it is possible that one-pot difluorination might work better than monofluorination (particularly if the remaining proton is involved in the decomposition). However, time constraints prohibited further studies.

Experimental

Unless stated otherwise, all manipulations were performed under argon or vacuum using standard Schlenk line or glove box techniques. Glassware was oven- or flame-dried and allowed to cool under vacuum or argon. Solvents were distilled under nitrogen from sodium/benzophenone (pentane, diethyl ether), calcium hydride (dichloromethane), magnesium (ethanol, *tert*-butanol), or sodium (toluene), and sparged with argon for 30-60 seconds immediately before use. Benzene-d_6 and chloroform-d_1 were purchased from Sigma-Aldrich or Cambridge Isotope Laboratories in 1-mL ampoules and used without purification.

The following starting materials were obtained from commercial sources and used as received unless stated otherwise: aluminum powder (Sigma-Aldrich), dibromomethane (Sigma-Aldrich), iodine (Fisher), phosphorus trichloride (Sigma-Aldrich), phosphoryl chloride (Sigma-Aldrich), phenol (Sigma-Aldrich), 60% sodium hydride dispersion in mineral oil (Sigma-Aldrich), cesium fluoride (Sigma-Aldrich), trifluoromethyltrimethylsilane (Oakwood), hydrogen chloride (Sigma-Aldrich, 1.0 M in diethyl ether), neopentyl glycol (Sigma-Aldrich), diethyl phosphite (Sigma-Aldrich), phosphorus pentasulfide (Sigma-Aldrich), Lawesson's reagent (Sigma-Aldrich), methyl iodide (Sigma-Aldrich).

NMR spectra were acquired on Varian spectrometers (Unity 400, Unity 500, VXR 500, and Unity Inova 600) at room temperature. Positive chemical shifts indicate shifts to higher frequency relative to the following standards: internal $SiMe_4$ (^1H and ^{13}C, set by assigning appropriate shifts to residual solvent signals), external $CFCl_3$ in $CDCl_3$ (^{19}F), and external H_3PO_4 in D_2O (^{31}P). Default instrument parameters were used unless stated otherwise. Spectra were processed using the MestReNova NMR software package; manual phasing, peak picking, and integration methods were employed, and polynomial or Bernstein polynomial (typically of order 3-8) baseline corrections were employed if warranted. Simulations of ^{19}F and ^{31}P NMR spectra were performed using the MestReNova spin simulation tool within the NMR software package.

Tetrachloro Methylenediphosphine, $Cl_2PCH_2PCl_2$. This is a modification of a literature procedure.[18] To a 2-L 3-necked round-bottomed flask equipped with a gas inlet, reflux condenser, and mechanical stirring paddle was added Al powder (125 g, 4.6 mol). CH_2Cl_2 (1 L, 15.6 mol) was added, followed by CH_2Br_2 (85 mL, 1.2 mol) and iodine (a few crystals). The mixture was refluxed with vigorous stirring for 4 days, then cooled to room temperature, giving an orange solution and gray powder. To a separate 5-L 3-necked round-bottomed flask equipped with gas inlet, water-cooled reflux condenser, and mechanical stirring paddle was added PCl_3 (480 mL, 5.5 mol), and the flask was cooled to 0 °C. With both the aluminum mixture and the PCl_3 being rapidly stirred, the aluminum-containing slurry was transferred portion-wise to the PCl_3 via a 1/8-inch bore Teflon cannula over the course of 4 h by short, repeated applications of argon pressure to the source flask while venting the receiving flask. The green-gray mixture was allowed to warm slowly to room temperature overnight by allowing the ice bath to melt (allowing the mixture to warm too rapidly can result in an uncontrolled exotherm and flash-boiling of the CH_2Cl_2). The mixture was refluxed for 2 h and then cooled to room temperature.

The flask was then equipped with a 500-mL pressure-equalizing liquid addition funnel. $POCl_3$ (430 mL, 4.6 mol) was added to the addition funnel, and then added to the reaction mixture dropwise over 3 h (addition of CH_2Cl_2 is sometimes necessary if precipitated solids make stirring too difficult). The mixture was refluxed for 4 h, cooled to room temperature, and placed into a freezer at –20 °C to complete precipitation of $POCl_3 \cdot AlCl_3$. The brown solution was filtered through a filter cannula, the residue was washed with CH_2Cl_2 (300 mL), and the wash was filtered and added to the original filtrate. After the majority of the CH_2Cl_2 was removed by atmospheric pressure distillation, the remaining CH_2Cl_2, PCl_3, and $POCl_3$ were removed at room temperature under vacuum to leave an oil, from which $Cl_2PCH_2PCl_2$ was distilled under vacuum at 27-35 °C and 10^{-2} Torr as a pale yellow liquid. Yield: 50 mL (16%). ^{1}H NMR (C_6D_6): δ 2.52 (t, J_{PH} = 16 Hz). $^{31}P\{^1H\}$ NMR (C_6D_6): δ 176 (s).

Tetraphenyl Methylenediphosphonite, $(PhO)_2PCH_2P(OPh)_2$. This is a modification of a literature procedure.[25] To a 1-L 2-necked round-bottomed flask equipped with a magnetic stir bar, gas inlet, and addition funnel was added NaH (22.9 g of a 60% dispersion in mineral oil, 573 mmol). The NaH was washed with pentane (3 × 100 mL) to remove the mineral oil, the washings being removed by cannula filtration. Et_2O (200 mL) was added to the flask, and the addition funnel was filled with a solution of phenol (52.6 g, 559 mmol) in Et_2O (200 mL). The flask was cooled to 0 °C and, with vigorous stirring, the phenol solution was added dropwise at a rate to keep the Et_2O below reflux; CAUTION: if the stirring rate is too high, the stir bar can break the flask. After the addition was complete, the mixture was stirred for 1 h, and then the addition funnel was charged with a solution of $Cl_2PCH_2PCl_2$ (19 mL, 140 mmol) in Et_2O (100 mL). The chlorodiphosphine was added dropwise to the NaOPh mixture with vigorous stirring at a rate to keep the Et_2O below reflux (addition of Et_2O is sometimes necessary to maintain stirring as NaCl

precipitates). After the addition was complete, the mixture was stirred for 1 h, and then allowed to settle overnight. The mixture was filtered through a filter cannula into a 1-L Schlenk flask, and most of the volatile material was removed from the filtrate under vacuum, leaving a clear and colorless liquid that contained product and some Et_2O. The yield was assumed to be quantitative. $^{31}P\{^1H\}$ NMR (Et_2O): δ 178 (s).

Bis[bis(trifluoromethyl)phosphino]methane, $(CF_3)_2PCH_2P(CF_3)_2$, dfmpm. In a glove box, a 500-mL Schlenk flask was charged with a magnetic stir bar and CsF (106.09 g, 0.70 mol) which had previously been dried at 120 °C under vacuum, ground into a fine powder in a glove box, and stored under argon. The flask was sealed, removed from the box, and placed under argon. To the CsF was added the solution of tetraphenyl methylenediphosphonite (~77 mL, 0.14 mol) in Et_2O (~75 mL) from the previous reaction, and the mixture was cooled to 0 °C. To the vigorously stirred mixture was added CF_3SiMe_3 (103 mL, 0.70 mol) by cannula over 15 min. After being stirred at 0 °C for 6 h, the yellow mixture was allowed to warm to room temperature overnight with continued stirring to give an off-white solid and a red-brown solution. A ^{31}P NMR spectrum of the solution showed complete disappearance of tetraphenyl methylenediphosphonite (δ 178) and formation of $Cs[(CF_3)_2PCHP(CF_3)_2]$ (δ 18.5). The mixture was filtered into a 1-L Schlenk flask, and the filtrate was concentrated to ~75 mL under vacuum at room temperature. The solution was cooled to 0 °C and treated with HCl (800 mL of a 1.0 M solution in Et_2O, 0.8 mol). As the HCl was added, the precipitation of CsCl necessitated increasing the stirring rate in order to maintain stirring. After the addition was complete, the solution was warmed to room temperature over 1 h, allowed to stand for 30 min until solids had settled, and then filtered. The Et_2O was removed from the filtrate by atmospheric pressure distillation, and the product was distilled in Bantamware at 79-86 °C under atmospheric pressure

to afford a clear and colorless liquid. Yield: 6.5 mL (21%). ^{1}H NMR (C_6D_6): δ 2.28 (t, J_{PH} = 2.7 Hz); there are also resonances from Et_2O (~5 mol%). $^{19}F\{^{1}H\}$ NMR (C_6D_6): δ –55.4 (m). $^{31}P\{^{1}H\}$ NMR (C_6D_6): δ –6.51 (m). The NMR data agree with literature values.[17]

2,2-Dimethyl-1,3-propanediyl Phosphorochloridite, $Me_2C(CH_2O)_2PCl$. This is a modification of a literature procedure.[46] To a 200-mL round-bottomed flask open to air was added neopentyl glycol (75.0 g, 0.72 mol), and then PCl_3 (75 mL, 0.86 mol) all in one portion. The reaction was allowed to proceed without stirring until evolution of HCl gas ceased (1-2 h), after which the reaction mixture was allowed to stand covered for a few days. The excess PCl_3 was removed under vacuum at room temperature, and the phosphorochloridite was distilled under vacuum at 66-78 °C and 10 Torr to give a clear and colorless oil. Yield: 85 mL (85%). ^{1}H NMR (C_6D_6): δ 4.02 (dd, J_{HH} = 10 Hz, J_{PH} = 6 Hz, 2H, CH_2), 3.04 (dd, J_{HH} = 10 Hz, J_{PH} = 11 Hz, 2H, CH_2), 0.84 (s, 3H, Me_2C), 0.08 (s, 3H, Me_2C). $^{31}P\{^{1}H\}$ NMR (C_6D_6): δ 148 (s).

Tetraethyl Methylenediphosphonate, $(EtO)_2P(O)CH_2P(O)(OEt)_2$. This is a modification of a literature procedure.[49] To a 500-mL 3-necked round-bottomed flask equipped with a magnetic stir bar, gas inlet, and addition funnel was added NaH (23.91 g of a 60% dispersion in mineral oil, 0.598 mol). The NaH was washed with pentane (3 × 100 mL) to remove the mineral oil, the washings being removed by cannula filtration. THF (100 mL) was added, and the addition funnel was charged with diethyl phosphite (70 mL, 0.543 mol). The diethyl phosphite was added dropwise with vigorous stirring at a rate to keep the THF below reflux. After the addition was complete, the mixture was stirred until evolution of hydrogen gas ceased and the reaction mixture had cooled to room temperature. The addition funnel was removed and freshly distilled CH_2Cl_2 (50 mL, 0.783 mol) was added. A reflux condenser was placed in the open neck, and the reaction mixture was heated to ~45 °C overnight. After the

reaction mixture had cooled to room temperature, it was quenched with water (150 mL), and the resulting mixture was extracted with CH_2Cl_2 (3 × 50 mL). The organic layers were combined and dried ($MgSO_4$), the solvent was removed under vacuum, and the diphosphonate was distilled under vacuum at 95-102 °C and 10^{-2} Torr to give a colorless viscous oil. Yield: 35 mL (52%). ^{1}H NMR ($CDCl_3$): δ 4.13 (dq, J_{HH} = 7.1 Hz, J_{PH} = 7.1 Hz, 8H, OC*H*$_2$Me), 2.40 (t, J_{PH} = 21.1 Hz, 2H, PCH_2P), 1.30 (t, J_{HH} = 7.1 Hz, 12H, OCH$_2$*Me*),. ^{1}H NMR (C_6D_6): δ 4.13 (m, 8H, OC*H*$_2$Me), 2.37 (t, J_{PH} = 20.9 Hz, 2H, PCH_2P), 1.08 (t, J_{HH} = 7.1 Hz, 12H, OCH$_2$*Me*). ^{31}P{^{1}H} NMR (C_6D_6): δ 20.2 (s).

Diethyl Thiophosphite, $(EtO)_2P(S)H$. This is a modification of a literature procedure.[57] To a 2-L 3-necked round-bottomed flask equipped with a reflux condenser and a mechanical stirring paddle was added Lawesson's reagent (131.86 g, 0.326 mol) and P_4S_{10} (72.47 g, 0.163 mol). Toluene (1 L) was added, followed by diethyl phosphite (70 mL, 0.543 mol). The mixture was heated to 100 °C with stirring for 2 h, at which time the ^{31}P NMR spectrum showed complete conversion of the diethyl phosphite, with minor side products present. The mixture was cooled to room temperature and filtered by cannula filtration, the solvent was removed under vacuum at room temperature, and the product was distilled under vacuum at 25-32 °C and 10^{-2} Torr to afford a pale yellow oil. Yield: 45 mL (59%). ^{1}H NMR ($CDCl_3$): δ 7.69 (d, J_{PH} = 647 Hz, 1H, PH), 4.10 (m, 4H, OC*H*$_2$Me), 1.29 (t, J_{HH} = 7.1 Hz, 6H, OCH$_2$*Me*). ^{31}P{^{1}H} NMR ($CDCl_3$): δ 69.8 (s).

Tetraethyl 2,2-Propylenediphosphonate, $(EtO)_2P(O)CMe_2P(O)(OEt)_2$. To a 100-mL Schlenk flask equipped with a magnetic stir bar was added NaH (1.9 g of a 60% dispersion in mineral oil, 47.5 mmol) under argon. The NaH was washed with pentane (3 × 10 mL) to remove the mineral oil, the washings being removed via filter cannula. THF (10 mL) was added, and

tetraethyl methylenediphosphonate (3.1 mL, 12.5 mmol,), was added dropwise by means of a gas-tight syringe. After the addition was complete, the mixture was stirred until evolution of hydrogen gas ceased and the reaction mixture had cooled to room temperature (~30 min). The mixture was cooled to 0 °C in an ice bath, and MeI (3.1 mL, 49.8 mmol) was added dropwise by means of a gas-tight syringe. The mixture was warmed to room temperature and stirred for 1 h. It was then quenched with water (50 mL), and extracted with CH_2Cl_2 (3 × 50 mL). The organic layers were combined and dried ($MgSO_4$), and the solvent was removed under vacuum at room temperature to give a pale yellow viscous oil, which upon standing formed colorless crystals. Yield: 2.5 g (63%). ^{1}H NMR (C_6D_6): δ 4.15 (dq, J_{HH} = 7.1 Hz, J_{PH} = 7.1 Hz, 8H, OC*H*$_2$Me), 1.40 (t, J_{PH} = 16.2 Hz, 6H, CMe_2), 1.30 (t, J_{HH} = 7.1 Hz, 12H, OCH_2*Me*). ^{31}P{^{1}H} NMR ($CDCl_3$): δ 28.3 (s). The NMR data are consistent with previous reports.[75-78]

References

1. Kosolapoff, G. M.; Maier, L., In *Organic Phosphorus Compounds*; 2nd ed.; Wiley-Interscience: New York, 1972; Vol. 1.
2. van der Boom, M. E.; Milstein, D. *Chem. Rev.* **2003**, *103*, 1759-1792.
3. Espinet, P.; Soulantica, K. *Coord. Chem. Rev.* **1999**, *193-195*, 499-556.
4. Hartwig, J. F. *Organotransition Metal Chemistry: From Bonding to Catalysis*; 1st ed.; University Science Books: Sausalito, 2010.
5. Wolfe, J. P.; Wagaw, S.; Buchwald, S. L. *J. Am. Chem. Soc.* **1996**, *118*, 7215-7216.
6. Driver, M. S.; Hartwig, J. F. *J. Am. Chem. Soc.* **1996**, *118*, 7217-7218.
7. Louie, J.; Driver, M. S.; Mamann, B. C.; Hartwig, J. F. *J. Org. Chem.* **1997**, *62*, 1268-1273.
8. Knowles, W. S.; Sabacky, M. J. *Chem. Commun.* **1968**, 1445-1446.

9. Vineyard, B. D.; Knowles, W. S.; Sabacky, M. J.; Bachman, G. L.; Weinkauff, D. J. *J. Am. Chem. Soc.* **1977**, *99*, 5946-5952.

10. Kitamura, M.; Ohkuma, T.; Inoue, S.; Sayo, N.; Kumobayashi, H.; Akutagawa, S.; Ohta, T.; Takaya, H.; Noyori, R. *J. Am. Chem. Soc.* **1988**, *110*, 629-631.

11. Ohkuma, T.; Ooka, H.; Yamakawa, M.; Ikariya, T.; Noyori, R. *J. Org. Chem.* **1996**, *61*, 4872-4873.

12. Fryzuk, M. D.; Bosnich, B. *J. Am. Chem. Soc.* **1977**, *99*, 6262-6267.

13. Apel, J.; Grobe, J. *Z. Anorg. Allg. Chem.* **1979**, *453*, 53-67.

14. Merwin, R. K.; Schnabel, R. C.; Koola, J. D.; Roddick, D. M. *Organometallics* **1992**, *11*, 2972-2978.

15. Bennett, B. L.; Hoerter, J. M.; Houlis, J. F.; Roddick, D. M. *Organometallics* **2000**, *19*, 615-621.

16. Flener, C. *Quantum Mechanical Analysis of Donor-Acceptor Interactions in Organometallic Complexes and Comparative Analysis of Class Size and Teacher Experience on Student Satisfaction and Learning.* Ph.D. Thesis, University of Illinois, Urbana, IL, 2009.

17. Phillips, I. G.; Ball, R. G.; Cavell, R. G. *Inorg. Chem.* **1988**, *27*, 4038-4045.

18. Manojlovic-Muir, L.; Jobe, I. R.; Maya, B. J.; Puddephatt, R. J. *J. Chem. Soc., Dalton Trans.* **1987**, 2117-2124.

19. Murphy-Jolly, M. B.; Lewis, L. C.; Caffyn, A. J. M. *Chem. Commun.* **2005**, 4479-4480.

20. Prakash, G. K. S.; Yudin, A. K. *Chem. Rev.* **1997**, *97*, 757-786.

21. Singh, R. P.; Vij, A.; Kirchmeier, R. L.; Shreeve, J. M. *Inorg. Chem.* **2000**, *39*, 375-377.

22. Panne, P.; Naumann, D.; Hoge, B. *J. Fluorine Chem.* **2001**, *112*, 283-286.

23. Tworowska, I.; Dabkowski, W.; Michalski, J. *Angew. Chem. Int. Ed.* **2001**, *40*, 2898-2900.

24. Hietkamp, S.; Sommer, H.; Stelzer, O. *Angew. Chem. Int. Ed.* **1982**, *21*, 376-377.

25. Karsch, H. H. *Z. Naturforsch., B: Anorg. Chem., Org. Chem.* **1983**, *38B*, 1027-1030.

26. Carty, A. J.; Harris, R. K. *Chem. Commun.* **1967**, 234-236.

27. Harris, R. K. *Can. J. Chem.* **1964**, *42*, 2275-2281.

28. Finer, E. G.; Harris, R. K. *Mol. Phys.* **1967**, *12*, 457-467.

29. Karsch, H. H. *Z. Naturforsch., B: Anorg. Chem., Org. Chem.* **1979**, *34B*, 1178-1182.

30. Finer, E. G.; Harris, R. K.; Bond, M. R.; Keat, R.; Shaw, R. A. *J. Mol. Spectrosc.* **1970**, *33*, 72-83.

31. Ogilvie, F. B.; Jenkins, J. M.; Verkade, J. G. *J. Am. Chem. Soc.* **1970**, *92*, 1916-1923.

32. Hilton, J.; Sutcliffe, L. H. *Prog. Nucl. Magn. Reson. Spectrosc.* **1975**, *10*, 27-39.

33. Swindell, R. R.; Schreeve, J. M. *Inorg. Nucl. Chem. Lett.* **1972**, *8*, 759-762.

34. Mallory, F. B.; Mallory, C. W.; Butler, K. E.; Lewis, M. B.; Xia, A. Q.; Luzik Jr, E. D.; Fredenburgh, L. E.; Ramanjulu, M. M.; Van, Q. N.; Francl, M. M.; Freed, D. A.; Wray, C. C.; Hann, C.; Nerz-Stormes, M.; Carroll, P. J.; Chirlian, L. E. *J. Am. Chem. Soc.* **2000**, *122*, 4108-4116.

35. Peralta, J. E.; Contreras, R. H.; Snyder, J. P. *Chem. Commun.* **2000**, 2025-2026.

36. Schwartz, R.; Seelig, J.; Künnecke, B. *Magn. Reson. Chem.* **2004**, *42*, 512-517.

37. Alkorta, I.; Elguero, J. *Struct. Chem.* **2004**, *15*, 117-120.

38. Bertini, F.; Grasselli, P.; Zubiani, G.; Cainelli, G. *Tetrahedron* **1970**, *26*, 1281-1290.

39. Pascali, V.; Tangari, N.; Umani-Ronchi, A. *J. Chem. Soc., Perkin Trans. 1* **1973**, 1166-1168.

40. Bruin, J. W.; Schat, G.; Akkerman, O. S.; Bickelhaupt, F. *J. Organomet. Chem.* **1985**, *288*, 13-25.

41. Gurak, J. A.; Chinn, J. W., Jr.; Lagow, R. J. *J. Am. Chem. Soc.* **1982**, *104*, 2637-2639.

42. Gudnason, P. I.; Arnason, I. *Org. Lett.* **2009**, *11*, 2015-2017.

43. Takai, K.; Kakiuchi, T.; Kataoka, Y.; Utimoto, K. *J. Org. Chem.* **1994**, *59*, 2668-2670.

44. Matsubara, S.; Oshima, K.; Matsuoka, H.; Matsumoto, K.; Ishikawa, K.; Matsubara, E. *Chem. Lett.* **2005**, *34*, 952-953.

45. Hewertson, W.; Smith, B. C.; Shaw, R. A.; Lintvedt, R. L., *Diphenyl Phosphorochloridite (Diphenyl Monochlorophosphite)* In *Inorg. Synth.*; Holtzlaw, H., F., Ed.; John Wiley & Sons, Inc.: Hoboken, 2007; Vol. 8, p 68-71.

46. Jew, R. L. *Steric and Electronic Effects Induced by Ancillary Ligand Substitutions on Cyclopentadienyl Osmium Complexes.* Ph.D. Thesis, University of Illinois, Urbana, IL, 2008.

47. Suzuki, H.; Fuchita, T.; Iwasa, A.; Mishina, T. *Synthesis* **1978**, 905-908.

48. King, R. B.; Sundaram, P. M. *J. Org. Chem.* **1984**, *49*, 1784-1789.

49. Leadbetter, M. R.; Brown, R. W.; McKenna, M. M. U.S. Patent 5,688,983, Nov. 18, 1997.

50. Imamoto, T.; Takeyama, T.; Kusumoto, T. *Chem. Lett.* **1985**, *14*, 1491-1492.

51. Imamoto, T.; Kikuchi, S.-i.; Miura, T.; Wada, Y. *Org. Lett.* **2001**, *3*, 87-90.

52. Kenny, N. P.; Rajendran, K. V.; Gilheany, D. G. *Chem. Commun.* **2015**, *51*, 16561-16564.

53. Corey, E. J.; Danheiser, R. L.; Chandrasekaran, S. *J. Org. Chem.* **1976**, *41*, 260-265.

54. Fritzsche, H.; Hasserodt, U.; Korte, F. *Chem. Ber.* **1965**, *98*, 171-174.

55. Berthod, M.; Favre-Reguillon, A.; Mohamad, J.; Mignani, G.; Docherty, G.; Lemaire, M. *Synlett* **2007**, 1545-1548.

56. Maier, L. *J. Inorg. Nucl. Chem.* **1962**, *24*, 275-283.

57. McKenna, C. E.; Li, Z. U.S. Patent 6,284,909 B1, Sep. 4, 2001.

58. Hays, H. R.; Kosolapoff, G. M. U.S. Patent 3,445,522, May 20, 1969.

59. Adams, J. J.; Lau, A.; Arulsamy, N.; Roddick, D. M. *Inorg. Chem.* **2007**, *46*, 11328-11334.

60. Humphreys, A. S.; Filipovska, A.; Berners-Price, S. J.; Koutsantonis, G. A.; Skelton, B. W.; White, A. H. *Dalton Trans.* **2007**, 4943-4950.

61. Berven, B. M.; Koutsantonis, G. A. *Synthesis* **2008**, 2626-2630.

62. Burch, G. M.; Goldwite, H.; Haszeldine, R. N. *J. Chem. Soc.* **1963**, 1083-1091.

63. Yurchenko, R. I.; Lavrova, E. E.; Voitsekhovskaya, O. M.; Yurchenko, A. G. *J. Gen. Chem. USSR (Engl. Transl.)* **1984**, *54*, 2366-2367.

64. Issleib, K.; Kuemmel, R. *Chem. Ber.* **1967**, *100*, 3331-3342.

65. Markl, G.; Weber, W.; Weiβ, W. *Chem. Ber.* **1985**, *118*, 2365-2395.

66. Markl, G.; Amrhein, J.; Stoiber, T.; Striebl, U.; Kreitmeier, P. *Tetrahedron* **2002**, *58*, 2551-2567.

67. Lindner, E.; Schmid, M.; Wald, J.; Queisser, J. A.; Gepraegs, M.; Wegner, P.; Nachtigal, C. *J. Organomet. Chem.* **2000**, *602*, 173-187.

68. Field, L. D.; Wilkinson, M. P. *Tetrahedron Lett.* **1997**, *38*, 2779-2782.

69. Dahlenburg, L.; Kaunert, A. *Eur. J. Inorg. Chem.* **1998**, *1998*, 885-887.

70. Kischkel, H.; Roeschenthaler, G.-V. *Chem. Ber.* **1985**, *118*, 4842-4848.

71. Tavtorkin, A. N.; Toloraya, S. A.; Nifant'ev, E. E.; Nifant'ev, I. E. *Tetrahedron Lett.* **2011**, *52*, 824-825.

72. Wadsworth, W. S., *Synthetic Applications of Phosphoryl-Stabilized Anions* In *Organic Reactions*; Dauben, W. G., Ed.; John Wiley & Sons, Inc.: New York, 1977; Vol. 25, p 73-253.

73. Quimby, O. T.; Curry, J. D.; Nicholson, D. A.; Prentice, J. B.; Roy, C. H. *J. Organomet. Chem.* **1968**, *13*, 199-207.

74. Taylor, S. D.; Kotoris, C. C.; Dinaut, A. N.; Chen, M.-J. *Tetrahedron* **1998**, *54*, 1691-1714.

75. Wang, T. S. T.; Mojdehi, G. E.; Fawwaz, R. A.; Johnson, P. M. *J. Nucl. Med.* **1979**, *20*, 1066-1070.

76. Seyferth, D.; Marmor, R. S. *J. Organomet. Chem.* **1973**, *59*, 237-245.

77. Teulade, M. P.; Savignac, P.; Aboujaoude, E. E.; Lietge, S.; Collignon, N. *J. Organomet. Chem.* **1986**, *304*, 283-300.

78. Yuan, C.; Ding, Y. *Huaxue Xuebao* **1987**, *45*, 1213-1216.

Chapter 3. Synthesis, characterization, and low-temperature protonation of an osmium methyl complex bearing a fluorinated diphosphine ligand

Introduction

As mentioned in chapter 1, protonation of transition metal hydride complexes has been used for decades as a strategy to synthesize metal dihydrogen complexes.[1-3] Dihydrogen complexes are the observed products of such reactions, however, only if certain kinetic and thermodynamic conditions are fulfilled. If the dihydrogen tautomer is more stable than the *cisoid*-dihydride form (an equilibrium that can be affected through choice of the ancillary ligands), then the observed product of protonation will be a dihydrogen complex if (a) the *transoid*-dihydride structure is higher in energy and either protonation occurs *cisoid* or it occurs *transoid* and the *cisoid*/*transoid* isomerization rate is fast, or (b) the *transoid*-dihydride is lower in energy but protonation occurs *cisoid* and the *cisoid*/*transoid* isomerization rate is slow.

The same considerations hold for the formation of coordinated alkane complexes by protonation of the corresponding transition metal alkyl complexes. In studies of electron-rich piano stool complexes $Cp'M(PR_3)_2H$ and $Cp'M(PR_3)_2Me$, in which Cp′ = various cyclopentadienyl derivatives and $(PR_3)_2$ = bis(monophosphines) or diphosphines with backbones longer than one carbon, protonation generally occurs with *cis* regiochemistry, but the resulting *cis* products rapidly rearrange to the more stable *trans*-dihydride or *trans*-hydrido(methyl) species.[4-7] Formation of the dihydrogen and alkane products (or their *cis*-dihydride and *cis*-hydrido(methyl) tautomers, respectively) is thus favored by using methylene diphosphines, $R_2PCH_2PR_2$, as the phosphine ligands. Such phosphines have two main effects: electronically, they destabilize the *trans* form because the diphosphine bite angle is less than optimal for such species, and sterically, they favor *cis* protonation by occluding the *trans* protonation pathway.

In 1998, we reported that the low-temperature protonation of the Os^{II} methyl complex $(C_5Me_5)Os(dmpm)(CH_3)$, where dmpm is the methylene diphosphine $Me_2PCH_2PMe_2$, affords the *cis*-methyl/hydride complex $[(C_5Me_5)Os(dmpm)(CH_3)H]^+$.[8] This compound was the first example of an alkyl/hydride complex that is in dynamic equilibrium with its alkane tautomer on the NMR time scale: the interconversion with $[(C_5Me_5)Os(dmpm)CH_4]^+$ occurs at a rate of 160 sec^{-1} at –100 °C. The methane complex, however, was not directly observed, and instead its presence was deduced from spin saturation transfer and line broadening studies of the exchange process.[8] Density functional theory (DFT) calculations suggested that the methane tautomer lies only about 5 kcal mol^{-1} higher in energy than the methyl/hydride complex.[9]

The small energy difference between the methyl/hydride complex and its methane tautomer prompted us to investigate whether the relative energies of these two forms could be reversed (so that the methane form was the more stable) by suitable modification of the ancillary ligands. In particular, decreasing the electron richness of the osmium center should achieve this result by disfavoring oxidative addition of the C–H bond (or, equivalently, favoring reductive coupling, which is the reverse of oxidative addition). Attempts to reduce the electron richness of the Os center by changing the cyclopentadienyl ligand from C_5Me_5 to C_5Me_4H, C_5H_4Me, and C_5H_5 failed to accomplish the expected stabilization of a methane complex, as did changing the phosphine from dmpm to its phenyl analog bis(diphenylphosphino)methane (dppm).[10,11] At this point, in order to guide future experimental work, we carried out a series of benchmarked[12] DFT calculations to evaluate the relative energies of various $[(C_5R_5)Os(diphosphine)(CH_3)H]^+$ and $[(C_5R_5)Os(diphosphine)CH_4]^+$ complexes bearing differently substituted cyclopentadienyl and diphosphine ligands.[13]

Our DFT analyses confirmed the experimental result that varying the number of methyl groups attached to the cyclopentadienyl ligand has only very small effects on the relative energies of the methyl hydride and methane tautomers. On the other hand, varying the substituents on the diphosphine ligands has a significant impact on the relative energies of these two tautomers (Figure 3.1). Thus, replacing dmpm with its fluorinated analogs $(CF_3)_2PCH_2P(CF_3)_2$ (dfmpm) or $(CF_3)_2PCF_2P(CF_3)_2$ (dfmpfm) should achieve the desired result: in both cases, the methane complex should be more stable than its methyl/hydride tautomer by approximately 2 kcal mol^{-1}, and there should be a barrier of over 14 kcal mol^{-1} for methane dissociation.[13] The perfluorophosphine dfmpfm presented a greater synthetic challenge than dfmpm, so we chose to employ the latter, whose synthesis is described in chapter 2.

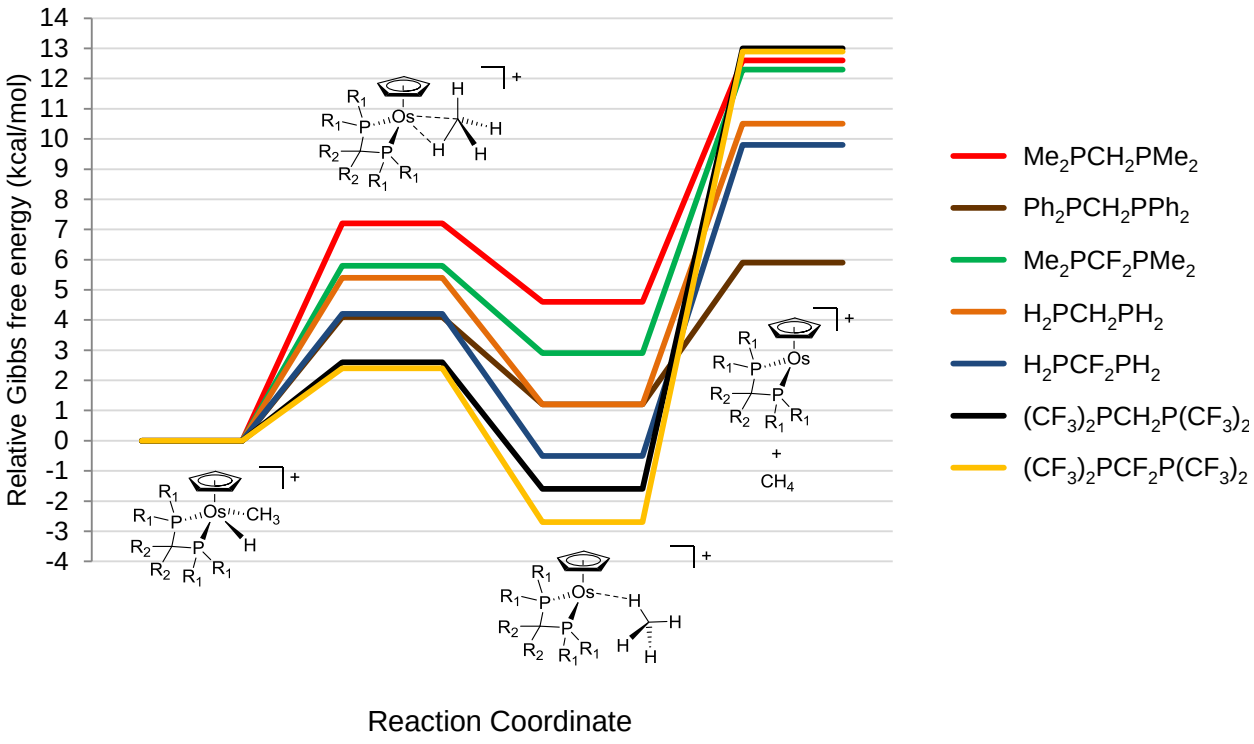

Figure 3.1. Relative energies of four tautomers along the reaction coordinate from osmium methyl/hydride to free methane for seven $[(C_5H_5)Os(diphosphine)CH_4]^+$ complexes at –100 °C. The energies were normalized by setting the methyl/hydride tautomers to 0 kcal mol^{-1}.

Results and Discussion

Synthesis of $(C_5Me_5)Os(dfmpm)Me$. Our group has previously described the preparation of the Os^{III} compound $(C_5Me_5)_2Os_2Br_4$ as a useful entry into mono(cyclopentadienyl)osmium complexes.[14,15] To date, our standard route to $(C_5Me_5)Os(diphosphine)(alkyl)$ compounds has involved reductive cleavage of the $(C_5Me_5)_2Os_2Br_4$ dimer with 1,5-cyclooctadiene (cod) in refluxing ethanol to form the Os^{II} product $(C_5Me_5)Os(cod)Br$.[15] Treatment of the latter with a diphosphine effects exchange and affords $(C_5Me_5)Os(diphosphine)Br$,[16] which can be alkylated by a three-step procedure to furnish the desired osmium alkyl complex.[4,17]

In part to simplify the synthetic procedure, however, we investigated the direct reaction between $(C_5Me_5)_2Os_2Br_4$ and dfmpm, which, if successful, would decrease the number of reaction steps by one. Treatment of $(C_5Me_5)_2Os_2Br_4$ with excess dfmpm in refluxing ethanol does give some $(C_5Me_5)Os(dfmpm)Br$, but the isolated yield is very poor (<1%), which is consistent with our previous experience with unfluorinated phosphines.[16] We hypothesized that the phosphine and the ethanol solvent were not effective in reducing Os^{III} to Os^{II}, so that stronger reductants would be needed to form the desired Os^{II} product. Indeed, repeating the reaction in the presence of zinc dust significantly improved the yield of $(C_5Me_5)Os(dfmpm)Br$. If one equiv. of Zn is added, the yield is modest (~20%), but if four equiv. of Zn are added, the yield increases to ~60% on scales up to several hundred milligrams. Although efforts to carry out this reaction on gram or multigram scales have thus far afforded much lower yields, the results suggest that the direct synthesis of bromoosmium(II) complexes from $(C_5Me_5)_2Os_2Br_4$ and zinc may be a general one that would work for non-fluorinated phosphines as well.

Conveniently, the bromoosmium(II) product $(C_5Me_5)Os(dfmpm)Br$ can be isolated as a pure, solvent-free solid by sublimation at 60-70 °C and 10^{-2} Torr. The orange product is air-stable for days in the solid state. The air stability is consistent with the electron withdrawing nature of the dfmpm ligand, which should make the Os^{II} product less electron rich than its dmpm analog, and therefore harder to oxidize.

The ^1H NMR spectrum of $(C_5Me_5)Os(dfmpm)Br$ is similar to that of the analogous dmpm complex $(C_5Me_5)Os(dmpm)Br$: the C_5Me_5 resonance is a triplet at δ 1.63 with J_{PH} = 2.1 Hz (vs. δ 1.93 with J_{PH} = 1.6 Hz for the dmpm compound), and the CH_2 protons appear as two doublets of triplets at δ 3.43 and 5.33 (vs. δ 3.28 and 4.45 for the dmpm compound).[16] The ^{31}P NMR coordination chemical shift (the chemical shift of the diphosphine complex minus the chemical shift of the free diphosphine) for the dfmpm compound is δ –19.6, versus δ –13.8 for the dmpm analog.[16,18]

The $^{31}P\{^1H\}$ NMR line shape of $(C_5Me_5)Os(dfmpm)Br$ is a complex multiplet (although simpler than that seen for free dfmpm) due to coupling with the twelve fluorine atoms. The ^{19}F NMR spectrum features two resonances, one for the CF_3 groups that are proximal to the C_5Me_5 ring, and one for those that are distal. The $^{19}F\{^1H\}$ NMR line shapes are also much less complex than seen for free dfmpm (both resonances are doublets), and are indicative[19] of a smaller coupling constant between the two magnetically inequivalent phosphorus nuclei (see chapter 2 for a discussion of the second-order effects in the spectra of free dfmpm). Simulations of the ^{19}F and ^{31}P NMR spectra are harder to match with experimental spectra than was the case for free dfmpm, probably owing to the reduced symmetry of the coordinated dfmpm ligand compared to free dfmpm; the best matches are obtained when $^3J_{PP'}$ is roughly 20 Hz and $^2J_{PF}$ is about 65 Hz.

Single crystals of $(C_5Me_5)Os(dfmpm)Br$ were obtained as orange prisms by cooling a saturated pentane solution to –20 °C overnight. The three-legged piano stool structure is apparent in the ORTEP plot (Figure 3.2): the diphosphine and the bromide group form the three legs and the C_5Me_5 ring forms the seat. The Os–Br bond length (2.55 Å) and diphosphine bite angle (70°) are consistent with the structures of other osmium diphosphine complexes with piano stool geometries.[4,10]

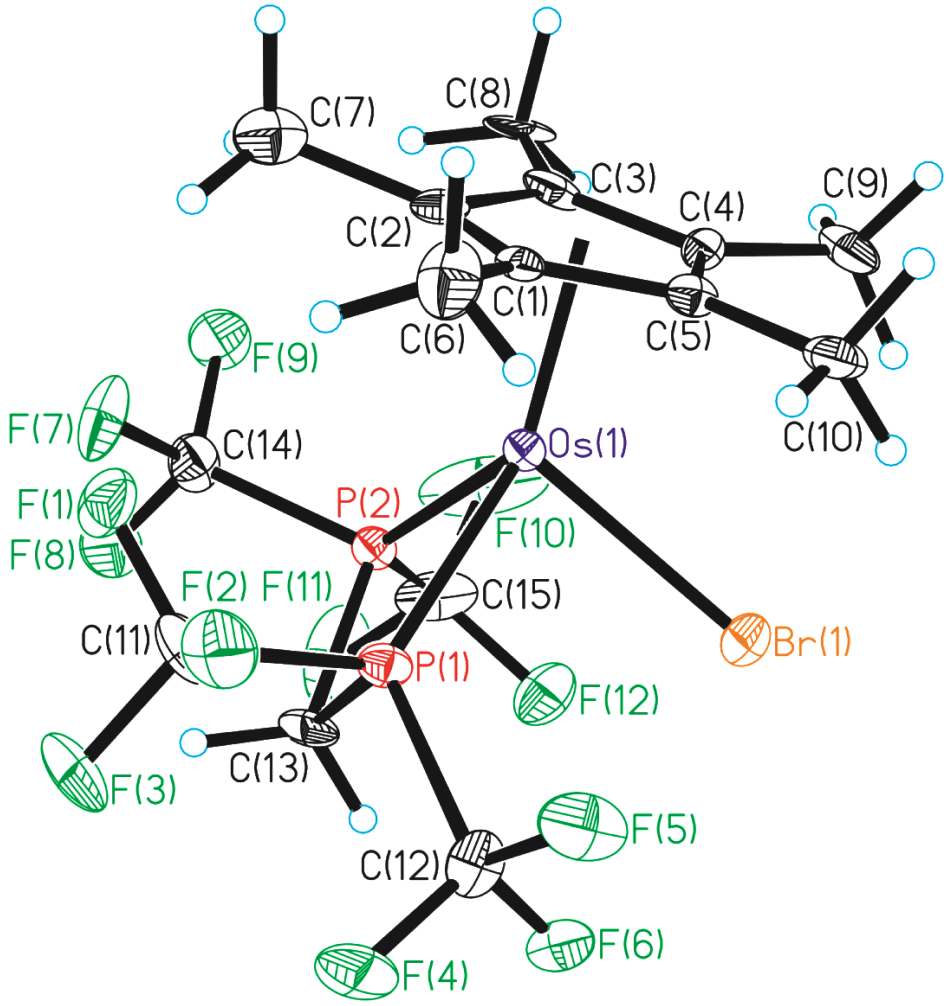

Figure 3.2. An ORTEP view of the X-ray crystal structure of $(C_5Me_5)Os(dfmpm)Br$. All non-hydrogen atoms are shown as 30% probability ellipsoids, and all hydrogen atoms are placed in idealized positions and depicted as arbitrarily-sized spheres.

In the conversion of $(C_5R_5)Os(PR_3)_2Br$ complexes to the corresponding $(C_5R_5)Os(PR_3)_2Me$ methyl compounds, we have typically used dimethylmagnesium because it reacts more cleanly than methyllithium or methyl Grignard reagents. When the phosphines are unidentate, the alkylations are typically complete after a few hours at room temperature. In contrast, when the phosphines are bidentate the alkylations are remarkably sluggish: even with a large excess of dimethylmagnesium, conversion of the dmpm compound $(C_5Me_5)Os(dmpm)Br$ to the corresponding methyl complex required 17 days in tetrahydrofuran (THF) at room temperature.[4] This sluggishness arises because dissociation of the bromide group or a diphosphine arm is extremely slow for these kinetically inert d^6 Os^{II} complexes,[4] and the latter process is further disfavored by the chelate effect.

We find that $(C_5Me_5)Os(dfmpm)Br$ is even more inert: it failed to react with dimethylmagnesium in THF at all, even after the mixture had been heated to reflux for one week. Indeed, we expect the substitution kinetics of this election-poor osmium complex to be even slower than for the analogous dmpm compound owing to (i) the strong metal-to-ligand backbonding to dfmpm, which should increase metal-diphosphine bond strengths, and (ii) the electron-poorer nature of the Os center, which should bind more strongly to the bromide as well.

In an effort to overcome these kinetic barriers, we made two adjustments to the alkylation conditions. First, we increased the reaction temperature by changing the reaction solvent from refluxing THF (b.p. 66 °C) to refluxing toluene (b.p. 111 °C). Second, we employed Lewis acidic alkylating agents such as dimethylzinc and trimethylaluminum, which have the added attraction that they are more soluble than methyllithium and methylmagnesium reagents in hydrocarbon solvents (the bromoosmium complex with dfmpm is itself very soluble in hydrocarbons). Our hypothesis was that these Lewis acidic reagents would assist in the

dissociation of the bromide (or phosphine) ligand, and thereby would promote the alkylation reaction. In addition, these alkylating agents are poorer bases than organolithium and organomagnesium species, and thus are not likely to deprotonate the acidic CH_2 protons of the diphosphine ligand.

We first tested trimethylaluminum as the methylating agent. Treatment of (C_5Me_5)Os(dfmpm)Br with an excess of trimethylaluminum in toluene at room temperature failed to produce any methylosmium product. After the toluene solution had been heated to reflux overnight, significant amounts of unreacted starting material remained, along with new species whose ^{19}F and ^{31}P NMR spectra strongly suggested that C–F activation had occurred. This outcome is not particularly surprising owing to the large thermochemical strength of Al–F bonds.

This result prompted us to try dimethylzinc, which is a milder alkylating agent that is commercially available in hydrocarbon solutions. Treatment of (C_5Me_5)Os(dfmpm)Br with excess dimethylzinc in toluene at room temperature gave no reaction, but heating the toluene solution to reflux overnight resulted in complete consumption of starting material and generation of new resonances in the ^{19}F and ^{31}P NMR spectra that were consistent with a clean methylation reaction. The completion of the alkylation reaction is signaled by a change in the solution color from bright orange to a cloudy pale yellow; typically, for addition of five equiv. of dimethylzinc, the reaction is complete after 2 h in refluxing toluene. The methyl complex can be isolated solvent-free and in high yield by removing the solvent and carrying out sublimation at 40-50 °C and 10^{-2} Torr. The product is an air-stable yellow solid. Scheme 3.1 shows the synthetic route to (C_5Me_5)Os(dfmpm)Me, which is achieved in 33% overall yield from osmium tetroxide.

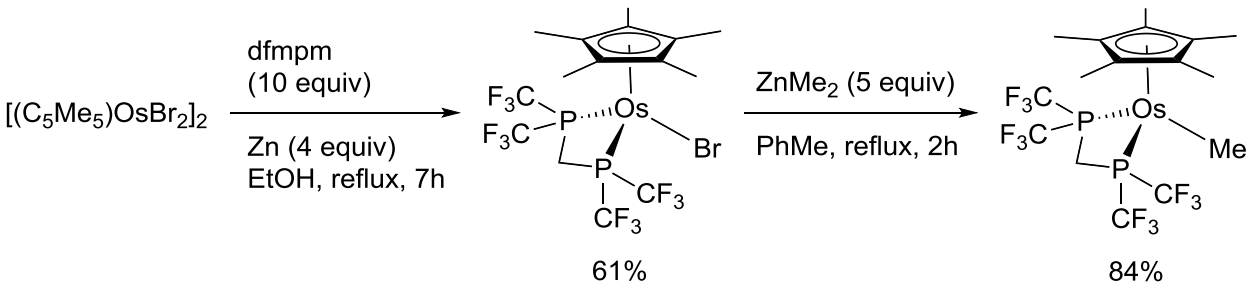

Scheme 3.1. Synthetic route to $(C_5Me_5)Os(dfmpm)Me$, starting from known $(C_5Me_5)_2Os_2Br_4$.

The ^{1}H, ^{13}C, ^{19}F, and ^{31}P NMR spectra of $(C_5Me_5)Os(dfmpm)Me$ (see Figure 3.3) are very similar to those of $(C_5Me_5)Os(dfmpm)Br$, except for additional resonances for the Os–Me group. The ^{1}H NMR line shape of this additional Os–Me resonance is quite remarkable, however: it exhibits resolvable coupling not only to the two phosphorus nuclei, but also to six of the twelve fluorine nuclei, and thus is a triplet of septets. In the $^{13}C\{^{1}H\}$ spectrum, the Os–Me group gives a resonance at δ –43.2, which is somewhat shielded relative to the δ –34.8 chemical shift for the analogous dmpm complex.[4]

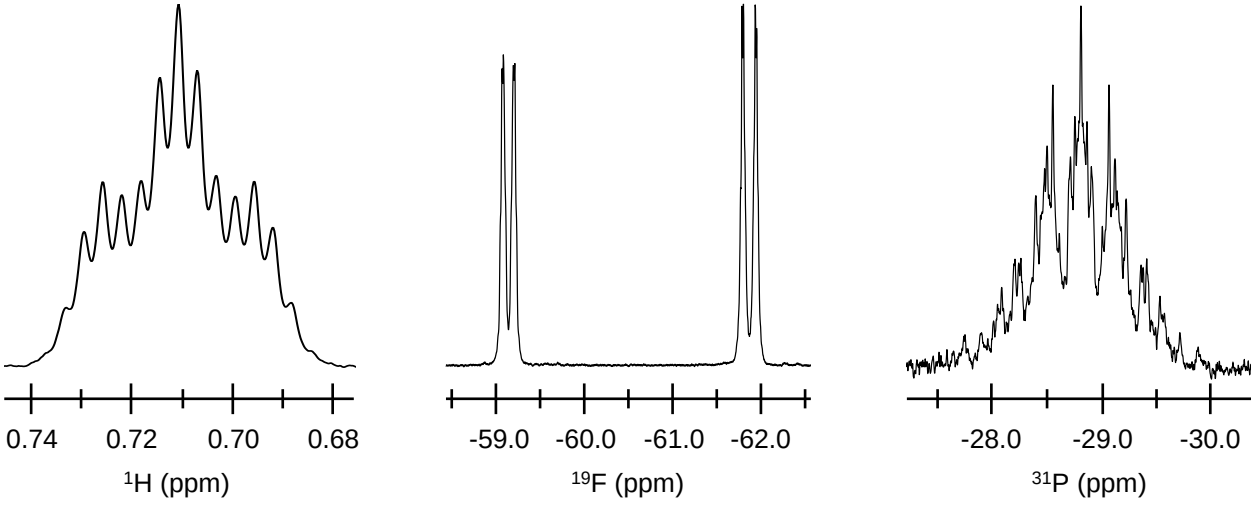

Figure 3.3. Selected regions of the ^{1}H, ^{19}F, and ^{31}P NMR spectra of $(C_5Me_5)Os(dfmpm)Me$ in C_6D_6. In the ^{1}H spectrum, only the osmium-bound methyl resonance is shown.

Single crystals of $(C_5Me_5)Os(dfmpm)Me$ were obtained as yellow prisms by cooling a saturated pentane solution to –20 °C overnight. The three-legged piano stool structure is apparent in the ORTEP plot (Figure 3.4): the diphosphine and the methyl group form the three legs and the C_5Me_5 ring forms the seat. The Os–CH_3 bond length (2.18 Å) and diphosphine bite angle (70°) are consistent with the structures of other osmium diphosphine complexes with piano stool geometries.[4,10]

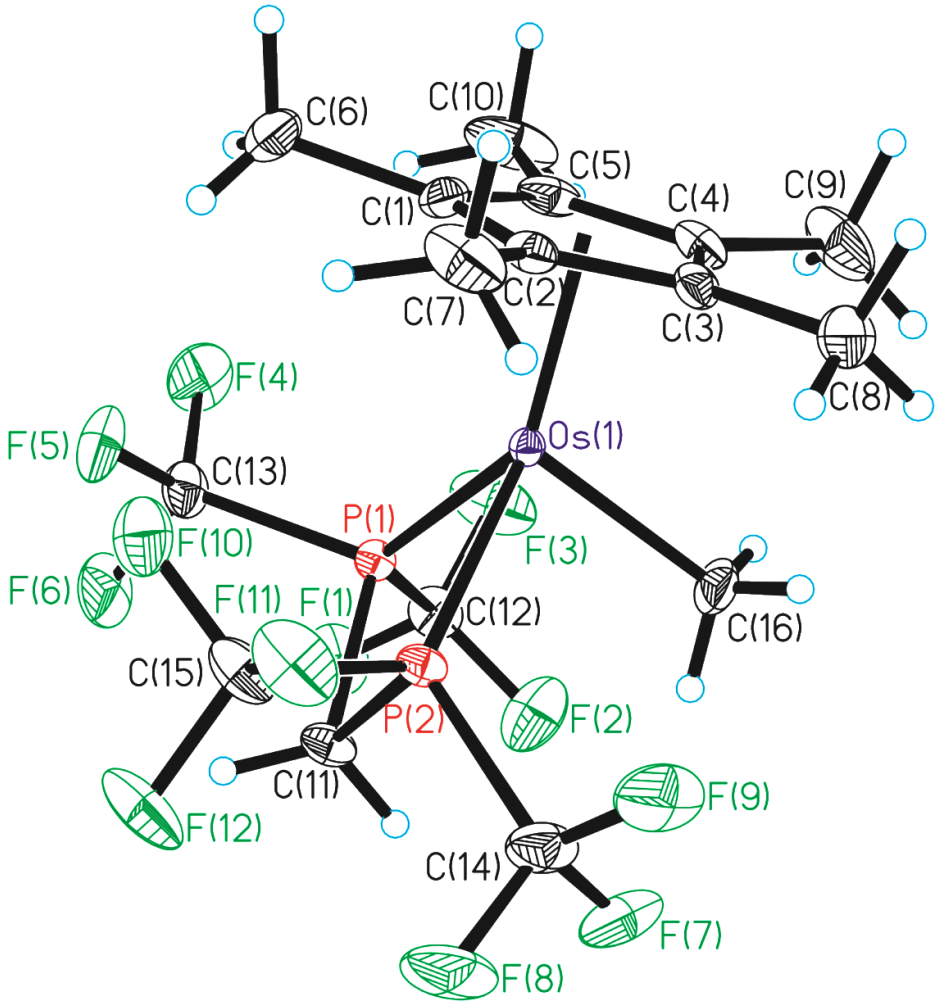

Figure 3.4. An ORTEP view of the X-ray crystal structure of $(C_5Me_5)Os(dfmpm)Me$. All non-hydrogen atoms are shown as 30% probability ellipsoids, and all hydrogen atoms except those of the Os–CH_3 group are placed in idealized positions and depicted as arbitrarily-sized spheres. The Os–CH_3 hydrogen atoms were located in the difference map and refined isotropically.

Low-temperature protonation of $(C_5Me_5)Os(dfmpm)Me$. In our previous studies of the protonation of osmium methyl complexes, we employed the carbon-based acid bis(trifluoromethanesulfonyl)methane, $(CF_3SO_2)_2CH_2$, as the protonating agent. This acid has the advantage that it and its conjugate base give separate resonances in the ^1H NMR spectrum, so that integration of these peaks gives a good estimate of the number of equiv. of protons that have been delivered to the osmium complex.[4,10,11] In addition, the acid is a solid (and therefore it is easy to weigh out precise amounts for protonation reactions), and not particularly hygroscopic.

Treatment of $(C_5Me_5)Os(dfmpm)Me$ with $(CF_3SO_2)_2CH_2$ in $CDCl_2F$ at –130 °C failed to protonate the osmium methyl complex. Even after the reaction mixture had been kept at room temperature for a week, only a small resonance for free methane was observed; most of the osmium methyl complex was still intact. The lack of reaction is a direct consequence of the significant electron-withdrawing effect of the dfmpm ligand, which makes the osmium center too poor a base to be protonated by $(CF_3SO_2)_2CH_2$.

In their work, Brookhart and coworkers used the acid $HBAr^F_4{\cdot}(Et_2O)_2$, (Ar^F = 3,5-bis(trifluoromethyl)phenyl) as their proton source.[20] This acid is stronger than $(CF_3SO_2)_2CH_2$ (see below), and therefore we investigated the low-temperature protonation of $(C_5Me_5)Os(dfmpm)Me$ with $HBAr^F_4{\cdot}(Et_2O)_2$. After adding this acid to a sample kept at –120 °C, a small singlet at δ –1.98 appeared in the ^1H NMR spectrum whose chemical shift was consistent with our expectations for a methane coordination complex. However, at this temperature the extent of protonation is too small for additional studies: typically, only a few percent of the osmium methyl complex is converted to this new species. We believe that this new species is mostly generated during sample preparation, when transient warming is unavoidable: considerable amounts of starting material remained intact and the intensity of the resonance at δ

–1.98 did not increase even after the sample was kept for many hours in the NMR probe at –120 °C. Subsequent studies showed that protonation of (C_5Me_5)Os(dfmpm)Me with $HBAr^F_4\cdot(Et_2O)_2$ becomes kinetically competent only above –70 °C, a temperature at which the species responsible for the resonance at δ –1.98 decomposes very rapidly.

Thus, we sought a more effective acid. Although $(CF_3SO_2)_2CH_2$ was not sufficiently acidic for our needs, it had other attractive features, and for this reason we turned to its nitrogen analog, bis(trifluoromethanesulfonyl)imide, $(CF_3SO_2)_2NH$. In dimethylsulfoxide (DMSO) the pKa's of $(CF_3SO_2)_2CH_2$[21] and $(CF_3SO_2)_2NH$[22] are both 2.1, but in the gas phase the imide is clearly the stronger acid: the Gibbs free energy for ionization, ΔG_{acid}, is 300.6 kcal mol^{-1} for $(CF_3SO_2)_2CH_2$ but 286.5 kcal mol^{-1} for $(CF_3SO_2)_2NH$.[23,24] The gas phase data should be more relevant[25] to acidities in poorly hydrogen-bonding solvents such as $CDCl_2F$. Indeed, our results follow the gas phase acidities: $(CF_3SO_2)_2NH$ is able to protonate (C_5Me_5)Os(dfmpm)Me in $CDCl_2F$ (see below), whereas $(CF_3SO_2)_2CH_2$ is not.

To our knowledge, the pKa of $HBAr^F_4\cdot(Et_2O)_2$ has not been reported,[26] but it is probably a stronger acid than either $(CF_3SO_2)_2CH_2$ or $(CF_3SO_2)_2NH$: for the diethyloxonium cation, ΔG_{acid} = 200.2[27] kcal mol^{-1} and its reported pKa is –3.5.[28] Our results, however, suggest that protonation of (C_5Me_5)Os(dfmpm)Me with $HBAr^F_4\cdot(Et_2O)_2$ is kinetically slow in $CDCl_2F$, despite its higher thermodynamic acidity. In order to further explore the issue of kinetics vs. thermodynamics in the protonation step, we also investigated triflic acid, CF_3SO_2OH, for which ΔG_{acid} is 299.5 kcal mol^{-1}.[23] Thus, the gas-phase acidity of CF_3SO_2OH is almost identical to that of $(CF_3SO_2)_2CH_2$. As we report below, triflic acid is very effective in protonating (C_5Me_5)Os(dfmpm)Me, whereas $(CF_3SO_2)_2CH_2$ is not. We propose that the difference relates to the steric size of these protonating

agents: for $(CF_3SO_2)_2CH_2$ the thermodynamic driving force is favorable but not large in magnitude, and protonation is slow owing to its much larger steric bulk vs. CF_3SO_2OH.

Treatment of (C_5Me_5)Os(dfmpm)Me with $(CF_3SO_2)_2NH$ in $CDCl_2F$ at –130 °C, followed by warming to –110 °C, gives a resonance at δ –1.94 that is similar to the one seen at δ –1.98 in the $HBAr^F_4\cdot(Et_2O)_2$ experiment,[29] but with significantly greater intensity. The same result is also achieved by treatment with CF_3SO_2OH (Figure 3.5 left). With $(CF_3SO_2)_2NH$, after the sample is kept at –110 °C for 10 min, about 35% of the methyl complex is converted to this new species; at longer times (ca. 1 h), the methyl complex disappears completely and is converted to the product that is responsible for this new signal, along with some free methane. With CF_3SO_2OH, conversion appears to be complete by the time the sample is inserted into the spectrometer.

In order to confirm that the new resonance at δ –1.94 is the result of protonation of the methyl group, we protonated the analogous ^{13}C-labeled complex (C_5Me_5)Os(dfmpm)$^{13}CH_3$ with $(CF_3SO_2)_2NH$. In the resulting ^{1}H NMR spectrum, the resonance at δ –1.94 is split into a doublet with J_{CH} = 127 Hz (Figure 3.5 middle). For comparison, J_{CH} is 125 Hz for free methane and 131 Hz for the parent osmium methyl complex. The ^{13}C NMR spectrum of the product of low-temperature protonation shows a binomial quintet at δ –45.1 (Figure 3.5 right) with the same J_{CH} coupling constant of 127 Hz seen in the ^{1}H NMR spectrum. This ^{13}C NMR resonance is significantly shielded relative to the chemical shift of δ –3.65 seen for free methane; the shift is similar but not identical to that of δ –45.0 seen at –110 °C for (C_5Me_5)Os(dfmpm)Me (the Os–Me resonance moves slightly to more negative chemical shifts as the temperature is decreased). We have observed ^{13}C NMR spectra in which both this new protonation product and (C_5Me_5)Os(dfmpm)Me are present simultaneously; the latter, of course, gives a resonance that is a binomial quartet instead of a quintet.

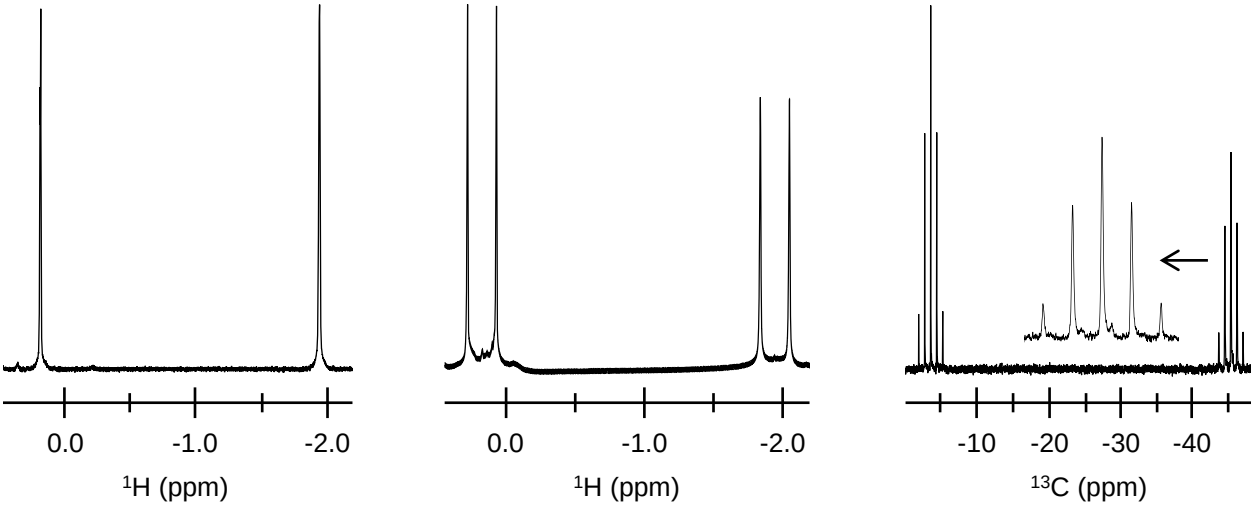

Figure 3.5. Selected regions of the ^{1}H NMR spectrum of [(C_5Me_5)Os(dfmpm)CH_4][OTf] (left) in $CDCl_2F$ at –105 °C, the ^{1}H NMR spectrum of [(C_5Me_5)Os(dfmpm)$^{13}CH_4$][$N(Tf)_2$] (middle) and the ^{1}H-coupled ^{13}C NMR spectrum of [(C_5Me_5)Os(dfmpm)$^{13}CH_4$] [$N(Tf)_2$] (right) in $CDCl_2F$ at –110 °C. The expansion in the ^{13}C NMR spectrum shows the detail of the Os–$^{13}CH_4$ resonance. The resonances at δ 0.18 in the ^{1}H NMR spectra and at δ –3.65 in the ^{13}C NMR spectrum are due to free methane.

We have previously shown that low-temperature protonation of (C_5R_5)Os(dmpm)Me complexes (containing the unfluorinated diphosphine dmpm) generates classical methyl/hydride complexes that give separate methyl and hydride resonances in the ^{1}H NMR spectra at –120 °C. These resonances broaden at higher temperatures owing to a chemical exchange process involving interconversion with a transient methane coordination complex that cannot be directly observed.[4,10,11] The quintet seen in the ^{13}C NMR spectrum upon protonation of the dfmpm complex (C_5Me_5)Os(dfmpm)Me is consistent with only two scenarios: a classical methyl/hydride complex whose methyl and hydride hydrogen atoms are exchanging so rapidly that only one average resonance is observed, or a methane coordination complex undergoing rapid exchange between the bridging and terminal hydrogen sites. We can rule out the former possibility as follows.

If protonation affords a classical methyl/hydride complex, the $^{1}J_{CH}$ coupling constant within the methyl group should be essentially unchanged from the 131 Hz value seen for the methyl complex $(C_5Me_5)Os(dfmpm)^{13}CH_3$. The two-bond H–Os–C coupling constant between the hydride and the methyl carbon in the methyl/hydride complex should be very small, probably less than 10 Hz.[30-32] If the methyl/hydride complex is in the fast exchange limit, then the exchange-averaged coupling constant should be about ¾(131 Hz) + ¼(10 Hz) ≈ 100 Hz. This value is clearly inconsistent with the coupling constant seen for the quintet generated upon low-temperature protonation of $(C_5Me_5)Os(dfmpm)^{13}CH_3$. The observed value of the $^{1}J_{CH}$ coupling constant of 127 Hz, which is very similar to that seen for free methane (125 Hz), strongly supports the conclusion that the protonation product is a coordinated methane complex, $[(C_5Me_5)Os(dfmpm)CH_4]^+$.

The $^{31}P\{^{1}H\}$ NMR spectrum of $[(C_5Me_5)Os(dfmpm)CH_4]^+$ exhibits a resonance at δ –20.3 that is an apparent septet due to resolvable coupling to six of the twelve fluorine atoms, with J_{PF} = 78.8 Hz. This chemical shift is deshielded by about 11 ppm relative to that of the parent methyl compound (δ –31.6 at –110 °C).

Isotopic perturbation of resonance studies for $[(C_5Me_5)Os(dfmpm)^{13}CH_4]^+$. The NMR spectra show that all four hydrogen atoms of the coordinated methane ligand are chemically equivalent, which must mean that the terminal (not coordinated to osmium) and bridging (coordinated to osmium) C–H groups of the methane ligand are undergoing fast chemical exchange on the NMR time scale. Therefore, the observed ^{1}H NMR chemical shift of δ –1.94 for the coordinated methane ligand is a weighted average of terminal and bridging C–H groups in the "frozen" structure. The mathematical formulas that describe the averaging depend on the coordination mode as follows, where δ is the observed (exchange-averaged) chemical

shift, δ_T is the chemical shift for a hydrogen atom in a terminal site, and δ_B is the chemical shift for a hydrogen atom in a bridging site (see chapter 1 for a description of possible coordination modes for metal-bound methane).

$\boldsymbol{\kappa^1/\eta^2}$**:** $$\boldsymbol{\delta = \frac{3}{4}\delta_T + \frac{1}{4}\delta_B} \quad \textbf{(3.1)}$$

$\boldsymbol{\kappa^2}$**:** $$\boldsymbol{\delta = \frac{1}{2}\delta_T + \frac{1}{2}\delta_B} \quad \textbf{(3.2)}$$

$\boldsymbol{\kappa^3}$**:** $$\boldsymbol{\delta = \frac{1}{4}\delta_T + \frac{3}{4}\delta_B} \quad \textbf{(3.3)}$$

In chapter 1, we noted that isotopic perturbation of resonance (IPR) has been used to determine the coordination mode of metal-bound alkane ligands by studying how the average NMR chemical shift depends on the extent of deuteration. In the present case, the four coordinated methane isotopologs capable of producing a ^{1}H NMR signal are CH_4, CH_3D, CH_2D_2, and CHD_3.

The fundamental reason that the chemical shift changes as a function of deuterium content is that C–D bonds have a greater reduced mass μ than C–H bonds. A well-known result from quantum mechanics is that zero point energies for chemical bonds are given by $\frac{1}{2}h\sqrt{k/\mu}$, where *h* is Planck's constant and *k* is the bond force constant; for a given value of *k*, the zero point energy will be smaller for deuterium than for hydrogen. Consequently, if there is an equilibrium between two sites with different force constants, the zero point energy of a mixed H/D system will be lower if deuterium atoms occupy the sites with the larger force constant and hydrogen atoms occupy the sites with the smaller force constant. What this means for a coordinated methane complex is that the deuterium atoms preferentially occupy terminal sites and the hydrogen atoms preferentially occupy bridging sites, because the latter should have the lower C–H force constant.

The above analysis can be described quantitatively by introducing a Boltzmann factor into equations 3.1-3.3 that accounts for the energy increase that accompanies swapping a hydrogen atom in a bridging site with a deuterium atom in a terminal site. The exchange-averaged chemical shifts of the different methane isotopologs are described by equations 3.4-3.15 below, where $\delta_{Os–CH_4}$, $\delta_{Os–CH_3D}$, $\delta_{Os–CH_2D_2}$, and $\delta_{Os–CHD_3}$ are the exchange-averaged chemical shifts of the CH_4, CH_3D, CH_2D_2, and CHD_3 complexes, respectively; ΔE_{BI} is the Boltzmann isotope energy difference due to the zero point energy effect; R is the gas constant; T is the temperature; and the other variables are defined as described for equations 3.1-3.3. In deriving these equations, we make the assumption that the chemical shifts of the hydrogen atoms are independent of the H/D composition in the other three sites. Indeed, the secondary isotope effect in free methane is quite small: the chemical shifts of the ^1H nuclei in CH_4 and CHD_3 differ by less than 0.05 ppm.[33] Nevertheless, for greater accuracy, we corrected for the secondary isotope effect before applying these equations, as described in the Experimental Section.

$\boldsymbol{\kappa^1/\eta^2}$:

$$\delta_{Os-CH_4} = \frac{3\delta_T+\delta_B}{4} \quad \textbf{(3.4)}$$

$$\delta_{Os-CH_3D} = \frac{\left(2+e^{-\frac{\Delta E_{BI}}{RT}}\right)\delta_T+\delta_B}{3+e^{-\frac{\Delta E_{BI}}{RT}}} \quad \textbf{(3.5)}$$

$$\delta_{Os-CH_2D_2} = \frac{\left(1+2e^{-\frac{\Delta E_{BI}}{RT}}\right)\delta_T+\delta_B}{2+2e^{-\frac{\Delta E_{BI}}{RT}}} \quad \textbf{(3.6)}$$

$$\delta_{Os-CHD_3} = \frac{\left(3e^{-\frac{\Delta E_{BI}}{RT}}\right)\delta_T+\delta_B}{1+3e^{-\frac{\Delta E_{BI}}{RT}}} \quad \textbf{(3.7)}$$

$\boldsymbol{\kappa^2}$:

$$\delta_{Os-CH_4} = \frac{\delta_T+\delta_B}{2} \quad \textbf{(3.8)}$$

$$\delta_{Os-CH_3D} = \frac{\left(1+2e^{-\frac{\Delta E_{BI}}{RT}}\right)\delta_T+\left(2+e^{-\frac{\Delta E_{BI}}{RT}}\right)\delta_B}{3+3e^{-\frac{\Delta E_{BI}}{RT}}} \quad \textbf{(3.9)}$$

$$\delta_{Os-CH_2D_2} = \frac{\left(2e^{-\frac{\Delta E_{BI}}{RT}} + e^{-\frac{2\Delta E_{BI}}{RT}}\right)\delta_T + \left(1 + 2e^{-\frac{\Delta E_{BI}}{RT}}\right)\delta_B}{1 + 4e^{-\frac{\Delta E_{BI}}{RT}} + e^{-\frac{2\Delta E_{BI}}{RT}}} \quad \textbf{(3.10)}$$

$$\delta_{Os-CHD_3} = \frac{\left(e^{-\frac{\Delta E_{BI}}{RT}}\right)\delta_T + \delta_B}{1 + e^{-\frac{\Delta E_{BI}}{RT}}} \quad \textbf{(3.11)}$$

κ^3:

$$\delta_{Os-CH_4} = \frac{\delta_T + 3\delta_B}{4} \quad \textbf{(3.12)}$$

$$\delta_{Os-CH_3D} = \frac{\left(e^{-\frac{\Delta E_{BI}}{RT}}\right)\delta_T + \left(1 + 2e^{-\frac{\Delta E_{BI}}{RT}}\right)\delta_B}{1 + 3e^{-\frac{\Delta E_{BI}}{RT}}} \quad \textbf{(3.13)}$$

$$\delta_{Os-CH_2D_2} = \frac{\left(e^{-\frac{\Delta E_{BI}}{RT}}\right)\delta_T + \left(2 + e^{-\frac{\Delta E_{BI}}{RT}}\right)\delta_B}{2 + 2e^{-\frac{\Delta E_{BI}}{RT}}} \quad \textbf{(3.14)}$$

$$\delta_{Os-CHD_3} = \frac{\left(e^{-\frac{\Delta E_{BI}}{RT}}\right)\delta_T + 3\delta_B}{3 + e^{-\frac{\Delta E_{BI}}{RT}}} \quad \textbf{(3.15)}$$

Equations 3.4-3.15 reveal that the exchange-averaged chemical shifts of the CH_4, CH_3D, CH_2D_2, and CHD_3 isotopologs depend on the coordination mode (i.e., the number of terminal sites and the number of bridging sites). Under the reasonable assumption that δ_B is shielded with respect to δ_T,[5,12,19] the exchange-averaged chemical shift for the methane complex moves to more negative chemical shifts with increasing deuterium incorporation. More interestingly, the four exchange-averaged chemical shifts form a pattern that is diagnostic of the coordination mode (Figure 3.6). Specifically, for the κ^1/η^2 coordination modes, each successive deuterium incorporation causes a *greater* change in chemical shift; for the κ^2 coordination mode, each successive deuterium incorporation causes approximately the *same* change in chemical shift; and for the κ^3 coordination mode, each successive deuterium incorporation causes a *smaller* change in chemical shift.

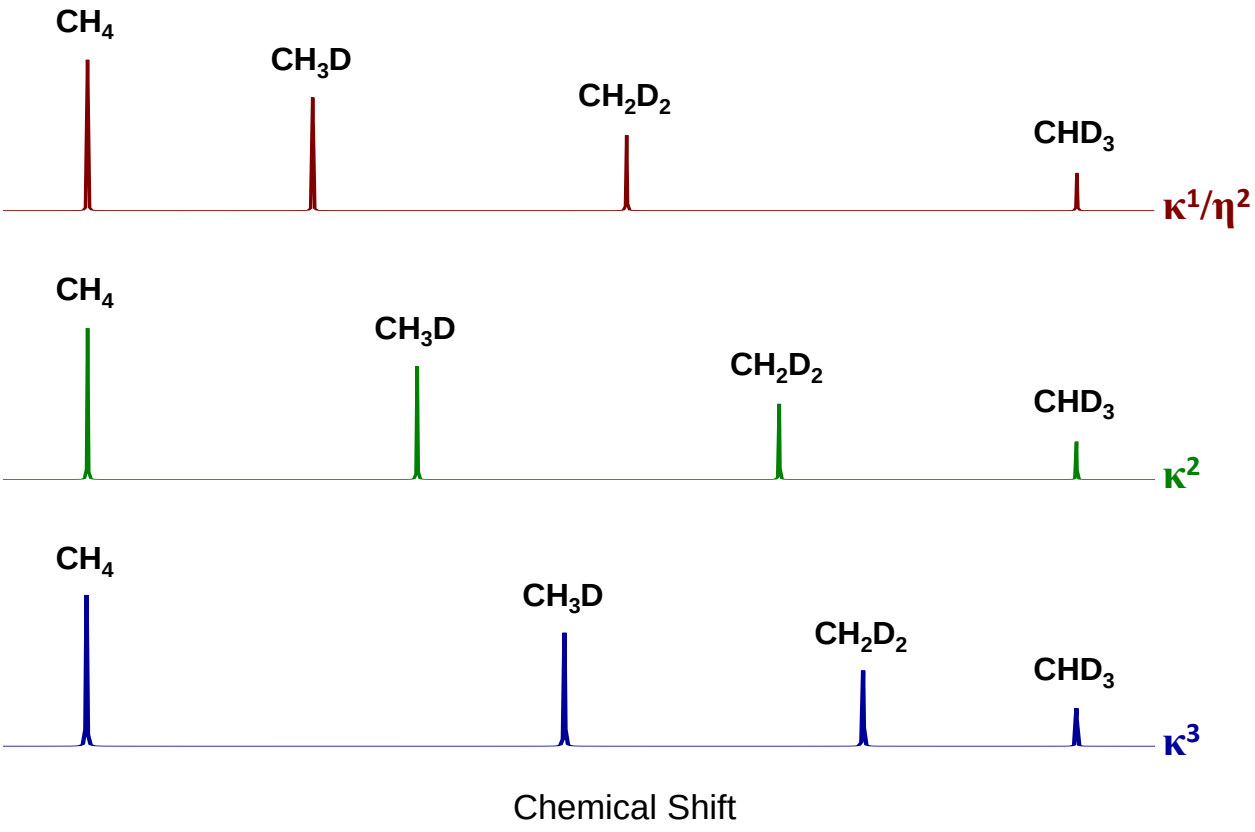

Figure 3.6. Calculated ^{1}H NMR patterns of the methane resonances of $[(C_5Me_5)Os(dfmpm)CH_nD_{4-n}]^+$, where *n* is 1-4, for the κ^1/η^2, κ^2, and κ^3 coordination modes.

Assignment of the methane coordination mode. To perform the IPR study, a 1:1 mixture of $(C_5Me_5)Os(dfmpm)^{13}CH_3$ and $(C_5Me_5)Os(dfmpm)^{13}CHD_2$ was treated with a 1:2 mixture of $(CF_3SO_2)_2NH$ and $(CF_3SO_2)_2ND$ in $CDCl_2F$ at –110 °C. In this way, all four isotopologs of the methane coordination complex – $[(C_5Me_5)Os(dfmpm)^{13}CH_4][N(SO_2CF_3)_2]$, $[(C_5Me_5)Os(dfmpm)^{13}CH_3D][N(SO_2CF_3)_2]$, $[(C_5Me_5)Os(dfmpm)^{13}CH_2D_2][N(SO_2CF_3)_2]$, and $[(C_5Me_5)Os(dfmpm)^{13}CHD_3][N(SO_2CF_3)_2]$ – should be generated in one NMR tube. In initial experiments, the resonances due to the CH_3D and CHD_3 isotopologs were almost absent, which suggested that little or no deuterium transfer from $(CF_3SO_2)_2ND$ was taking place. One possibility is that protonation occurs with a significant kinetic isotope effect (i.e., k_H/k_D is much

greater than one). Another possibility is that the acid mixture rapidly undergoes proton/deuterium exchange with adventitious proton sources (possibly silanol groups on the glass walls of the NMR tube). We found that significant amounts of the CH_3D and CHD_3 isotopologs of the coordinated methane complex could be generated provided that the NMR tube was pre-conditioned with a 3:1 mixture of DCl/HCl before it was dried and used. Even so, the CH_3D and CHD_3 isotopologs were formed in smaller amounts than the CH_4 and CH_2D_2 isotopologs.

The resulting ^{1}H NMR spectrum (Figure 3.7) contains four resonances (all doublets as a result of the 100% ^{13}C labeling) with separations that clearly match only one of the calculated patterns: that for the κ^1/η^2 coordination modes. *Methane is bound to osmium in our complex by means of only one bridging hydrogen atom*.

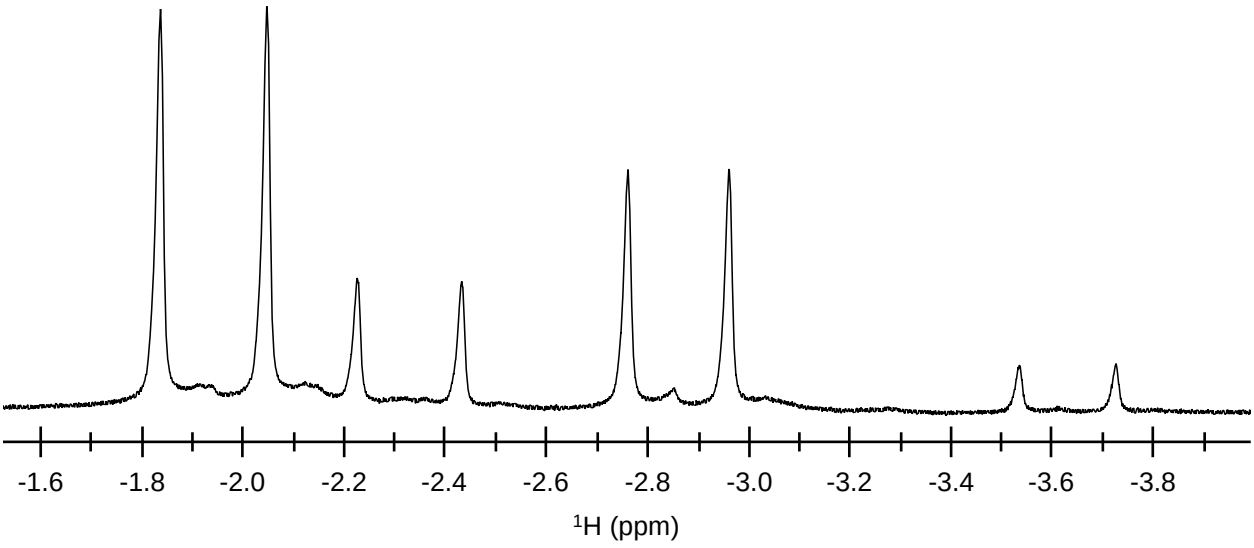

Figure 3.7. Selected region of the ^{1}H NMR spectrum of $[(C_5Me_5)Os(dfmpm)^{13}CH_nD_{4-n}]^+$, where *n* is 1-4, at –110 °C in $CDCl_2F$ showing the four coordinated methane isotopologs.

Quantification of chemical shifts, coupling constants, and the Boltzmann isotope energy difference in coordinated methane. Having determined that the coordination mode of the methane complex is either κ^1 or η^2, we can now solve equations 3.4-3.7 analytically to determine the values of the terminal hydrogen chemical shift δ_T, the bridging hydrogen chemical shift δ_B, and the Boltzmann isotope energy difference ΔE_{BI}. From the chemical shifts of δ –1.94, –2.33, –2.86, and –3.63 for the CH_4, CH_3D, CH_2D_2, and CHD_3 isotopologs, respectively, we determined that $\delta_T = 0.39 \pm 0.05$, $\delta_B = -8.92 \pm 0.17$, and $\Delta E_{BI} = 0.264 \pm 0.005$ kcal mol^{-1}. The chemical shift of the terminal hydrogen atoms is close to that seen for free alkanes, as might be expected. The chemical shift of the bridging hydrogen atom is similar to that seen for related Os^{II} hydrides.[16] The Boltzmann isotope energy difference is about twice the value of 0.13 ± 0.01 kcal mol^{-1} reported by Calvert and Shapley for their agostic osmium methyl complex[34] but is very similar to the value of 0.23 ± 0.03 kcal mol^{-1} reported by Ball and coworkers for $(C_5H_4Pr^i)Re(CO)_2$(pentane).[35]

The same analysis can be performed for the C–H coupling constants by replacing the chemical shifts (δ) in equations 3.4-3.7 with coupling constants (J) to give equations 3.16-3.19. As we did for the chemical shifts, we assumed that $^1J_{CH}$ is independent of the H/D composition in the other three sites for the derivation, and then corrected for the secondary isotope effect before applying the equations, as described in the Experimental Section; for free methane, $^1J_{CH}$ differs by only 1 Hz between CH_4 and CHD_3.[36]

$$J_{\mathbf{Os-CH_4}} = \frac{3J_T + J_B}{4} \qquad \textbf{(3.16)}$$

$$J_{\mathbf{Os-CH_3D}} = \frac{\left(2+e^{-\frac{\Delta E_{BI}}{RT}}\right)J_T + J_B}{3+e^{-\frac{\Delta E_{BI}}{RT}}} \qquad \textbf{(3.17)}$$

$$J_{\mathbf{Os-CH_2D_2}} = \frac{\left(\mathbf{1+2e^{-\frac{\Delta E_{BI}}{RT}}}\right)J_T + J_B}{\mathbf{2+2e^{-\frac{\Delta E_{BI}}{RT}}}} \quad \textbf{(3.18)}$$

$$J_{\mathbf{Os-CHD_3}} = \frac{\left(\mathbf{3e^{-\frac{\Delta E_{BI}}{RT}}}\right)J_T + J_B}{\mathbf{1+3e^{-\frac{\Delta E_{BI}}{RT}}}} \quad \textbf{(3.19)}$$

Though it may not be readily apparent from Figure 3.6, the coupling constants decrease upon successive deuterium incorporation: 126 Hz, 124 Hz, 120 Hz, and 115 Hz for the CH_4, CH_3D, CH_2D_2, and CHD_3 isotopologs, respectively. Solving equations 3.16-3.19 yields the following values: J_T = 141 ± 4 Hz, J_B = 83 ± 11 Hz, and ΔE_{BI} = 0.273 ± 0.063 kcal mol^{-1}. Note that the Boltzmann isotope energy difference determined from the chemical shift data and from the coupling constant data are identical within error, as they should be.

The 83 Hz coupling constant for the bridging hydrogen atom (as well as the large Boltzmann isotope energy difference) shows the significant extent to which the bridging C–H bond of methane is weakened by coordination to osmium. Interestingly, the terminal C–H coupling constant of 141 Hz is significantly larger than that of free methane, presumably because these C–H bonds strengthen (and/or increase their s-character[37,38]) to compensate for the weakened bridging C–H bond.

DFT calculations suggest the bridging C–H bond in the model complex $[(C_5H_5)Os(dfmpm)CH_4]^+$ is lengthened by ~0.07 Å.[13] For free methane, it has been calculated that stretching one C–H bond causes all four J_{CH} coupling constants to increase, provided that the amount of stretching is not too large.[39] For a lengthening of one bond by 0.07 Å, the coupling constants in free methane are calculated to increase (from the normal value of 124 Hz) to 125 Hz for the stretched bond and to 128 Hz for the other three bonds. The coupling constants we observe differ significantly from these values. We conclude that formation of the three-center

Os···H–C interaction not only stretches one bond, it also causes a significant change in the bonding within methane: the bridging C–H bond loses significant carbon s-character, whereas the other three C–H bonds gain s-character.

Is the carbon atom interacting with the Os center? The chemical shift pattern observed in the IPR study is consistent with both κ^1 and η^2 coordination modes, which differ in whether there is (η^2) or is not (κ^1) significant orbital overlap between the carbon atom and the osmium atom. Ball and coworkers[35] have suggested that strong shielding of the ^{13}C NMR resonances of coordinated alkanes indicates the presence of an η^2 interaction; if true, the strongly shielded chemical shift of the methane ligand in the ^{13}C NMR spectrum of $[(C_5Me_5)Os(dfmpm)^{13}CH_4]^+$ would indicate that this ligand adopts an η^2 coordination mode. However, our earlier DFT calculations clearly show that the Os–CH_4 linkage is κ^1 and that there is essentially no overlap between Os and C: the Os–C distance of 2.571 Å is far too long,[40] and the Os–H–C angle of 115° is far too obtuse.[13] These metrics are consistent with other theoretical studies of transition metal alkane complexes.[9,41,42]

We propose that the strong shielding seen in the ^{13}C NMR spectrum is *not* due to the presence of a direct Os–C bond, but conversely is a direct result of the *weakness* of the Os–CH_4 interaction. The weakness of this interaction causes this d^6 osmium center to have a ligand field that is effectively five-coordinate rather than six-coordinate, so that one of the empty d-orbitals of sigma antibonding character drops significantly in energy. The shielding reflects diamagnetic anisotropy associated with the presence of low-lying paramagnetic excited states that mix into the ground state.[43]

This same diamagnetic anisotropy effect is responsible for the strongly shielded hydride resonances of certain five-coordinate d^6 iridium hydrides,[44] and we believe it is also likely

responsible for the strongly shielded ^{129}Xe chemical shifts in $(C_5H_4Pr^i)Re(CO)(PF_3)Xe$ and related compounds.[45] We therefore conclude that the coordination mode of the methane ligand in $[(C_5Me_5)Os(dfmpm)CH_4]^+$ is κ^1. The η^2 coordination mode is, instead, an intermediate or transition state that is responsible for the interconversion of the methyl/hydride and coordinated methane tautomers.[13]

Kinetic analysis of methane loss from $[(C_5Me_5)Os(dfmpm)CH_4][OTf]$. When a sample of the methane complex $[(C_5Me_5)Os(dfmpm)CH_4][OTf]$ in $CDCl_2F$ is warmed from –110 °C to –105 °C, the ^{1}H NMR resonance due to the coordinated methane ligand decreases exponentially in intensity and a resonance due to free methane grows in. The decay follows first-order kinetics with half-lives of 153, 44, and 12 min at –105, –100, and –95 °C, respectively. An Eyring plot (Figure 3.8) for this decomposition reaction yields values for the enthalpy and entropy of activation for methane loss of $\Delta H^{\ddagger}$ = 14.9 ± 1.5 kcal mol^{-1} and $\Delta S^{\ddagger}$ = 12.3 ± 8.8 cal mol^{-1} K^{-1}, which correspond to a Gibbs free energy of activation for methane loss, $\Delta G^{\ddagger}$, of 12.8 ± 0.1 kcal mol^{-1} at –100 °C. This value is comparable to the 14.6 kcal mol^{-1} activation energy calculated for $[(C_5H_5)Os(dfmpm)CH_4]^+$ in our earlier DFT work.[13] It is also similar to the activation energy for methane dissociation of 13.5 kcal mol^{-1} seen for the unfluorinated $[(C_5Me_5)Os(dmpm)(CH_3)H]^+$ complex,[8] and to the value of 14.5 ± 0.4 kcal mol^{-1} observed for a rhodium methane complex.[20]

The dissociation barrier is a thermodynamic measure of the stabilization that arises from overlap between methane and the $[(C_5Me_5)Os(dfmpm)]^+$ fragment, minus the energetic cost of distorting the methane molecule (i.e., of weakening one C–H bond) and the osmium fragment to the geometries seen in the Os-methane complex (the latter distortion is small, and we will assume that this energy term is negligible). The bridging and terminal C–H coupling constants

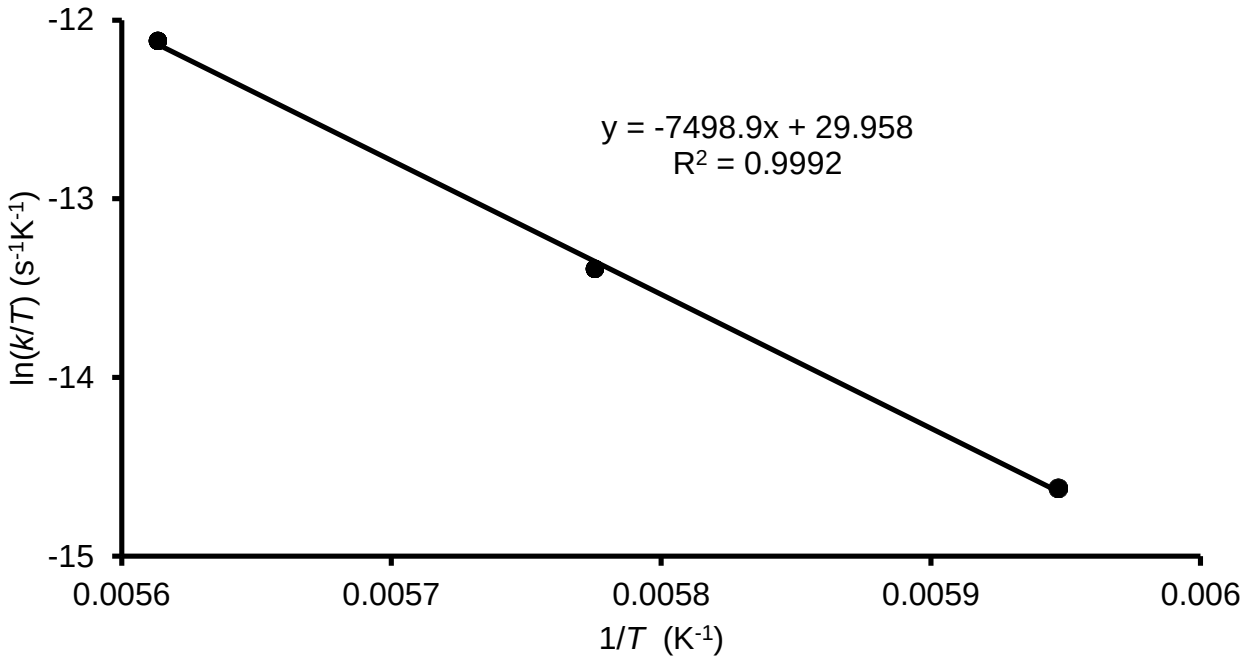

Figure 3.8. Eyring plot of the rate of methane loss from $[(C_5Me_5)Os(dfmpm)CH_4][OTf]$ as a function of temperature. The reaction rates were obtained at –105, –100, and –95 °C.

deduced from the IPR study suggest that the structure of methane is quite significantly perturbed. As mentioned above, DFT calculations suggest that the bridging C–H bond is lengthened by ~0.07 Å when methane coordinates to the Os center;[46] the energetic cost of this distortion is known to be ~1.5 kcal mol^{-1}.[47] This distortion energy is recovered when methane dissociates; thus we can estimate that the Os-methane overlap energy is about 1.5 kcal mol^{-1} larger than the observed dissociation energy, or ~14 kcal mol^{-1}.

Conclusions. The structural information about the coordinated methane complex described herein provides valuable new insights on the binding and activation of light alkanes by transition metal complexes. In particular, our combined NMR and DFT analysis indicates that (1) binding in our methane complex occurs by means of one bridging hydrogen atom, and (2) orbital overlap between the transition metal and a carbon atom of the alkane is *not* required for

substantial binding energy between the transition metal and the alkane. Importantly, we have shown that IPR studies can be used to determine the structures of transition metal alkane complexes prepared by low-temperature protonation of transition metal alkyl complexes (previous IPR studies have all been carried out with transition metal alkane complexes that had been prepared by photolysis of transition metal carbonyl complexes in isotopic mixtures of the liquid alkane[35]). This protonation methodology is particularly advantageous for full solution NMR characterization of cationic transition metal alkane complexes, because cationic species are generally not soluble in liquid alkanes.

Experimental

Unless stated otherwise, all manipulations were performed under argon or vacuum using standard Schlenk line or glove box techniques. Glassware was oven- or flame-dried and allowed to cool under vacuum or argon. Solvents were distilled under nitrogen from sodium/benzophenone (pentane, diethyl ether), magnesium (ethanol), or sodium (toluene), and sparged with argon for 30-60 seconds immediately before use.

Benzene-d_6 was purchased from Sigma-Aldrich or Cambridge Isotope Laboratories in 1-mL ampoules and used without purification. The following starting materials were obtained from commercial sources and used as received unless stated otherwise: dimethylzinc (Strem, 1.2 M solution in toluene), iodomethane-^{13}C (Sigma-Aldrich), iodomethane-$^{13}C,d_2$ (Sigma-Aldrich), lithium powder (Sigma-Aldrich), bis(trifluoromethane)sulfonimide (Matrix Scientific, dried over $MgSO_4$ and sublimed), lithium bis(trifluoromethane)sulfonimide (Oakwood), sulfuric acid-D_2 (Alfa Aesar). The compounds $(C_5Me_5)_2Os_2Br_4$[15] and $CDCl_2F$[48] were prepared according to published procedures, and the $CDCl_2F$ was doubly distilled and stored in a PTFE-sealed glass

vessel over Linde 3A or 4A molecular sieves. The carbon acid $(CF_3SO_2)_2CH_2$ was generously donated by Dr. Alan Siedle of the 3M Corporation and was purified by sublimation prior to use.

NMR spectra were acquired on Varian spectrometers (Unity 400, Unity 500, VXR 500, and Unity Inova 600) at room temperature, unless specified otherwise. Positive chemical shifts indicate shifts to higher frequency relative to the following chemical shift standards: $SiMe_4$ (^1H and ^{13}C, set by assigning appropriate shifts to residual solvent signals), external $CFCl_3$ in $CDCl_3$ (^{19}F), and external H_3PO_4 in D_2O (^{31}P). Default instrument parameters were used unless stated otherwise. NMR spectra were processed with the MestReNova NMR software package; manual phasing, peak picking, and integration methods were employed, and polynomial or Bernstein polynomial (typically of order 3-8) baseline corrections were employed. The NMR probe temperature was calibrated with methanol.[49]

FTIR spectra were acquired on a Thermo Nicolet IR200 spectrometer as mineral oil mulls between KBr plates. IR spectra were processed using the OMNIC® software package[50] with automatic baseline corrections. Melting points were acquired on a Thomas-Hoover Uni-Melt apparatus in sealed capillaries under argon. Elemental analyses were performed by the University of Illinois Microanalysis Laboratory and are reported as the average of two runs. X-ray crystallographic data were collected by the University of Illinois George L. Clark X-Ray Facility and 3M Materials Laboratory. The initial solution for the (C_5Me_5)Os(dfmpm)Br structure was obtained by Dr. Danielle Gray in the X-ray Facility, whereas the solution for the (C_5Me_5)Os(dfmpm)Me structure was obtained by the authors. Both structures were refined by the authors.

(Pentamethylcyclopentadienyl)bromo[bis(bis(trifluoromethyl)phosphino)methane]-osmium(II), (C_5Me_5)Os(dfmpm)Br. In a glove box, a 100-mL Schlenk flask equipped with a

magnetic stir bar was charged with $(C_5Me_5)_2Os_2Br_4$ (500.0 mg, 0.515 mmol) and zinc dust (135.0 mg, 2.06 mmol); the flask was removed from the box and kept under argon. Distilled ethanol (50 mL) was added, followed by dfmpm (1.1 mL, 5.0 mmol). The flask was equipped with a reflux condenser, and the brown mixture was heated to reflux. Upon reaching reflux, the brown slurry changed to a cloudy dark orange solution. After the mixture had refluxed for 6 h, the volatile materials were removed under vacuum and the orange-brown solid was extracted with pentane (2 x 25 mL). The extracts were filtered and combined, and the solution was taken to dryness under vacuum to give a red-orange solid. The residue was sublimed onto a water-cooled cold finger at 60-70 °C and 10^{-2} Torr to give 289.5 mg (37%) of (C_5Me_5)Os(dfmpm)Br as a bright orange powder. The remaining residue was taken into a glove box and ground into a finer powder with a spatula, and was then sublimed as above to give 184.9 mg (24%) of additional product. Total yield: 474.4 mg (61%). M.p.: 240-243 °C. Anal. Calcd. for $C_{15}H_{17}BrF_{12}OsP_2$: C, 23.8; H, 2.26; N, 0.00. Found: C, 23.7; H, 2.14; N, 0.51. ^{1}H NMR (C_6D_6): δ 5.33 (dt, J_{HH} = 16.7 Hz, J_{PH} = 10.9 Hz, 1H, PCH_2P), 3.43 (dt, J_{HH} = 16.7 Hz, J_{PH} = 12.4 Hz, 1H, PCH_2P), 1.63 (t, J_{PH} = 2.1 Hz, 15H, C_5Me_5). ^{19}F{^{1}H} NMR (C_6D_6): δ –55.1 (m), –59.8 (m). ^{31}P{^{1}H} NMR (C_6D_6): δ –26.1 (m). IR (cm^{-1}): 2252 (w), 1339 (m), 1180 (vs), 1150 (vs), 1096 (s), 1035 (m), 776 (s), 745 (w), 693 (s), 659 (m), 616 (w), 589 (s), 556 (s), 518 (w), 483 (s), 452 (s), 424 (w).

(Pentamethylcyclopentadienyl)(methyl)[bis(bis(trifluoromethyl)phosphino)methane] osmium(II), (C_5Me_5)Os(dfmpm)CH_3. In a glove box, an 80-mL Schlenk tube equipped with a magnetic stir bar was charged with (C_5Me_5)Os(dfmpm)Br (150.0 mg, 0.20 mmol); the tube was removed from the box and kept under argon. Distilled toluene (10 mL) was added, followed by $ZnMe_2$ (0.83 mL, 1.2 M solution in toluene, 0.99 mmol). The orange solution was heated to reflux for 2 h, resulting in formation of a cloudy yellow solution. The volatile materials were

removed under vacuum, and the residue was extracted with pentane (2 x 25 mL). The extracts were filtered and combined, taken to dryness under vacuum, and the residue was sublimed onto a water-cooled cold finger at 40-50 °C and 10^{-2} Torr as a yellow powder. Yield: 115.2 mg (84%). M.p.: 218-220 °C. Anal. Calcd. for $C_{16}H_{20}F_{12}OsP_2$: C, 27.8; H, 2.91; N, 0.00. Found: C, 27.1; H, 2.79; N, 0.56. ^{1}H NMR (C_6D_6): δ 5.04 (dt, J_{HH} = 16.7 Hz, J_{PH} = 11.6 Hz, 1H, PCH_2P), 3.25 (dt, J_{HH} = 16.7 Hz, J_{PH} = 12.1 Hz, 1H, PCH_2P), 1.61 (t, J_{PH} = 2.0 Hz, 15H, C_5Me_5), 0.71 (t-sept, J_{PH} = 7.5 Hz, J_{FH} = 1.8 Hz, 3H, Os–Me). $^{13}C\{^1H\}$ NMR (C_6D_6): δ 93.6 (t, J_{PC} = 2.8 Hz, C_5Me_5), 53.8 (t, J_{PC} = 25.3 Hz, PCH_2P), 9.54 (s, C_5Me_5), –43.2 (m, Os–CH_3). $^{19}F\{^1H\}$ NMR (C_6D_6): δ –59.1 (m), –61.9 (m). $^{31}P\{^1H\}$ NMR (C_6D_6): δ –28.8 (m). IR (cm^{-1}): 2239 (w), 1355 (m), 1232 (m), 1181 (vs), 1146 (vs), 1109 (vs), 1081 (s), 1030 (m), 770 (m), 754 (w), 742 (w), 705 (m), 648 (m), 599 (m), 558 (m), 519 (w), 491 (m), 452 (m), 436 (w), 409 (m).

Bis(methyl-^{13}C)zinc, Zn($^{13}CH_3)_2$. $Zn(^{13}CH_3)_2$ was synthesized according to a modified literature procedure.[51] In a glove box, an 80-mL Schlenk tube equipped with a magnetic stir bar was charged with zinc granules (426.6 mg, 6.5 mmol) and lithium powder (90.6 mg, 13.0 mmol); the tube was removed from the box and kept under argon. Distilled Et_2O (10 mL) was added, followed by $^{13}CH_3I$ (0.81 mL, 13.0 mmol). The mixture was refluxed for 5 d, allowed to cool to room temperature, and filtered to give a clear and very pale yellow solution of $Zn(^{13}CH_3)_2$ (~8 mL of a ~0.6 M solution as judged by ^{1}H NMR integration). Yield: ~80%. ^{1}H NMR (C_6D_6/Et_2O): δ –0.44 (d, J_{CH} = 121 Hz); there is also a resonance due to $Zn(O^{13}CH_3)_2$ (~30 mol%) at δ 3.59 (d, J_{CH} = 138 Hz). $^{13}C\{^1H\}$ NMR (C_6D_6/Et_2O): δ –6.48 (s); there is also a resonance due to $Zn(O^{13}CH_3)_2$ at δ 53.4.

Bis(methyl-^{13}C,d_2)zinc, Zn($^{13}CHD_2)_2$. $Zn(^{13}CHD_2)_2$ was synthesized as described above for $Zn(^{13}CH_3)_2$, except that $^{13}CHD_2I$ was used as the electrophile, to give a clear and colorless

solution of $Zn(^{13}CHD_2)_2$ (~10 mL of a ~0.5 M solution as judged by ^1H NMR integration). Yield: ~80%. ^1H NMR (C_6D_6/Et_2O): δ –0.61 (d, J_{CH} = 121 Hz). $^{13}C\{^1H\}$ NMR (C_6D_6/Et_2O): δ –7.12 (1:2:3:2:1 p, J_{CD} = 18.6 Hz).

(Pentamethylcyclopentadienyl)(methyl-^{13}C)[bis(bis(trifluoromethyl)phosphino)-methane]osmium(II), (C_5Me_5)Os(dfmpm)$^{13}CH_3$. This compound was synthesized as described for $(C_5Me_5)Os(dfmpm)CH_3$, except that $Zn(^{13}CH_3)_2$ was used as the alkylating agent. Yield: 28.9 mg (59%). M.p.: 215-217 °C. Anal. Calcd. for $C_{15}{}^{13}CH_{20}F_{12}OsP_2$: C, 27.8; H, 2.91; N, 0.00. Found: C, 27.4; H, 2.71; N, 0.34. ^1H NMR (C_6D_6): δ 5.04 (dt, J_{HH} = 16.7 Hz, J_{PH} = 11.6 Hz, 1H, PCH_2P), 3.25 (dt, J_{HH} = 16.7 Hz, J_{PH} = 12.1 Hz, 1H, PCH_2P), 1.61 (t, J_{PH} = 2.0 Hz, 15H, C_5Me_5), 0.71 (dtsept, J_{CH} = 131 Hz, J_{PH} = 7.4 Hz, J_{FH} = 1.9 Hz, 3H, Os–$^{13}CH_3$). $^{13}C\{^1H\}$ NMR (C_6D_6): δ 93.6 (t, J_{PC} = 2.8 Hz, C_5Me_5), 9.55 (s, C_5Me_5), –43.2 (m, Os–$^{13}CH_3$). $^{19}F\{^1H\}$ NMR (C_6D_6): δ –59.2 (m), –61.9 (m). $^{31}P\{^1H\}$ NMR (C_6D_6): δ –28.8 (m). IR (cm^{-1}): 2362 (w), 2335 (w), 2243 (w), 1355 (m), 1226 (m), 1181 (vs), 1146 (vs), 1109 (vs), 1081 (s), 1030 (m), 770 (m), 754 (w), 742 (w), 705 (m), 648 (w), 599 (m), 558 (m), 519 (w), 490 (m), 451 (m), 435 (w), 410 (m).

(Pentamethylcyclopentadienyl)(methyl-^{13}C,d$_2$)[bis(bis(trifluoromethyl)phosphino)-methane]osmium(II), (C_5Me_5)Os(dfmpm)$^{13}CHD_2$. This compound was synthesized as described for $(C_5Me_5)Os(dfmpm)CH_3$, except that $Zn(^{13}CHD_2)_2$ was used as the alkylating agent. Yield: 157.5 mg (75%). M.p.: 216-218 °C. Anal. Calcd. for $C_{15}{}^{13}CH_{18}D_2F_{12}OsP_2$: C, 27.8; H, 3.19; N, 0.00. Found: C, 27.5; H, 2.70; N, 0.80. ^1H NMR (C_6D_6): δ 5.03 (dt, J_{HH} = 16.7 Hz, J_{PH} = 11.5 Hz, 1H, PCH_2P), 3.24 (dt, J_{HH} = 16.7 Hz, J_{PH} = 12.1 Hz, 1H, PCH_2P), 1.60 (t, J_{PH} = 1.94 Hz, 15H, C_5Me_5), 0.67 (dm, J_{CH} = 131 Hz, 1H, Os–$^{13}CHD_2$). $^{19}F\{^1H\}$ NMR (C_6D_6): δ –59.2 (m), –61. 9 (m). $^{31}P\{^1H\}$ NMR (C_6D_6): δ –28.9 (m). IR (cm^{-1}): 2195 (w), 2129 (w), 1353 (m), 1179

(vs), 1144 (vs), 1109 (vs), 1081 (s), 1030 (m), 767 (s), 751 (w), 742 (w), 704 (s), 647 (m), 596 (s), 558 (s), 517 (w), 492 (s), 451 (s), 410 (m).

***N*-Deuterobis(trifluoromethanesulfonyl)imide, $(CF_3SO_2)_2ND$.** $(CF_3SO_2)_2ND$ was synthesized according to a modified literature procedure.[52] In a glove box, a small Schlenk tube equipped with a magnetic stir bar was charged with $LiN(SO_2CF_3)_2$ (1.0 g, 3.5 mmol) and D_2SO_4 (5.0 mL, 93 mmol); a water-cooled cold finger was inserted, and the tube was removed from the box. The mixture was heated to 50 °C with stirring under static vacuum (10^{-2} Torr). After 12 h, colorless crystals had collected on the cold finger, leaving a brown solution at the bottom of the Schlenk tube. The apparatus was taken into a glove box, and the colorless to white crystals of $(CF_3SO_2)_2ND$ were collected and stored in a Schlenk tube in the glove box. Yield: 0.93 g (95%).

General method for $[(C_5Me_5)Os(dfmpm)(methane)]^+$ isotopologs synthesis. Note: See Appendix A for detailed procedures; Krytox™ grease (DuPont)[53] was used instead of silicone grease to lubricate glass joints because it is more resistant to leaching by $CDCl_2F$. In a glove box, an oven-dried 5 mm NMR tube topped with a female 14/20 ground-glass joint was charged with the appropriate (C_5Me_5)Os(dfmpm)methyl isotopolog or mixture of isotopologs (~10 mg, 14.4 μmol). The appropriate bis(trifluoromethane)sulfonimide isotopolog or mixture of isotopologs (~5 mg, 17.8 μmol) was added, being careful to avoid contact between the two reagents. A vacuum transfer apparatus was attached to the NMR tube via the ground-glass joint and the stopcocks were all closed. The NMR tube was removed from the box and attached to the Schlenk line by means of the vacuum transfer apparatus, still being careful to avoid contact of the acid with the osmium compound (the two will react in the solid state at room temperature). The NMR tube was inserted into a spinner for the NMR spectrometer, placed into a liquid nitrogen bath, and $CDCl_2F$ (1-1.5 mL) was vacuum transferred to the NMR tube. The NMR tube was placed

under static vacuum and flame-sealed, and the NMR tube was inserted into a pre-cooled NMR probe (–135 °C). Tuning, matching, and shimming were performed, and spectra were obtained. To measure the barrier for methane loss, spectra were obtained every 300 seconds. Peak integrals were measured relative to an internal standard; for example, small resonances due to hexanes were often used for this purpose (the hexanes being introduced through the use of hexanes-moistened Kimwipes® tissues[54] used to clean the ground-glass joint atop the NMR tube).

(Pentamethylcyclopentadienyl)(methane)[bis(bis(trifluoromethyl)phosphino)-methane]osmium(II) bis(trifluoromethanesulfonyl)imide, [(C_5Me_5)Os(dfmpm)CH_4]-[$N(SO_2CF_3)_2$]. ^{1}H NMR (C_6D_6, –110 °C): δ 5.79 (m, 1H, PCH_2P), 4.25 (m, 1H, PCH_2P), 2.02 (s, 15H, C_5Me_5), –1.94 (s, 4H, Os–CH_4). $^{31}P\{^1H\}$ NMR (C_6D_6): δ –20.3 ("sept," J_{PF} = 78.8 Hz).

(Pentamethylcyclopentadienyl)(methane-^{13}C)[bis(bis(trifluoromethyl)phosphino)-methane]osmium(II) bis(trifluoromethanesulfonyl)imide, [(C_5Me_5)Os(dfmpm)$^{13}CH_4$]-[$N(SO_2CF_3)_2$]. ^{1}H NMR (C_6D_6, –110 °C): δ 5.79 (m, 1H, PCH_2P), 4.25 (m, 1H, PCH_2P), 2.02 (s, 15H, C_5Me_5), –1.94 (d, J_{CH} = 126 Hz, 4H, Os–$^{13}CH_4$). ^{13}C NMR (C_6D_6): δ 98.1 (br s, C_5Me_5), 10.2 (q, J_{CH} = 130 Hz, C_5Me_5), –45.1 (quint, J_{CH} = 126 Hz, Os–$^{13}CH_4$). $^{31}P\{^1H\}$ NMR (C_6D_6): δ –20.2 ("sept," J_{PF} = 76.4 Hz).

(Pentamethylcyclopentadienyl)(methane-^{13}C,d)[bis(bis(trifluoromethyl)phosphino)-methane]osmium(II) bis(trifluoromethanesulfonyl)imide, [(C_5Me_5)Os(dfmpm)$^{13}CH_3D$]-[$N(SO_2CF_3)_2$]. ^{1}H NMR (C_6D_6, –110 °C): δ 5.79 (m, 1H, PCH_2P), 4.25 (m, 1H, PCH_2P), 2.02 (s, 15H, C_5Me_5), –2.33 (d, J_{CH} = 124 Hz, 4H, Os–$^{13}CH_4$). ^{13}C NMR (C_6D_6): δ 98.1 (br s, C_5Me_5), 10.2 (q, J_{CH} = 130 Hz, C_5Me_5), –45.1 (m, Os–$^{13}CH_3D$). $^{31}P\{^1H\}$ NMR (C_6D_6): δ –20.2 ("sept," J_{PF} = 76.4 Hz).

(Pentamethylcyclopentadienyl)(methane-^{13}C,d_2)[bis(bis(trifluoromethyl)phosphino)-methane]osmium(II) bis(trifluoromethanesulfonyl)imide, [(C_5Me_5)Os(dfmpm)$^{13}CH_2D_2$]-[$N(SO_2CF_3)_2$]. ^{1}H NMR (C_6D_6, –110 °C): δ 5.80 (m, 1H, PCH_2P), 4.26 (m, 1H, PCH_2P), 2.02 (s, 15H, C_5Me_5), –2.86 (d, J_{CH} = 120 Hz, 4H, Os–$^{13}CH_4$). ^{13}C NMR (C_6D_6): δ 98.1 (br s, C_5Me_5), 10.2 (q, J_{CH} = 130 Hz, C_5Me_5), –45.1 (m, Os–$^{13}CH_2D_2$). ^{31}P{^{1}H} NMR (C_6D_6): δ –20.2 ("sept," J_{PF} = 76.4 Hz).

(Pentamethylcyclopentadienyl)(methane-^{13}C,d_3)[bis(bis(trifluoromethyl)phosphino)-methane]osmium(II) bis(trifluoromethanesulfonyl)imide, [(C_5Me_5)Os(dfmpm)$^{13}CHD_3$]-[$N(SO_2CF_3)_2$]. ^{1}H NMR (C_6D_6, –110 °C): δ 5.80 (m, 1H, PCH_2P), 4.26 (m, 1H, PCH_2P), 2.02 (s, 15H, C_5Me_5), –3.63 (d, J_{CH} = 115 Hz, 4H, Os–$^{13}CH_4$). ^{13}C NMR (C_6D_6): δ 98.1 (br s, C_5Me_5), 10.2 (q, J_{CH} = 130 Hz, C_5Me_5), –45.1 (m, Os–$^{13}CHD_3$). ^{31}P{^{1}H} NMR (C_6D_6): δ –20.2 ("sept," J_{PF} = 76.4 Hz).

NMR Data Analysis. For the ^{1}H NMR spectrum of [(C_5Me_5)Os(dfmpm)$^{13}CH_nD_{4-n}$]-[$N(SO_2CF_3)_2$] at –110 °C in $CDCl_2F$, line fitting was performed and optimized on the region containing the resonances for the four coordinated methane isotopologs before performing peak picking. This procedure was employed in order to minimize the error in the chemical shift values, which were used for IPR analysis. For the ^{1}H NMR spectra of [(C_5Me_5)Os(dfmpm)$^{13}CH_4$][OTf] in $CDCl_2F$ that were used for kinetic analysis of methane loss, Whittaker smoother baseline corrections were employed with parameters carefully selected to remove baseline modulations without impacting resonances. This procedure was employed in order to maximize the accuracy and consistency of the peak areas used to perform the kinetic analysis.

Before using them in calculations of the chemical shifts of the frozen methane structure, the measured chemical shift values for the CH_4, CH_3D, CH_2D_2, and CHD_3 complexes were corrected for the secondary isotope effects[33] seen in free methane (e.g., the observed chemical shift of δ –2.33 for the CH_3D complex was corrected to δ –2.31 by removing the 0.02 ppm upfield secondary isotope shift observed between free CH_4 and free CH_3D). Similarly, the measured C–H coupling constants for the CH_4, CH_3D, CH_2D_2, and CHD_3 complexes were corrected for the secondary isotope effects[36] seen in free methane (e.g., the observed C–H coupling constant of 123.7 Hz for the CH_3D complex was corrected to 124.1 Hz by removing the 0.4 Hz decrease in the coupling constant observed between free CH_4 and free CH_3D). The coupling constant correction for the CH_2D_2 complex was estimated to be 0.7 Hz by interpolation.

The rate constant for dissociation of methane was determined from the slope of the plot of the natural logarithm of peak areas for the coordinated methane resonance versus time.

Error Analysis. The error in the NMR probe temperature was estimated to be 1 K. The error in the rate constant for dissociation of methane was estimated to be 10% from the RMS deviation of points from the best-fit line relating the natural logarithm of peak areas for the coordinated methane resonance versus time, and from the uncertainty in integration values. The errors in the enthalpy,[55] entropy,[55] and Gibbs free energy[56] of activation for dissociation of methane were computed according to the following propagation of error formulas, where $\sigma\Delta H^{\ddagger}$, $\sigma\Delta S^{\ddagger}$, and $\sigma\Delta G^{\ddagger}$ are the errors in the enthalpy, entropy, and Gibbs free energy of activation in J mol^{-1}, J mol^{-1} K^{-1}, and J mol^{-1}, respectively; R is the gas constant; T is the NMR probe temperature in K; T_{max} is the maximum NMR probe temperature used for the Eyring plot in K; T_{min} is the minimum NMR probe temperature used for the Eyring plot in K; k_B is the Boltzmann constant; k is the rate constant for the decomposition reaction in Hz; k_{max} is the maximum rate

constant for the Eyring plot in Hz; k_{min} is the minimum rate constant for the Eyring plot in Hz; h is Planck's constant; σ_T is the error in temperature in K; σ_k is the error in the rate constant in Hz; $\Delta T = (T_{max} - T_{min})$; and $\Delta L = [\ln(k_{max}/T_{max}) - \ln(k_{min}/T_{min})]$.

$$(\boldsymbol{\sigma\Delta H^{\ddagger}})^{\mathbf{2}} = \left(\frac{\boldsymbol{RT_{max}T_{min}}}{\boldsymbol{\Delta T}}\right)^{\mathbf{2}} \left\{\left[\left(\mathbf{1} + \boldsymbol{T_{min}}\frac{\boldsymbol{\Delta L}}{\boldsymbol{\Delta T}}\right)^{\mathbf{2}} + \left(\mathbf{1} + \boldsymbol{T_{max}}\frac{\boldsymbol{\Delta L}}{\boldsymbol{\Delta T}}\right)^{\mathbf{2}}\right]\left(\frac{\boldsymbol{\sigma_T}}{\boldsymbol{T}}\right)^{\mathbf{2}} + \mathbf{2}\left(\frac{\boldsymbol{\sigma_k}}{\boldsymbol{k}}\right)^{\mathbf{2}}\right\}$$

$$(\boldsymbol{\sigma\Delta S^{\ddagger}})^{\mathbf{2}} = \left(\frac{\boldsymbol{R}}{\boldsymbol{\Delta T}}\right)^{\mathbf{2}} \left\{\left[\boldsymbol{T_{max}}^{\mathbf{2}}\left(\mathbf{1} + \boldsymbol{T_{min}}\frac{\boldsymbol{\Delta L}}{\boldsymbol{\Delta T}}\right)^{\mathbf{2}} + \boldsymbol{T_{min}}^{\mathbf{2}}\left(\mathbf{1} + \boldsymbol{T_{max}}\frac{\boldsymbol{\Delta L}}{\boldsymbol{\Delta T}}\right)^{\mathbf{2}}\right]\left(\frac{\boldsymbol{\sigma_T}}{\boldsymbol{T}}\right)^{\mathbf{2}} + \left(\boldsymbol{T_{max}}^{\mathbf{2}} + \boldsymbol{T_{min}}^{\mathbf{2}}\right)\left(\frac{\boldsymbol{\sigma_k}}{\boldsymbol{k}}\right)^{\mathbf{2}}\right\}$$

$$(\boldsymbol{\sigma\Delta G^{\ddagger}})^{\mathbf{2}} = (\boldsymbol{RT})^{\mathbf{2}}\left[\left(\mathbf{1} + \ln\frac{\boldsymbol{k_B T}}{\boldsymbol{kh}}\right)^{\mathbf{2}}\left(\frac{\boldsymbol{\sigma_T}}{\boldsymbol{T}}\right)^{\mathbf{2}} + \left(\frac{\boldsymbol{\sigma_k}}{\boldsymbol{k}}\right)^{\mathbf{2}}\right]$$

The errors in the measured chemical shifts of the CH_4, CH_3D, CH_2D_2, and CHD_3 complexes were estimated to be 0.001, 0.002, 0.004, and 0.005 ppm, respectively, and the errors in the measured coupling constants were estimated to be 0.20, 0.22, 0.24, and 0.22 Hz, respectively. The errors reported for the terminal and bridging chemical shifts and coupling constants and the Boltzmann isotope energy difference values were computed according to the following propagation of error formulas, where $\sigma\delta_T$ and $\sigma\delta_B$ are the errors in the terminal and bridging chemical shifts, respectively, in ppm; $\sigma\delta_{CH4}$, $\sigma\delta_{CH3D}$, $\sigma\delta_{CH2D2}$, and $\sigma\delta_{CHD3}$, are the errors in the measured (exchange-averaged) chemical shifts of the CH_4, CH_3D, CH_2D_2, and CHD_3 complexes, respectively, in ppm; σJ_T and σJ_B are the errors in the terminal and bridging C–H coupling constants, respectively, in Hz; σJ_{CH4}, σJ_{CH3D}, σJ_{CH2D2}, and σJ_{CHD3} are the errors in the measured (exchange-averaged) C–H coupling constants of the CH_4, CH_3D, CH_2D_2, and CHD_3 complexes, respectively, in Hz; $\sigma\Delta E_{BI}$ is the error in the Boltzmann isotope energy difference; and the other variables are defined as described previously in this chapter. The propagation of error formulas were derived with the aid of Mathematica®.[57]

$$(\sigma\delta_T)^2 = \frac{1}{16}\left[\left(4\left[\frac{\delta_{Os-CH_4}\left(\delta_{Os-CH_3D}-\delta_{Os-CH_2D_2}\right)^2}{\left(\delta_{Os-CH_4}-2\delta_{Os-CH_3D}+\delta_{Os-CH_2D_2}\right)^2}\right]^2 + 36\left[\frac{\delta_{Os-CH_4}\left(\delta_{Os-CH_2D_2}-\delta_{Os-CHD_3}\right)^2}{\left(\delta_{Os-CH_4}-3\delta_{Os-CH_2D_2}+2\delta_{Os-CHD_3}\right)^2}\right]^2\right.\right.$$

$$\left.+ 9\left[\frac{\delta_{Os-CH_4}\left(\delta_{Os-CH_3D}-\delta_{Os-CHD_3}\right)^2}{\left(2\delta_{Os-CH_4}-3\delta_{Os-CH_3D}+\delta_{Os-CHD_3}\right)^2}\right]^2\right)\left(\frac{\sigma\delta_{Os-CH_4}}{\delta_{Os-CH_4}}\right)^2$$

$$+\left(\left[\frac{\delta_{Os-CH_3D}\left(\delta_{Os-CH_4}-\delta_{Os-CH_2D_2}\right)^2}{\left(\delta_{Os-CH_4}-2\delta_{Os-CH_3D}+\delta_{Os-CH_2D_2}\right)^2}\right]^2 + 4\left[\frac{\delta_{Os-CH_3D}\left(\delta_{Os-CH_4}-\delta_{Os-CHD_3}\right)^2}{\left(2\delta_{Os-CH_4}-3\delta_{Os-CH_3D}+\delta_{Os-CHD_3}\right)^2}\right]^2\right.$$

$$\left.+ 4\left[\frac{\delta_{Os-CH_3D}\left(\delta_{Os-CH_2D_2}-\delta_{Os-CHD_3}\right)^2}{\left(\delta_{Os-CH_3D}-2\delta_{Os-CH_2D_2}+\delta_{Os-CHD_3}\right)^2}\right]^2\right)\left(\frac{\sigma\delta_{Os-CH_3D}}{\delta_{Os-CH_3D}}\right)^2$$

$$+\left(4\left[\frac{\delta_{Os-CH_2D_2}\left(\delta_{Os-CH_4}-\delta_{Os-CH_3D}\right)^2}{\left(\delta_{Os-CH_4}-2\delta_{Os-CH_3D}+\delta_{Os-CH_2D_2}\right)^2}\right]^2 + 4\left[\frac{\delta_{Os-CH_2D_2}\left(\delta_{Os-CH_4}-\delta_{Os-CHD_3}\right)^2}{\left(\delta_{Os-CH_4}-3\delta_{Os-CH_2D_2}+2\delta_{Os-CHD_3}\right)^2}\right]^2\right.$$

$$\left.+\left[\frac{\delta_{Os-CH_2D_2}\left(\delta_{Os-CH_3D}-\delta_{Os-CHD_3}\right)^2}{\left(\delta_{Os-CH_3D}-2\delta_{Os-CH_2D_2}+\delta_{Os-CHD_3}\right)^2}\right]^2\right)\left(\frac{\sigma\delta_{Os-CH_2D_2}}{\delta_{Os-CH_2D_2}}\right)^2$$

$$+\left(9\left[\frac{\delta_{Os-CHD_3}\left(\delta_{Os-CH_4}-\delta_{Os-CH_2D_2}\right)^2}{\left(\delta_{Os-CH_4}-3\delta_{Os-CH_2D_2}+2\delta_{Os-CHD_3}\right)^2}\right]^2 + 36\left[\frac{\delta_{Os-CHD_3}\left(\delta_{Os-CH_4}-\delta_{Os-CH_3D}\right)^2}{\left(2\delta_{Os-CH_4}-3\delta_{Os-CH_3D}+\delta_{Os-CHD_3}\right)^2}\right]^2\right.$$

$$\left.\left.+ 4\left[\frac{\delta_{Os-CHD_3}\left(\delta_{Os-CH_3D}-\delta_{Os-CH_2D_2}\right)^2}{\left(\delta_{Os-CH_3D}-2\delta_{Os-CH_2D_2}+\delta_{Os-CHD_3}\right)^2}\right]^2\right)\left(\frac{\sigma\delta_{Os-CHD_3}}{\delta_{Os-CHD_3}}\right)^2\right]$$

$$(\sigma\delta_B)^2 = \frac{1}{16}\left[\left(4\left[2\delta_{Os-CH_4} - \frac{3\delta_{Os-CH_4}(\delta_{Os-CH_3D} - \delta_{Os-CH_2D_2})^2}{(\delta_{Os-CH_4} - 2\delta_{Os-CH_3D} + \delta_{Os-CH_2D_2})^2}\right]^2 + 4\left[2\delta_{Os-CH_4} - \frac{9\delta_{Os-CH_4}(\delta_{Os-CH_2D_2} - \delta_{Os-CHD_3})^2}{(\delta_{Os-CH_4} - 3\delta_{Os-CH_2D_2} + 2\delta_{Os-CHD_3})^2}\right]^2 + \left[4\delta_{Os-CH_4} - \frac{9\delta_{Os-CH_4}(\delta_{Os-CH_3D} - \delta_{Os-CHD_3})^2}{(2\delta_{Os-CH_4} - 3\delta_{Os-CH_3D} + \delta_{Os-CHD_3})^2}\right]^2\right)\left(\frac{\sigma\delta_{Os-CH_4}}{\delta_{Os-CH_4}}\right)^2$$

$$+ 9\left(\left[\frac{\delta_{Os-CH_3D}(\delta_{Os-CH_4} - \delta_{Os-CH_2D_2})^2}{(\delta_{Os-CH_4} - 2\delta_{Os-CH_3D} + \delta_{Os-CH_2D_2})^2}\right]^2 + 4\left[\frac{\delta_{Os-CH_3D}(\delta_{Os-CH_4} - \delta_{Os-CHD_3})^2}{(2\delta_{Os-CH_4} - 3\delta_{Os-CH_3D} + \delta_{Os-CHD_3})^2}\right]^2 + 4\left[\frac{\delta_{Os-CH_3D}(\delta_{Os-CH_2D_2} - \delta_{Os-CHD_3})^2\left[8(\delta_{Os-CH_3D} - \delta_{Os-CH_2D_2})(\delta_{Os-CH_3D} - 2\delta_{Os-CH_2D_2} + \delta_{Os-CHD_3}) - (\delta_{Os-CH_3D} - \delta_{Os-CHD_3})^2\right]}{(\delta_{Os-CH_3D} - 4\delta_{Os-CH_2D_2} + 3\delta_{Os-CHD_3})^2(\delta_{Os-CH_3D} - 2\delta_{Os-CH_2D_2} + \delta_{Os-CHD_3})^2}\right]^2\right)\left(\frac{\sigma\delta_{Os-CH_3D}}{\delta_{Os-CH_3D}}\right)^2$$

$$+ 9\left(4\left[\frac{\delta_{Os-CH_2D_2}(\delta_{Os-CH_4} - \delta_{Os-CH_3D})^2}{(\delta_{Os-CH_4} - 2\delta_{Os-CH_3D} + \delta_{Os-CH_2D_2})^2}\right]^2 + 4\left[\frac{\delta_{Os-CH_2D_2}(\delta_{Os-CH_4} - \delta_{Os-CHD_3})^2}{(\delta_{Os-CH_4} - 3\delta_{Os-CH_2D_2} + 2\delta_{Os-CHD_3})^2}\right]^2 + \left[\frac{\delta_{Os-CH_2D_2}(\delta_{Os-CH_3D} - \delta_{Os-CHD_3})^3(3\delta_{Os-CH_3D} - 8\delta_{Os-CH_2D_2} + 5\delta_{Os-CHD_3})}{(\delta_{Os-CH_3D} - 4\delta_{Os-CH_2D_2} + 3\delta_{Os-CHD_3})^2(\delta_{Os-CH_3D} - 2\delta_{Os-CH_2D_2} + \delta_{Os-CHD_3})^2}\right]^2\right)\left(\frac{\sigma\delta_{Os-CH_2D_2}}{\delta_{Os-CH_2D_2}}\right)^2$$

$$+ \left(81\left[\frac{\delta_{Os-CHD_3}(\delta_{Os-CH_4} - \delta_{Os-CH_2D_2})^2}{(\delta_{Os-CH_4} - 3\delta_{Os-CH_2D_2} + 2\delta_{Os-CHD_3})^2}\right]^2 + 324\left[\frac{\delta_{Os-CHD_3}(\delta_{Os-CH_4} - \delta_{Os-CH_3D})^2}{(2\delta_{Os-CH_4} - 3\delta_{Os-CH_3D} + \delta_{Os-CHD_3})^2}\right]^2 + 4\left[\frac{\delta_{Os-CHD_3}(\delta_{Os-CH_3D} - \delta_{Os-CH_2D_2})^2\left[8(\delta_{Os-CH_3D} - 2\delta_{Os-CH_2D_2} + \delta_{Os-CHD_3})^2 - 3(\delta_{Os-CH_3D} - 4\delta_{Os-CH_2D_2} + 3\delta_{Os-CHD_3})^2\right]}{(\delta_{Os-CH_3D} - 4\delta_{Os-CH_2D_2} + 3\delta_{Os-CHD_3})^2(\delta_{Os-CH_3D} - 2\delta_{Os-CH_2D_2} + \delta_{Os-CHD_3})^2}\right]^2\right)\left(\frac{\sigma\delta_{Os-CHD_3}}{\delta_{Os-CHD_3}}\right)^2\Bigg]$$

$$(\sigma\Delta E_{\mathrm{BI}})^2 = \left(\frac{RT}{2}\right)^2 \left[\left(\left[\frac{\delta_{\mathrm{Os-CH_4}}(\delta_{\mathrm{Os-CH_3D}} - \delta_{\mathrm{Os-CH_2D_2}})}{(2\delta_{\mathrm{Os-CH_4}} - 3\delta_{\mathrm{Os-CH_3D}} + \delta_{\mathrm{Os-CH_2D_2}})(\delta_{\mathrm{Os-CH_3D}} - \delta_{\mathrm{Os-CH_2D_2}})} \right]^2 + \left[\frac{\delta_{\mathrm{Os-CH_4}}(\delta_{\mathrm{Os-CH_2D_2}} - \delta_{\mathrm{Os-CHD_3}})}{(2\delta_{\mathrm{Os-CH_4}} - 3\delta_{\mathrm{Os-CH_2D_2}} + \delta_{\mathrm{Os-CHD_3}})(\delta_{\mathrm{Os-CH_2D_2}} - \delta_{\mathrm{Os-CHD_3}})} \right]^2 \right.$$

$$\left. + 16 \left[\frac{\delta_{\mathrm{Os-CH_4}}(\delta_{\mathrm{Os-CH_3D}} - \delta_{\mathrm{Os-CHD_3}})}{(8\delta_{\mathrm{Os-CH_4}} - 9\delta_{\mathrm{Os-CH_3D}} + \delta_{\mathrm{Os-CHD_3}})(\delta_{\mathrm{Os-CH_3D}} - \delta_{\mathrm{Os-CHD_3}})} \right]^2 \right) \left(\frac{\sigma\delta_{\mathrm{Os-CH_4}}}{\delta_{\mathrm{Os-CH_4}}} \right)^2$$

$$+ \left(\left[\frac{\delta_{\mathrm{Os-CH_3D}}(\delta_{\mathrm{Os-CH_4}} - \delta_{\mathrm{Os-CH_2D_2}})}{(2\delta_{\mathrm{Os-CH_4}} - 3\delta_{\mathrm{Os-CH_3D}} + \delta_{\mathrm{Os-CH_2D_2}})(\delta_{\mathrm{Os-CH_3D}} - \delta_{\mathrm{Os-CH_2D_2}})} \right]^2 + 16 \left[\frac{\delta_{\mathrm{Os-CH_3D}}(\delta_{\mathrm{Os-CH_4}} - \delta_{\mathrm{Os-CHD_3}})}{(8\delta_{\mathrm{Os-CH_4}} - 9\delta_{\mathrm{Os-CH_3D}} + \delta_{\mathrm{Os-CHD_3}})(\delta_{\mathrm{Os-CH_3D}} - \delta_{\mathrm{Os-CHD_3}})} \right]^2 \right.$$

$$\left. + 16 \left[\frac{\delta_{\mathrm{Os-CH_3D}}(\delta_{\mathrm{Os-CH_2D_2}} - \delta_{\mathrm{Os-CHD_3}})}{(3\delta_{\mathrm{Os-CH_3D}} - 4\delta_{\mathrm{Os-CH_2D_2}} + \delta_{\mathrm{Os-CHD_3}})(\delta_{\mathrm{Os-CH_3D}} - 4\delta_{\mathrm{Os-CH_2D_2}} + 3\delta_{\mathrm{Os-CHD_3}})} \right]^2 \right) \left(\frac{\sigma\delta_{\mathrm{Os-CH_3D}}}{\delta_{\mathrm{Os-CH_3D}}} \right)^2$$

$$+ \left(\left[\frac{\delta_{\mathrm{Os-CH_2D_2}}(\delta_{\mathrm{Os-CH_4}} - \delta_{\mathrm{Os-CH_3D}})}{(2\delta_{\mathrm{Os-CH_4}} - 3\delta_{\mathrm{Os-CH_3D}} + \delta_{\mathrm{Os-CH_2D_2}})(\delta_{\mathrm{Os-CH_3D}} - \delta_{\mathrm{Os-CH_2D_2}})} \right]^2 + \left[\frac{\delta_{\mathrm{Os-CH_2D_2}}(\delta_{\mathrm{Os-CH_4}} - \delta_{\mathrm{Os-CHD_3}})}{(2\delta_{\mathrm{Os-CH_4}} - 3\delta_{\mathrm{Os-CH_2D_2}} + \delta_{\mathrm{Os-CHD_3}})(\delta_{\mathrm{Os-CH_2D_2}} - \delta_{\mathrm{Os-CHD_3}})} \right]^2 \right.$$

$$\left. + 16 \left[\frac{\delta_{\mathrm{Os-CH_2D_2}}(\delta_{\mathrm{Os-CH_3D}} - \delta_{\mathrm{Os-CHD_3}})}{(3\delta_{\mathrm{Os-CH_3D}} - 4\delta_{\mathrm{Os-CH_2D_2}} + \delta_{\mathrm{Os-CHD_3}})(\delta_{\mathrm{Os-CH_3D}} - 4\delta_{\mathrm{Os-CH_2D_2}} + 3\delta_{\mathrm{Os-CHD_3}})} \right]^2 \right) \left(\frac{\sigma\delta_{\mathrm{Os-CH_2D_2}}}{\delta_{\mathrm{Os-CH_2D_2}}} \right)^2$$

$$+ \left(\left[\frac{\delta_{\mathrm{Os-CHD_3}}(\delta_{\mathrm{Os-CH_4}} - \delta_{\mathrm{Os-CH_2D_2}})}{(2\delta_{\mathrm{Os-CH_4}} - 3\delta_{\mathrm{Os-CH_2D_2}} + \delta_{\mathrm{Os-CHD_3}})(\delta_{\mathrm{Os-CH_2D_2}} - \delta_{\mathrm{Os-CHD_3}})} \right]^2 + 16 \left[\frac{\delta_{\mathrm{Os-CHD_3}}(\delta_{\mathrm{Os-CH_4}} - \delta_{\mathrm{Os-CH_3D}})}{(8\delta_{\mathrm{Os-CH_4}} - 9\delta_{\mathrm{Os-CH_3D}} + \delta_{\mathrm{Os-CHD_3}})(\delta_{\mathrm{Os-CH_3D}} - \delta_{\mathrm{Os-CHD_3}})} \right]^2 \right.$$

$$\left. + 16 \left[\frac{\delta_{\mathrm{Os-CHD_3}}(\delta_{\mathrm{Os-CH_3D}} - \delta_{\mathrm{Os-CH_2D_2}})}{(3\delta_{\mathrm{Os-CH_3D}} - 4\delta_{\mathrm{Os-CH_2D_2}} + \delta_{\mathrm{Os-CHD_3}})(\delta_{\mathrm{Os-CH_3D}} - 4\delta_{\mathrm{Os-CH_2D_2}} + 3\delta_{\mathrm{Os-CHD_3}})} \right]^2 \right) \left(\frac{\sigma\delta_{\mathrm{Os-CHD_3}}}{\delta_{\mathrm{Os-CHD_3}}} \right)^2$$

$$+ \left(\left[\ln \sqrt{\frac{\delta_{\mathrm{Os-CH_3D}} - \delta_{\mathrm{Os-CH_2D_2}}}{2\delta_{\mathrm{Os-CH_4}} - 3\delta_{\mathrm{Os-CH_3D}} + \delta_{\mathrm{Os-CH_2D_2}}}} \right]^2 + \left[\ln \sqrt{\frac{3(\delta_{\mathrm{Os-CH_2D_2}} - \delta_{\mathrm{Os-CHD_3}})}{2\delta_{\mathrm{Os-CH_4}} - 3\delta_{\mathrm{Os-CH_2D_2}} + \delta_{\mathrm{Os-CHD_3}}}} \right]^2 + \left[\ln \sqrt{\frac{3(\delta_{\mathrm{Os-CH_3D}} - \delta_{\mathrm{Os-CHD_3}})}{8\delta_{\mathrm{Os-CH_4}} - 9\delta_{\mathrm{Os-CH_3D}} + \delta_{\mathrm{Os-CHD_3}}}} \right]^2 \right.$$

$$\left. + \left[\ln \sqrt{-\frac{\delta_{\mathrm{Os-CH_3D}} - 4\delta_{\mathrm{Os-CH_2D_2}} + 3\delta_{\mathrm{Os-CHD_3}}}{3\delta_{\mathrm{Os-CH_3D}} - 4\delta_{\mathrm{Os-CH_2D_2}} + \delta_{\mathrm{Os-CHD_3}}}} \right]^2 \right) \left(\frac{\sigma T}{T} \right)^2 \Bigg]$$

$$(\sigma J_T)^2 = \frac{1}{16}\left[\left(4\left[\frac{J_{Os-CH_4}(J_{Os-CH_3D} - J_{Os-CH_2D_2})^2}{(J_{Os-CH_4} - 2J_{Os-CH_3D} + J_{Os-CH_2D_2})^2}\right]^2 + 36\left[\frac{J_{Os-CH_4}(J_{Os-CH_2D_2} - J_{Os-CHD_3})^2}{(J_{Os-CH_4} - 3J_{Os-CH_2D_2} + 2J_{Os-CHD_3})^2}\right]^2\right.\right.$$

$$\left.\left. + 9\left[\frac{J_{Os-CH_4}(J_{Os-CH_3D} - J_{Os-CHD_3})^2}{(2J_{Os-CH_4} - 3J_{Os-CH_3D} + J_{Os-CHD_3})^2}\right]^2\right)\left(\frac{\sigma J_{Os-CH_4}}{J_{Os-CH_4}}\right)^2$$

$$+\left(\left[\frac{J_{Os-CH_3D}(J_{Os-CH_4} - J_{Os-CH_2D_2})^2}{(J_{Os-CH_4} - 2J_{Os-CH_3D} + J_{Os-CH_2D_2})^2}\right]^2 + 4\left[\frac{J_{Os-CH_3D}(J_{Os-CH_4} - J_{Os-CHD_3})^2}{(2J_{Os-CH_4} - 3J_{Os-CH_3D} + J_{Os-CHD_3})^2}\right]^2\right.$$

$$\left. + 4\left[\frac{J_{Os-CH_3D}(J_{Os-CH_2D_2} - J_{Os-CHD_3})^2}{(J_{Os-CH_3D} - 2J_{Os-CH_2D_2} + J_{Os-CHD_3})^2}\right]^2\right)\left(\frac{\sigma J_{Os-CH_3D}}{J_{Os-CH_3D}}\right)^2$$

$$+\left(4\left[\frac{J_{Os-CH_2D_2}(J_{Os-CH_4} - J_{Os-CH_3D})^2}{(J_{Os-CH_4} - 2J_{Os-CH_3D} + J_{Os-CH_2D_2})^2}\right]^2 + 4\left[\frac{J_{Os-CH_2D_2}(J_{Os-CH_4} - J_{Os-CHD_3})^2}{(J_{Os-CH_4} - 3J_{Os-CH_2D_2} + 2J_{Os-CHD_3})^2}\right]^2\right.$$

$$\left. + \left[\frac{J_{Os-CH_2D_2}(J_{Os-CH_3D} - J_{Os-CHD_3})^2}{(J_{Os-CH_3D} - 2J_{Os-CH_2D_2} + J_{Os-CHD_3})^2}\right]^2\right)\left(\frac{\sigma J_{Os-CH_2D_2}}{J_{Os-CH_2D_2}}\right)^2$$

$$+\left(9\left[\frac{J_{Os-CHD_3}(J_{Os-CH_4} - J_{Os-CH_2D_2})^2}{(J_{Os-CH_4} - 3J_{Os-CH_2D_2} + 2J_{Os-CHD_3})^2}\right]^2 + 36\left[\frac{J_{Os-CHD_3}(J_{Os-CH_4} - J_{Os-CH_3D})^2}{(2J_{Os-CH_4} - 3J_{Os-CH_3D} + J_{Os-CHD_3})^2}\right]^2\right.$$

$$\left.\left. + 4\left[\frac{J_{Os-CHD_3}(J_{Os-CH_3D} - J_{Os-CH_2D_2})^2}{(J_{Os-CH_3D} - 2J_{Os-CH_2D_2} + J_{Os-CHD_3})^2}\right]^2\right)\left(\frac{\sigma J_{Os-CHD_3}}{J_{Os-CHD_3}}\right)^2\right]$$

$$(\sigma J_B)^2 = \frac{1}{16}\left[\left(4\left[2J_{Os-CH_4} - \frac{3J_{Os-CH_4}(J_{Os-CH_3D} - J_{Os-CH_2D_2})^2}{(J_{Os-CH_4} - 2J_{Os-CH_3D} + J_{Os-CH_2D_2})^2}\right]^2 + 4\left[2J_{Os-CH_4} - \frac{9J_{Os-CH_4}(J_{Os-CH_2D_2} - J_{Os-CHD_3})^2}{(J_{Os-CH_4} - 3J_{Os-CH_2D_2} + 2J_{Os-CHD_3})^2}\right]^2\right.\right.$$

$$\left.\left. + \left[4J_{Os-CH_4} - \frac{9J_{Os-CH_4}(J_{Os-CH_3D} - J_{Os-CHD_3})^2}{(2J_{Os-CH_4} - 3J_{Os-CH_3D} + J_{Os-CHD_3})^2}\right]^2\right)\left(\frac{\sigma J_{Os-CH_4}}{J_{Os-CH_4}}\right)^2\right.$$

$$+ 9\left(\left[\frac{J_{Os-CH_3D}(J_{Os-CH_4} - J_{Os-CH_2D_2})^2}{(J_{Os-CH_4} - 2J_{Os-CH_3D} + J_{Os-CH_2D_2})^2}\right]^2 + 4\left[\frac{J_{Os-CH_3D}(J_{Os-CH_4} - J_{Os-CHD_3})^2}{(2J_{Os-CH_4} - 3J_{Os-CH_3D} + J_{Os-CHD_3})^2}\right]^2\right.$$

$$\left. + 4\left[\frac{J_{Os-CH_3D}(J_{Os-CH_2D_2} - J_{Os-CHD_3})^2\left[8(J_{Os-CH_3D} - J_{Os-CH_2D_2})(J_{Os-CH_3D} - 2J_{Os-CH_2D_2} + J_{Os-CHD_3}) - (J_{Os-CH_3D} - J_{Os-CHD_3})^2\right]}{(J_{Os-CH_3D} - 4J_{Os-CH_2D_2} + 3J_{Os-CHD_3})^2(J_{Os-CH_3D} - 2J_{Os-CH_2D_2} + J_{Os-CHD_3})^2}\right]^2\right)\left(\frac{\sigma J_{Os-CH_3D}}{J_{Os-CH_3D}}\right)^2$$

$$+ 9\left(4\left[\frac{J_{Os-CH_2D_2}(J_{Os-CH_4} - J_{Os-CH_3D})^2}{(J_{Os-CH_4} - 2J_{Os-CH_3D} + J_{Os-CH_2D_2})^2}\right]^2 + 4\left[\frac{J_{Os-CH_2D_2}(J_{Os-CH_4} - J_{Os-CHD_3})^2}{(J_{Os-CH_4} - 3J_{Os-CH_2D_2} + 2J_{Os-CHD_3})^2}\right]^2\right.$$

$$\left. + \left[\frac{J_{Os-CH_2D_2}(J_{Os-CH_3D} - J_{Os-CHD_3})^3(3J_{Os-CH_3D} - 8J_{Os-CH_2D_2} + 5J_{Os-CHD_3})}{(J_{Os-CH_3D} - 4J_{Os-CH_2D_2} + 3J_{Os-CHD_3})^2(J_{Os-CH_3D} - 2J_{Os-CH_2D_2} + J_{Os-CHD_3})^2}\right]^2\right)\left(\frac{\sigma J_{Os-CH_2D_2}}{J_{Os-CH_2D_2}}\right)^2$$

$$+ \left(81\left[\frac{J_{Os-CHD_3}(J_{Os-CH_4} - J_{Os-CH_2D_2})^2}{(J_{Os-CH_4} - 3J_{Os-CH_2D_2} + 2J_{Os-CHD_3})^2}\right]^2 + 324\left[\frac{J_{Os-CHD_3}(J_{Os-CH_4} - J_{Os-CH_3D})^2}{(2J_{Os-CH_4} - 3J_{Os-CH_3D} + J_{Os-CHD_3})^2}\right]^2\right.$$

$$\left. + 4\left[\frac{J_{Os-CHD_3}(J_{Os-CH_3D} - J_{Os-CH_2D_2})^2\left[8(J_{Os-CH_3D} - 2J_{Os-CH_2D_2} + J_{Os-CHD_3})^2 - 3(J_{Os-CH_3D} - 4J_{Os-CH_2D_2} + 3J_{Os-CHD_3})^2\right]}{(J_{Os-CH_3D} - 4J_{Os-CH_2D_2} + 3J_{Os-CHD_3})^2(J_{Os-CH_3D} - 2J_{Os-CH_2D_2} + J_{Os-CHD_3})^2}\right]^2\right)\left(\frac{\sigma J_{Os-CHD_3}}{J_{Os-CHD_3}}\right)^2\Bigg]$$

$$(\sigma\Delta E_{\mathrm{BI}})^2 = \left(\frac{RT}{2}\right)^2 \left[\left(\left[\frac{J_{\mathrm{Os-CH_4}}(J_{\mathrm{Os-CH_3D}} - J_{\mathrm{Os-CH_2D_2}})}{(2J_{\mathrm{Os-CH_4}} - 3J_{\mathrm{Os-CH_3D}} + J_{\mathrm{Os-CH_2D_2}})(J_{\mathrm{Os-CH_3D}} - J_{\mathrm{Os-CH_2D_2}})}\right]^2 + \left[\frac{J_{\mathrm{Os-CH_4}}(J_{\mathrm{Os-CH_2D_2}} - J_{\mathrm{Os-CHD_3}})}{(2J_{\mathrm{Os-CH_4}} - 3J_{\mathrm{Os-CH_2D_2}} + J_{\mathrm{Os-CHD_3}})(J_{\mathrm{Os-CH_2D_2}} - J_{\mathrm{Os-CHD_3}})}\right]^2 \right.$$

$$\left. + 16\left[\frac{J_{\mathrm{Os-CH_4}}(J_{\mathrm{Os-CH_3D}} - J_{\mathrm{Os-CHD_3}})}{(8J_{\mathrm{Os-CH_4}} - 9J_{\mathrm{Os-CH_3D}} + J_{\mathrm{Os-CHD_3}})(J_{\mathrm{Os-CH_3D}} - J_{\mathrm{Os-CHD_3}})}\right]^2\right)\left(\frac{\sigma J_{\mathrm{Os-CH_4}}}{J_{\mathrm{Os-CH_4}}}\right)^2$$

$$+ \left(\left[\frac{J_{\mathrm{Os-CH_3D}}(J_{\mathrm{Os-CH_4}} - J_{\mathrm{Os-CH_2D_2}})}{(2J_{\mathrm{Os-CH_4}} - 3J_{\mathrm{Os-CH_3D}} + J_{\mathrm{Os-CH_2D_2}})(J_{\mathrm{Os-CH_3D}} - J_{\mathrm{Os-CH_2D_2}})}\right]^2 + 16\left[\frac{J_{\mathrm{Os-CH_3D}}(J_{\mathrm{Os-CH_4}} - J_{\mathrm{Os-CHD_3}})}{(8J_{\mathrm{Os-CH_4}} - 9J_{\mathrm{Os-CH_3D}} + J_{\mathrm{Os-CHD_3}})(J_{\mathrm{Os-CH_3D}} - J_{\mathrm{Os-CHD_3}})}\right]^2 \right.$$

$$\left. + 16\left[\frac{J_{\mathrm{Os-CH_3D}}(J_{\mathrm{Os-CH_2D_2}} - J_{\mathrm{Os-CHD_3}})}{(3J_{\mathrm{Os-CH_3D}} - 4J_{\mathrm{Os-CH_2D_2}} + J_{\mathrm{Os-CHD_3}})(J_{\mathrm{Os-CH_3D}} - 4J_{\mathrm{Os-CH_2D_2}} + 3J_{\mathrm{Os-CHD_3}})}\right]^2\right)\left(\frac{\sigma J_{\mathrm{Os-CH_3D}}}{J_{\mathrm{Os-CH_3D}}}\right)^2$$

$$+ \left(\left[\frac{J_{\mathrm{Os-CH_2D_2}}(J_{\mathrm{Os-CH_4}} - J_{\mathrm{Os-CH_3D}})}{(2J_{\mathrm{Os-CH_4}} - 3J_{\mathrm{Os-CH_3D}} + J_{\mathrm{Os-CH_2D_2}})(J_{\mathrm{Os-CH_3D}} - J_{\mathrm{Os-CH_2D_2}})}\right]^2 + \left[\frac{J_{\mathrm{Os-CH_2D_2}}(J_{\mathrm{Os-CH_4}} - J_{\mathrm{Os-CHD_3}})}{(2J_{\mathrm{Os-CH_4}} - 3J_{\mathrm{Os-CH_2D_2}} + J_{\mathrm{Os-CHD_3}})(J_{\mathrm{Os-CH_2D_2}} - J_{\mathrm{Os-CHD_3}})}\right]^2 \right.$$

$$\left. + 16\left[\frac{J_{\mathrm{Os-CH_2D_2}}(J_{\mathrm{Os-CH_3D}} - J_{\mathrm{Os-CHD_3}})}{(3J_{\mathrm{Os-CH_3D}} - 4J_{\mathrm{Os-CH_2D_2}} + J_{\mathrm{Os-CHD_3}})(J_{\mathrm{Os-CH_3D}} - 4J_{\mathrm{Os-CH_2D_2}} + 3J_{\mathrm{Os-CHD_3}})}\right]^2\right)\left(\frac{\sigma J_{\mathrm{Os-CH_2D_2}}}{J_{\mathrm{Os-CH_2D_2}}}\right)^2$$

$$+ \left(\left[\frac{J_{\mathrm{Os-CHD_3}}(J_{\mathrm{Os-CH_4}} - J_{\mathrm{Os-CH_2D_2}})}{(2J_{\mathrm{Os-CH_4}} - 3J_{\mathrm{Os-CH_2D_2}} + J_{\mathrm{Os-CHD_3}})(J_{\mathrm{Os-CH_2D_2}} - J_{\mathrm{Os-CHD_3}})}\right]^2 + 16\left[\frac{J_{\mathrm{Os-CHD_3}}(J_{\mathrm{Os-CH_4}} - J_{\mathrm{Os-CH_3D}})}{(8J_{\mathrm{Os-CH_4}} - 9J_{\mathrm{Os-CH_3D}} + J_{\mathrm{Os-CHD_3}})(J_{\mathrm{Os-CH_3D}} - J_{\mathrm{Os-CHD_3}})}\right]^2 \right.$$

$$\left. + 16\left[\frac{J_{\mathrm{Os-CHD_3}}(J_{\mathrm{Os-CH_3D}} - J_{\mathrm{Os-CH_2D_2}})}{(3J_{\mathrm{Os-CH_3D}} - 4J_{\mathrm{Os-CH_2D_2}} + J_{\mathrm{Os-CHD_3}})(J_{\mathrm{Os-CH_3D}} - 4J_{\mathrm{Os-CH_2D_2}} + 3J_{\mathrm{Os-CHD_3}})}\right]^2\right)\left(\frac{\sigma J_{\mathrm{Os-CHD_3}}}{J_{\mathrm{Os-CHD_3}}}\right)^2$$

$$+ \left(\left[\ln\sqrt{\frac{J_{\mathrm{Os-CH_3D}} - J_{\mathrm{Os-CH_2D_2}}}{2J_{\mathrm{Os-CH_4}} - 3J_{\mathrm{Os-CH_3D}} + J_{\mathrm{Os-CH_2D_2}}}}\right]^2 + \left[\ln\sqrt{\frac{3(J_{\mathrm{Os-CH_2D_2}} - J_{\mathrm{Os-CHD_3}})}{2J_{\mathrm{Os-CH_4}} - 3J_{\mathrm{Os-CH_2D_2}} + J_{\mathrm{Os-CHD_3}}}}\right]^2 + \left[\ln\sqrt{\frac{3(J_{\mathrm{Os-CH_3D}} - J_{\mathrm{Os-CHD_3}})}{8J_{\mathrm{Os-CH_4}} - 9J_{\mathrm{Os-CH_3D}} + J_{\mathrm{Os-CHD_3}}}}\right]^2 \right.$$

$$\left. + \left[\ln\sqrt{-\frac{J_{\mathrm{Os-CH_3D}} - 4J_{\mathrm{Os-CH_2D_2}} + 3J_{\mathrm{Os-CHD_3}}}{3J_{\mathrm{Os-CH_3D}} - 4J_{\mathrm{Os-CH_2D_2}} + J_{\mathrm{Os-CHD_3}}}}\right]^2\right)\left(\frac{\sigma T}{T}\right)^2\Bigg]$$

Crystallographic Details. Single crystals of $(C_5Me_5)Os(dfmpm)Br$ were mounted on glass fibers with Paratone®-N oil (Exxon)[58] and immediately cooled to -173 °C in a cold nitrogen gas stream on the diffractometer. Standard peak search and indexing procedures gave rough cell dimensions, and least squares refinement using 3313 reflections yielded the cell dimensions given in Table 1.

Data were collected with an area detector by using the measurement parameters listed in Table 1. The metric parameters of the lattice indicated orthorhombic symmetry, but the diffraction intensities were more consistent with monoclinic symmetry with β = 90.008(2)°. The systematic absences for 0*k*0, $k \neq 2n$, and *h*0*l*, $l \neq 2n$, were uniquely consistent with the space group $P2_1/c$, which was confirmed by the success of the subsequent refinement. The measured intensities were reduced to structure factor amplitudes and their estimated standard deviations (esd's) by correction for background, scan speed, and Lorentz and polarization effects. Six frame series were integrated and filtered for statistical outliers using SAINT,[59] then corrected for absorption by multi-scan methods using SADABS v2014/5.[60] The minimum and maximum transmission factors were 0.604 and 0.728. No decay correction was applied. Symmetry equivalent reflections were averaged to yield the set of unique data. All 8140 unique data were used in the least squares refinement.

Correct positions for the osmium and bromine atoms were deduced from a Patterson map (SHELXTL).[61] Subsequent least-squares refinement and difference Fourier calculations revealed the positions of the remaining non-hydrogen atoms, although early in the refinement some restraints were applied to aid the least-squares convergence. The analytical approximations to the scattering factors were used, and all structure factors were corrected for both real and imaginary components of anomalous dispersion. At this point, the nearness of β to 90°, the large values of the weighted and unweighted residuals, and the large number of reflections for which $I_{obs} >> I_{calc}$ suggested that the crystal was twinned by pseudomerohedry. Applying the twin law that relates

hkl to $\bar{h}\bar{k}l$, i.e., rotation about the *c**-axis, led to a substantial reduction in the residuals, and all model restraints could be lifted. The intensities were calculated from the equation $I = xI_a + (1-x)I_b$, where *x* is a scale factor that relates the volumes of the twin components. The scale factor refined to a value of 0.318(1). The quantity minimized by the least-squares program was $\Sigma w(F_o^2 - F_c^2)^2$, where $w = \{[\sigma(F_o^2)]^2 + (0.267P)^2\}^{-1}$ and $P = (F_o^2 + 2F_c^2)/3$. In the final cycle of least

Table 3.1. Crystallographic data for $(C_5Me_5)Os(dfmpm)Br$ at 100 K.

formula	$C_{15}H_{17}BrF_{12}OsP_2$
FW (g mol^{-1})	757.34
λ (Å)	0.71073
crystal system	monoclinic
space group	$P2_1/c$
a (Å)	11.562(2)
b (Å)	15.822(3)
c (Å)	242.194(5)
α (°)	90
β (°)	90.008(7)
γ (°)	90
V (Å^3)	4425.7(16)
Z	8
ρ_{calc} (g cm^{-3})	2.273
μ (mm^{-1})	7.81
absorption correction	multi-scan
max. min. transm. factors	0.604, 0.430
data/restraints/parameters	8140/0/728
goodness-of-fit on F^2	1.022
*R*1 [$I > 2\sigma(I)$]	0.0832
w*R*2 (all data)	0.1074
largest diff. peak and hole (e·Å^{-3})	1.353/–1.921

squares, independent anisotropic displacement factors were refined for the non-hydrogen atoms. Hydrogen atoms were placed in idealized locations with the methylene and methyl C-H distances equal to 0.99 and 0.98 Å, respectively; displacement parameters for the methylene and methyl hydrogens were set equal to 1.2 and 1.5 times U_{eq} for the attached carbon, respectively. Successful convergence was indicated by the maximum shift/error of 0.003 for the last cycle. Final refinement parameters are given in Table 1. The largest peak in the final Fourier difference map (1.35 eÅ^{-3}), which was located 0.72 Å from Os2, is a heavy atom ripple. A final analysis of variance between observed and calculated structure factors showed no apparent errors.

Single crystals of (C_5Me_5)Os(dfmpm)Me grown by cooling a saturated pentane solution to –20 °C under argon were mounted on glass fibers with Paratone®-N oil (Exxon)[58] and immediately cooled to –100 °C in a cold nitrogen gas stream on the diffractometer. Standard peak search and indexing procedures gave rough cell dimensions, and least squares refinement using 9788 reflections yielded the cell dimensions given in Table 3.2.

Data were collected with an area detector by using the measurement parameters listed in Table 3.2. The triclinic lattice and the average values of the normalized structure factors suggested the space group $P\bar{1}$, which was confirmed by the success of the subsequent refinement. The measured intensities were reduced to structure factor amplitudes and their estimated standard deviations (esd's) by correction for background, scan speed, and Lorentz and polarization effects. Twenty-four frame series were integrated and filtered for statistical outliers using SAINT,[59] then corrected for absorption by face-indexed methods using SADABS v2012/1.[60] The maximum and minimum transmission factors were 0.605 and 0.208. Symmetry equivalent reflections were averaged to yield the set of unique data. All 5438 unique data were used in the least squares refinement.

Correct positions for the osmium and phosphorus atoms were deduced from a Patterson map (SHELXTL).[62] Subsequent least-squares refinement and difference Fourier calculations revealed the positions of the remaining non-hydrogen atoms. The quantity minimized by the least-squares program was $\Sigma w(F_o^2 - F_c^2)^2$, where $w = \{[\sigma(F_o^2)]^2 + (0.160P)^2 + 0.197P\}^{-1}$ and $P = (F_o^2 + 2F_c^2)/3$. The analytical approximations to the scattering factors were used, and all

Table 3.2. Crystallographic data for $(C_5Me_5)Os(dfmpm)Me$ at 173 K.

formula	$C_{16}H_{20}F_{12}OsP_2$
FW (g mol^{-1})	692.49
λ (Å)	0.71073
crystal system	triclinic
space group	$P\bar{1}$
a (Å)	8.5360(8)
b (Å)	9.0259(9)
c (Å)	14.8664(14)
α (°)	92.993(5)
β (°)	99.785(5)
γ (°)	106.416(5)
V (Å^3)	1076.60(18)
Z	2
ρ_{calc} (g cm^{-3})	2.136
μ (mm^{-1})	6.174
absorption correction	face-indexed
max. min. transm. factors	0.605, 0.208
data/restraints/parameters	5438/0/298
goodness-of-fit on F^2	1.063
*R*1 [$I > 2\sigma(I)$]	0.0187
w*R*2 (all data)	0.0398
largest diff. peak and hole (e·Å^{-3})	0.644/–0.560

structure factors were corrected for both real and imaginary components of anomalous dispersion. In the final cycle of least squares, independent anisotropic displacement factors were refined for the non-hydrogen atoms. All of the hydrogen atoms could be located in the difference maps, but in the final model only those on the Os–CH_3 group were refined freely with independent isotropic displacement parameters; the remaining hydrogen atoms were placed in idealized positions with calculated displacement parameters. The C_5Me_5 methyl groups were allowed to rotate about the C–C axis to find the best least-squares positions. The displacement parameters for methylene hydrogens were set equal to 1.2 times U_{eq} for the attached carbon; those for C_5Me_5 methyl hydrogens were set to 1.5 times U_{eq}. An isotropic extinction parameter was refined to a final value of $x = 7(2) \times 10^{-7}$ where F_c is multiplied by the factor $k[1 + F_c^2 x\lambda^3/\sin 2\theta]^{-1/4}$ with k being the overall scale factor. Successful convergence was indicated by the maximum shift/error of 0.003 for the last cycle. Final refinement parameters are given in Table 1. The largest peak in the final Fourier difference map (0.64 eÅ^{-3}) was located 1.12 Å from Os1. A final analysis of variance between observed and calculated structure factors showed no apparent errors.

CIF and FCF files for the structures of (C_5Me_5)Os(dfmpm)Br and (C_5Me_5)Os(dfmpm)Me are available free of charge from the Cambridge Crystallographic Data Centre under CCDC numbers 1873058 and 1405251, respectively.[63]

References

1. Crabtree, R. H.; Lavin, M. *J. Chem. Soc., Chem. Commun.* **1985**, 794-795.
2. Crabtree, R. H.; Lavin, M.; Bonneviot, L. J. *J. Am. Chem. Soc.* **1986**, *108*, 4032-4037.
3. Kubas, G. J. *Metal Dihydrogen and σ-Bond Complexes: Structure, Theory, and Reactivity*; Kluwer Academic Publishers: New York, 2001.

4. Gross, C. L. *Pentamethylcyclopentadienyl Osmium Chemistry: An Approach to Transition Metal Alkane Complexes.* Ph.D. Thesis, University of Illinois, Urbana, IL, 1997.

5. Conroy-Lewis, F. M.; Simpson, S. J. *J. Chem. Soc., Chem. Commun.* **1987**, 1675-1676.

6. Chinn, M. S.; Heinekey, D. M. *J. Am. Chem. Soc.* **1990**, *112*, 5166-5175.

7. Jia, G.; Ng, W. S.; Yao, J. *Organometallics* **1996**, *15*, 5039-5045.

8. Gross, C. L.; Girolami, G. S. *J. Am. Chem. Soc.* **1998**, *120*, 6605-6606.

9. Martin, R. L. *J. Am. Chem. Soc.* **1999**, *121*, 9459-9460.

10. Jew, R. L. *Steric and Electronic Effects Induced by Ancillary Ligand Substitutions on Cyclopentadienyl Osmium Complexes.* Ph.D. Thesis, University of Illinois, Urbana, IL, 2008.

11. Dickinson, P. W. *Trispyrazolylborate and Tetramethylcyclopentadienyl Osmium Chemistry: Toward Methane Coordination Complexes.* Ph.D. Thesis, University of Illinois, Urbana, IL, 2006.

12. Flener-Lovitt, C.; Woon, D. E.; Dunning, T. H.; Girolami, G. S. *J. Phys. Chem. A* **2010**, *114*, 1843-1851.

13. Flener, C. *Quantum Mechanical Analysis of Donor-Acceptor Interactions in Organometallic Complexes and Comparative Analysis of Class Size and Teacher Experience on Student Satisfaction and Learning.* Ph.D. Thesis, University of Illinois, Urbana, IL, 2009.

14. Gross, C. L.; Wilson, S. R.; Girolami, G. S. *J. Am. Chem. Soc.* **1994**, *116*, 10294-10295.

15. Gross, C. L.; Brumaghim, J. L.; Jefferis, J. M.; Dickinson, P. W.; Girolami, G. S.; Gribble, C. W.; Tilley, T. D. *Inorg. Synth.* **2014**, *36*, 72-77.

16. Gross, C. L.; Girolami, G. S. *Organometallics* **1996**, *15*, 5359-5367.

17. Brumaghim, J. L. *Synthesis, Characterization, and Ring-Opening Metathesis Polymerization Activity of Pentamethylcyclopentadienyl Osmium Complexes.* Ph.D. Thesis, University of Illinois, Urbana, IL, 1999.

18. Karsch, H. H.; Schmidbaur, H. *Z. Naturforsch., B: Anorg. Chem., Org. Chem.* **1977**, *32B*, 762-767.

19. Harris, R. K. *Can. J. Chem.* **1964**, *42*, 2275-2281.

20. Bernskoetter, W. H.; Schauer, C. K.; Goldberg, K. I.; Brookhart, M. *Science* **2009**, *326*, 553-556.

21. Bordwell, F. G.; Branca, J. C.; Hughes, D. L.; Olmstead, W. N. *J. Org. Chem.* **1980**, *45*, 3305-3313.

22. Chipanina, N. N.; Sterkhova, I. V.; Aksamentova, T. N.; Sherstyannikova, L. V.; Kukhareva, V. A.; Shainyan, B. A. *Russ. J. Gen. Chem.* **2008**, *78*, 2363-2373.

23. Koppel, I. A.; Taft, R. W.; Anvia, F.; Zhu, S.-Z.; Hu, L.-Q.; Sung, K.-S.; DesMarteau, D. D.; Yagupolskii, L. M.; Yagupolskii, Y. L.; Ignat'ev, N. V.; Kondratenko, N. V.; Volkonskii, A. Y.; Vlasov, V. M.; Notario, R.; Maria, P.-C. *J. Am. Chem. Soc.* **1994**, *116*, 3047-3057.

24. Leito, I.; Raamat, E.; Kütt, A.; Saame, J.; Kipper, K.; Koppel, I. A.; Koppel, I.; Zhang, M.; Mishima, M.; Yagupolskii, L. M.; Garlyauskayte, R. Y.; Filatov, A. A. *J. Phys. Chem. A* **2009**, *113*, 8421-8424.

25. Stoyanov, E. S.; Kim, K.-C.; Reed, C. A. *J. Phys. Chem. A* **2004**, *108*, 9310-9315.

26. The pKa values and associated references were obtained from the Internet Bond-energy Databank (*i*BonD), © Tsinghua University and Nankai University, all rights reserved. http://ibond.nankai.edu.cn

27. Lias, S. G.; Liebman, J. F.; Levin, R. D. *J. Phys. Chem. Ref. Data* **1984**, *13*, 695-808.

28. *Ionisation Constants of Organic Acids in Solution* In *IUPAC Chemical Data*; Serjeant, E. P., Dempsey, B., Eds.; Pergamon Press: Oxford, UK, 1979; Vol. 23.

29. At these low temperatures, it is likely that some ion paring occurs, leading to a small difference in chemical shift for the same cation in the presence of two different counteranions.

30. Bullock, R. M.; Headford, C. E. L.; Hennessy, K. M.; Kegley, S. E.; Norton, J. R. *J. Am. Chem. Soc.* **1989**, *111*, 3897-3908.

31. Schwartz, D. J.; Ball, G. E.; Andersen, R. A. *J. Am. Chem. Soc.* **1995**, *117*, 6027-6040.

32. Although examples of transition metal *cisoid*-methyl/hydride complexes abound, in our survey of the literature we found only one report[30] of a non-zero $^{2}J_{CH}$ value (7.8 Hz) for a transition metal *cisoid*-methyl/hydride complex ($Cp_2W(^{13}CH_3)H^+$). A $^{2}J_{CH}$ value was not reported for [(^{i}Pr)$_2$P(CH$_2$)$_2$P(^{i}Pr)$_2$]Pt(μ-Me)(μ-H)Yb(C$_5$Me$_5$)$_2$,[31] but the line shape of the μ-Me portion of the ^{13}C NMR spectrum at –70 °C is consistent with a $^{2}J_{CH}$ value ≤ 10 Hz.

33. Bernheim, R. A.; Lavery, B. J. *J. Chem. Phys.* **1965**, *42*, 1464.

34. Calvert, R. B.; Shapley, J. R. *J. Am. Chem. Soc.* **1978**, *100*, 7726-7727.

35. Lawes, D. J.; Geftakis, S.; Ball, G. E. *J. Am. Chem. Soc.* **2005**, *127*, 4134-4135.

36. Bennett, B.; Raynes, W. T.; Anderson, C. W. *Spectrochim. Acta* **1989**, *45A*, 821-827.

37. Brookhart, M.; Green, M. L. H. *J. Organomet. Chem.* **1983**, *250*, 395-408.

38. Sauer, S. P. A.; Raynes, W. T. *J. Chem. Phys.* **2000**, *113*, 3121-3129.

39. Raynes, W. T.; Geertsen, J.; Oddershede, J. *Chem. Phys. Lett.* **1992**, *197*, 516-524.

40. Cordero, B.; Gomez, V.; Platero-Prats, A. E.; Reves, M.; Echeverria, J.; Cremades, E.; Barragan, F.; Alvarez, S. *Dalton Trans.* **2008**, 2832-2838.

41. Chan, B.; Ball, G. E. *J. Chem. Theory Comput.* **2013**, *9*, 2199-2208.

42. Bergman, R. G.; Cundari, T. R.; Gillespie, A. M.; Gunnoe, T. B.; Harman, W. D.; Klinckman, T. R.; Temple, M. D.; White, D. P. *Organometallics* **2003**, *22*, 2331-2337.

43. Ruiz-Morales, Y.; Schreckenbach, G.; Ziegler, T. *Organometallics* **1996**, *15*, 3920-3923.

44. Garbacz, P.; Terskikh, V. V.; Ferguson, M. J.; Bernard, G. M.; Kędziorek, M.; Wasylishen, R. E. *J. Phys. Chem. A* **2014**, *118*, 1203-1212.

45. Ball, G. E.; Darwish, T. A.; Geftakis, S.; George, M. W.; Lawes, D. J.; Portius, P.; Rourke, J. P. *Proc. Natl. Acad. Sci. U.S.A.* **2005**, *102*, 1853-1858.

46. Unpublished DFT calculations[13] show that coordination of methane to the related osmium fragment $[(C_5H_5)Os(dfmpm)]^+$ results in elongation of the coordinated C–H bond to 1.153 Å.

47. Duchovic, R. J.; Hase, W. L.; Schlegel, H. B.; Frisch, M. J.; Raghavachari, K. *Chem. Phys. Lett.* **1982**, *89*, 120-125.

48. Siegel, J. S.; Anet, F. A. L. *J. Org. Chem.* **1988**, *53*, 2629-2630.

49. VT-Calibration Manual, Bruker Instruments, Inc.

50. OMNIC® is a registered trademark of Thermo Electron Scientific Instruments LLC.

51. Smit, C. J.; Van Der Koppel, N. C. G.B. Patent 2,268,489 A, December 1, 1994.

52. Desmarteau, D. D.; Witz, M. *J. Fluorine Chem.* **1991**, *52*, 7-12.

53. Krytox™ is a trademark of The Chemours Company FC, LLC.

54. Kimwipes® is a registered trademark of Kimberly-Clark Worldwide, Inc.

55. Morse, P. M.; Spencer, M. D.; Wilson, S. R.; Girolami, G. S. *Organometallics* **1994**, *13*, 1646-1655.

56. Shelby, Q. D.; Lin, W.; Girolami, G. S. *Organometallics* **1999**, *18*, 1904-1910.

57. Mathematica® Version 11.2.0.0, ©1988-2017 Wolfram Research, Inc. Mathematica® is a registered trademark of Wolfram Research, Inc.

58. Paratone® is a registered trademark of Chevron Intellectual Property LLC.

59. SAINT Version 8.34A, ©2014 Bruker AXS, all rights reserved.

60. Krause, L.; Herbst-Irmer, R.; Sheldrick, G. M.; Stalke, D. *J. Appl. Crystallogr.* **2015**, *48*, 3-10.

61. SHELXTL Version 2014/6, ©1993-2014 Bruker AXS, all rights reserved.

62. SHELXTL Version 6.12, ©2001 Bruker AXS, all rights reserved.

63. These crystallographic data files will not be made publically available by the CCDC until the structures are published in a scientific journal article.

Chapter 4. Attempts to form a ruthenium methane complex and an osmium ethane complex, and suggestions for future progress

Introduction

The previous chapter detailed the successful generation and characterization of an osmium complex featuring methane as a ligand. Several efforts were also made toward the generation of other ruthenium and osmium complexes with light alkanes, and these efforts are discussed in this chapter.

In 1998, Gross and Girolami showed that protonation of the Os^{II} complex $(C_5Me_5)Os(dmpm)Me$, where dmpm is bis(dimethylphosphino)methane, gave an equilibrium mixture of a classical methyl/hydride complex and a methane coordination complex, but the equilibrium strongly favored the methyl/hydride tautomer (so much so that the methane complex was not directly detectable in solution).[1] This finding showed that the $(C_5Me_5)Os(dmpm)^+$ fragment is sufficiently electron rich to fully populate the C–H σ* orbitals of methane and thus favor the oxidative addition product. In order to reverse the relative thermodynamic stabilities of the methyl/hydride and methane tautomers, the metal center must be rendered slightly less electron rich. The previous chapter related one successful strategy to achieve this outcome: by changing the ligand set, in particular by changing the phosphine from dmpm to a fluorinated analog.

Another way to moderate the electron richness of a metal center is to change the metal. In particular, the ruthenium fragment $(C_5Me_5)Ru(dmpm)^+$ should be less electron rich than its Os analog,[2-5] and thus should show promise for the generation and characterization of transition metal alkane complexes. Similar reasoning led Brookhart and coworkers to switch from a square-planar iridium complex that exists as a classical methyl/hydride species[6] to its rhodium

analog, which forms a rhodium methane complex that was amenable to characterization by solution NMR spectroscopy.[7]

In fact, many years ago our group attempted to generate a ruthenium methane complex by low-temperature protonation of the ruthenium methyl complex $(C_5Me_5)Ru(dmpm)Me$.[8] Trifluoroacetic acid was the only acid studied, and the temperature during the protonation reaction, –78 °C, was—in retrospect—too high. As a result, the protonation afforded no observable methyl/hydride or methane coordination complex; only free methane was seen, along with the ruthenium byproduct $(C_5Me_5)Ru(dmpm)(\kappa^1\text{-}O_2CCF_3)$.

In view of our subsequent success in generating osmium methyl/hydride[9-11] and methane complexes by protonation of the corresponding osmium methyl complexes at or below –110 °C in $CDCl_2F$ solvent, we decided to revisit the protonation of $(C_5Me_5)Ru(dmpm)Me$ at similarly low temperatures. We also describe our initial efforts to prepare an osmium ethane complex.

Results and Discussion

Attempts to generate a ruthenium methane complex. The methyl compound $(C_5Me_5)Ru(dmpm)Me$ can readily be synthesized by our previously published route.[8] Briefly, $RuCl_3\cdot(H_2O)_x$ is treated with C_5Me_5H in refluxing methanol to give $[(C_5Me_5)RuCl_2]_2$, which is reduced with $Na[Et_3BH]$ in tetrahydrofuran to the tetramer $[(C_5Me_5)RuCl]_4$. The tetramer is cleaved with 1,5-cyclooctadiene (cod) in tetrahydrofuran to give $(C_5Me_5)Ru(cod)Cl$, which reacts with dmpm in tetrahydrofuran to yield $(C_5Me_5)Ru(dmpm)Cl$. Alkylation of this chloro compound with dimethylmagnesium in diethyl ether affords the methyl compound $(C_5Me_5)Ru(dmpm)Me$.

In our reinvestigation of the protonation of this methyl complex, we treated it with $(CF_3SO_2)_2CH_2$ at –130 °C in $CDCl_2F$. At this temperature, the ^1H NMR spectrum (Figure 4.1)

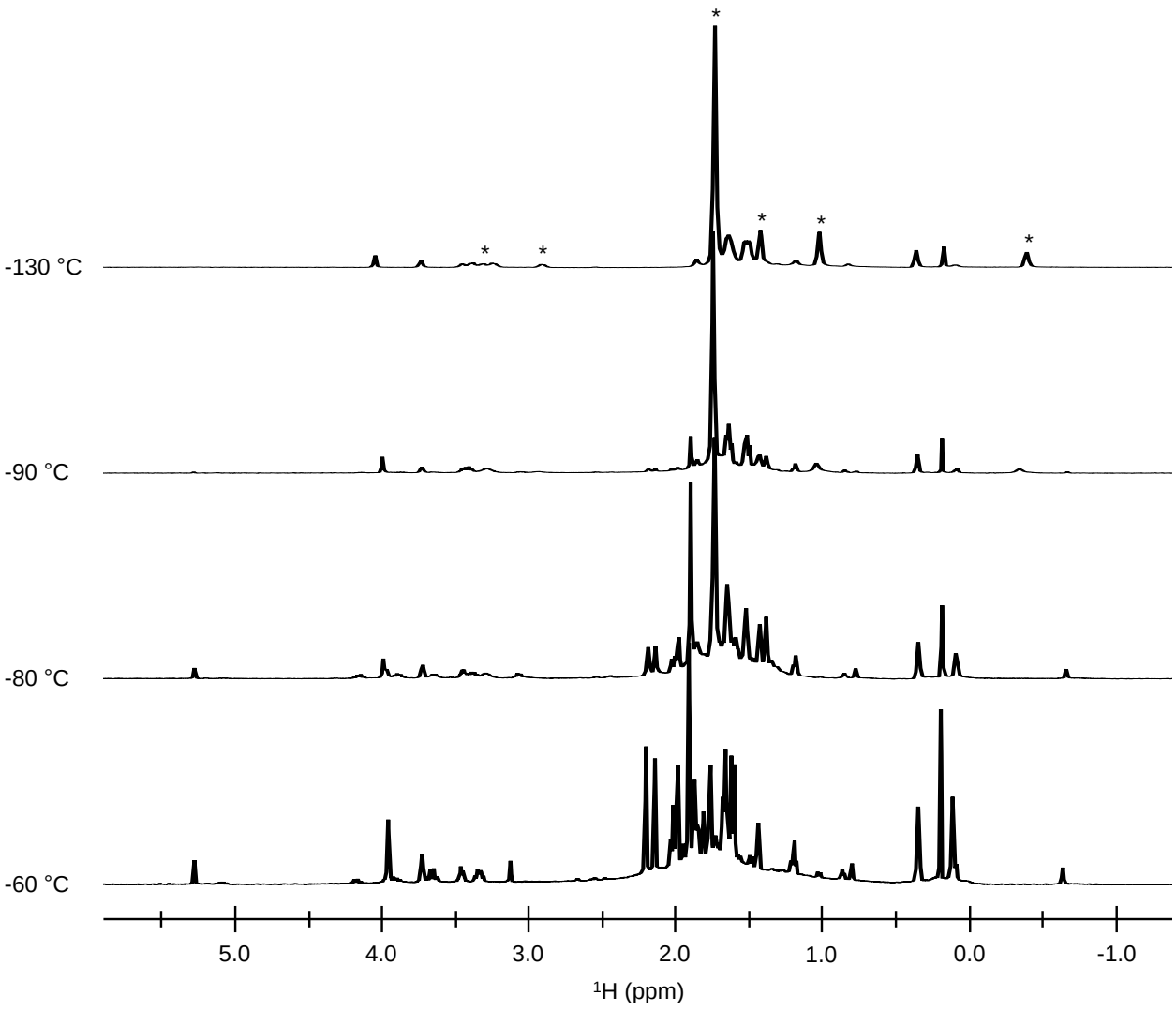

Figure 4.1. Selected region of stacked ^{1}H NMR spectra resulting from treatment of $(C_5Me_5)Ru(dmpm)Me$ with $(CF_3SO_2)_2CH_2$ in $CDCl_2F$ at –130 °C. The asterisks (*) indicate the resonances due to $(C_5Me_5)Ru(dmpm)Me$, the resonance at δ 0.16 is that of free methane, and the resonance at δ 4.04 (which moves to δ 3.97 at –60 °C) is due to $[(CF_3SO_2)_2CH]^-$.

contains resonances due to unreacted $(C_5Me_5)Ru(dmpm)Me$ and small amounts of free methane, the latter probably resulting from transient warming during sample preparation. Some unidentified byproducts are also present. Raising the temperature incrementally results in the increasingly rapid disappearance of the methyl complex (by –80 °C it has been completely consumed) and formation of additional free methane, but with no sign of a methane complex at

any time. We conclude from these observations that the ruthenium center is indeed less electron rich than its osmium analog, so much so that the protonation with the carbon acid $(CF_3SO_2)_2CH_2$ is kinetically slow until temperatures are reached (ca. –80 °C) at which the methane coordination complex, if formed, is not stable toward dissociation.

At –80 and –60 °C, ruthenium hydride resonances are seen at δ –19.4 (s), –20.4 (t, J_{PH} = 16.8 Hz), and –21.8 (s), consistent with solvent activation.[9,12] Furthermore, the presence of a resonance for dichloromethane (δ 5.28) at temperatures of –90 °C and higher is suggestive of activation of solvent C–F bonds. In analogy to the behavior seen for the corresponding osmium system,[9] these solvent activation reactions occur after the 16-electron $[(C_5Me_5)Ru(dmpm)]^+$ fragment is generated by dissociation of methane.

Treatment of $(C_5Me_5)Ru(dmpm)Me$ with the stronger acid $(CF_3SO_2)_2NH$ results in complete consumption of the starting material and loss of methane, even at –130 °C, and formation of two new ruthenium hydrides, as judged from the presence in the ^1H NMR spectrum (Figure 4.2) of resonances between δ –5 and –9. One of these hydrides gives a doublet of doublets at δ –5.77, with the two P–H coupling constants being 27.5 and 18 Hz, and the other is a doublet at δ –5.64 with J_{PH} = 11.5 Hz; the integrations of these two resonances are nearly the same. The $^{31}P\{^1H\}$ NMR spectrum (Figure 4.3) also shows that there are two major protonation products at –130 °C: one of these gives an AB quartet with δ_A = –21.6, δ_B = –23.9, and J_{AB} = 100 Hz, and the other gives a singlet at δ –29; some minor products (with yields of less than 10%) are formed as well.

The doublet of doublets at δ –5.77 in the ^1H NMR spectrum and the AB quartet in the $^{31}P\{^1H\}$ NMR spectrum are both indicative of protonation of $(C_5Me_5)Ru(dmpm)Me$ to form a hydride complex of the form $[(C_5Me_5)Ru(dmpm)X(H)]^+$ in which the X and hydride groups

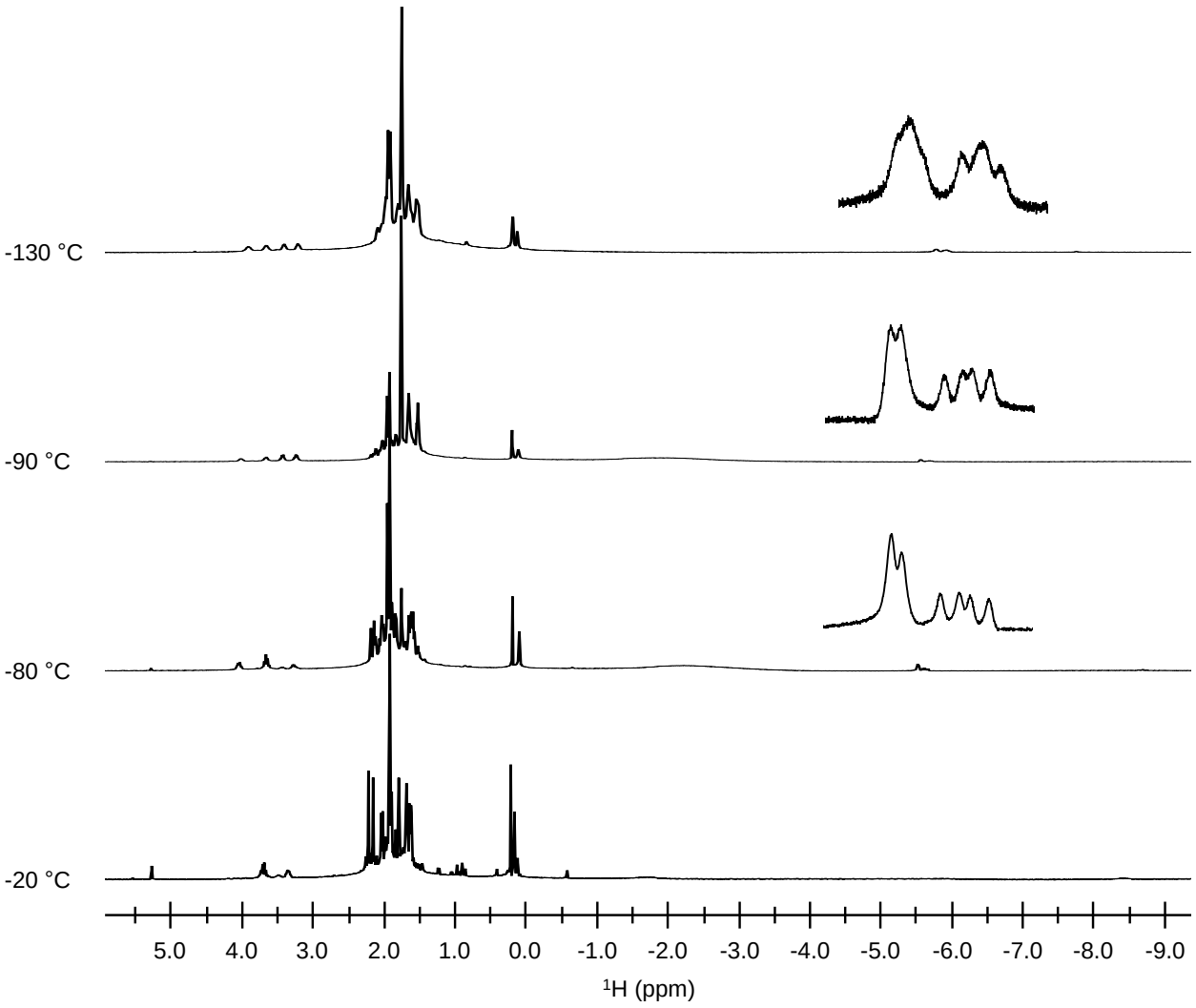

Figure 4.2. Selected region of stacked ^{1}H NMR spectra resulting from treatment of $(C_5Me_5)Ru(dmpm)Me$ with $(CF_3SO_2)_2NH$ in $CDCl_2F$ at –130 °C. The insets show detail of the hydride resonances around δ –5.5. The resonance at δ 0.18 is that of free methane.

occupy cisoid positions in a four-legged piano stool structure. Protonation of the analogous osmium complex gives a similar classical methyl/hydride product with a cisoid geometry, $[(C_5Me_5)Os(dmpm)Me(H)]^+$; the hydride resonance of this species is also a doublet of doublets with similar P–H coupling constants of 39.6 and 18.2 Hz, and the $^{31}P\{^{1}H\}$ NMR spectrum of this osmium complex also is an AB quartet with a similar J_{AB} coupling constant of 114 Hz.[1,9]

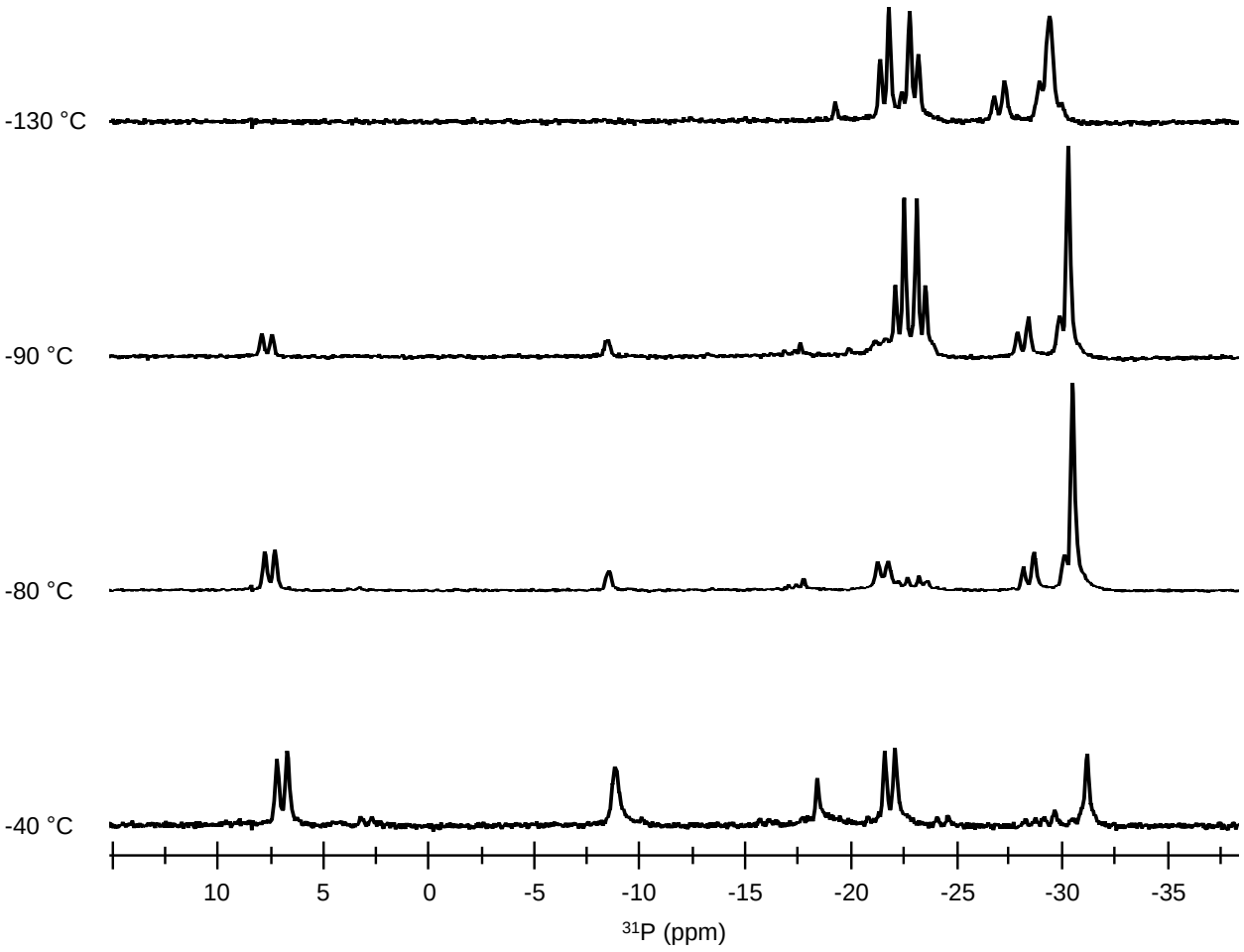

Figure 4.3. Selected region of stacked ^{31}P NMR spectra resulting from treatment of $(C_5Me_5)Ru(dmpm)Me$ with $(CF_3SO_2)_2NH$ in $CDCl_2F$ at –130 °C.

We can exclude the possibility that the X group in $[(C_5Me_5)Ru(dmpm)X(H)]^+$ is methyl on several grounds. First, there is no resonance in the ^1H NMR spectrum corresponding to a ruthenium-bound methyl group. Second, by comparison with our results for the analogous osmium system,[1] we would expect the hydride resonance of this species to exhibit line broadening above –130 °C owing to exchange with the methyl protons, but it does not, even though this exchange process should have a lower barrier than in the osmium compound. Third, if X were methyl, we would expect this complex to undergo reductive elimination at temperatures lower than the –80 to –90 °C temperatures at which this process takes place in the

analogous osmium complex. Although this $[(C_5Me_5)Ru(dmpm)X(H)]^+$ complex does eventually decompose upon warming, it is still quite evident in the spectrum at –40 °C, and its decomposition occurs without concomitant growth of the resonance for free methane. We can also exclude the possibility that X is Cl or F derived from the solvent; these complexes should be stable at room temperature, whereas this $[(C_5Me_5)Ru(dmpm)X(H)]^+$ complex is not. It is possible that X is $N(SO_2CF_3)_2$; a few transition metal coordination complexes of this anion are known.[13,14]

The species that gives the ^1H NMR doublet at δ –5.64 and the $^{31}P\{^1H\}$ NMR singlet at δ –29 is tentatively assigned as the known cationic ruthenium dihydride $[(C_5Me_5)Ru(dmpm)H_2]^+$.[15] At room temperature in dichloromethane solution, as the BAr^F_4 salt, this compound exists as a 94:6 mixture of the cisoid form (which exists as a molecular dihydrogen complex) and the transoid classical dihydride form, respectively. The reported ^{31}P NMR chemical shift for the cisoid form of δ –31 is consistent with our observation of a singlet at δ –29; the ^1H NMR chemical shift of δ –7.77 is less consistent, and it is not clear whether the different chemical shift can be attributed to the different temperature, solvent, and counterion we employed, or indicates that the complex we see is not this dihydride cation (a definitive experiment, which we have not done, is to protonate the known[8] hydride $(C_5Me_5)Ru(dmpm)H$ with $(CF_3SO_2)_2NH$ at low temperature in $CDCl_2F$). The doublet ^1H NMR line shape, however, is entirely consistent with an AA′XX′ spin system, as we have seen for the cisoid form of the analogous osmium complex $[(C_5Me_5)Os(dmpm)H_2]^+$.[9] The line shape is actually not a doublet, but instead the two lines are the most intense components of a second-order pattern; the weaker components of the pattern are lost in the baseline of the spectrum. Finally, integrations of the ^{31}P NMR resonances suggest that the $[(C_5Me_5)Ru(dmpm)X(H)]^+$ and $[(C_5Me_5)Ru(dmpm)H_2]^+$ complexes are present in a 2:1

molar ratio, respectively; this molar ratio is also consistent with the observation in the ^{1}H NMR spectrum that the integrated intensities of the doublet of doublets due to $[(C_5Me_5)Ru(dmpm)X(H)]^+$ and the apparent doublet due to $[(C_5Me_5)Ru(dmpm)H_2]^+$ are about equal.

The ^{1}H and ^{31}P NMR resonances due to the $[(C_5Me_5)Ru(dmpm)X(H)]^+$ start to disappear when the sample is warmed above –80 °C. At –60 and –40 °C, ruthenium methylidene resonances grow in at δ 15.6 (d, J_{HH} = 2.5 Hz) and 14.6 (td, J_{PH} = 8.6 Hz, J_{HH} = 2.5 Hz). In studies of the protonation of related osmium methyl complexes, the formation of hydride and methylidene complexes was observed after dissociation of methane; this transformation is thought to involve activation of the solvent.[9,12] Once again, as in the reaction of $(C_5Me_5)Ru(dmpm)Me$ with the carbon acid $(CF_3SO_2)_2CH_2$, a resonance for dichloromethane grows in as the temperature is raised, consistent with solvent activation.

All these observations indicate that the problem with the earlier ruthenium work was not that the temperature during the protonation step was too high, but rather that the stability of the methane complex is too low.

Attempts to generate an osmium ethyl complex. In view of the successful generation and characterization of an osmium methane complex detailed in chapter 3, we sought to extend the chemistry to other light alkane complexes. We therefore turned to the preparation of the ethyl precursor $(C_5Me_5)Os(dfmpm)Et$, which upon being protonated may afford an ethane coordination complex. The most obvious route to the ethyl precursor complex is treatment of $(C_5Me_5)Os(dfmpm)Br$ with an excess of diethylzinc in refluxing toluene, in analogy to the method we used successfully to prepare the osmium methyl complex (see chapter 3). Consistent with our observations in the methylation reaction, the reaction mixture changed from clear

orange to cloudy yellow as the reaction progressed; an excess of diethylzinc – we used ~5 equiv – appears to be necessary for the reaction to occur in a reasonable time. However, sublimation of the reaction residue gave a mixture of compounds as judged by NMR spectroscopy (Figure 4.4-4.6).

The desired ethyl complex (C_5Me_5)Os(dfmpm)Et was the principal component of the mixture: in the ^{1}H NMR spectrum (Figure 4.4), the methylene protons of the ethyl group appear as a quartet (J_{HH} = 7.4 Hz) of multiplets at δ 1.88 (partly obscured by a sharp triplet due to another species; see below) and the methyl protons of the ethyl group appear as a triplet at δ 1.56 (J_{HH} = 7.4 Hz). The multiplet structure for the methylene protons arises from coupling to the phosphorus and fluorine atoms of the dfmpm ligand, as seen for the corresponding methyl

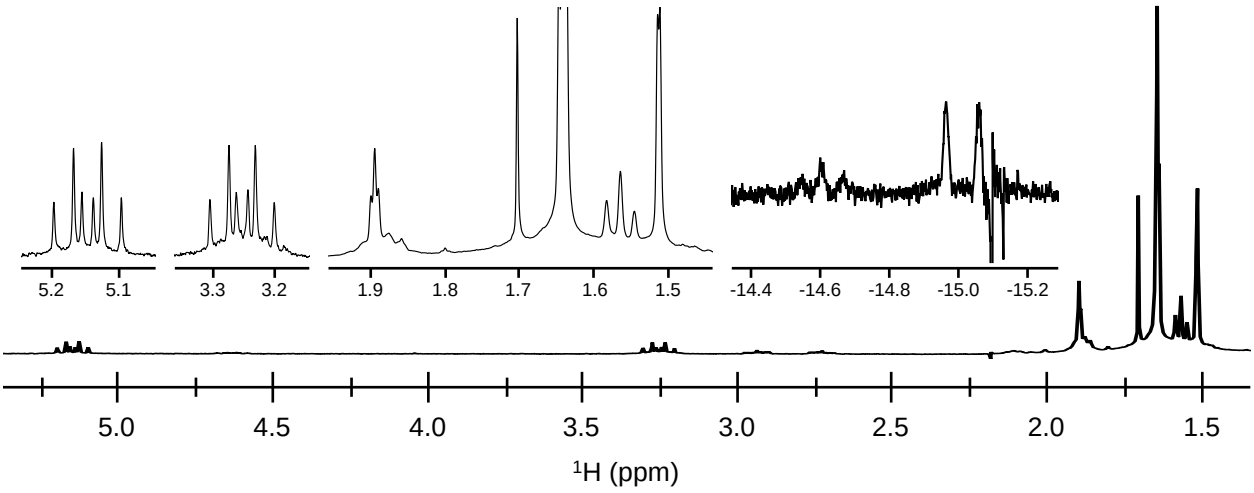

Figure 4.4. Selected region of the ^{1}H NMR spectrum in C_6D_6 resulting from treatment of (C_5Me_5)Os(dfmpm)Br with $ZnEt_2$ in refluxing toluene, followed by sublimation. The four insets show expansions of the regions near δ 5.2, near δ 3.25, between δ 2.0 and 1.4, and the hydride region. In the first three insets, all the peaks are due to (C_5Me_5)Os(dfmpm)Et except for the sharp triplet at δ 1.89 (the C_5Me_5 peak of (C_5Me_5)Os(dfmpm)H), the sharp singlet at δ 1.70 (probably the C_5Me_5 peak of $(C_5Me_5)_2$Os), and the sharp doublet at δ 1.51 (the C_5Me_5 peak of (C_5Me_5)Os(κ^1-dfmpm)(C_2H_4)H).

complex described in chapter 3. The dmpm analog $(C_5Me_5)Os(dmpm)Et$, which has been synthesized previously in our group,[12] has an ^1H NMR spectrum that is similar to that of $(C_5Me_5)Os(dfmpm)Et$ (excluding the additional PMe_2 resonances), except that the chemical shifts of the methylene and methyl resonances are almost exactly reversed: these groups give a quartet at δ 1.57 (J_{HH} = 8.0 Hz) and a triplet at δ 1.89 (J_{HH} = 7.0 Hz), respectively. The ^{19}F NMR spectrum of $(C_5Me_5)Os(dmpm)Et$ has two resonances for the two pairs of CF_3 groups (i.e., proximal and distal with respect to the C_5Me_5 ring) at δ –58.7 and –61.4 (Figure 4.5); these are deshielded by about 0.5 ppm with respect to the corresponding resonances for the analogous OsMe complex. The $^{31}P\{^1H\}$ NMR chemical shift of $(C_5Me_5)Os(dfmpm)Et$ (δ –31.8, see Figure 4.6) is shielded by 3 ppm relative to that of $(C_5Me_5)Os(dfmpm)Me$ (δ –28.8).

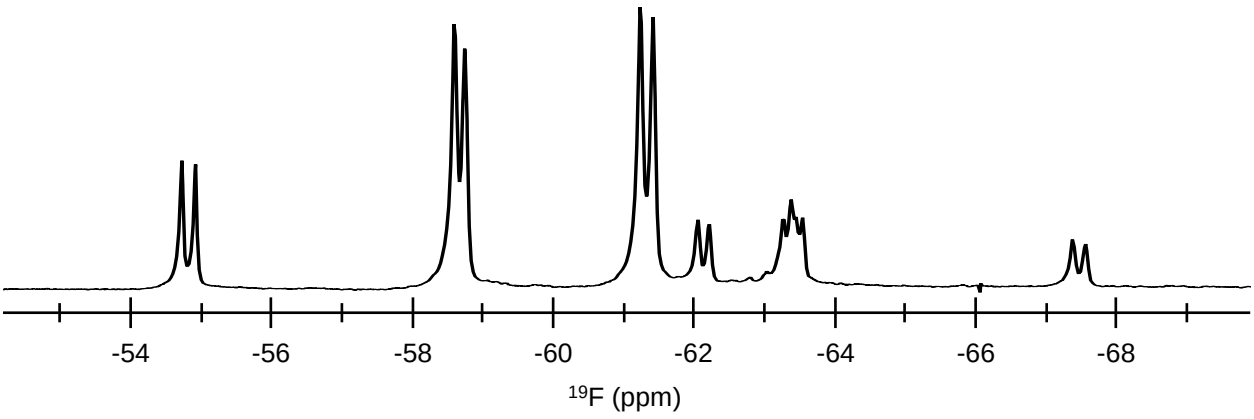

Figure 4.5. ^{19}F NMR spectrum in C_6D_6 of the mixture of $(C_5Me_5)Os(dfmpm)Et$, $(C_5Me_5)Os(\kappa^1\text{-}dfmpm)(C_2H_4)H$, and $(C_5Me_5)Os(dfmpm)H$ that is formed when $(C_5Me_5)Os(dfmpm)Br$ is treated with $ZnEt_2$ in refluxing toluene. The resonances are identified in the text; some extraneous small peaks outside this region are not shown.

About 60 mol % of the sublimate was $(C_5Me_5)Os(dfmpm)Et$; the balance consisted primarily of two different osmium hydride compounds, one of which contains coordinated ethylene (the result of β-hydrogen elimination). The ^1H, ^{19}F, and ^{31}P NMR spectra are consistent with the two osmium hydride byproducts being $(C_5Me_5)Os(\kappa^1\text{-}dfmpm)(C_2H_4)H$, which gives the

doublet at δ –15.0 in the ^{1}H NMR spectrum, and (C_5Me_5)Os(dfmpm)H, which gives the triplet at δ –14.6; in both cases the coupling is to ^{31}P spins, and the multiplicity indicates the number of phosphorus atoms bound to the osmium center.

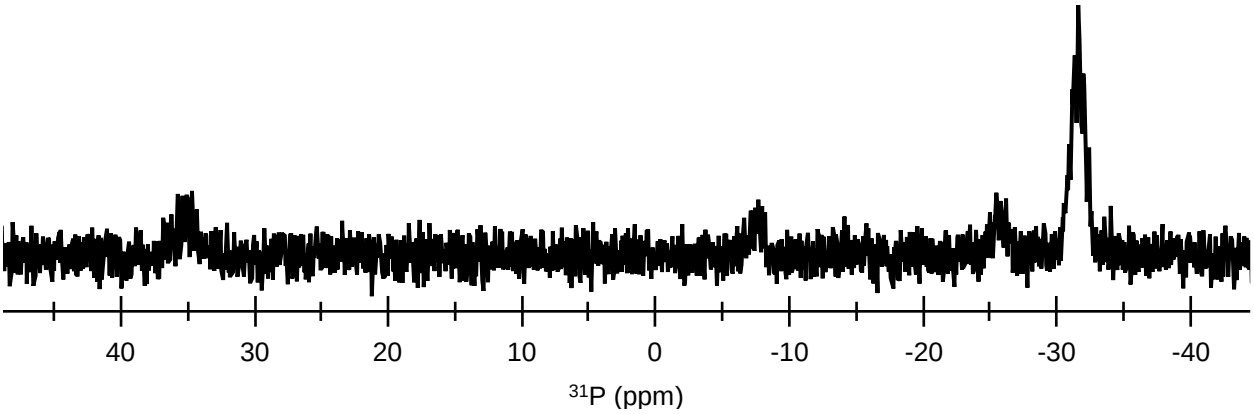

Figure 4.6. ^{31}P NMR spectrum in C_6D_6 of the mixture of (C_5Me_5)Os(dfmpm)Et, (C_5Me_5)Os(κ^1-dfmpm)(C_2H_4)H, and (C_5Me_5)Os(dfmpm)H that is formed when (C_5Me_5)Os(dfmpm)Br is treated with $ZnEt_2$ in refluxing toluene. The resonances are identified in the text.

In (C_5Me_5)Os(κ^1-dfmpm)(C_2H_4)H, the ethylene ligand gives four ^{1}H NMR resonances at δ 2.94, 2.73, 0.85, and 0.79 (Figure 4.7). The spin system is ABCDX, which shows that rotation of the ethylene ligand about the Os–C_2H_4 bond is slow on the NMR time scale, and that there are observable couplings to a fifth spin X, which is the bound phosphorus atom of the κ^1-dfmpm ligand. The resonances for the A and B spins near δ 2.8 have line shapes that clearly are based on an AB quartet in which each component is split into a doublet of doublets. The resonances for the C and D spins are strongly second-order because the chemical shifts of these two spins are very close to one another. The coupling constants within the ABCDX spin system were derived from matching the experimental line shapes to those calculated from a simulation: J_{AB} = 15 Hz, J_{AC} = –1 Hz, J_{AD} = 11 Hz, J_{AX} = 4.5 Hz, J_{BC} = 10 Hz, J_{BD} = –1 Hz, J_{BX} = 4.5 Hz, J_{CD} = 9 Hz, J_{CX} = 2 Hz, and J_{DX} = 2 Hz; the coupling constant signs are relative.[16] The 2 Hz couplings of the C

and D spins to spin X (due to the coordinated phosphorus atom) are estimates; these couplings are not resolved but instead increase the apparent line widths in the CD part of the spectrum.

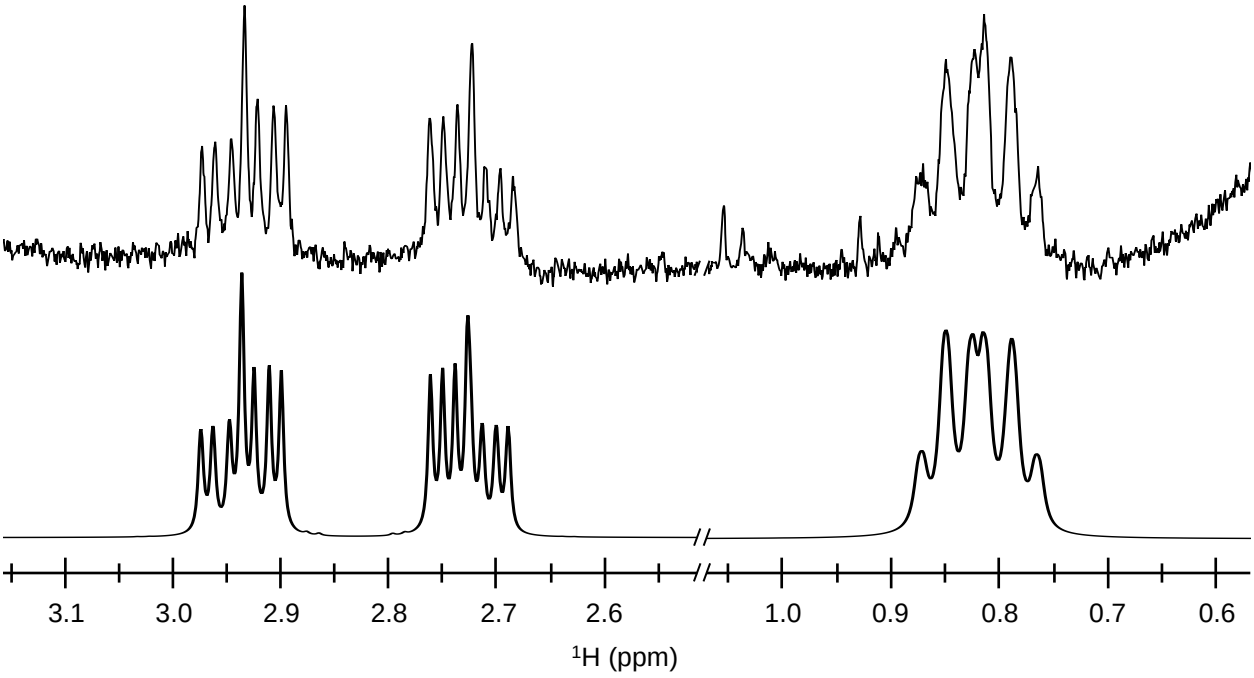

Figure 4.7. Experimental (top) and simulated (bottom) ^{1}H NMR resonances for the ethylene ligand of $(C_5Me_5)Os(\kappa^1\text{-dfmpm})(C_2H_4)H$ in C_6D_6. The simulation parameters (chemical shifts and coupling constants) are described in the text. Note the broken baselines and ppm scale.

In free alkenes, the magnitude of the J_{HH} coupling constants involving the vinylic hydrogen atoms decrease in the order *trans* (19 Hz) > *cis* (12 Hz) > *gem* (2.5 Hz).[17] For alkene ligands bound to transition metals, the relative sizes of the three J_{HH} coupling constants is not necessarily in this same order: in a dinuclear tungsten(III) alkoxide, for example, the J_{HH} coupling constants within a coordinated ethylene ligand decrease in the order *cis* (11 Hz) > *trans* (8 Hz) > *gem* (7 Hz), as determined unambiguously from a deuterium labeling study.[18] Several osmium ethylene/hydride complexes are known,[19-22] including the osmium(II) tris(pyrazolylborate) compound $[TpOs(C_2H_4)_2(PPr^i_3)]^+$, which is d_6 and octahedral like $(C_5Me_5)Os(\kappa^1\text{-dfmpm})(C_2H_4)H$. In this TpOs compound, the ethylene ligands give a ^{1}H NMR

spectrum consistent with an AA′BB′ spin system, with $J_{AA'} = J_{BB'} = 13.0$ Hz, $J_{AB} = -0.9$ Hz, and $J_{AB'} = 9.0$ Hz.[23] In view of the C_s symmetry of this TpOs compound, in which the two ethylene ligands lie off of the mirror plane (but are related to one another by it), the four hydrogen atoms on each ethylene ligand should be chemically inequivalent and should give an ABCD spin system. The observed AA′BB′ spin system shows that these ethylene ligands must be spinning rapidly about their Os–C_2H_4 axes; such a rotation exchanges hydrogen atoms that are *trans* to one another across the C=C double bond. From this information, the *trans* coupling must be between the A and A′ spins (and between B and B′), which is the largest J_{HH} coupling constant (13 Hz) of the three. Therefore the J_{HH} coupling constants in this TpOs compound follow the same trend as seen for free alkenes: *trans* > *cis* > *gem*. From the simulation, the J_{HH} coupling constants in (C_5Me_5)Os(κ^1-dfmpm)(C_2H_4)H have the following magnitude: 1 Hz, 10 Hz, and ~12 Hz, the latter being the average of one coupling of 15 Hz and another of 9 Hz. One possible assignment is *trans* (~12 Hz) > *cis* (~10 Hz) > *gem* (~1 Hz), but this would mean that the ethylene hydrogen atoms with similar chemical shifts occupy *trans* positions on the ethylene ligand, which seems unlikely. We believe that a more reasonable assignment for the coupling constants in (C_5Me_5)Os(κ^1-dfmpm)(C_2H_4)H is *cis* (~12 Hz) > *trans* (~10 Hz) > *gem* (~1 Hz), which would mean that the ethylene hydrogen atoms proximal to the phosphine have similar chemical shifts (as do the ethylene hydrogen atoms that are proximal to the hydride ligand).

In the $^{19}F\{^1H\}$ NMR spectrum of (C_5Me_5)Os(κ^1-dfmpm)(C_2H_4)H (Figure 4.5), all four CF_3 groups are chemically inequivalent: two of these (on the non-coordinated phosphorus atom) accidentally have exactly the same chemical shift of δ –54.9 and the other two (on the Os-coordinated phosphorus atom) appear at δ –62.2 and –63.5. In the $^{31}P\{^1H\}$ NMR spectrum (Figure 4.6), the non-coordinated phosphorus atom appears at δ –7.69 (which is close to the

chemical shift of δ –6.51 for the free phosphine) and the coordinated atom appears at δ 35.1. The latter is considerably deshielded (by over 50 ppm) relative to the chemical shifts of δ –18 to –31 seen for (C_5Me_5)Os(dfmpm)X compounds (X = Br, OTf, Me, Et, H) in which the phosphine is bidentate. This difference can be ascribed in part to the inductive effect of the strongly π-accepting ethylene ligand, but mostly to the known "ring effect" on the ^{31}P NMR chemical shift of chelating diphosphines.[24] We have previously reported an example of this effect in a pair of osmium(II) complexes, in which the chemical shift of the coordinated P atom of a unidentate methylene diphosphine (dmpm) is deshielded by over 30 ppm relative to the chemical shift seen for a chelating form of the same phosphine.[25]

The ^{1}H NMR spectrum of the hydride (C_5Me_5)Os(dfmpm)H (Figure 4.4) is very similar to that of its unfluorinated analog, (C_5Me_5)Os(dmpm)H,[9,26] except of course for the lack of the PMe_2 resonances. The chemical shift for the hydride ligand in (C_5Me_5)Os(dfmpm)H (δ –14.6) is only slightly upfield of that seen for (C_5Me_5)Os(dmpm)H (δ –13.9). The ^{19}F NMR spectrum of (C_5Me_5)Os(dmpm)H (Figure 4.5) has two resonances for the two pairs of CF_3 groups at δ –63.4 and –67.5; these are shielded by about 5 ppm with respect to the corresponding resonances for both the analogous OsMe and OsEt complexes. The ^{31}P{^{1}H} NMR chemical shift of (C_5Me_5)Os(dfmpm)H (δ –25.8, see Figure 4.6) is deshielded by 3 and 6 ppm with respect to the analogous OsMe and OsEt complexes, respectively.

We subsequently found that (C_5Me_5)Os(dfmpm)Et can be prepared with much smaller amounts of the hydride byproducts if the alkylation reaction is carried out for a longer time (3 days) at a lower temperature (50 °C in toluene). Under these conditions (C_5Me_5)Os(dfmpm)Et constitutes about 85 mol % of the sublimate (Figure 4.8). A small amount of the (C_5Me_5)Os(dfmpm)Br starting material was also seen in this sample. Temperatures significantly

lower than 50 °C, however, are ineffective: when the alkylation was attempted at room temperature with excess diethylzinc, no reaction occurred even after 3 days.

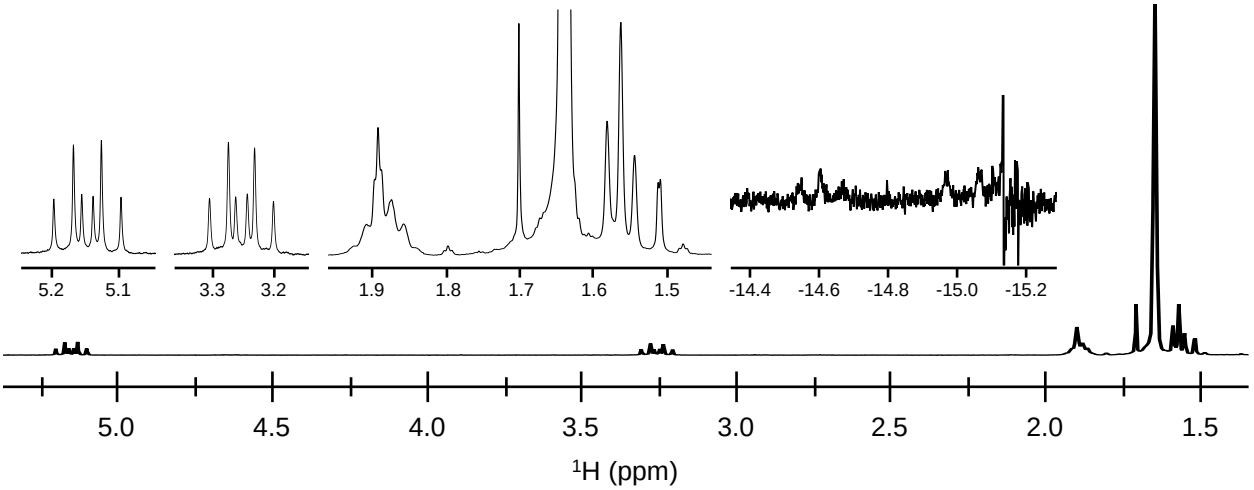

Figure 4.8. Selected region of the ^{1}H NMR spectrum in C_6D_6 resulting from treatment of (C_5Me_5)Os(dfmpm)Br with $ZnEt_2$ in toluene at 50 °C, followed by sublimation. The insets are the same as described in Figure 4.4.

In order to further minimize the amount of hydride byproducts formed, we investigated whether the alkylation could be performed at lower temperatures by replacing the bromide ligand with a more labile leaving group. Trifluoromethanesulfonate (triflate) is an excellent leaving group and has proven useful in reducing reaction times in our previous osmium chemistry.[9-12] We found that reaction of (C_5Me_5)Os(dfmpm)Br with silver triflate failed to afford the desired osmium triflate compound, so we pursued a two-step route. Conversion of (C_5Me_5)Os(dfmpm)Br to (C_5Me_5)Os(dfmpm)Me by the methods described in chapter 3, followed by treatment of this methyl compound with triflic acid in pentane, gave (C_5Me_5)Os(dfmpm)OTf as a sublimable orange solid in decent yield. Addition of exactly one equivalent of triflic acid is crucial to obtaining good yield and purity.

Treatment of (C_5Me_5)Os(dfmpm)OTf with diethylzinc in toluene at room temperature for 30 minutes gave a cloudy yellow solution, a promising sign. However, after removing the

solvent under vacuum and extracting with pentane, both the ^{19}F and ^{31}P NMR spectra of the pentane extract indicated that (C_5Me_5)Os(dfmpm)H was the main component present; only a relatively small amount of (C_5Me_5)Os(dfmpm)Et was present in the reaction mixture. It appears that the presence of the triflate anion promotes β-hydrogen elimination of the Os–Et group, even at room temperature (possibly owing to the Lewis acidity of the zinc triflate byproduct), but that higher temperatures are required to form the ethylene/hydride complex.

Suggestions for further progress

Ruthenium chemistry. Although we have had no success to date generating ruthenium alkane complexes, there are some strategies we believe might be effective. Our results suggest that the (C_5Me_5)Ru(dmpm)$^+$ fragment is insufficiently electron rich to populate one of the C–H σ* orbitals and form a strong bond with methane; i.e., methane is not far enough along the oxidative addition pathway[27,28] to create a significant barrier to loss of methane. Although the ligand framework on our piano-stool ruthenium complexes is already quite electron-rich, there are a couple of ways in which the electron richness of the ruthenium center could be further increased.

First, the electron-donating capacity of the diphosphine (dmpm) could be increased by dialkylating the methylene backbone. This approach is preferable to increasing the donor properties of the phosphine by changing the terminal alkyl groups from methyl to cyclohexyl or *tert*-butyl because we know from our experimental and DFT studies that increasing the steric bulk about the metal center decreases the metal-alkane binding energy.[9-11,29] Second, the electron-donating capacity of the cyclopentadienyl ring could be increased by replacing one or more of the five ring substituents with alkoxy, alkylsulfide, dialkylamino, or dialkylphosphino groups. Again, however, we know that such modifications do not always have the desired effect

if the increase in ligand steric size counteracts any electronically-induced increase in the metal-alkane binding energy.[9-11,29]

A different strategy for progress with the ruthenium chemistry would be to *decrease* the electron density of the ruthenium center, thus promoting greater *σ-donation* from a C–H bond of methane to ruthenium and thereby strengthening the bond between the two. This kind of interaction, which may be operative in Brookhart's rhodium methane complex,[7] is known to be responsible for the stability of a large number of transition metal dihydrogen complexes.[28] It is possible, therefore, that protonation of ruthenium alkyl complexes bearing the dfmpm ligand, (C_5Me_5)Ru(dfmpm)R, would afford observable alkane coordination complexes.

Osmium chemistry. Considering that (C_5Me_5)Os(dfmpm)Et was obtained in highest purity when (C_5Me_5)Os(dfmpm)Br was alkylated with $ZnEt_2$ at 50 °C in toluene for several days, it may prove advantageous to carry out the reaction at a slightly lower temperature for a longer time. Alternatively, pure (C_5Me_5)Os(dfmpm)Et might be obtainable by alkylating (C_5Me_5)Os(dfmpm)OTf with an excess of diethylzinc or at temperatures below 20 °C.

If such changes do not sufficiently improve the purity of the ethyl complex obtained, a better leaving group may be necessary. In view of the success we have had utilizing $(CF_3SO_2)_2NH$ (Tf_2NH) as a strong acid, (C_5Me_5)Os(dfmpm)NTf_2 may be a useful starting material. In addition to any advantage NTf_2 may confer as a leaving group, the acid Tf_2NH is an easily handled solid and thus can be weighed out precisely in small amounts much more easily than can TfOH, which is an extremely caustic liquid. Other possible leaving groups are iodide, $BAr^F{}_4$, or SbF_6, although the latter two anions will give salts that probably cannot be purified by sublimation.

It is possible that some of the osmium hydrides are formed by β-hydrogen elimination during the sublimation of the crude (C_5Me_5)Os(dfmpm)Et. If so, then crystallization is an obvious alternative purification method, although this method often gives product contaminated with small amounts of silicone grease, whose ^{1}H NMR resonance overlaps with (and often obscures) the resonance due to free methane in the protonation experiments. If this overlap proves to be a problem (as it was in protonation studies of (C_5Me_5)Os(dfmpm)Me), Krytox™ grease[30] can be used to lubricate and seal the ground-glass joints in the ethylation reaction.

Experimental

Unless stated otherwise, all manipulations were performed under argon or vacuum using standard Schlenk line or glove box techniques. Glassware was oven- or flame-dried and allowed to cool under vacuum or argon. The following starting materials were obtained from commercial sources and used as received unless stated otherwise: diethylzinc (Strem, 10 wt.% in hexanes), trifluoromethanesulfonic acid (Sigma-Aldrich). The compounds (C_5Me_5)Ru(dmpm)Me[8] and $CDCl_2F$[31] were prepared according to published procedures, and the $CDCl_2F$ was doubly distilled and stored in a PTFE-sealed glass vessel over Linde 3A or 4A molecular sieves. The compound (C_5Me_5)Os(dfmpm)Me was prepared as described in chapter 3.

NMR spectra were acquired on Varian spectrometers (Unity 400, Unity 500, VXR 500, and Unity Inova 600) at room temperature, unless specified otherwise. Positive chemical shifts indicate shifts to higher frequency relative to the following chemical shift standards: $SiMe_4$ (^{1}H, set by assigning appropriate shifts to residual solvent signals), external $CFCl_3$ in $CDCl_3$ (^{19}F), and external H_3PO_4 in D_2O (^{31}P). Default instrument parameters were used unless stated otherwise. NMR spectra were processed with the MestReNova NMR software package; manual phasing, peak picking, and integration methods were employed, and polynomial or Bernstein

polynomial (typically of order 3-8) baseline corrections were employed. Simulations of ^{1}H NMR spectra were performed using the MestReNova spin simulation tool within the NMR software package. FTIR spectra were acquired on a Thermo Nicolet IR200 spectrometer as mineral oil mulls between KBr plates. IR spectra were processed using the OMNIC® software package[32] with automatic baseline corrections.

(Pentamethylcyclopentadienyl)(trifluoromethanesulfonato)[bis(bis(trifluoromethyl)-phosphino)methane]osmium(II), (C_5Me_5)Os(dfmpm)OTf. Note: Because triflic acid is a caustic liquid, it is difficult to measure out milligram quantities precisely. We found it best to prepare a dilute solution of TfOH in CH_2Cl_2 on a larger scale, from which aliquots could be taken containing the desired amount of acid. The CH_2Cl_2 is then removed from the aliquot under vacuum, and the resulting acid is suspended in a suitable reaction solvent. Thus, triflic acid (33 mg, 0.217 mmol, obtained by evaporation of 2.17 mL of a 0.1 M solution in CH_2Cl_2) was suspended in pentane (2 mL) and cooled to 0 °C; to this vigorously stirred suspension was added a solution of (C_5Me_5)Os(dfmpm)Me (150.0 mg, 0.217 mmol) in pentane (10 mL). The mixture was allowed to warm to room temperature and then was stirred for 30 min, during which time the solution color changed from clear yellow to clear orange. The volatile materials were removed under vacuum, and the residue was extracted with Et_2O (10 mL). The extract was filtered, the filtrate was taken to dryness under vacuum, and the residue was sublimed onto a water-cooled cold finger at 70-80 °C and 10^{-2} Torr. No yield was recorded for this preparation, but material for analysis was obtained. ^{1}H NMR (C_6D_6): δ 5.53 (dt, J_{HH} = 16.8 Hz, J_{PH} = 11.0 Hz, 1H, PCH_2P), 3.68 (dt, J_{HH} = 16.7 Hz, J_{PH} = 12.6 Hz, 1H, PCH_2P), 1.45 (t, J_{PH} = 2.1 Hz, 15H, C_5Me_5). ^{19}F NMR (C_6D_6): δ –56.4 (d, J_{PF} = 74.5 Hz, 6F, $P(CF_3)_2$), –59.0 (m, 6F, $P(CF_3)_2$), –77.2 (m, 3F, OTf). ^{31}P NMR (C_6D_6): δ –18.1 (m). IR (cm^{-1}): 1506 (w), 1354 (w), 1323 (m), 1235 (m), 1210

(m), 1182 (m), 1144 (s), 1094 (w), 1031 (w), 1008 (m), 780 (w), 702 (w), 655 (w), 635 (w), 590 (w), 562 (w), 519 (w), 485 (w), 460 (w), 427 (w).

A yield for this reaction was graciously supplied by Mr. Brian Trinh. The preparation was similar to the above, except that the scale was larger (1.5 mmol TfOH and 1.4 mmol (C_5Me_5)Os(dfmpm)Me in 40 mL of pentane), the reactants were combined at room temperature, and the reaction mixture was stirred at room temperature overnight to give an orange powder. The product was isolated by filtration and dried under vacuum. Yield: 659.4 mg (55%). Unreacted (C_5Me_5)Os(dfmpm)Me (32%) can be recovered by taking the yellow filtrate to dryness under vacuum. ^{1}H and ^{19}F NMR data are consistent with those reported above.

(Pentamethylcyclopentadienyl)(ethyl)[bis(bis(trifluoromethyl)phosphino)methane]-osmium(II), (C_5Me_5)Os(dfmpm)Et. To a solution of (C_5Me_5)Os(dfmpm)Br (55.5 mg, 0.073 mmol) in toluene (5 mL) was added diethylzinc (0.063 mL, 15.8 wt. % in toluene, 0.073 mmol). The solution was heated to 50 °C overnight, during which time no visible change had occurred. More diethylzinc (0.25 mL, 15.8 wt. % in toluene, 0.29 mmol) was added, and the mixture was heated to 50 °C for 2.5 more days, after which the solution was cloudy and pale yellow in color. The volatile materials were removed under vacuum, and the residue was extracted with pentane (3 x 10 mL); the extracts were filtered and combined, and the solvent was removed under vacuum. The residue was sublimed onto a water-cooled cold finger at 45-50 °C and 10^{-2} Torr. Yield: ~14 mg (~85% is (C_5Me_5)Os(dfmpm)Et, ~20% yield). ^{1}H NMR (C_6D_6): δ 5.15 (dt, J_{HH} = 16.6 Hz, J_{PH} = 11.7 Hz, 1H, PCH_2P), 3.25 (dt, J_{HH} = 16.6 Hz, J_{PH} = 12.0 Hz, 1H, PCH_2P), 1.88 (m, 2H, $OsCH_2CH_3$), 1.64 (t, J_{PH} = 2.0 Hz, 15H, C_5Me_5), 1.56 (t, J_{HH} = 7.4 Hz, 3H, $OsCH_2CH_3$). ^{19}F NMR (C_6D_6): δ –58.7 (m), –61.4 (m). ^{31}P NMR (C_6D_6): δ –31.8 (m). Small amounts of two other compounds were present in the sublimate, as described below.

(Pentamethylcyclopentadienyl)(hydrido)(ethylene)[κ^1-bis(bis(trifluoromethyl)-phosphino)methane]osmium(II), (C_5Me_5)Os(κ^1-dfmpm)(CH_2=CH_2)H. This compound was formed as a minor byproduct in the synthesis of (C_5Me_5)Os(dfmpm)Et. ^{1}H NMR (C_6D_6): δ 2.94 (ddd, A of ABCD with J_{AB} = 15.6 Hz, J_{AC} = 3.6 Hz, J_{AD} = 12.0 Hz, 1H, OsC_2H_4), 2.73 (ddd, B of ABCD with J_{BC} = 11.0 Hz, J_{BD} = 4.0 Hz, 1H, OsC_2H_4), 2.11 (m, 2H, PCH_2P), 1.51 (d, J_{PH} = 1.2 Hz, 15H, C_5Me_5), 0.84 (m, C of ABCD with J_{CD} = 15.0 Hz, 1H, OsC_2H_4), 0.80 (m, D of ABCD, 1H, OsC_2H_4), –15.0 (d, J_{PH} = 38.2 Hz, 1H, OsH). ^{19}F NMR (C_6D_6): δ –54.9 (d, J_{PH} = 73.5 Hz, 6F, non-coordinated P(CF_3)$_2$ groups), –62.2 (d, J_{PH} = 60.9 Hz, 3F, coordinated P(CF_3)$_2$ group), –63.5 (d, J_{PH} = 61.8 Hz, 3F, coordinated P(CF_3)$_2$ group). ^{31}P NMR (C_6D_6): δ 35.1 (m, 1P, coordinated P(CF_3)$_2$ group), –7.69 (m, 1P, non-coordinated P(CF_3)$_2$ group).

(Pentamethylcyclopentadienyl)(hydrido)[bis(bis(trifluoromethyl)phosphino)-methane]osmium(II), (C_5Me_5)Os(dfmpm)H. This compound was formed as a minor byproduct in the synthesis of (C_5Me_5)Os(dfmpm)Et. ^{1}H NMR (C_6D_6): δ 4.63 (dtd, J_{HH} = 17.0 Hz, J_{PH} = 11.5 Hz, J_{HH} = 3.2 Hz, 1H, PCH_2P), 3.24 (dtd, J_{HH} = 17.0 Hz, J_{PH} = 12.4 Hz, J_{HH} = 1.9 Hz, 1H, PCH_2P), 1.89 (t, J_{PH} = 2.0 Hz, 15H, C_5Me_5), –14.6 (t, J_{PH} = 24.1 Hz, 1H, OsH). ^{19}F NMR (C_6D_6): δ –63.4 (d, J_{PH} = 71.9 Hz, 6F), –67.5 (d, J_{PH} = 65.0 Hz, 6F). ^{31}P NMR (C_6D_6): δ –25.8 (m).

Low-temperature protonation of (C_5Me_5)Ru(dmpm)Me. Note: See Appendix A for detailed procedures; Krytox™ grease (DuPont)[30] was used instead of silicone grease to lubricate the glass joints because it is more resistant to leaching by $CDCl_2F$. In a glove box, an oven-dried 5 mm NMR tube topped with a female 14/20 ground-glass joint was charged with (C_5Me_5)Ru(dmpm)Me (~7.5 mg, 19 μmol when Tf_2CH_2 was the acid used, or ~15 mg, 39 μmol when Tf_2NH was the acid used). Bis(trifluoromethanesulfonyl)methane (~6 mg, 21 μmol) or

bis(trifluoromethane)sulfonimide (~8 mg, 28 μmol) was added, being careful to avoid contact between the two reagents when Tf_2NH was the acid used. A vacuum transfer apparatus was attached to the NMR tube via the ground-glass joint and the stopcocks were all closed. The NMR tube was removed from the box and attached to the Schlenk line by means of the vacuum transfer apparatus, still being careful to avoid contact of the acid with the ruthenium compound when Tf_2NH was the acid used (the two will react in the solid state at room temperature). The NMR tube was inserted into a spinner for the NMR spectrometer, placed into a liquid nitrogen bath, and $CDCl_2F$ (1-1.5 mL) was vacuum transferred to the NMR tube. The NMR tube was placed under static vacuum and flame-sealed, and the NMR tube was inserted into a pre-cooled NMR probe (–135 °C). Tuning, matching, and shimming were performed, and spectra were obtained at the specified temperatures.

References

1. Gross, C. L.; Girolami, G. S. *J. Am. Chem. Soc.* **1998**, *120*, 6605-6606.
2. Based on comparisons of redox potentials for Ru and Os compounds with identical ligand frameworks. References 3-5 show such comparisons for monometallic (3 and 5) and bimetallic (4) compounds.
3. Shao, J.-Y.; Zhong, Y.-W. *Inorg. Chem.* **2013**, *52*, 6464-6472.
4. Nagashima, T.; Nakabayashi, T.; Suzuki, T.; Kanaizuka, K.; Ozawa, H.; Zhong, Y.-W.; Masaoka, S.; Sakai, K.; Haga, M.-a. *Organometallics* **2014**, *33*, 4893-4904.
5. Gong, Z.-L.; Yao, C.-J.; Shao, J.-Y.; Nie, H.-J.; Tang, J.-H.; Zhong, Y.-W. *Sci. China: Chem.* **2017**, *60*, 583-590.
6. Bernskoetter, W. H.; Hanson, S. K.; Buzak, S. K.; Davis, Z.; White, P. S.; Swartz, R.; Goldberg, K. I.; Brookhart, M. *J. Am. Chem. Soc.* **2009**, *131*, 8603-8613.

7. Bernskoetter, W. H.; Schauer, C. K.; Goldberg, K. I.; Brookhart, M. *Science* **2009**, *326*, 553-556.

8. Lin, W.; Wilson, S. R.; Girolami, G. S. *Organometallics* **1997**, *16*, 2987-2994.

9. Gross, C. L. *Pentamethylcyclopentadienyl Osmium Chemistry: An Approach to Transition Metal Alkane Complexes.* Ph.D. Thesis, University of Illinois, Urbana, IL, 1997.

10. Dickinson, P. W. *Trispyrazolylborate and Tetramethylcyclopentadienyl Osmium Chemistry: Toward Methane Coordination Complexes.* Ph.D. Thesis, University of Illinois, Urbana, IL, 2006.

11. Jew, R. L. *Steric and Electronic Effects Induced by Ancillary Ligand Substitutions on Cyclopentadienyl Osmium Complexes.* Ph.D. Thesis, University of Illinois, Urbana, IL, 2008.

12. Brumaghim, J. L. *Synthesis, Characterization, and Ring-Opening Metathesis Polymerization Activity of Pentamethylcyclopentadienyl Osmium Complexes.* Ph.D. Thesis, University of Illinois, Urbana, IL, 1999.

13. Bohle, D. S.; Chua, Z. *Organometallics* **2015**, *34*, 1074-1084.

14. Biancalana, L.; Bresciani, G.; Chiappe, C.; Marchetti, F.; Pampaloni, G.; Pomelli, C. S. *Phys. Chem. Chem. Phys.* **2018**, *20*, 5057-5066.

15. Law, J. K.; Mellow, H.; Heinekey, D. M. *J. Am. Chem. Soc.* **2002**, *24*, 1024-1030.

16. The AB coupling constant of 15 Hz and the CD coupling constant of 9 Hz are between similar sets of hydrogen atoms, and therefore should be similar to one another. The CD coupling constant, however, may be larger than 9 Hz: the uncertainty in this coupling constant is at least several Hz, in part because the CD portion of the spectrum is rather

broad and in part because the CD coupling constant is correlated with the chemical shift difference between the C and D spins. A small change in one of these parameters changes the value in the other, and a range of values can fit the observed line shape.

17. Pretsch, E.; Clerc, T.; Seibl, J.; Simon, W. *Tables of Spectral Data for Structure Determination of Organic Compounds*; 2nd ed.; *Transl.* Biemann, K.; Springer-Verlag: Berlin Heidelberg New York Tokyo, 1983.
18. Chisholm, M. H.; Huffman, J. C.; Hampden-Smith, M. J. *J. Am. Chem. Soc.* **1989**, *111*, 5284-5299.
19. Werner, H.; Zenkert, K. *J. Chem. Soc., Chem. Commun.* **1985**, 1607-1608.
20. Johnson, T. J.; Albinati, A.; Koetzle, T. F.; Ricci, J.; Eisenstein, O.; Huffman, J. C.; Caulton, K. G. *Inorg. Chem.* **1994**, *33*, 4966-4976.
21. Ferrando, G.; Caulton, K. G. *Inorg. Chem.* **1999**, *38*, 4168-4170.
22. Albertin, G.; Antoniutti, S.; Botter, A.; Castro, J. *Z. Anorg. Allg. Chem.* **2016**, *642*, 250-254.
23. Bajo, S.; Esteruelas, M. A.; López, A. M.; Oñate, E. *Organometallics* **2011**, *30*, 5710-5715.
24. Garrou, P. E. *Chem. Rev.* **1981**, *81*, 229-266.
25. Dickinson, P. W.; Girolami, G. S. *Inorg. Chem.* **2006**, *45*, 5215-5224.
26. Gross, C. L.; Girolami, G. S. *Organometallics* **1996**, *15*, 5359-5367.
27. Crabtree, R. H. *J. Chem. Soc., Dalton Trans.* **2001**, 2437-2450.
28. Kubas, G. J. *Metal Dihydrogen and σ-Bond Complexes: Structure, Theory, and Reactivity*; Kluwer Academic Publishers: New York, 2001.

29. Flener, C. *Quantum Mechanical Analysis of Donor-Acceptor Interactions in Organometallic Complexes and Comparative Analysis of Class Size and Teacher Experience on Student Satisfaction and Learning.* Ph.D. Thesis, University of Illinois, Urbana, IL, 2009.

30. Krytox™ is a trademark of The Chemours Company FC, LLC.

31. Siegel, J. S.; Anet, F. A. L. *J. Org. Chem.* **1988**, *53*, 2629-2630.

32. OMNIC® is a registered trademark of Thermo Electron Scientific Instruments LLC.

Chapter 5. Design of molecular precursors for the bottom-up construction of graphene nanostructures with atomically precise edge structures

Introduction

Graphene – single layers of graphite consisting of a hexagonal network of carbon one atom thick – is a fascinating material. One consequence of its extended two-dimensional π structure is that the conduction band is low enough in energy to overlap with the valence band, so that graphene is a rare example of a 2D electrical conductor.[1] As a result, graphene has been studied intensively for its potential use in future "nanoelectronic" devices.[1-12] In particular, graphene's high charge carrier mobility makes it an attractive candidate for high frequency electronics,[8] and its flexibility and physical robustness (for a 2D material) render it attractive for a variety of future applications, such as flexible electronics and transparent electrodes.[7,13] However, the absence of an appreciable band gap renders graphene problematic for uses that require materials with switching behavior (e.g., field-effect transistors) due to the lack of an off state.[14]

Because of the tremendous potential utility of a semiconducting form of graphene, many theoretical studies have been directed toward determining how to imbue graphene with a band gap.[15,16] One of the most promising approaches is reducing the dimensions of graphene from an extended sheet to a narrow ribbon on the order of a few nanometers in width. Such constructs are called graphene nanoribbons – GNRs.[15,16] Electronic perturbations from the edges of a graphene sheet increasingly affect the electronic properties as the width of the GNR narrows, and the molecular edge arrangement (armchair versus zig-zag) also impacts the electronic properties: GNRs with armchair edges are predicted to exhibit larger bandgaps than those with zig-zag edges.[16]

It has been challenging to confirm these theoretical predictions experimentally,[17] primarily because it is difficult to create graphene nanoribbons with edge structures that are perfectly defined, i.e., atomically precise. Scanning tunneling microscope (STM) lithography has succeeded in producing GNRs with widths as small as 2.5 nm whose bandgaps matched theory fairly well,[4] but STM lithography is unable to create GNRs whose edge structure is atomically precise. As a result, standing electron waves are seen in STM images of these GNRs, and these patterns become more irregular as the width of the lithographically generated GNRs is decreased, indicating disorder in the edge structure.[4] A few other methods for the generation of GNRs have been developed, such as etching with nickel nanoparticles[18] and scission of carbon nanotubes (CNTs),[19] but these methods also suffer from lack of atomic precision in the edge structure.

If GNRs could be constructed with atomically precise edges, they should exhibit better and more reproducible properties. A major breakthrough was achieved when Fasel and coworkers demonstrated the ability to form GNRs with precisely-defined edge structures by the debrominative polymerization of brominated polyaromatic hydrocarbons on gold surfaces, followed by thermally driven dehydrocyclization.[20] Although the directions of growth and the lengths of the resulting GNRs were not well-controlled, the edge structures were atomically precise (i.e., no missing or dangling bonds), and in addition the nature of the edge structure (armchair versus zig-zag) – and thus the bandgap[16] – could be completely controlled by the choice of the starting polyaromatic monomer.[20]

Methods for fabricating electronic components from graphene can be categorized as top-down (etching components from larger sheets of graphene by, e.g., lithography) and bottom-up (fabrication of the desired components from molecules, e.g., surface-assisted coupling of aromatic hydrocarbons). Top-down methods have the advantage of generally being more

amenable to large scale and high throughput, but are usually limited in resolution and control over edge structure. Bottom-up methods show greater promise for higher resolution and precise edge structure, but are generally not as scalable. The method of Fasel and coworkers represents one of the first steps toward successful bottom-up fabrication of GNRs, but much greater control over GNR length, position, and direction of growth will be needed to construct electronic components out of GNRs, and even then the throughput limitations will have to be overcome.

Despite the success of bottom-up GNR synthesis, most of the effort in experimental graphene research has continued to focus on growth of large graphene sheets, primarily by chemical vapor deposition (CVD),[6,10-12,21-30] usually using methane as the carbon source. Although in many respects CVD is an ideal method to carry out large scale graphene synthesis, the quality of CVD-grown graphene is quite sensitive to the identity and structure of the underlying growth surface. In particular, a clean surface (i.e., a surface possessing few nucleation sites) leads to higher quality films with fewer but larger domains.[28] What is still lacking, however, is the ability to grow graphene on large scale in precise locations for the direct construction of electronic components.

A method for creating patterns on hydrogen-passivated silicon with great spatial control has been developed by University of Illinois scientist Joe Lyding. His method involves the use of an STM tip to remove specific hydrogen atoms from hydrogen-passivated silicon surfaces (called depassivation).[31,32] This method can be used to create digitized (i.e., quantized) surface patterns with atomic resolution:[33] selective adsorption of various molecules on STM-depassivated silicon has been demonstrated.[34] An as-yet unrealized goal is to use such depassivated silicon surfaces in a hybrid top-down/bottom-up approach to construct graphene nanoelectronics, in which the top-down part consists of initial patterning and the bottom-up part consists of selective graphene

growth in the patterned areas. This chapter details our contributions to the goal, which at this point are still in their formative stages. The implementation of our ideas is the subject of our continuing collaboration with Professor Lyding and his research group.

Results and Discussion

Concepts for vacuum-based construction of graphene nanoelectronics. The work of Fasel and coworkers seemed to us to be a good starting point for our efforts to achieve the vacuum-based construction of graphene nanoelectronics. We envisioned that STM-patterning of hydrogen-passivated silicon followed by exposure to a polyaromatic hydrocarbon would result in selective adsorption of the hydrocarbon on the dehydrogenated areas of the patterned silicon surface. If the polyaromatic hydrocarbons can be further processed, it may be possible to develop precise control over the location, shape, and size of graphene nanostructures on silicon.

Because our collaborators have already developed the patterning technology,[31] our first step was to design volatile precursor molecules that could couple on a surface to form graphene or graphene-like carbon arrays. We chose to include in the project scope both precursors that could be adsorbed into sub-nanometer dehydrogenated areas on a silicon surface, as well as precursors capable of forming larger sheets of graphene on catalytically active surfaces such as gold, silver, and copper.

As Fasel and coworkers have shown, judicious placement of halogen atoms in the polyaromatic hydrocarbon precursors determines the shape of the graphene nanostructures that result from coupling and dehydrocyclization.[20] In order for a polyaromatic hydrocarbon to be a candidate precursor to graphene nanostructures, the following criteria should be satisfied:

1. The precursor should be volatile for facile deposition on a substrate.
2. The arrangement of carbon atoms generated by subsequent processing should not depend on which face of the precursor adsorbs to the substrate.
3. The halogen atoms, if any, should be positioned such that only one coupling arrangement is possible.
4. The structure formed after coupling should exhibit low steric strain.

Criterion 1 is self-explanatory; criteria 2-4 will become clearer from the following examples and figures.

The essential features that govern the growth of graphene or graphene-like structures from halogenated polyaromatic hydrocarbons can be nicely illustrated by considering a very simple precursor, 1,3,5-tris(2-bromophenyl)benzene (2-TBB).[35] For this molecule, debrominative coupling followed by dehydrocyclization is not expected to produce GNRs, but rather graphene sheets with periodic holes (Figure 5.1), if unrestricted growth is allowed to occur. The first step in Figure 5.1 is the debrominative coupling step, and the second is the

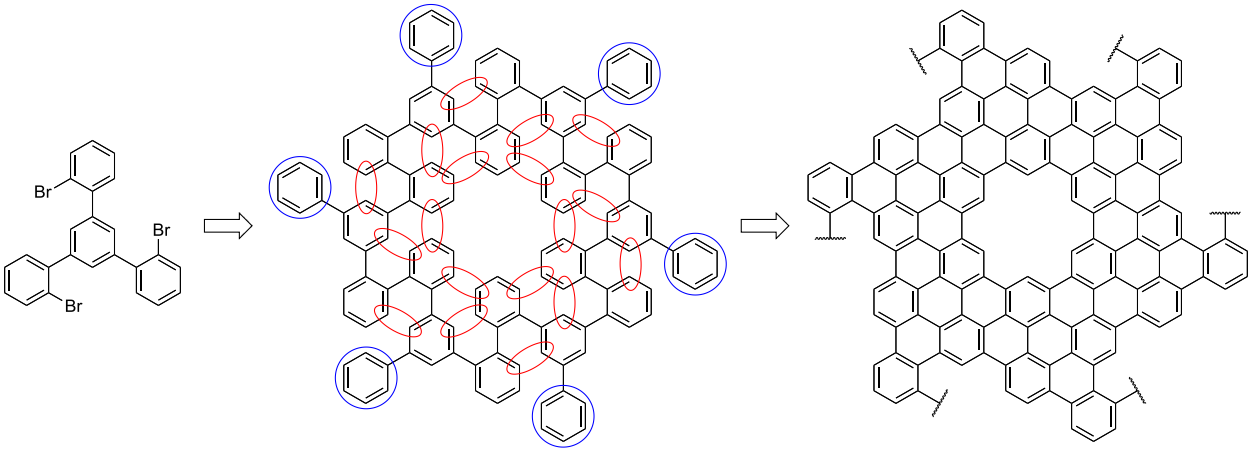

Figure 5.1. 1,3,5-tris(2-bromophenyl)benzene (left), the intermediate structure produced by debrominative coupling of the precursor molecule (middle), and the graphene structure produced by dehydrocyclization (right).

dehydrocyclization step. The blue circles in the middle structure designate phenyl rings that in principle can rotate to allieviate steric strain between neighboring rings, and the red ovals signify steric strain due to repulsive H-H contacts that cannot be relieved because the rings involved are constrained and cannot rotate. Although the graphene structure that would be produced by coupling of 2-TBB followed by dehydrocyclization is quite interesting ("holely" graphene), when considered in light of the four criteria, 2-TBB meets only criteria 1 (readily sublimable) and 3 (halogen placement permits only one coupling arrangement); different (enantiomeric) structures are formed depending on which face binds to the surface (criterion 2), and coupling of adjacent molecules generates serious steric penalties (criterion 4). We might expect, therefore, that 2-TBB would not work well to generate graphene structures, and in fact, this is the case (unpublished work by the Lyding group).

Let us next consider a different precursor, 2,2′-bis(2,5-dibromophenyl)biphenyl (2,2′-BBB), whose symmetry is such that it forms the same structure when bound to a surface by either face (Figure 5.2), so that – unlike 2-TBB – this molecule satisfies criterion 2. Figure 5.2 also shows that 2,2′-BBB should produce solid sheets of graphene with armchair edge structures; however, it is also apparent that the intermediate structure following initial surface-assisted

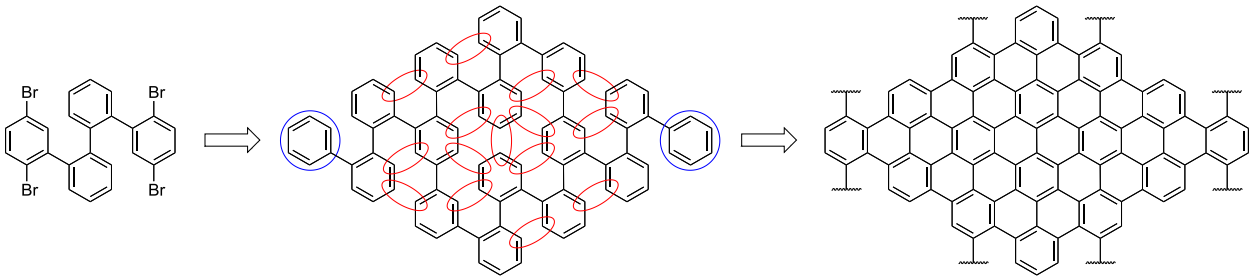

Figure 5.2. 2,2′-bis(2,5-dibromophenyl)biphenyl (left), the intermediate structure produced by coupling of the precursor molecule (middle), and the graphene structure produced by dehydrocyclization (right).

debrominative coupling suffers from considerable steric strain between neighboring phenylene rings. Therefore, 2,2′-BBB meets criteria 1, 2, and 3, but not 4 (the strain criterion).

Slight alteration of 2,2′-BBB to 2,6-bis(2,5-dibromophenyl)biphenyl (2,6-BBB) should alleviate most of the steric strain while leaving everything else essentially the same (Figure 5.3). The greatly reduced number of red ovals makes readily apparent the improvement in steric strain, which is a consequence of changing the connectivity so that there is a freely rotating phenyl ring in the 2,6-BBB molecule. Thus, 2,6-BBB satisfies all four precursor criteria.

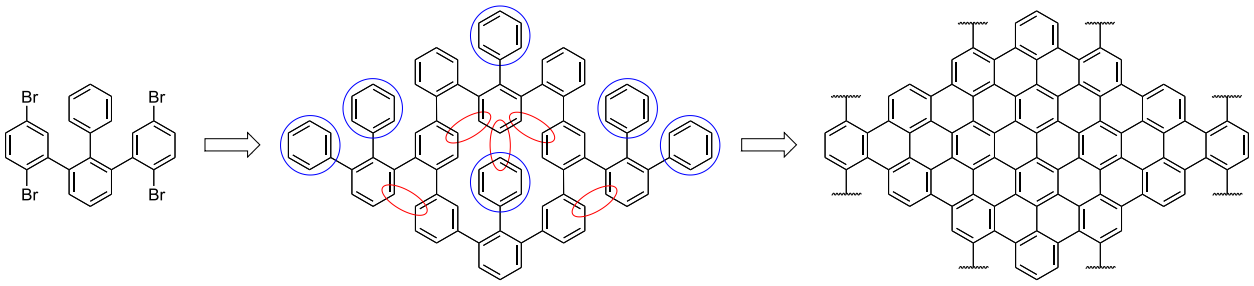

Figure 5.3. 2,6-bis(2,5-dibromophenyl)biphenyl (left), the intermediate structure produced by coupling of the precursor molecule (middle), and the graphene structure produced by dehydrocyclization (right).

Another precursor which also meets all the criteria is 1,4-bis(2,6-dibromophenyl)benzene (1,4-BBB). Figure 5.4 shows the precursor molecule, the expected intermediate structure, and the final graphene sheet profile. Only slight puckering is needed to relieve the steric strain in the intermediate structure formed by coupling of the precursor molecules.

The formation of GNRs from all of these precursors depends on the initial debrominative coupling step. As mentioned previously, adsorbing these molecules on pattered depassivated silicon should enable location control. But the dangling bonds of depassivated silicon are known to significantly perturb the electronic structure of adsorbed π-systems,[36] and one currently unanswered question is whether these perturbations interfere with the initial coupling step.

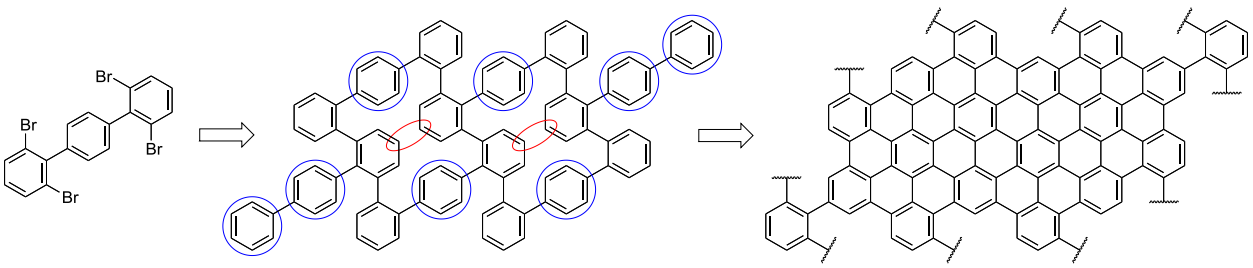

Figure 5.4. 1,4-bis(2,6-dibromophenyl)benzene (left), the intermediate structure produced by coupling of the precursor molecule (middle), and the graphene structure produced by dehydrocyclization (right).

Progress toward the synthesis of precursor molecules. 2-TBB was synthesized according to a modification of the published procedure.[35] The other precursors, however, were not known and syntheses had to be developed. For 2,2′-BBB, we envisioned a route starting with 2,2′-dinitrobiphenyl. We found that hydrogenation of this dinitro compound proceeded smoothly to the corresponding diamino compound in high yield.[37] Subsequent one-pot diazotization/iodination[38] of the diamino compound gave 2,2′-diiodobiphenyl. We expected that Suzuki coupling of this diiodo compound with 2,5-dibromophenylboronic acid should afford the desired 2,2′-BBB precursor. The boronic acid was synthesized by extra-low-temperature deprotonation of 1,4-dibromobenzene with lithium tetramethylpiperidide (LiTMP)[39] followed by trapping of the anion with trimethylborate and subsequent acidification. Unfortunately, coupling between the diiodide and the boronic acid did not proceed cleanly. Scheme 5.1 shows the attempted synthetic route for 2,2′-BBB.

For 2,6-BBB, we began with 1,3-dibromo-2-iodobenzene, which was synthesized from 1,3-dibromobenzene according to a literature procedure.[40] A Suzuki coupling of 1,3-dibromo-2-iodobenzene with phenylboronic acid gave 2,6-dibromobiphenyl. Treatment of the latter with activated magnesium (formed by reduction of magnesium chloride with powdered lithium),

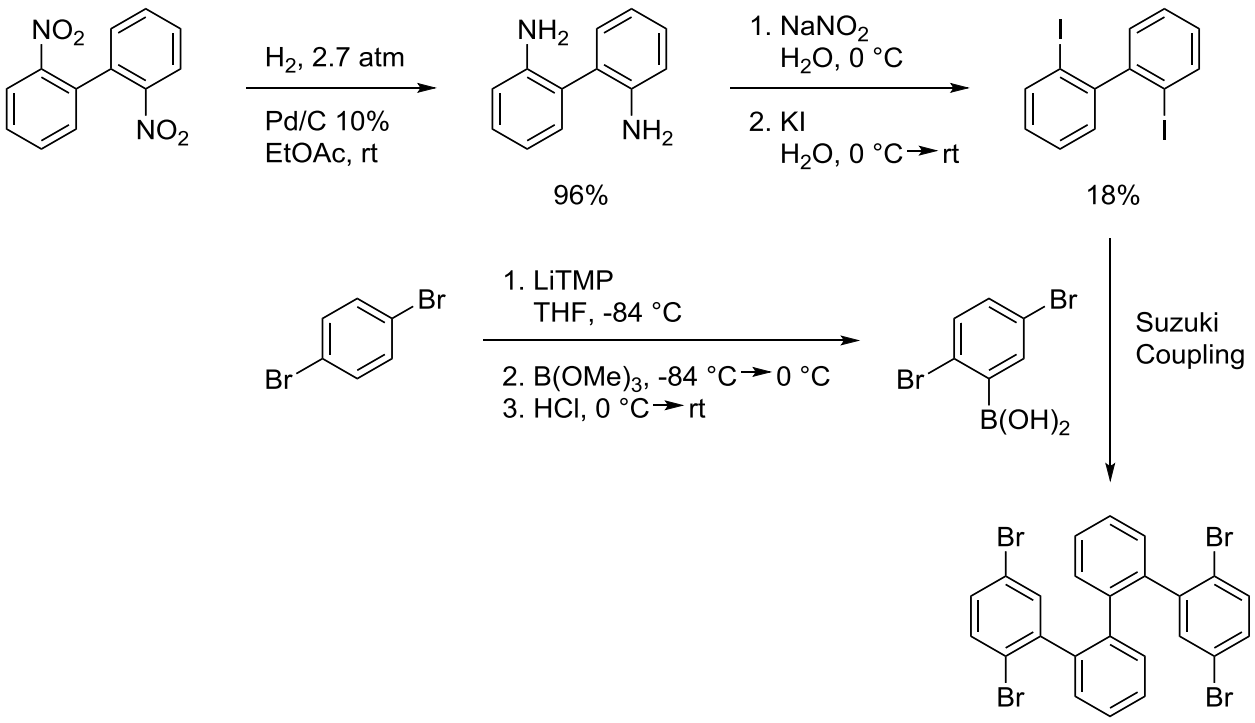

Scheme 5.1. Synthetic scheme for 2,2′-bis(2,5-dibromophenyl)biphenyl. The final Suzuki coupling did not yield the desired product.

followed by trapping with iodine, gave 2,6-diiodobiphenyl. Several attempts were made to couple the diiodide with 2,5-dibromophenylboronic acid, including conditions that worked well with the sterically encumbered 1,3-dibromo-2-iodobenzene,[41] but unfortunately, just as in the case of 2,2′-BBB, clean coupling was never achieved. Scheme 5.2 shows the attempted synthetic route for 2,6-BBB.

Because the polyarene core of 1,4-BBB is entirely different from those of the other precursors, the synthetic approach also differed significantly. Because 1,3-dibromo-2-iodobenzene was already on hand from the attempted synthesis of 2,6-BBB, 1,4-phenylenediboronic acid was the natural coupling partner, as it would directly yield 1,4-BBB. However, there turned out to be an additional challenge besides the steric hindrance of the iodide: the solubility of the diboronic acid was poor in the solvent mixture, requiring us to

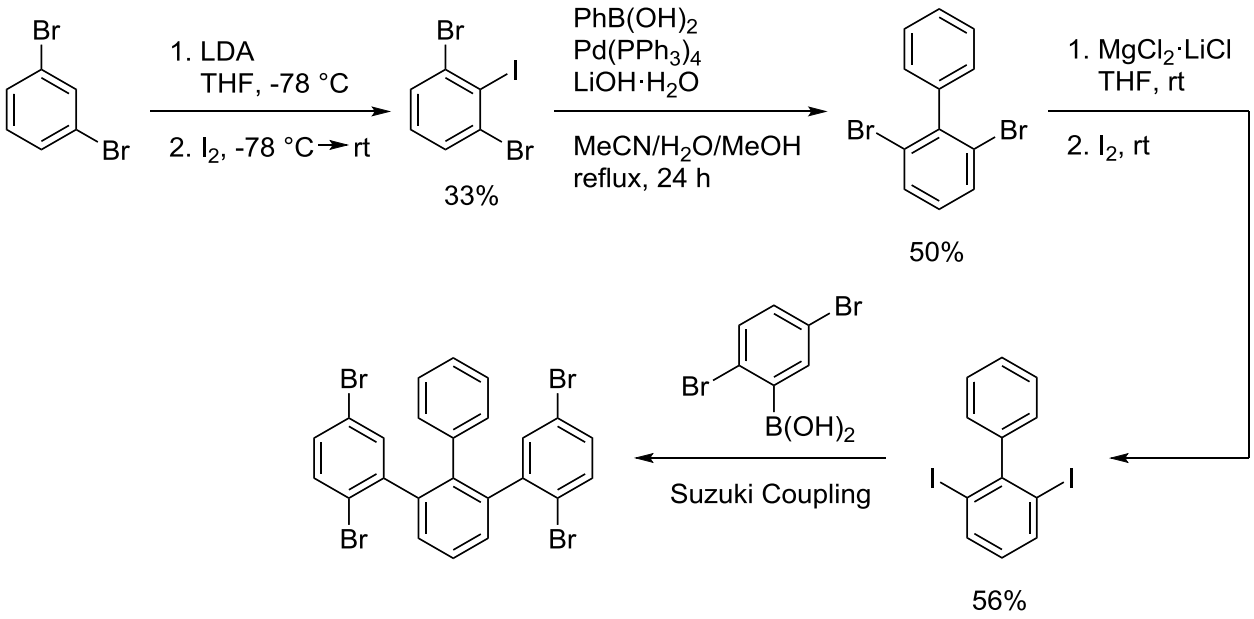

Scheme 5.2. Synthetic scheme for 2,6-bis(2,5-dibromophenyl)biphenyl. The final Suzuki coupling did not yield the desired product.

perform the reaction at low concentrations for extended time periods with methanol added to improve solubility. Scheme 5.3 shows the synthetic scheme for 1,4-BBB, which, to our satisfaction, did produce the desired product, albeit in low yield.

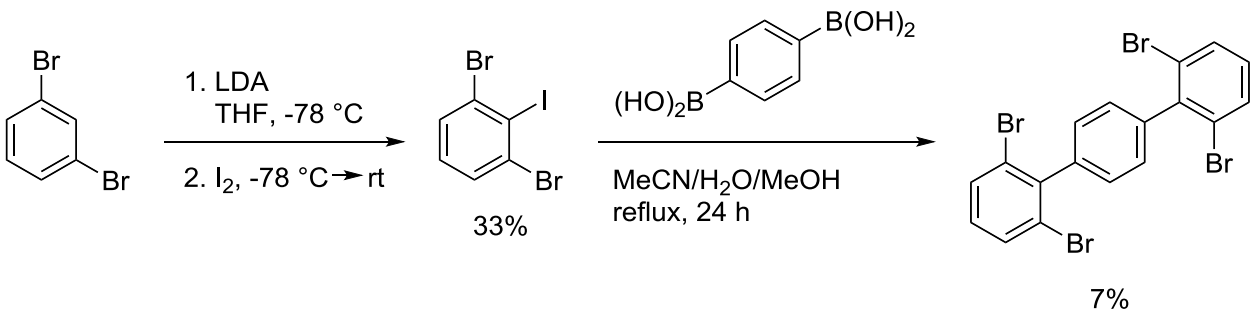

Scheme 5.3. Synthetic scheme for 1,4-bis(2,6-dibromophenyl)benzne. The final Suzuki coupling gave the desired product in low yield.

Preliminary surface chemistry of graphene precursor monomers. The two precursor molecules that were successfully synthesized were tested by our collaborators for their ability to serve as graphene or graphene-like arrays, both on gold and on patterned depassivated silicon surfaces. In preliminary experiments,[42] 2-TBB showed evidence that it adheres preferentially to the dehydrogenated regions of STM-depassivated silicon.

Concepts for solution-based construction of graphene nanoelectronics. Due to the limited success in our synthesis of new precursors and the inherent throughput limitations in the STM-based construction of graphene arrays, we turned to the possibility of constructing graphene nanoelectronics by solution methods. Sinitskii and coworkers have recently reported multiple examples[43-45] of solution synthesis of GNRs from polyaromatic hydrocarbons using the Yamamoto[46] and Scholl[47] reactions to accomplish the coupling and dehydrocyclization steps, respectively.

One issue with processing and depositing solution-synthesized GNRs is that graphene (like most undecorated polyaromatic hydrocarbons) is poorly soluble in many organic solvents due to the extensive π-stacking; however, methods for improving the solubility have been reported.[48,49] The use of sonication in polar[49] and/or high-boiling[50] solvents is one attractive method because it does not necessitate alterations in the chemical and structural nature of the graphene, thus giving us greater freedom to develop graphene structures that have ideal characteristics for electronic applications. Another possibility is to circumvent the solubility problem by processing GNRs on the surface of a solvent (e.g., Sinitskii and coworkers dissolved GNRs in chlorosulfonic acid and then added drops of this solution to water, resulting in self-assembly of the GNRs into a film on the water surface, from which the GNRs could be transferred to a suitable substrate[45]). Alternatively, Lyding and coworkers have shown that GNRs

formed by solution synthesis can be deposited by means of dry contact transfer, which has been shown to avoid the contamination commonly associated with solution deposition methods, and also does not depend on the GNRs being soluble in organic solvents.[51]

The general conceptual method for solution-based construction of graphene nanostructures that we find most appealing is iterative coupling. This method has been used for decades for the automated synthesis of peptides and more recently has proven useful for the efficient synthesis of large and complex polyene and polyarene molecules. In the case of peptide synthesis, the iterative reaction is the coupling of a carboxylic acid with an amine to form an amide, whereas in the case of the polyene and polyarene syntheses, the iterative reaction is a specialized case of Suzuki coupling involving the use of a protected boronic acid.[52,53] Because graphene is, in some sense, a two-dimensional dehydrogenated polymer of benzene, the iterative Suzuki coupling (or other carbon-carbon coupling reactions, e.g., Negishi coupling) of appropriate arene precursors could form graphene nanostructures. Iterative coupling is attractive for GNR formation because it relies on repetition of the same reaction (and thus, in principle, the same reaction conditions) to accomplish growth of GNRs, and because the number of iterative cycles performed determines precisely the length of the resultant GNRs.

In our initial experiments, we focused on GNRs constructed from the anthracene building blocks 9,10-dibromoanthracene and 10-bromoanthracene-9-boronic acid, both of which are commercially available. Because 10-bromoanthracene-9-boronic acid is bifunctional with regard to Suzuki coupling, it is inherently reactive with itself, and therefore in need of a biasing factor to ensure that it reacts only with the other anthracene building block. This biasing can be accomplished by modifying the 9,10-dibromoanthracene building block to make it more reactive. Because conditions have been discovered for coupling a boronic acid preferentially with an aryl

iodide in the presence of an aryl bromide, we envisioned that one end of 9,10-dibromoanthracene could be converted to an iodide,[54] followed by coupling with the bifunctional boronic acid, followed by conversion of one end of the resulting dibromide to an iodide, etc. After sufficiently long polyanthracene chains had formed, they would be dehydrocyclized to GNRs according to the method of Mullen and coworkers,[35,48,55] and then the bromides on both ends could be converted to thiols, providing a convenient handle for controlled solution deposition of the GNRs on metal (e.g., gold) electrodes.

Scheme 5.4 shows the general process for converting anthracenyl building blocks into GNRs for deposition on a surface with spatial precision. As a first step, we reproduced a literature procedure for the conversion of 9,10-dibromoanthracene to 9-bromo-10-iodoanthracene by lithium-halogen exchange followed by iodination.[54] Although initial attempts to couple this iodide with the bifunctional boronic acid have so far been unsuccessful, several variations on the approach detailed in Scheme 5.4 are possible if Suzuki coupling proves ineffective after additional effort. For example, other coupling strategies (e.g., Negishi coupling) could be employed.

Subsequent conversion of polyanthrylene chains to GNRs can best be effected using $FeCl_3$ as the oxidant (the Scholl reaction), as shown by the work of Mullen and coworkers,[35,47,48,55] as well as Sinitskii and coworkers,[43-45] for other polyaromatic precursors. If wider GNRs are desired, a different precursor approach would probably be required, due to the poorer stability of tetracene, pentacene, and higher acenes. Instead, iterative coupling starting with dibromopolyphenylene precursors, such as terphenyl or quinquephenyl derivatives, should work better, producing GNRs whose apparent monomer would be tetracene or heptacene, respectively.

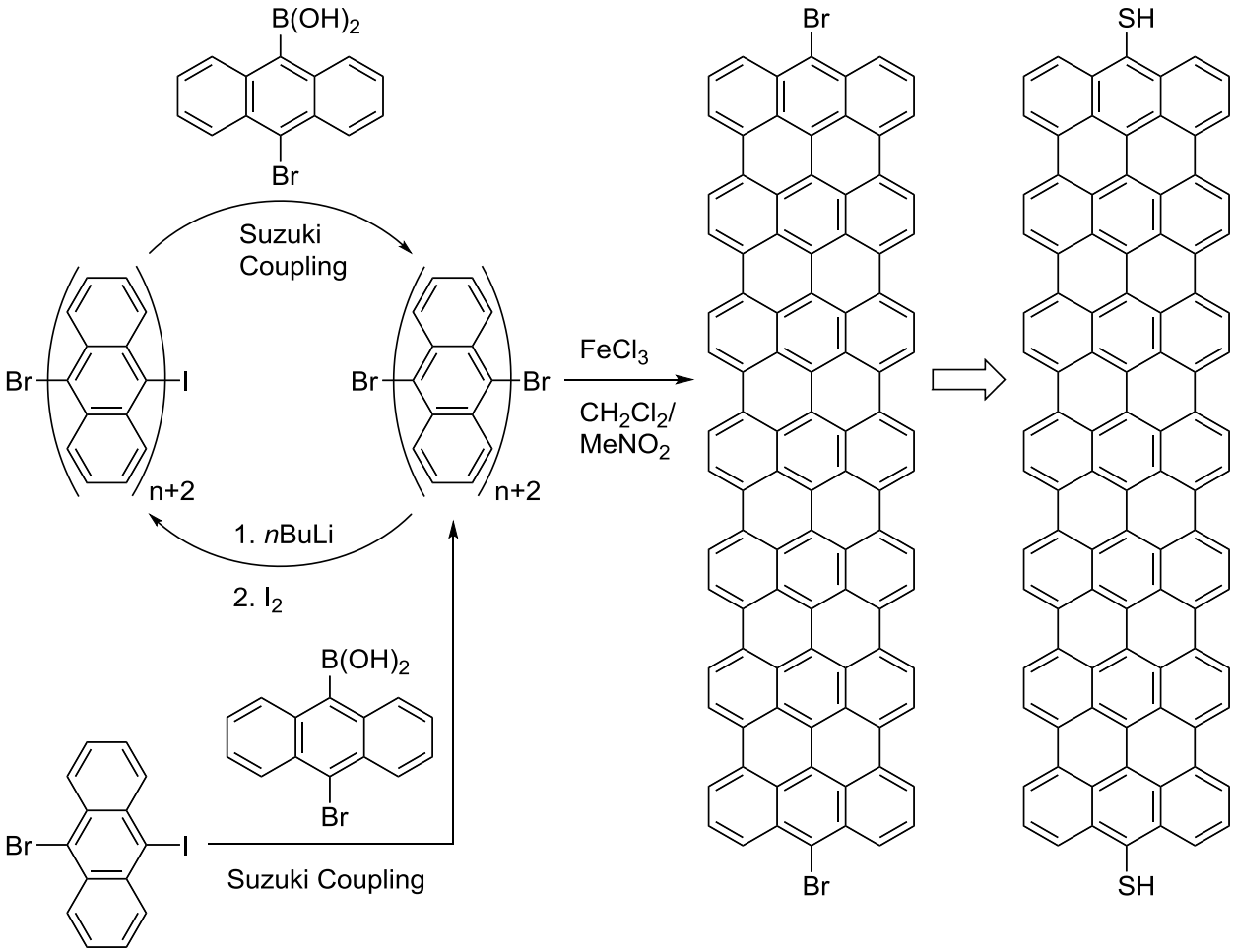

Scheme 5.4. Iterative coupling scheme for the solution-based formation of GNRs. The GNR length is determined by the number of times (n) the cycle is repeated. The installation of thiols on the ends would be for the purpose of adhesion to gold (or other thiophilic metal) electrodes.

Perhaps most exciting about the solution-based approach is the fact that, if a method for precise nanopatterning of thiophilic metal electrodes were developed, GNRs could be deposited on a surface in precise locations with precise orientations, thus taking a huge step toward fabrication of pristine graphene nanoelectronics. One initial idea for nanopatterning of thiophilic metal electrodes relates to the atomically precise patterning of hydrogen-passivated silicon[31,32] that was mentioned previously. If depassivation were stimulated at locations corresponding to the lengths of thiol-capped GNRs and the desired pitch of GNR nanowires, thiophilic metal

electrodes could conceivably be vapor deposited selectively at the depassivated sites, providing a framework for solution deposition of the GNRs themselves in the desired locations (Figure 5.5). Of course, the fact that the depassivation is accomplished with an STM tip works against high throughput, but parallel depassivation by many tips could mitigate this limitation.

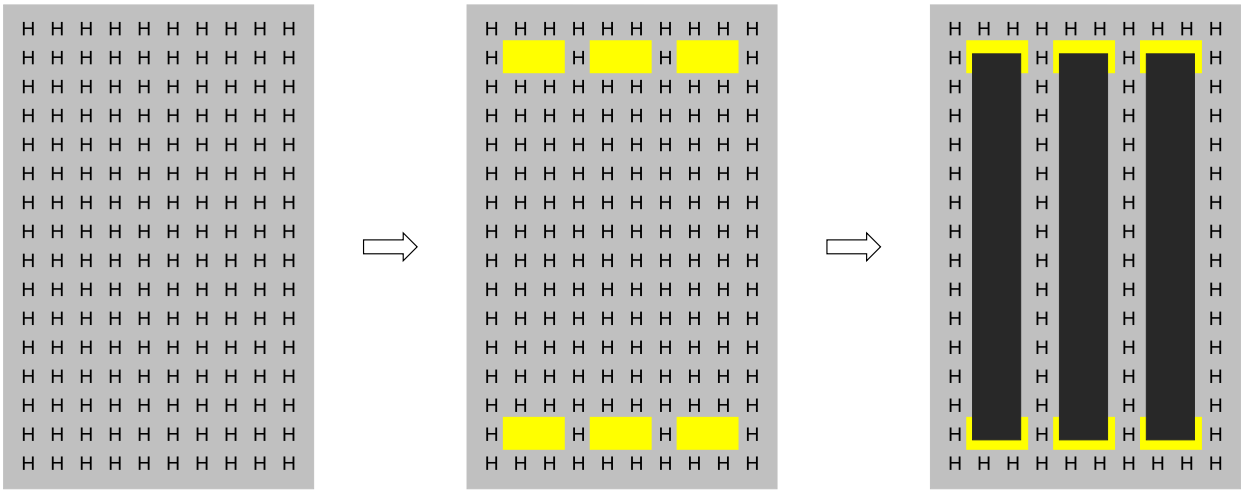

Figure 5.5. Representations of a hydrogen-passivated silicon surface (left), the same surface after STM-induced depassivation followed by vapor deposition of thiophilic metal electrodes (yellow) in the depassivated areas (middle), and the same surface after solution deposition of thiol-capped GNRs (dark gray) onto the electrodes (right).

Experimental

Unless stated otherwise, all manipulations were performed under argon or vacuum using standard Schlenk line or glove box techniques. Glassware was oven- or flame-dried and allowed to cool under vacuum or argon. Solvents were distilled under nitrogen from sodium/benzophenone (diethyl ether and tetrahydrofuran), magnesium (methanol and ethanol), boric anhydride (acetonitrile), or sodium (toluene), and sparged with argon for 30-60 seconds immediately before use.

Benzene-d_6, chloroform-d, and dichloromethane-d_2 were purchased from Sigma-Aldrich or Cambridge Isotope Laboratories in 1-mL ampoules and used without purification. The following starting materials were obtained from commercial sources and used as received unless stated otherwise: 2,2′-dinitrobiphenyl (Alfa Aesar), 1,3-dibromobenzene (Sigma-Aldrich), 1,4-dibromobenzene (Sigma-Aldrich), sodium nitrite (Sigma-Aldrich), potassium iodide (Fisher), magnesium chloride (Sigma-Aldrich), lithium powder (Sigma-Aldrich), 2,2,6,6-tetramethylpiperidine (Matrix Scientific), *n*-butyllithium (Sigma-Aldrich, 1.6 M solution in hexanes), trimethylborate (Sigma-Aldrich), hydrogen chloride (Sigma-Aldrich, 1.0 M in diethyl ether), iodine (Fisher), phenylboronic acid (Alfa Aesar, listed under "benzeneboronic acid"), lithium hydroxide hydrate (Fisher), diisopropylamine (Sigma-Aldrich), 1,4-phenylenebis(boronic acid) (Oakwood), 9,10-dibromoanthracene (Sigma-Aldrich), and tetrakis(triphenylphosphine)-palladium(0) (Strem). The compound 1,3-dibromo-2-iodobenzene were prepared according to a literature procedure,[40] and lithium 2,2,6,6-tetramethylpiperidide was prepared by treatment of a solution of 2,2,6,6-tetramethylpiperidine in pentane with *n*-butyllithium in hexanes at –78 °C, isolated by filtration, and dried under vacuum. Column chromatography was performed with SiliaFlash®[56] P60 silica gel purchased from SiliCycle and packed into columns as slurries in hexanes.

NMR spectra were acquired on Varian spectrometers (Unity 400, Unity Inova 400, Unity 500, and VXR 500) at room temperature, unless specified otherwise. Positive chemical shifts indicate shifts to higher frequency relative to the following chemical shift standards: $SiMe_4$ (^1H and ^{13}C, set by assigning appropriate shifts to residual solvent signals) and external BF_3 in $CDCl_3$ (^{11}B). Default instrument parameters were used unless stated otherwise. NMR spectra were processed using the MestReNova NMR software package; manual phasing, peak picking, and

integration methods were employed, and polynomial or Bernstein polynomial baseline corrections (typically of order 3-8) were employed.

1,3,5-Tris(2-bromophenyl)benzene, $C_6H_3(C_6H_4Br)_3$. This is a modification of a literature procedure.[35] A small oven-dried Schlenk tube was charged with 2′-bromoacetophenone (2.7 mL, 20.0 mmol), trifluoromethanesulfonic acid (0.2 mL, 2.3 mmol) was added by syringe, and the solution was heated under positive argon flow to 130 °C for 7 h with stirring. The dark brown solution was cooled to room temperature, quenched with water (20 mL), and extracted with CH_2Cl_2 (50 mL). The organic layer was dried with $MgSO_4$ and evaporated. The crude residue was purified by silica gel chromatography eluting with pentane/CH_2Cl_2 (6:1) to give a light yellow solid. The solid was recrystallized from hexanes/CH_2Cl_2 (~1:1) by suspending in 10 mL of hexanes, adding CH_2Cl_2 until the solid was completely dissolved, boiling off CH_2Cl_2 until saturation was reached, allowing the solution to cool to room temperature, and cooling to 0 °C to maximize yield. The white crystalline product was isolated by vacuum filtration and dried under vacuum. Yield: 1.336 g (37%). ^{1}H NMR ($CDCl_3$): δ 7.69 (dd, J_{HH} = 8.0 Hz, J_{HH} = 1.0 Hz, 3H, $C_6H_3(C_6\mathit{H}_4Br)_3$), 7.51 (s, 1H, $C_6\mathit{H}_3(C_6H_4Br)_3$), 7.47 (dd, J_{HH} = 7.6 Hz, J_{HH} = 1.7 Hz, 3H, $C_6H_3(C_6\mathit{H}_4Br)_3$), 7.38 (td, J_{HH} = 7.5 Hz, J_{HH} = 1.2 Hz, 3H, $C_6H_3(C_6\mathit{H}_4Br)_3$), 7.22 (td, J_{HH} = 7.7 Hz, J_{HH} = 1.7 Hz, 3H, $C_6H_3(C_6\mathit{H}_4Br)_3$).

2,2′-Diaminobiphenyl, $(C_6H_4NH_2)_2$. This is a modification of a literature procedure.[37] To a 85 mL Fisher-Porter bottle equipped with a magnetic stir bar and a gas pressure regulator were added 2,2′-dinitrobiphenyl (2.50 g, 10.2 mmol) and Pd/C (0.4 g, 10% Pd loading, 0.38 mmol). The bottle was evacuated and filled with argon (3 cycles), and then ethyl acetate (15 mL, sparged with argon for 30 seconds) was added by syringe. The gas regulator was attached to a hydrogen gas cylinder and the Fisher-Porter bottle was purged by pressurizing with hydrogen gas

to 3 atm and venting (3 cycles). The bottle was then charged with hydrogen gas (40 psi) and sealed, and the reaction mixture was stirred at room temperature for 3 days, repressurizing to 40 psi with hydrogen gas periodically until hydrogen gas ceased to be consumed. The system was then and vented to remove the excess hydrogen gas and purged with argon. The solution was separated from solid catalyst by vacuum filtration, solvent was removed under vacuum, and the pale yellow residue was dried in a vacuum desiccator overnight over $CaSO_4$ to give the product as an off-white solid. Yield: 1.81 g (96%). ^{1}H NMR ($CDCl_3$): δ 7.19 (td, J_{HH} = 7.7 Hz, J_{HH} = 1.6 Hz, 2H, $C_6H_4NH_2$), 7.13 (dd, J_{HH} = 7.5 Hz, J_{HH} = 1.5 Hz, 2H, $C_6H_4NH_2$), 6.84 (td, J_{HH} = 7.5 Hz, J_{HH} = 1.0 Hz, 2H, $C_6H_4NH_2$), 6.80 (dd, J_{HH} = 8.0 Hz, J_{HH} = 0.5 Hz, 2H, $C_6H_4NH_2$), 3.75 (s, 4H, $C_6H_4NH_2$).

2,2′-Diiodobiphenyl, $(C_6H_4I)_2$. To a 250 mL round-bottomed flask equipped with a magnetic stir bar was added a solution of 2,2′-diaminobiphenyl (1.81 g, 9.82 mmol) in aqueous HCl (120 mL, 8M). The solution was cooled to 0 °C, and a solution of sodium nitrite (1.438 g, 20.8 mmol) in deionized water (6.5 mL) was added dropwise, producing a pale yellow solution. After the mixture had been stirred for 30 min, a solution of KI (3.568 g, 21.5 mmol) in deionized water (10 mL) was added dropwise, resulting in evolution of bubbles and formation of a dark solution and a black solid. The mixture was warmed to room temperature and stirred overnight, then extracted with Et_2O (3 × 50 mL). The combined extracts were washed with aqueous sodium bisulfite (50 mL) and water (50 mL), dried ($MgSO_4$), and taken to dryness under vacuum. The residue was chromatographed on silica gel, eluting with hexanes, and the solvent was removed from the eluate under vacuum to give the product as a bright white solid. Yield: 0.718 g (18%). ^{1}H NMR ($CDCl_3$): δ 7.95 (dd, J_{HH} = 7.9 Hz, J_{HH} = 0.8 Hz, 2H), 7.43 (td, J_{HH} = 7.5 Hz, J_{HH} = 0.9 Hz, 2H), 7.20 (dd, J_{HH} = 7.6 Hz, J_{HH} = 1.5 Hz, 2H), 7.10 (td, J_{HH} = 7.8 Hz, J_{HH} = 1.6 Hz, 2H).

2,5-Dibromophenylboronic acid, $C_6H_3Br_2B(OH)_2$. To a 100 mL Schlenk flask equipped with a magnetic stir bar was added lithium 2,2,6,6-tetramethylpiperidide (1.72 g, 11.7 mmol). The flask was cooled to –78 °C, and THF (30 mL) was added. The mixture was cooled to –84 °C (EtOAc/N_2(l) bath), and a solution of 1,4-dibromobenzene (2.50 g, 10.6 mmol) in THF (20 mL) at –78 °C was added dropwise by means of an addition funnel. After the pale yellow slurry had stirred at –84 °C for 45 min, trimethylborate (1.40 mL, 12.6 mmol) was added dropwise by syringe, resulting in formation of a clear dark yellow solution. The mixture was stirred at –84 °C for 1 h, allowed to warm to 0 °C, and quenched with aqueous HCl (50 mL, 2M). The biphasic mixture was allowed to warm to room temperature, and was extracted with CH_2Cl_2 (3 × 100 mL). The combined organic extracts were washed with aqueous HCl, dried ($MgSO_4$), and taken to dryness under vacuum. The residue was recrystallized from aqueous acetone by suspending in 20 mL of acetone, adding water until the solid was completely dissolved, boiling off acetone until saturation was reached, allowing the solution to cool to room temperature, and cooling to 0 °C to maximize yield. The pale yellow crystalline product was isolated by vacuum filtration and dried under vacuum. This product was contaminated with water, and was therefore recrystallized from $CHCl_3$ by dissolving in 20 mL of boiling $CHCl_3$, boiling off the solvent until saturation was reached, allowing the solution to cool to room temperature, and cooling to 0 °C to maximize yield. The off-white crystalline product was isolated by vacuum filtration and dried under vacuum. Yield: 0.475 g (16%). ^{1}H NMR (C_6D_6): δ 7.98 (d, J_{HH} = 2.3 Hz, 1H, $C_6\mathit{H}_3Br_2B(OH)_2$), 6.97 (s, 2H, $C_6H_3Br_2B(O\mathit{H})_2$), 6.94 (d, J_{HH} = 8.5 Hz, 1H, $C_6\mathit{H}_3Br_2B(OH)_2$), 6.90 (dd, J_{HH} = 8.5 Hz, J_{HH} = 2.4 Hz, 1H, $C_6\mathit{H}_3Br_2B(OH)_2$). ^{11}B{^{1}H} NMR ($C_6D_6$): δ 25.5 (s, 1B).

2,6-Dibromobiphenyl, ($C_6H_3Br_2Ph$). To a 250 mL Schlenk flask equipped with a magnetic stir bar was added 1,3-dibromo-2-iodobenzene (2.00 g, 5.53 mmol), phenylboronic acid (0.674 g, 5.53 mmol), lithium hydroxide hydrate (0.928 g, 22.1 mmol), and tetrakis(triphenylphosphine)palladium (0.319 g, 0.280 mmol). Acetonitrile (150 mL) and water (15 mL, deoxygenated by bubbling with argon for 10 min) were added, and the yellow mixture was heated at 65 °C for 16 h, after which time TLC showed the presence of mostly starting materials. Methanol (50 mL) was added to improve dissolution of the starting materials, and the mixture was heated at 65 °C for another 24 h. The mixture was allowed to cool to room temperature, the organic solvents were removed under vacuum, and the aqueous portion that remained was extracted with CH_2Cl_2 (3 × 100 mL). The combined organic extracts were dried ($MgSO_4$) and taken to dryness under vacuum; the residue was chromatographed on silica gel, eluting with hexanes, and the solvent was removed from the eluate under vacuum to give the product as a white solid. Yield: 0.862 g (50%). ^{1}H NMR ($CDCl_3$): δ 7.63 (d, J_{HH} = 8.0 Hz, 2H, $C_6H_3Br_2Ph$), 7.46 (m, 3H, $C_6H_3Br_2Ph$), 7.21 (m, 2H, $C_6H_3Br_2Ph$), 7.07 (t, J_{HH} = 8.1 Hz, 1H, $C_6H_3Br_2Ph$).

2,6-Diiodobiphenyl, ($C_6H_3I_2Ph$). To a 100 mL Schlenk flask equipped with a magnetic stir bar was added anhydrous magnesium chloride (2.105 g, 22.1 mmol), lithium powder (0.307 g, 44.2 mmol), and THF (50 mL). A slight exotherm occurred. After the mixture had been stirred for 4 days, a fine black powder settled when stirring was halted, indicating the presence of magnesium metal rather than lithium metal. 2,6-Dibromobiphenyl (0.862 g, 2.76 mmol) was added all in one portion, and the mixture immediately became warm for several minutes, then cooled back to room temperature. After being stirred for 24 h, the suspension was transferred by cannula to a 250 mL Schlenk flask containing iodine (12.35 g, 48.7 mmol). The addition caused

warming of the solution nearly to reflux. After being stirred for 1 h, the reaction mixture was quenched with aqueous sodium thiosulfate (50 mL, 1M) to destroy excess iodine. Water (50 mL) was added, and the mixture was extracted with CH_2Cl_2 (3 × 150 mL). The combined organic extracts were dried ($MgSO_4$), and taken to dryness under vacuum. The residue was chromatographed on silica gel, eluting with hexanes. The resulting pale purple solution was washed with aqueous sodium thiosulfate (50 mL, 1M), and the organic layer was dried ($MgSO_4$) and taken to dryness under vacuum. The residue recrystallized from methanol by dissolving in 20 mL of boiling methanol, boiling off the solvent until saturation was reached, allowing the solution to cool to room temperature, and cooling to 0 °C to maximize yield. The white crystalline product was isolated by vacuum filtration and dried under vacuum. Yield: 0.628 g (56%). ^{1}H NMR ($CDCl_3$): δ 7.94 (d, J_{HH} = 7.9 Hz, 2H, $C_6H_3I_2$Ph), 7.46 (m, 3H, $C_6H_3I_2$*Ph*), 7.12 (m, 2H, $C_6H_3I_2$*Ph*), 6.68 (t, J_{HH} = 7.9 Hz, 1H, $C_6H_3I_2$Ph).

2,2″,6,6″-Tetrabromoterphenyl, $C_6H_4(C_6H_3Br_2)_2$. To a 1 L Schlenk flask equipped with a magnetic stir bar was added 1,3-dibromo-2-iodobenzene (2.00 g, 5.53 mmol), p-phenylenebis(boronic acid) (0.482 g, 2.91 mmol), lithium hydroxide hydrate (0.977 g, 23.3 mmol), and tetrakis(triphenylphosphine)palladium (0.336 g, 0.291 mmol). Acetonitrile (450 mL), methanol (150 mL), and water (30 mL, deoxygenated by bubbling with argon for 10 min) were added, and the yellow mixture was heated at 65 °C for 36 h. CAUTION: if the stirring rate is too high, the stir bar can break the flask. The mixture was allowed to cool to room temperature, the organic solvents were removed under vacuum, and the aqueous portion that remained was extracted with CH_2Cl_2 (3 × 150 mL). The combined organic extracts were dried ($MgSO_4$) and taken to dryness under vacuum. The residue was chromatographed on silica gel, eluting with hexanes, and the solvent was removed from the eluate under vacuum. The residue

was recrystallized from methanol by dissolving in 20 mL of boiling methanol, boiling off the solvent until saturation was reached, allowing the solution to cool to room temperature, and cooling to 0 °C to maximize yield. The white crystalline product was isolated by vacuum filtration and dried under vacuum. Yield: 0.105 g (7%). ^{1}H NMR ($CDCl_3$): δ 7.66 (d, J_{HH} = 8.0 Hz, 4H, $C_6H_4(C_6H_3Br_2)_2$), 7.29 (s, 4H, $C_6H_4(C_6H_3Br_2)_2$), 7.09 (t, J_{HH} = 8.0 Hz, 2H, $C_6H_4(C_6H_3Br_2)_2$).

9-Bromo-10-iodoanthracene, ($C_{10}H_8BrI$). This is a modification of a literature procedure.[54] To a small Schlenk tube equipped with a magnetic stir bar was added 9,10-dibromoanthracene (0.500 g, 1.49 mmol) and THF (50 mL). The solution was cooled to –78 °C, and *n*-butyllithium (1.10 mL, ~1.5M in hexanes, 1.64 mmol) was added dropwise by syringe, causing the yellow slurry to change color to a bright orange solution. After being stirred for 1 h, iodine (0.453 g, 1.79 mmol) was added all in one portion. The reaction mixture was allowed to warm to room temperature, quenched with aqueous sodium thiosulfate (10 mL, 1M) to destroy excess iodine, and extracted with CH_2Cl_2 (3 x 50 mL). The combined organic extracts were dried ($MgSO_4$) and taken to dryness under vacuum. The residue was recrystallized from toluene by dissolving in 10 mL of boiling toluene, boiling off the solvent until saturation was reached, allowing the solution to cool to room temperature, and cooling to 0 °C to maximize yield. The product was isolated as bright yellow needles by vacuum filtration and dried under vacuum. Yield: 0.445 g (78%). ^{1}H NMR ($CDCl_3$): δ 8.59 (m, 4H), 7.65 (m, 4H).

References

1. Novoselov, K. S.; Geim, A. K.; Morozov, S. V.; Jiang, D.; Zhang, Y.; Dubonos, S. V.; Grigorieva, I. V.; Firsov, A. A. *Science* **2004**, *306*, 666-669.

2. Han, M. Y.; Ozyilmaz, B.; Zhang, Y.; Kim, P. *Phys. Rev. Lett.* **2007**, *98*, 206805-1-206805-4.

3. Mullen, K.; Rabe, J. P. *Acc. Chem. Res.* **2008**, *41*, 511-520.

4. Tapaszto, L.; Dobrik, G.; Lambin, P.; Biro, L. P. *Nat. Nanotechnol.* **2008**, *3*, 397-401.

5. Bai, J.; Huang, Y. *Mater. Sci. Eng., R* **2010**, *70*, 341-353.

6. Chen, J.; Wen, Y.; Wu, B.; Huang, L.; Xue, Y.; Geng, D.; Wang, D.; Yu, G.; Liu, Y. *J. Am. Chem. Soc.* **2011**, *133*, 17548-17551.

7. Pang, S.; Hernandez, Y.; Feng, X.; Mullen, K. *Adv. Mater.* **2011**, *23*, 2779-2795.

8. Reddy, D.; Register, L. F.; Carpenter, G. D.; Banerjee, S. K. *J. Phys. D: Appl. Phys.* **2011**, *44*, 313001-1-313001-20.

9. Batzill, M. *Surf. Sci. Rep.* **2012**, *67*, 83-115.

10. Colombo, L.; Wallace, R. M.; Ruoff, R. S. *Proc. IEEE* **2012**, *101*, 1536-1556.

11. Lei, W.; Li, C.; Cole, M. T.; Qu, K.; Ding, S.; Zhang, Y.; Warner, J. H.; Wang, B.; Milne, W. I. *Carbon* **2013**, *56*, 255-263.

12. Wang, M.; Jang, S. K.; Jang, W.-J.; Kim, M.; Park, S.-Y.; Kim, S.-W.; Kahng, S.-J.; Choi, J.-Y.; Ruoff, R. S.; Song, Y. J.; Lee, S. *Adv. Mater.* **2013**, *25*, 2746-2752.

13. Liang, M.; Luo, B.; Zhi, L. *Int. J. Energy Res.* **2009**, *33*, 1161-1170.

14. Han, M.; Ozyilmaz, B.; Zhang, Y.; Jarillo-Herero, P.; Kim, P. *Phys. Status Solidi B* **2007**, *244*, 4134-4137.

15. Barone, V.; Hod, O.; Scuseria, G. E. *Nano Lett.* **2006**, *6*, 2748-2754.

16. Son, Y.-W.; Cohen, M. L.; Louie, S. G. *Phys. Rev. Lett.* **2006**, *97*, 216803-1-216803-4.

17. Ritter, K. A.; Lyding, J. W. *Nat. Mater.* **2009**, *8*, 235-242.

18. Campos, L. C.; Manfrinato, V. R.; Sanchez-Yamagishi, J. D.; Kong, J.; Jarillo-Herrero, P. *Nano Lett.* **2009**, *9*, 2600-2604.

19. Jiao, L.; Zhang, L.; Wang, X.; Diankov, G.; Dai, H. *Nature* **2009**, *458*, 877-880.

20. Cai, J.; Ruffieux, P.; Jaafar, R.; Bieri, M.; Braun, T.; Blankenburg, S.; Muoth, M.; Seitsonen, A. P.; Saleh, M.; Feng, X.; Mullen, K.; Fasel, R. *Nature* **2010**, *466*, 470-473.

21. Regmi, M.; Chisholm, M. F.; Eres, G. *Carbon* **2012**, *50*, 134-141.

22. Ding, G.; Zhu, Y.; Wang, S.; Gong, Q.; Sun, L.; Wu, T.; Xie, X.; Jiang, M. *Carbon* **2013**, *53*, 321-326.

23. Hagihara, Y.; Kajiwara, T.; Visikovskiy, A.; Tanaka, S. *Appl. Phys. Express* **2013**, *6*, 055102-1-055102-4.

24. Vlassiouk, I.; Fulvio, P.; Meyer, H.; Lavrik, N.; Dai, S.; Datskos, P.; Smirnov, S. *Carbon* **2013**, *54*, 58-67.

25. Wei, D.; Mitchell, J. I.; Tansarawiput, C.; Nam, W.; Qi, M.; Ye, P. D.; Xu, X. *Carbon* **2013**, *53*, 374-379.

26. Dhingra, S.; Hsu, J.-F.; Vlassiouk, I.; D'Urso, B. *Carbon* **2014**, *69*, 188-193.

27. Hsieh, Y.-P.; Hofmann, M.; Kong, J. *Carbon* **2014**, *67*, 417-423.

28. Magnuson, C. W.; Kong, X.; Ji, H.; Tan, C.; Li, H.; Piner, R.; Ventrice, C. A.; Ruoff, R. S. *J. Mater. Res.* **2014**, *29*, 403-409.

29. Takami, T.; Seino, R.; Yamazaki, K.; Ogino, T. *J. Phys. D: Appl. Phys.* **2014**, *47*, 094015-1-094015-7.

30. Yan, Z.; Peng, Z.; Tour, J. M. *Acc. Chem. Res.* **2014**, *47*, 1327-1337.

31. Lyding, J. W.; Shen, T.-C.; Hubacek, J. S.; Tucker, J. R.; Abeln, G. C. *Appl. Phys. Lett.* **1994**, *64*, 2010-2012.

32. Walsh, M. A.; Hersam, M. C. *Annu. Rev. Phys. Chem.* **2009**, *60*, 193-216.

33. Randall, J. N.; Ballard, J. B.; Lyding, J. W.; Schmucker, S.; Von Ehr, J. R.; Saini, R.; Xu, H.; Ding, Y. *Microelectron. Eng.* **2010**, *87*, 955-958.

34. Abeln, G. C.; Lee, S. Y.; Lyding, J. W.; Thompson, D. S.; Moore, J. S. *Appl. Phys. Lett.* **1997**, *70*, 2747-2749.

35. Feng, X.; Wu, J.; Enkelmann, V.; Mullen, K. *Org. Lett.* **2006**, *8*, 1145-1148.

36. Xu, Y.; He, K. T.; Schmucker, S. W.; Guo, Z.; Koepke, J. C.; Wood, J. D.; Lyding, J. W.; Aluru, N. R. *Nano Lett.* **2011**, *11*, 2735-2742.

37. Scarborough, C. C.; Popp, B. V.; Guzei, I. A.; Stahl, S. S. *J. Organomet. Chem.* **2005**, *690*, 6143-6155.

38. Vinod, T. K.; Hart, H. *J. Org. Chem.* **1991**, *56*, 5630-5640.

39. Luliński, S.; Serwatowski, J.; Szczerbińska, M. *Eur. J. Org. Chem.* **2008**, 1797-1801.

40. Leroux, F. R.; Bonnafoux, L.; Heiss, C.; Colobert, F.; Lanfranchi, D. A. *Adv. Synth. Catal.* **2007**, *349*, 2705-2713.

41. Fan, C.-A.; Ferber, B.; Kagan, H. B.; Lafon, O.; Lesot, P. *Tetrahedron: Assymetry* **2008**, *19*, 2666-2677.

42. The preliminary surface work mentioned in this paragraph was performed by Adrian Radocea, Lyding Research Group, Materials Science and Engineering Department, Beckman Insitute, University of Illinois.

43. Vo, T. H.; Shekhirev, M.; Kunkel, D. A.; Morton, M. D.; Berglund, E.; Kong, L.; Wilson, P. M.; Dowben, P. A.; Enders, A.; Sinitskii, A. *Nature Communications* **2014**.

44. Vo, T. H.; Shekhirev, M.; Kunkel, D. A.; Orange, F.; Guinel, M. J.-F.; Enders, A.; Sinitskii, A. *Chem. Commun.* **2014**, *50*, 4172-4174.

45. Pour, M. M.; Lashkov, A.; Radocea, A.; Liu, X.; Sun, T.; Lipatov, A.; Korlacki, R. A.; Shekhirev, M.; Aluru, N. R.; Lyding, J. W.; Sysoev, V.; Sinitskii *Nature Communications* **2017**.

46. Yamamoto, T.; Morita, A.; Miyazaki, Y.; Maruyama, T.; Wakayama, H.; Zhou, Z.-h.; Nakamura, Y.; Kanbara, T.; Sasaki, S.; Kubota, K. *Macromolecules* **1992**, *25*, 1214-1223.

47. Simpson, C. D.; Mattersteig, G.; Martin, K.; Gherghel, L.; Bauer, R. E.; Rader, H. J.; Mullen, K. *J. Am. Chem. Soc.* **2004**, *126*, 3139-3147.

48. Dossel, L.; Gherghel, L.; Feng, X.; Mullen, K. *Angew. Chem. Int. Ed.* **2011**, *50*, 2540-2543.

49. Coleman, J. N. *Acc. Chem. Res.* **2013**, *46*, 14-22.

50. Vo, T. H.; Shekhirev, M.; Lipatov, A.; Korlacki, R. A.; Sinitskii, A. *Faraday Discuss.* **2014**, *173*, 105-113.

51. Radocea, A.; Sun, T.; Vo, T. H.; Sinitskii, A.; Aluru, N. R.; Lyding, J. W. *Nano Lett.* **2017**, *17*, 170-178.

52. Li, J.; Balmer, S. G.; Gillis, E. P.; Fujii, S.; Schmidt, M. J.; Palazzolo, A. M. E.; Lehmann, J. W.; Morehouse, G. F.; Burke, M. D. *Science* **2015**, *347*, 1221-1226.

53. Li, J.; Grillo, A. S.; Burke, M. D. *Acc. Chem. Res.* **2015**, *48*, 2297-2307.

54. Nesterov, E. E.; Zhu, Z.; Swager, T. M. *J. Am. Chem. Soc.* **2005**, *127*, 10083-10088.

55. Yang, X.; Dou, X.; Mullen, K. *Chem. Asian J.* **2008**, *3*, 759-766.

56. SiliaFlash® is a registered trademark of SiliCycle Inc. Corporation Canada.

Appendix A. Detailed description of the optimized procedure for low-temperature NMR characterization of osmium methane complexes

As mentioned in the experimental section of chapter 3, it is essential that the osmium methyl precursor and the acid used for low-temperature protonation not come in contact with one another until they are frozen in liquid nitrogen, because they react even in the solid state at room temperature. The mixing of the osmium compound and the acid is best accomplished by the following procedure: In an argon-filled glove box, the osmium methyl precursor is loaded into a 5 mm NMR tube topped with a 14/20 female ground glass joint and the tube is tapped lightly to bring the material to the bottom of the tube. The tube is then tilted until it is nearly horizontal, and the acid is placed into the bulb of the 14/20 ground glass joint (just below the ground glass portion). A custom vacuum transfer apparatus (Figure A.1) is attached to the ground glass joint, which is lubricated with Krytox™ grease,[1] and the stopcocks as well as the NMR tube joint are secured with rubber bands. The apparatus is removed from the glove box, still maintaining the NMR tube in a horizontal position, and connected to a Schlenk line by a hose, from which the air is removed by three vacuum-fill cycles. The NMR tube is then inserted into a spinner for the NMR spectrometer until the spinner reaches the joint between the original NMR tube and the ground glass joint topper (the spinner usually cannot slide past this joint, because a rib is formed in the fabrication process). The apparatus is placed under static vacuum, and then, in one motion, the NMR tube is turned to a vertical position and inserted into a liquid nitrogen bath in a small cylindrical Dewar flask. The osmium methyl compound and the acid are thus frozen the moment they make contact, preventing premature reaction between the two. A PTFE screw-capped Schlenk flask containing $CDCl_2F$ solvent is attached to the other ground glass joint of the vacuum transfer apparatus (using Krytox™ grease as a lubricant), the apparatus and the NMR

tube are placed under static vacuum, and $CDCl_2F$ (~0.5 mL) is vacuum transferred into the frozen NMR tube.

In order to ensure full dissolution of the reactants in the solvent without substantial premature reaction between the two, the following procedure is employed: The NMR tube is removed from the liquid nitrogen bath to allow partial warming; as soon as the solvent thaws, the mixture is shaken for 2 seconds and reinserted into the liquid nitrogen bath. This thaw-shake-freeze cycle is repeated until no more solid reactants are visible, indicating complete dissolution. More $CDCl_2F$ (0.5 to 1 mL) is vacuum transferred to the NMR tube, and the solvent is thawed one more time, shaken to thoroughly mix the entire solution, and refrozen. Performing the dissolution in cycles with minimum solvent minimizes the time spent at elevated temperatures, minimizing loss of methane from the complex formed upon protonation. The Schlenk flask of $CDCl_2F$ is sealed and removed from the apparatus, the NMR tube is placed under static vacuum (still frozen in liquid nitrogen), and the NMR tube is flame-sealed just above the NMR tube/topper joint with a house gas/oxygen cylinder torch (flame-sealing should be practiced several times with NMR tubes containing only $CDCl_2F$ or some other solvent until one is comfortable with the process). During the entire process of handling the NMR tube once it is placed into the liquid nitrogen bath, it is important that the spinner never contact the liquid nitrogen bath (thermal shock can cause cracking). Once the flame-sealing is finished, the NMR tube is briefly removed from the liquid nitrogen bath and then reinserted into the liquid nitrogen bath through a 5 mm hole in the center of a foam cap for the Dewar flask. This cap keeps the liquid nitrogen bath from evaporating as quickly, but more importantly, it insulates the spinner from the bath, greatly reducing buildup of condensation and ice on the spinner. Figure A.1 shows the apparatus used for preparing the samples for low-temperature NMR characterization.

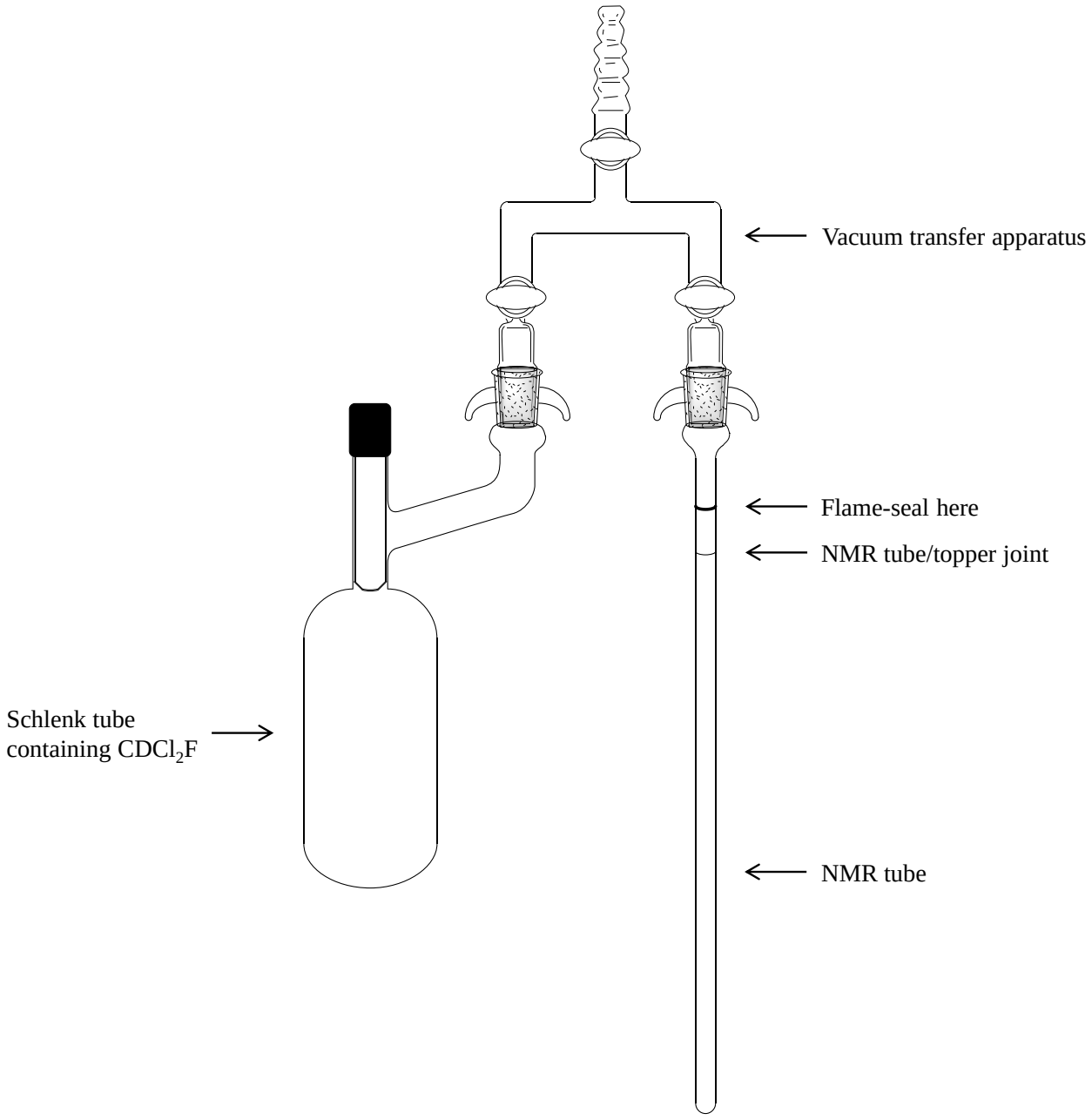

Figure A.1. Apparatus for preparing an NMR sample of $(C_5Me_5)Os(dfmpm)CH_3$ isotopologs + $(CF_3SO_2)_2NH/D$ in $CDCl_2F$ for low-temperature characterization of methane complexes.

Once the NMR sample is prepared, the NMR spectrometer can be prepared. The probe temperature is controlled by flowing dry nitrogen through coils immersed in a liquid nitrogen bucket (the normal method when the desired temperature is lower than –50 °C). It is best if the

tubing leading from the bucket to the probe is wrapped with an insulating foam jacket to limit ice buildup. The most important modification to the normal setup is to prevent condensation of water and buildup of ice near the top of the probe stack as follows. A four-inch long piece of PVC pipe with an inner diameter just large enough to fit over the top of the probe is placed into the end of an insulating foam jacket twelve inches long and of an appropriate diameter to fit snugly over the piece of pipe. The end of the foam jacket containing the pipe is placed over the top of the probe stack, and plastic tubing running from an argon cylinder is inserted through the insulating tube and into the mouth of the probe. A small stream of argon is continuously fed into the probe stack through this tube to exclude air and prevent condensation of water and buildup of ice. The argon tube and insulating jacket are removed only temporarily when inserting or ejecting NMR samples. It is important that the piece of PVC pipe is included, because placing the foam jacket directly over the top of the probe stack can result in small pieces of foam falling into the probe due to repeated scraping against the top of the probe stack every time the jacket is installed or removed.

A flame-sealed NMR tube containing pure $CDCl_2F$ is inserted into the probe, the shim files for $CDCl_3$ are selected, and adjustments for tuning, matching, and shimming are made from this point. The temperature of the probe is slowly decreased in 10-degree intervals, tuning and matching every 20 degrees and shimming every 40 degrees. In this way the proper tuning, matching, and shimming parameters are most easily attained at the very low temperatures necessary for the experiments. Once the probe temperature reaches –135 °C, the sample of pure solvent is ejected and the analyte sample is inserted. For best results, any condensation and/or ice must be wiped off the NMR tube and spinner with a Kimwipes® tissue[2] immediately before insertion of the sample into the probe; the wiping must be performed quickly in order to avoid

warming the sample. At such low temperatures, samples are not able to spin in the spectrometer, so the spinner is kept turned off at all times. Once the sample has remained in the probe 10 minutes to allow temperature equilibration, the temperature is slowly raised to the desired experimental temperature. A final round of tuning, matching, and shimming is performed, and the desired experiments are run. When acquiring ^{19}F or ^{31}P data, capacitor sticks for ^{19}F or ^{31}P are inserted into the bottom of the probe, and tuning and matching for these nuclei are performed. If significant difficulty with shimming is encountered (which is more likely at these low temperatures), automatic shimming on the *x*, *y*, and *z* parameters can be performed.

References

1. Krytox™ is a trademark of The Chemours Company FC, LLC.
2. Kimwipes® is a registered trademark of Kimberly-Clark Worldwide, Inc.

Appendix B. Full NMR spectra of all new compounds

Shown below are NMR spectra of all new compounds reported in this thesis, as well those of a few compounds that have been reported previously but whose syntheses were modified, gave different results (primarily differences in yields), or for which additional spectra were acquired beyond those previously reported. All spectra show the full spectral width. All spectra were acquired on Varian spectrometers, and the MestReNova NMR software package was used for post-acquisition processing. Particular spectrometers, acquisition parameters, and post-acquisition processing methods are described in the experimental sections of the relevant chapters.

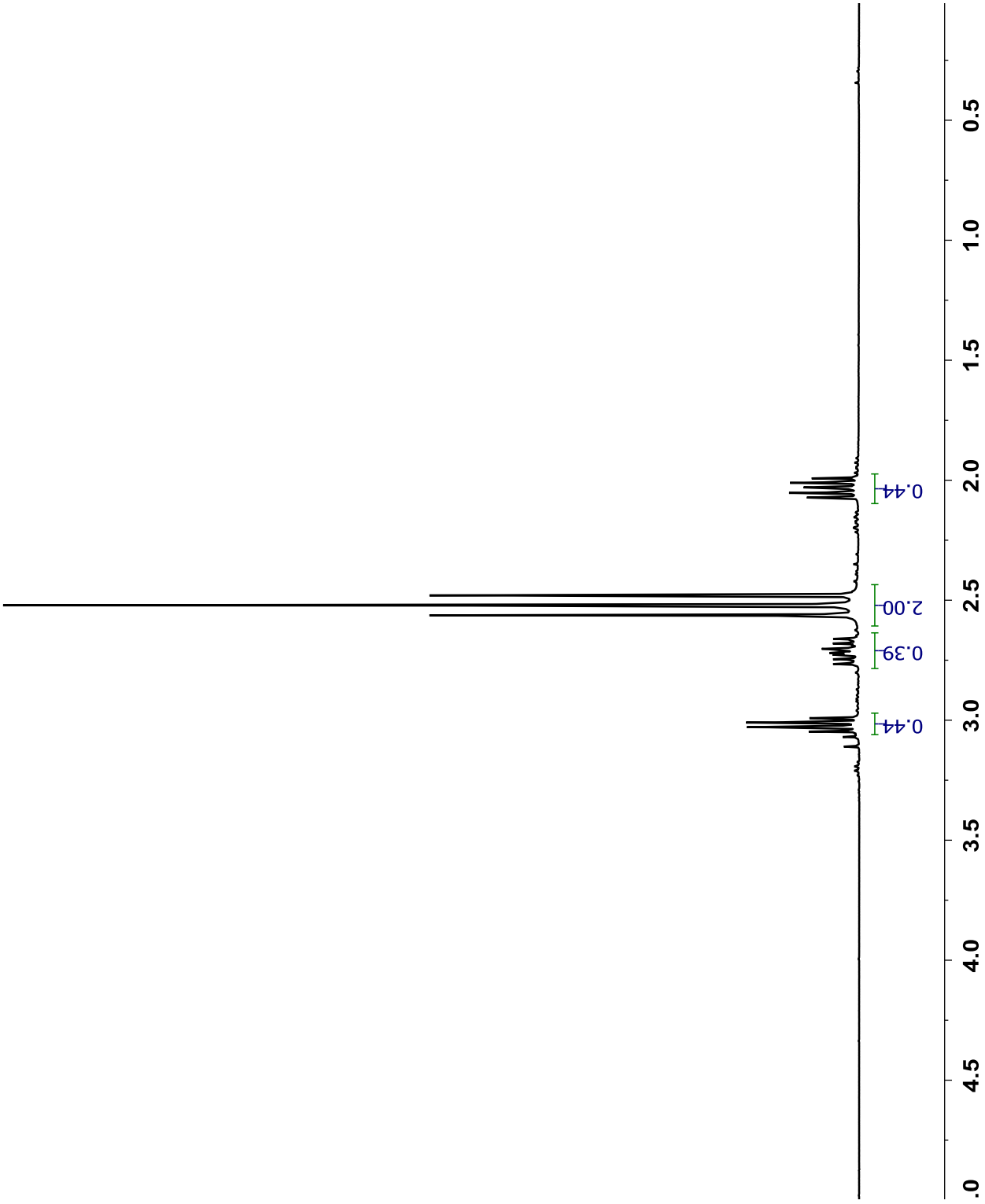

Figure B.1. ^{1}H NMR spectrum of $Cl_2PCH_2PCl_2$ in C_6D_6. Smaller peaks are due to impurities.

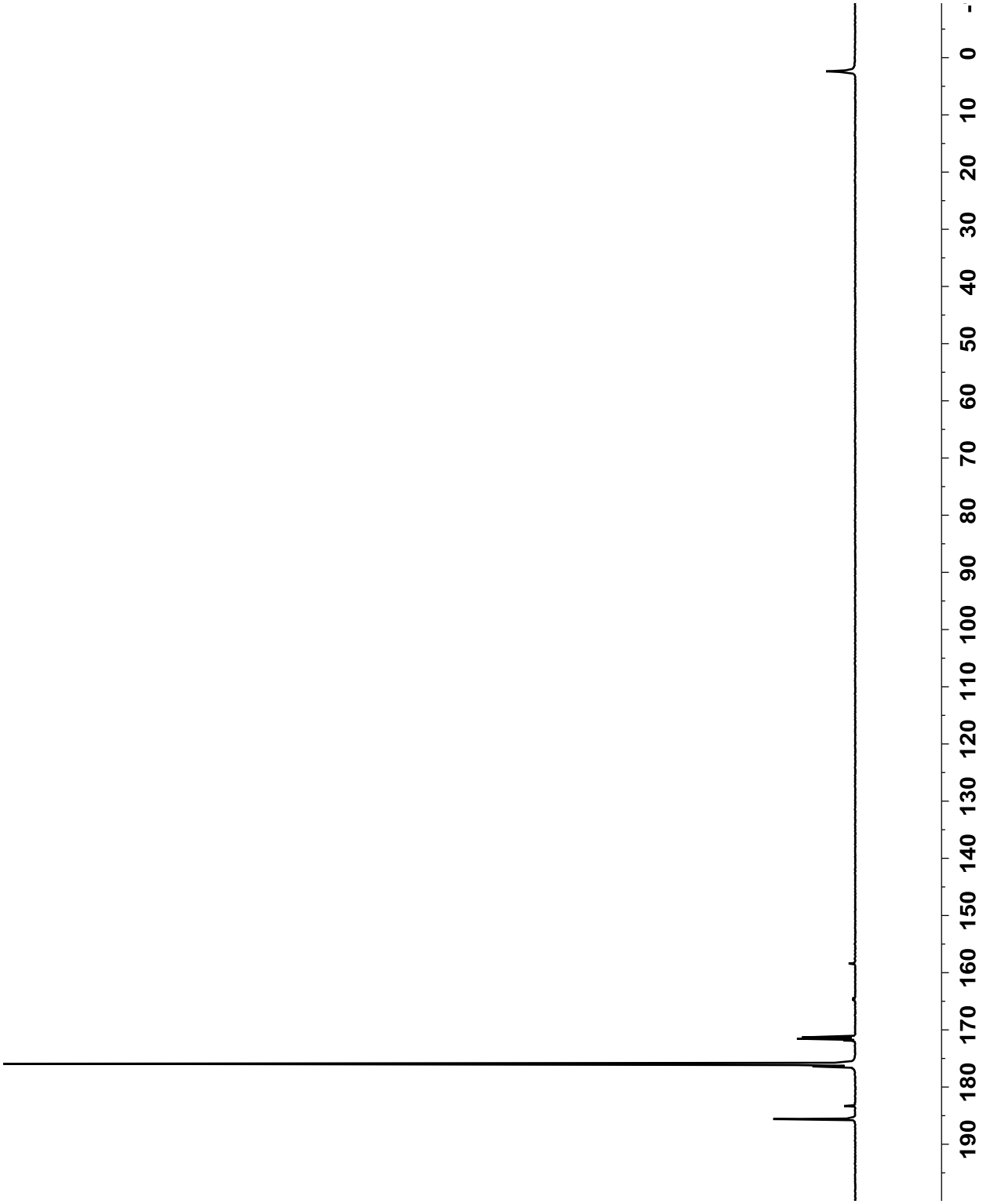

Figure B.2. ^{31}P NMR spectrum of $Cl_2PCH_2PCl_2$ in C_6D_6. Smaller peaks are due to impurities.

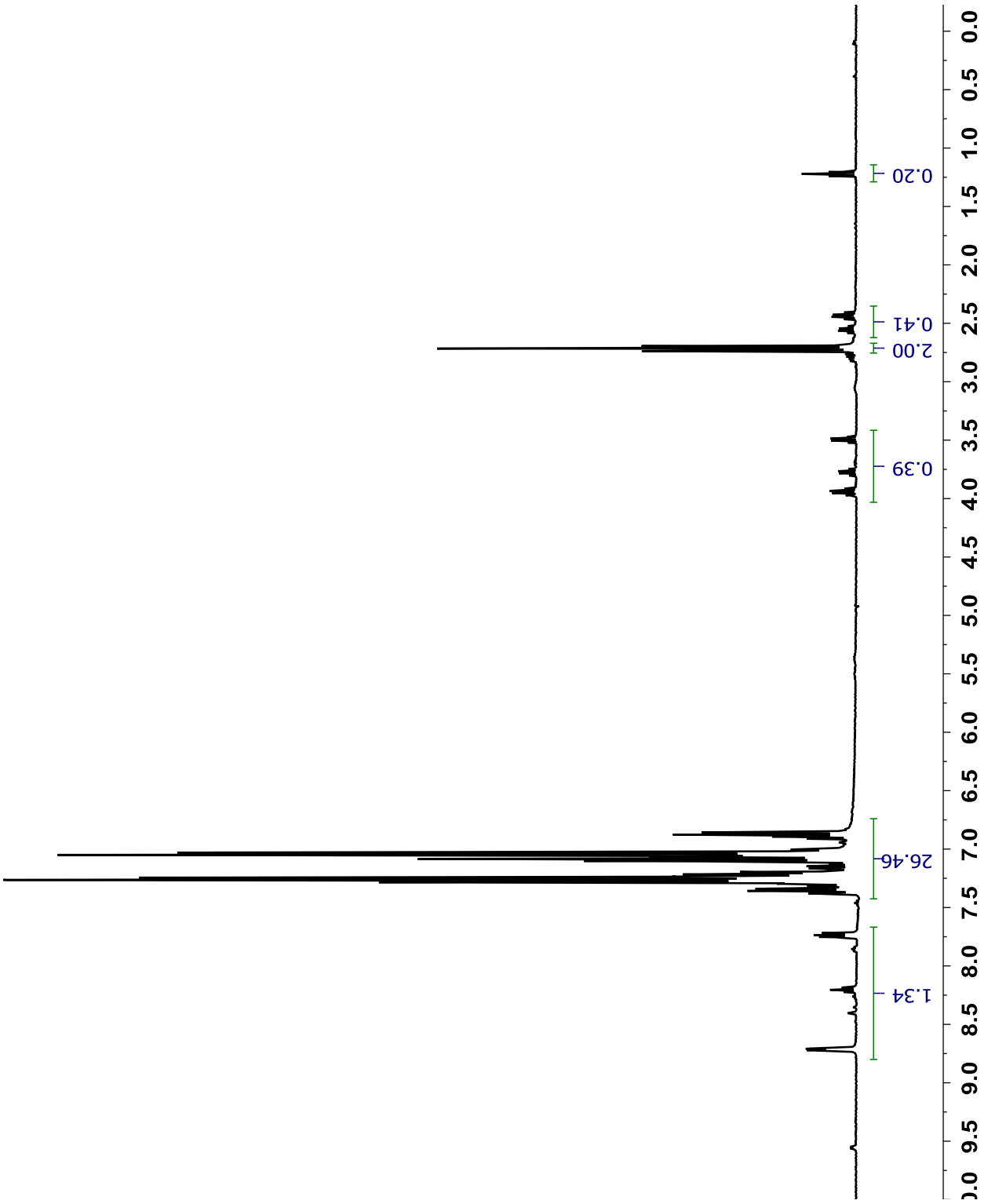

Figure B.3. ^{1}H NMR spectrum of $(PhO)_2PCH_2P(OPh)_2$ in $CDCl_3$. Smaller peaks are due to impurities.

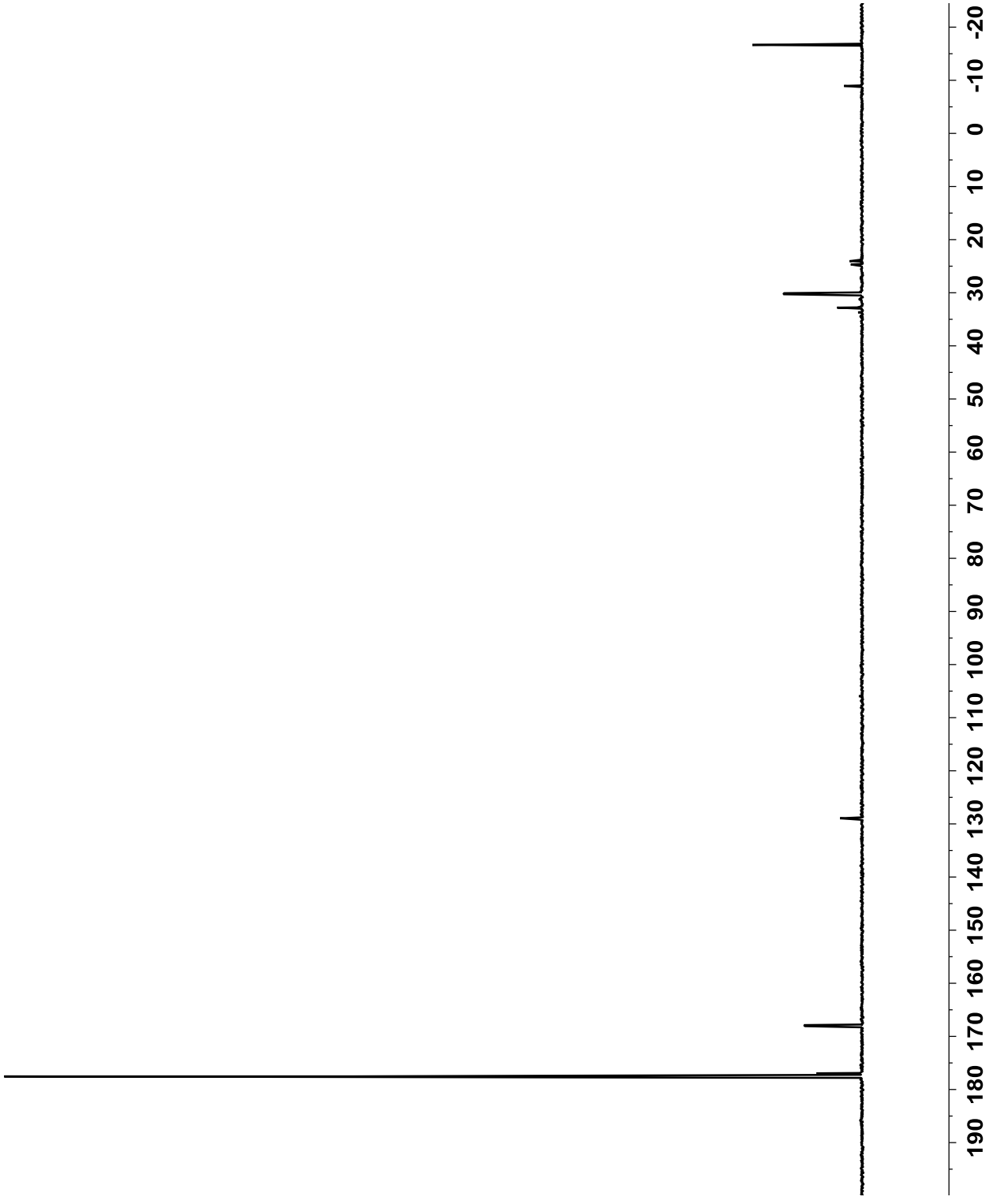

Figure B.4. ^{31}P NMR spectrum of $(PhO)_2PCH_2P(OPh)_2$ in $CDCl_3$. Smaller peaks are due to impurities.

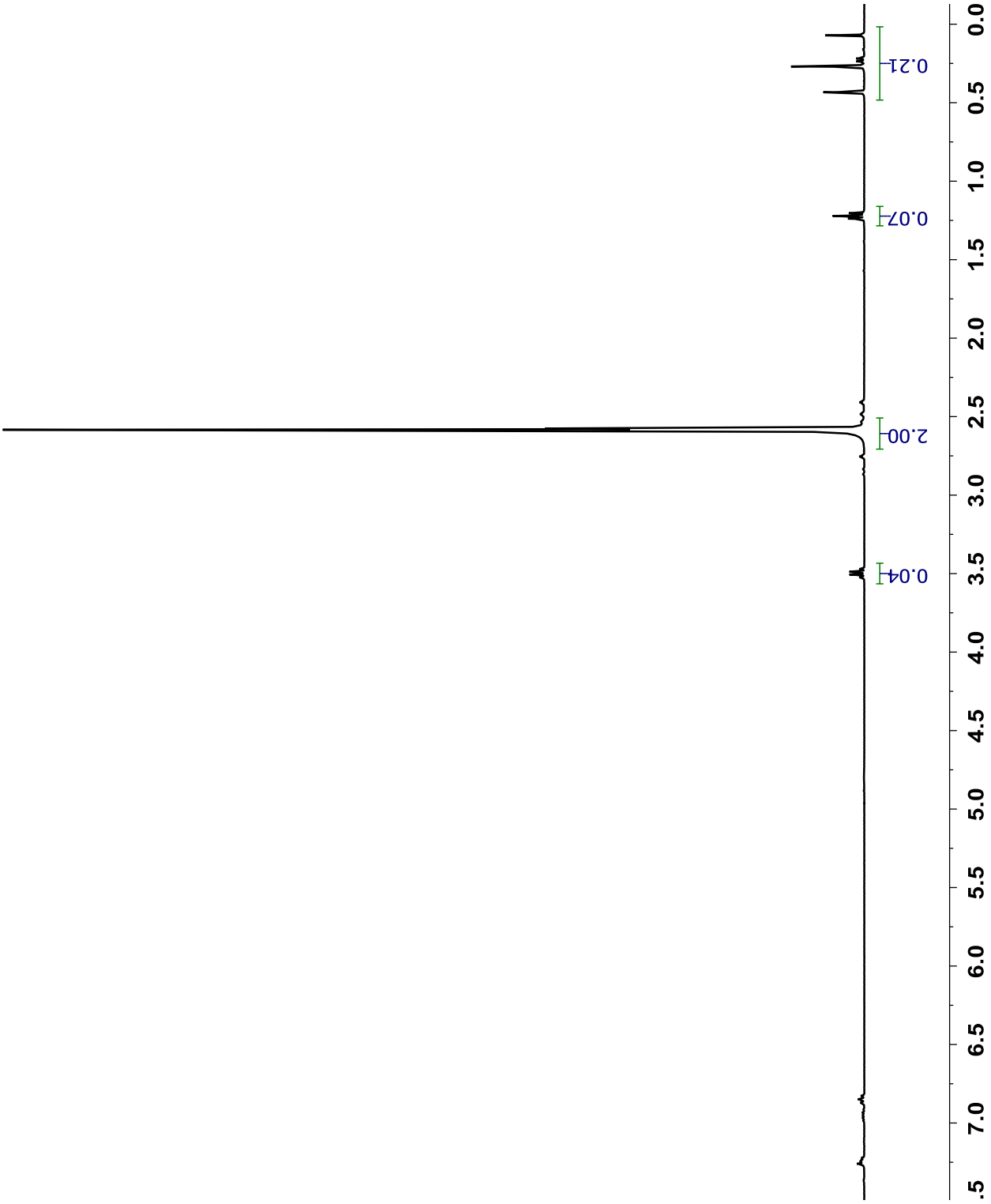

Figure B.5. ^{1}H NMR spectrum of $(CF_3)_2PCH_2P(CF_3)_2$ in $CDCl_3$. Minor contamination from diethyl ether, phenol derivatives, and aliphatic silicon-containing compounds can be seen.

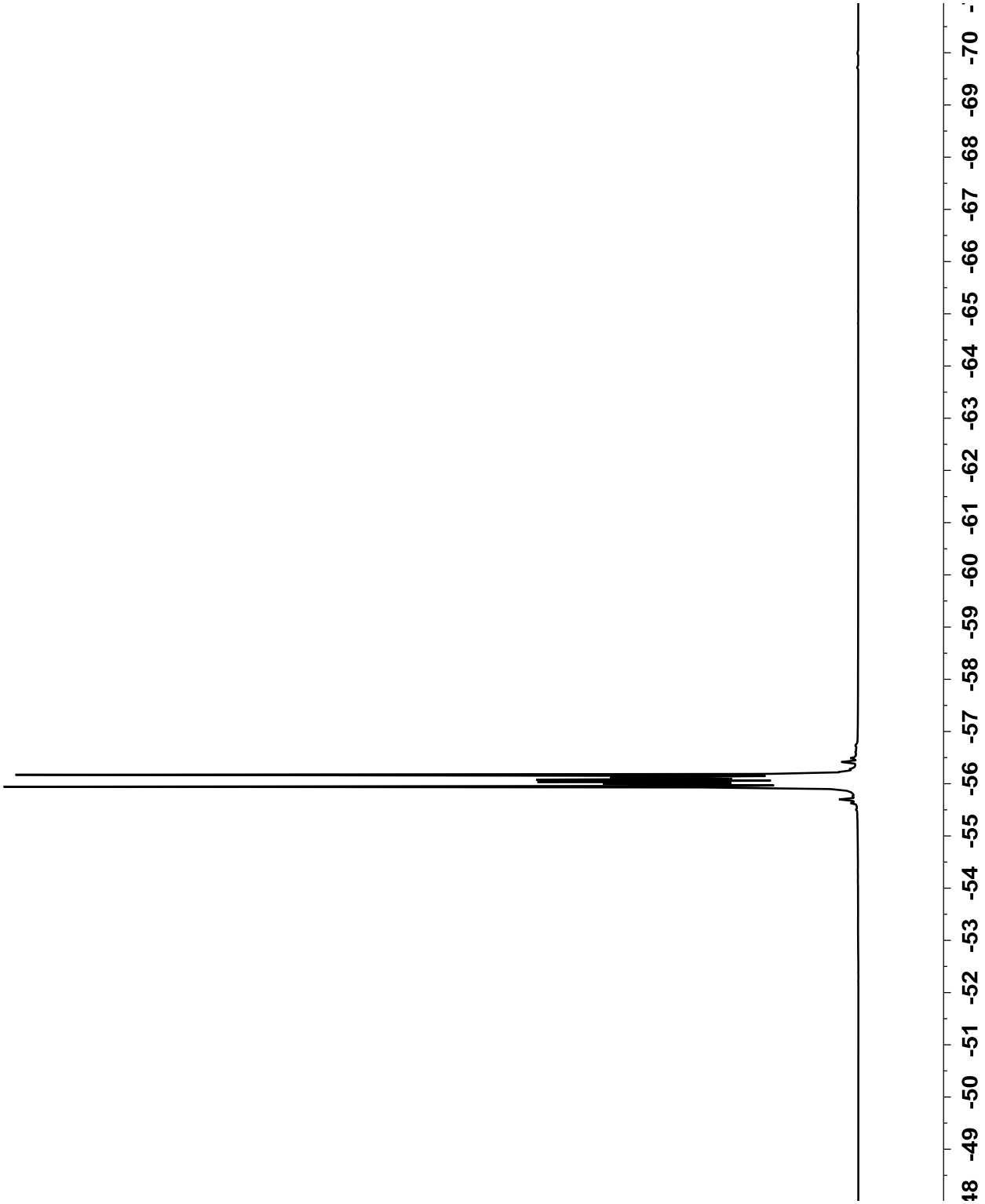

Figure B.6. ^{19}F NMR spectrum of $(CF_3)_2PCH_2P(CF_3)_2$ in $CDCl_3$. A resonance from a minor contaminant is barely visible around δ –70.

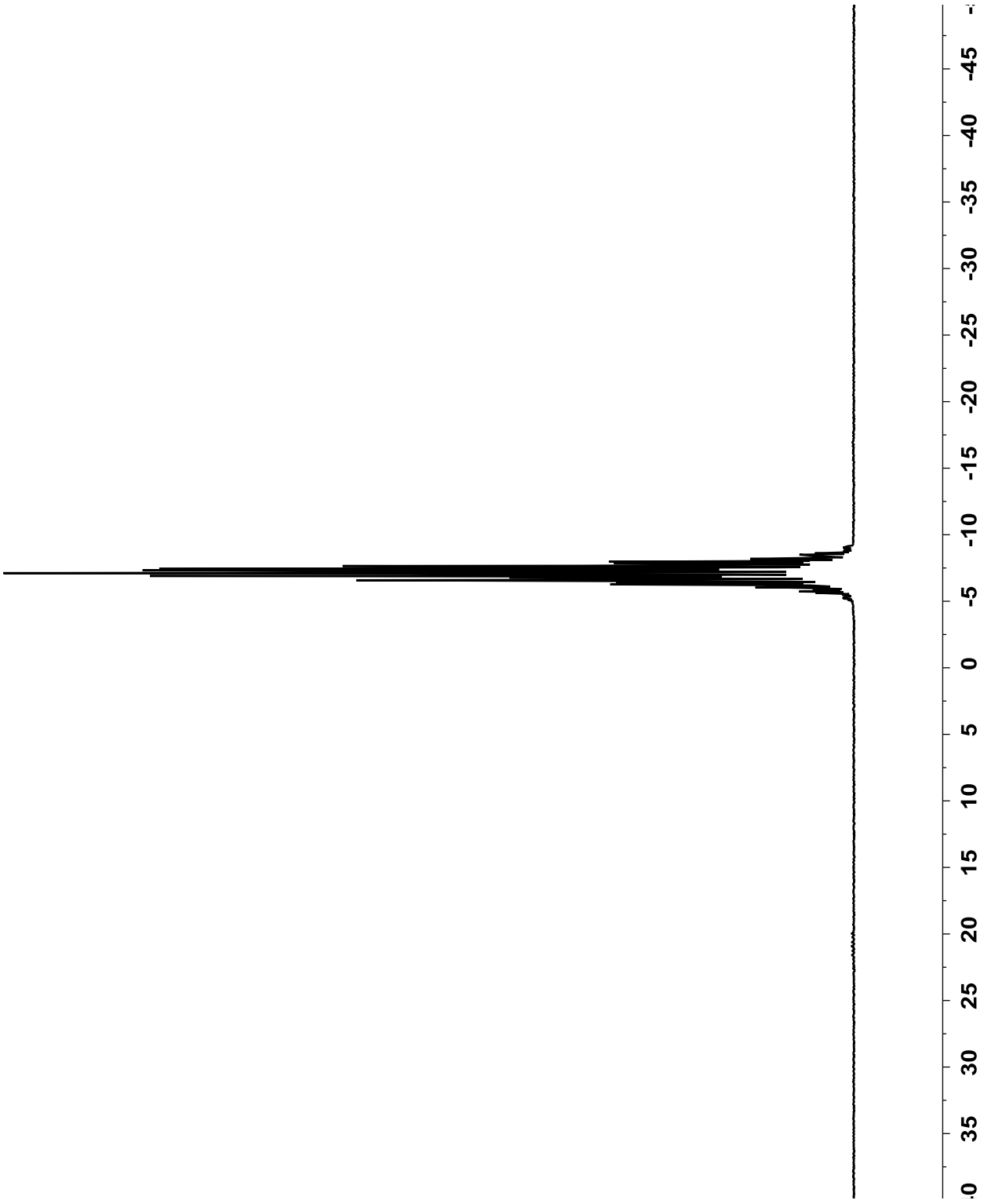

Figure B.7. ^{31}P NMR spectrum of $(CF_3)_2PCH_2P(CF_3)_2$ in $CDCl_3$. A resonance from a minor contaminant is barely visible around δ 20.

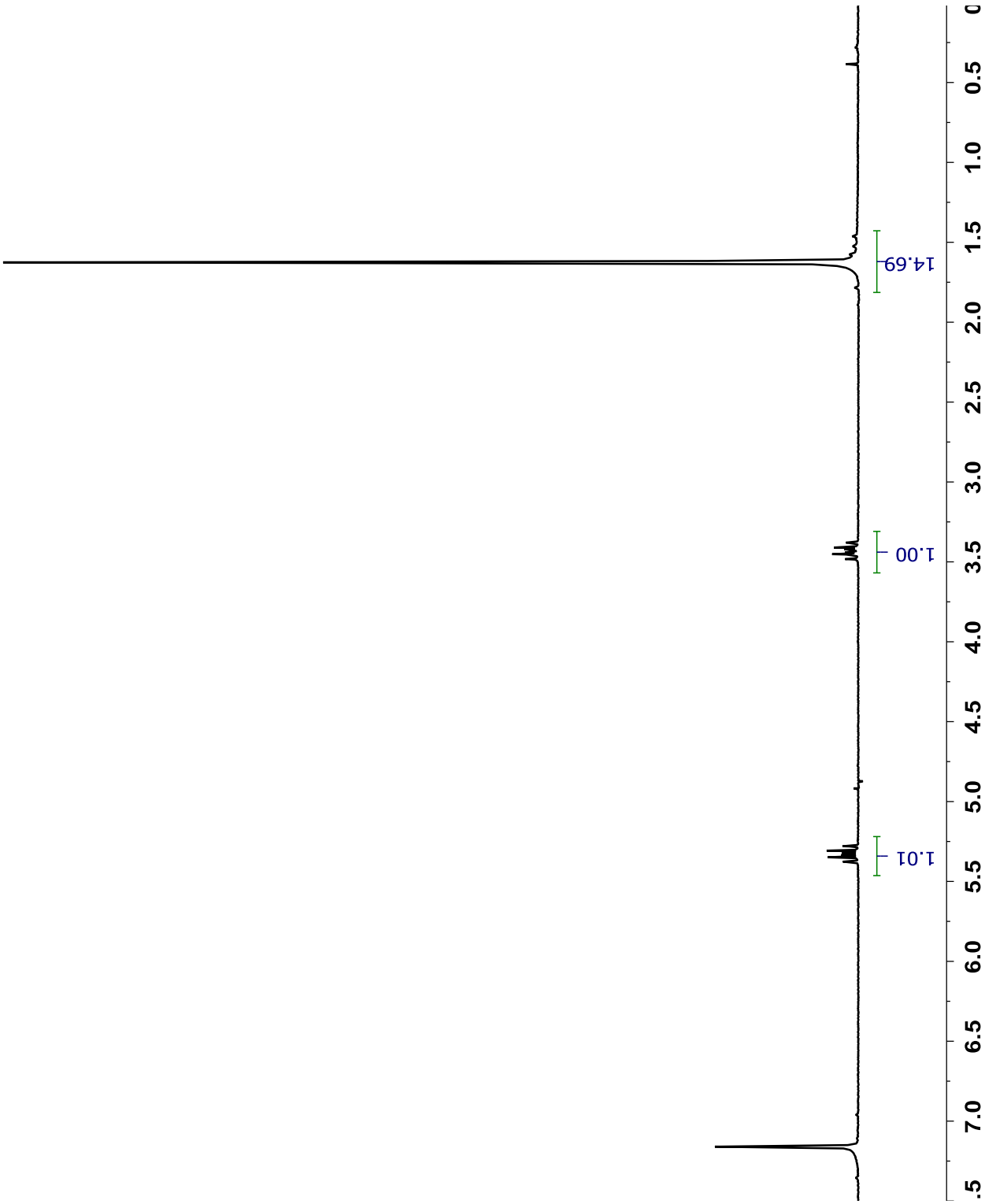

Figure B.8. ^{1}H NMR spectrum of Cp*Os(dfmpm)Br in C_6D_6. Minor contamination from water and silicone grease can be seen.

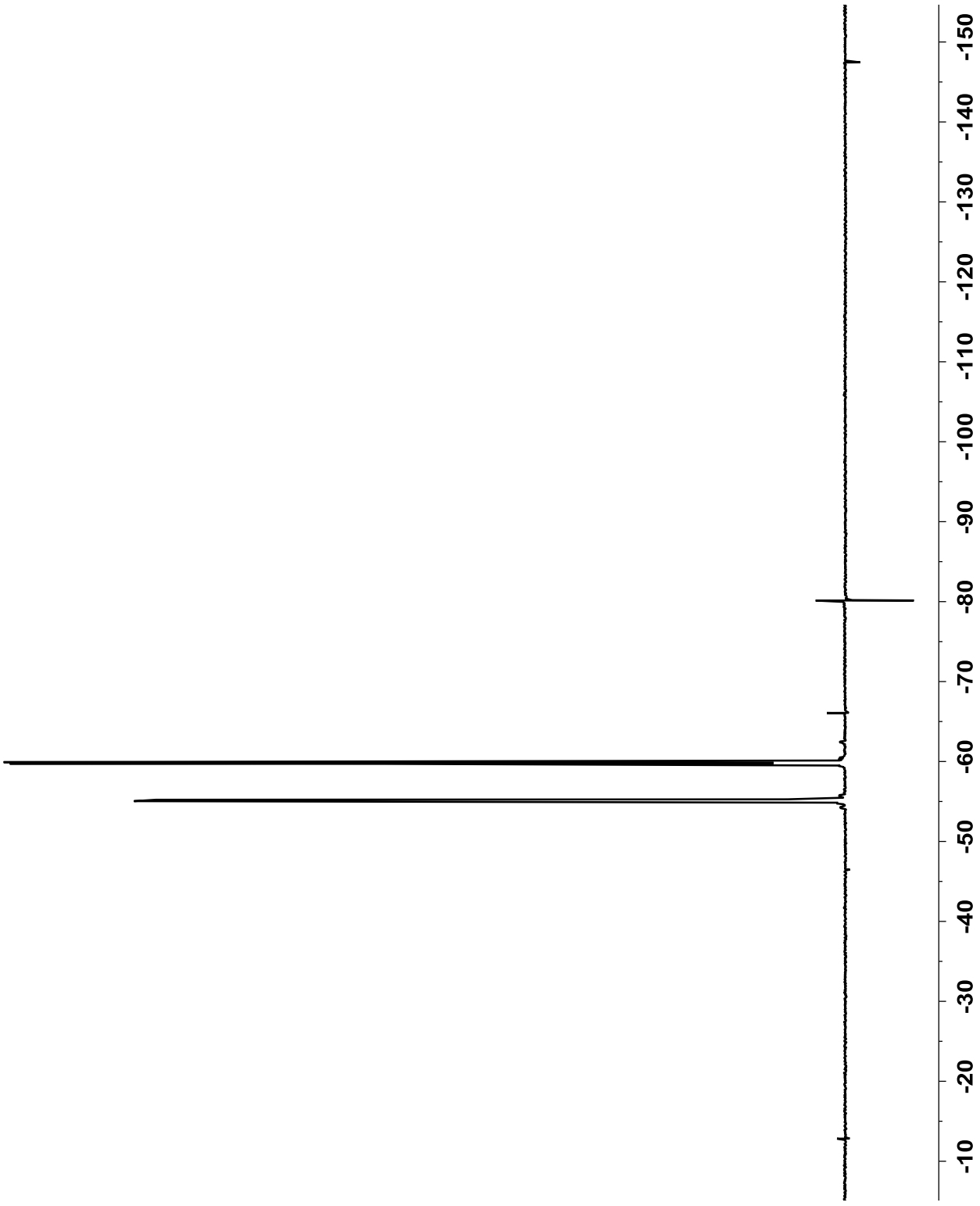

Figure B.9. ^{19}F NMR spectrum of Cp*Os(dfmpm)Br in C_6D_6.

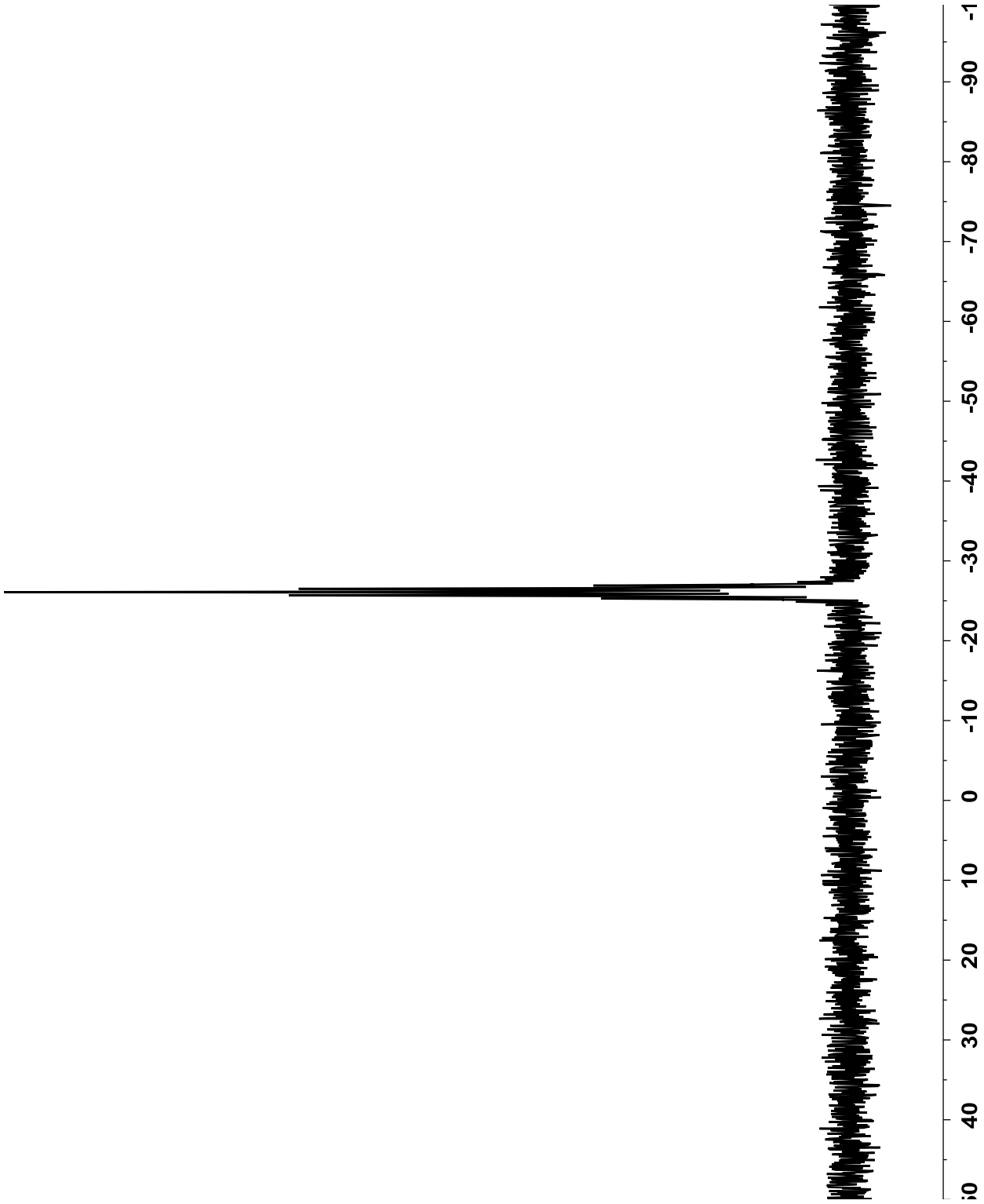

Figure B.10. ^{31}P NMR spectrum of Cp*Os(dfmpm)Br in C_6D_6.

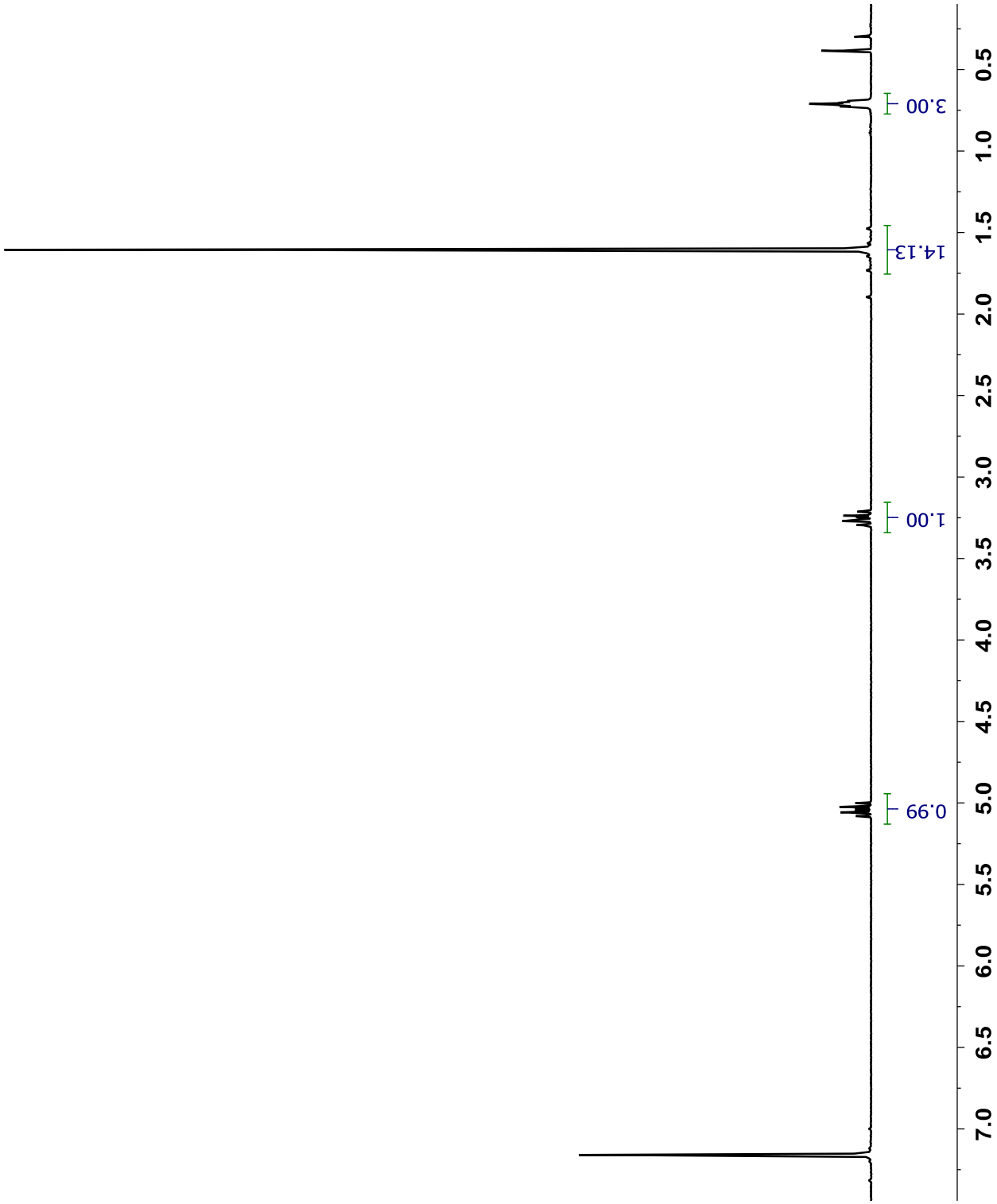

Figure B.11. ^{1}H NMR spectrum of Cp*Os(dfmpm)Me in C_6D_6. Minor contamination from water and silicone grease can be seen.

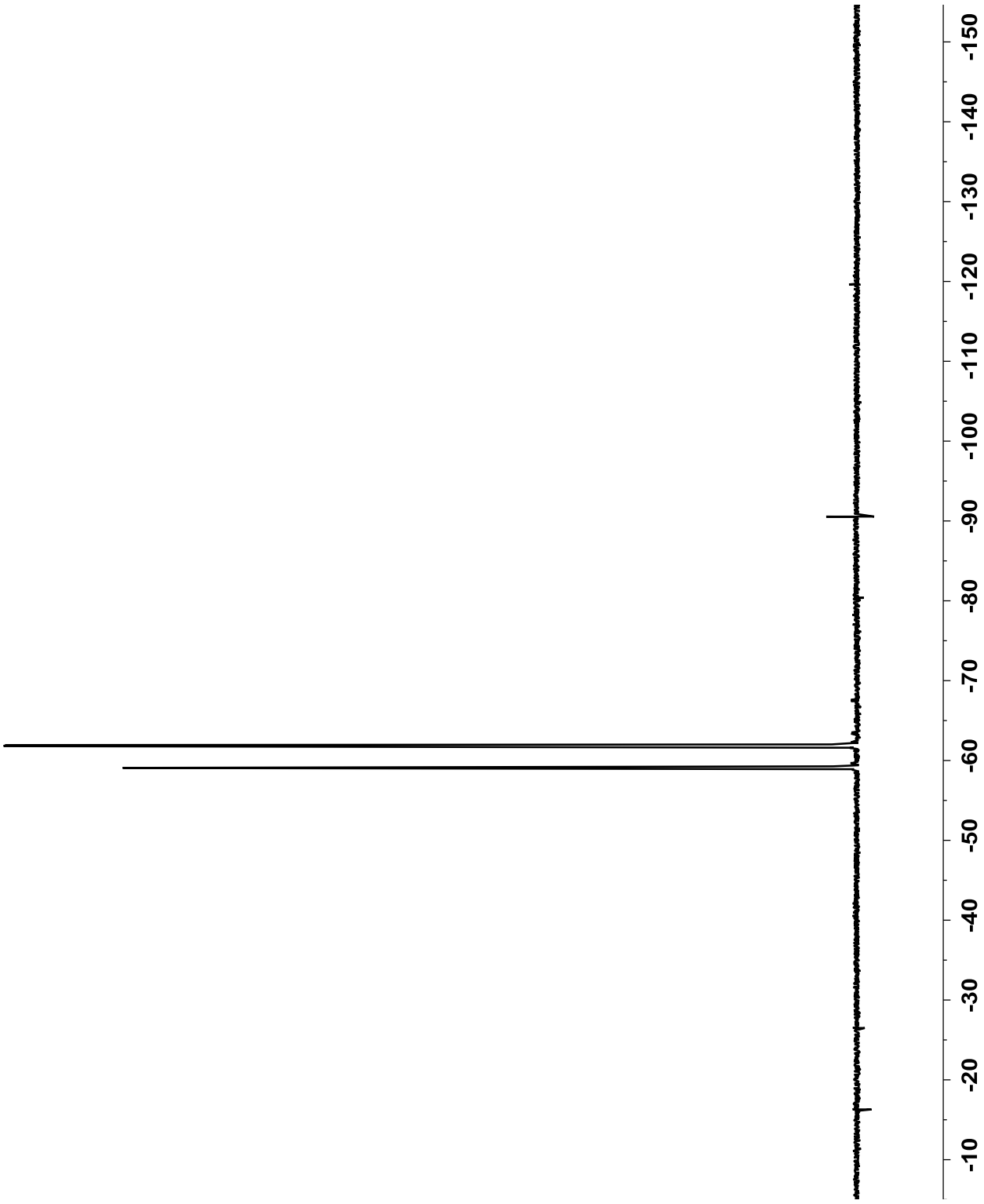

Figure B.12. ^{19}F NMR spectrum of Cp*Os(dfmpm)Me in C_6D_6.

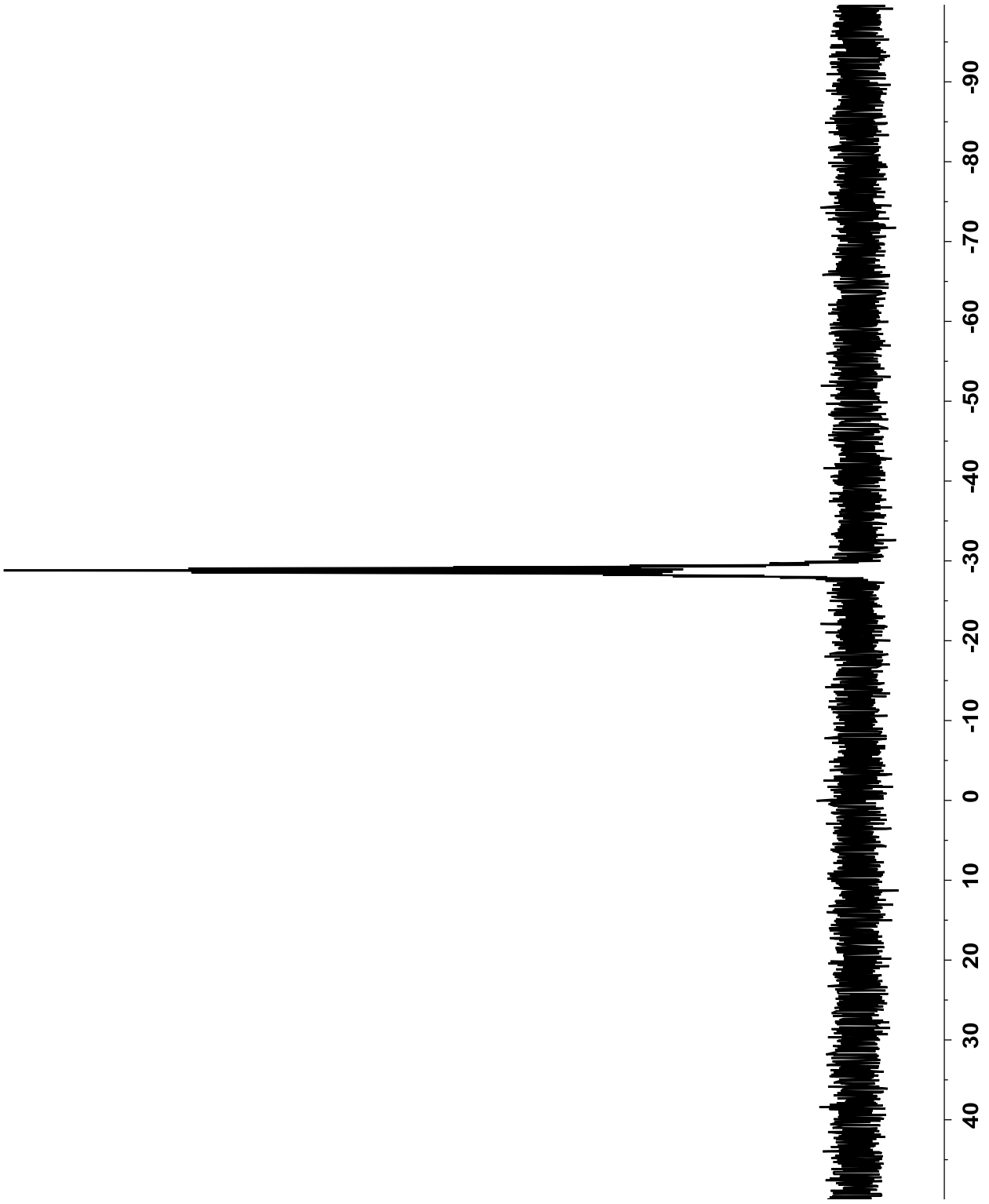

Figure B.13. ^{31}P NMR spectrum of Cp*Os(dfmpm)Me in C_6D_6.

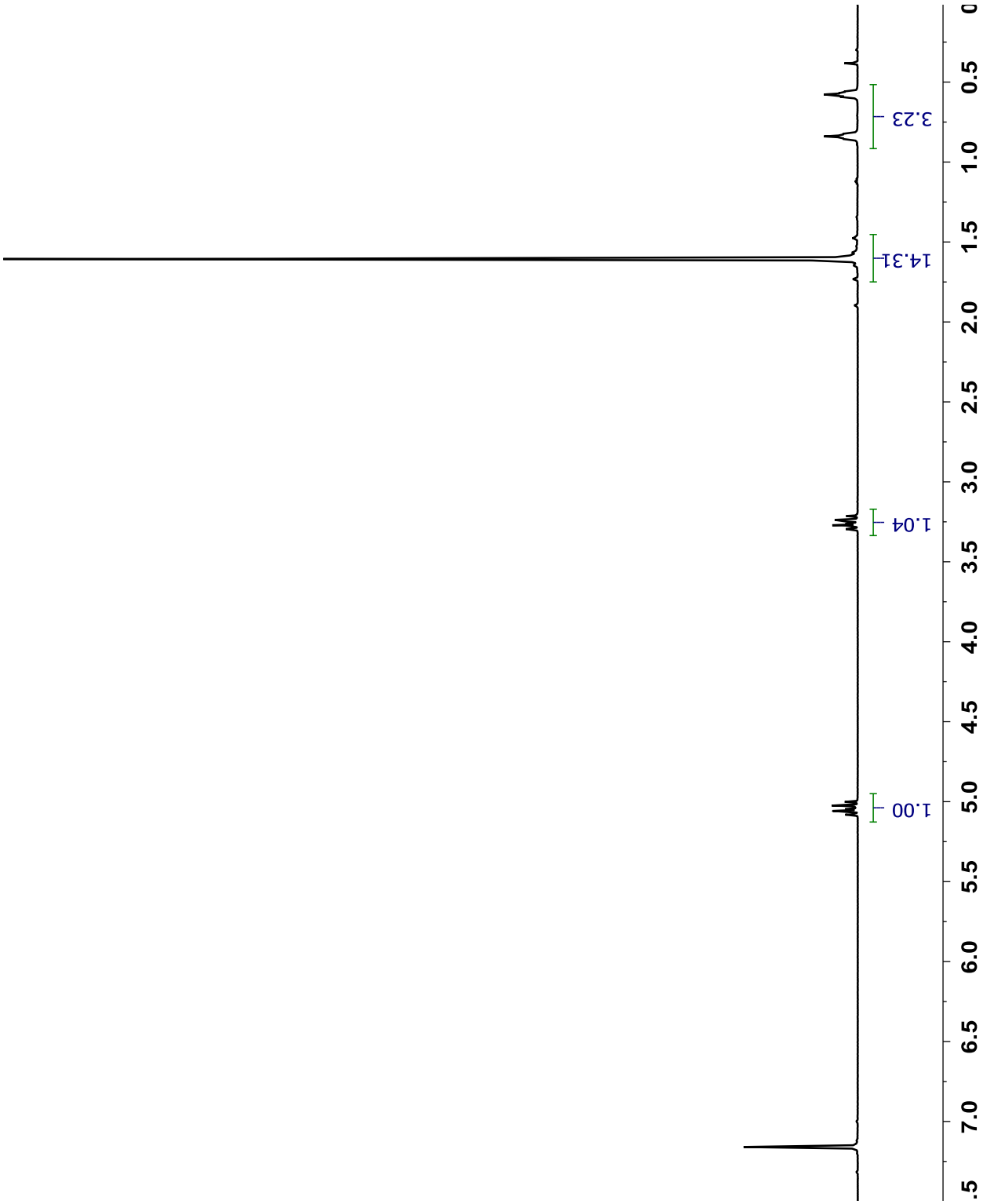

Figure B.14. ^{1}H NMR spectrum of Cp*Os(dfmpm)$^{13}CH_3$ in C_6D_6. Minor contamination from water can be seen.

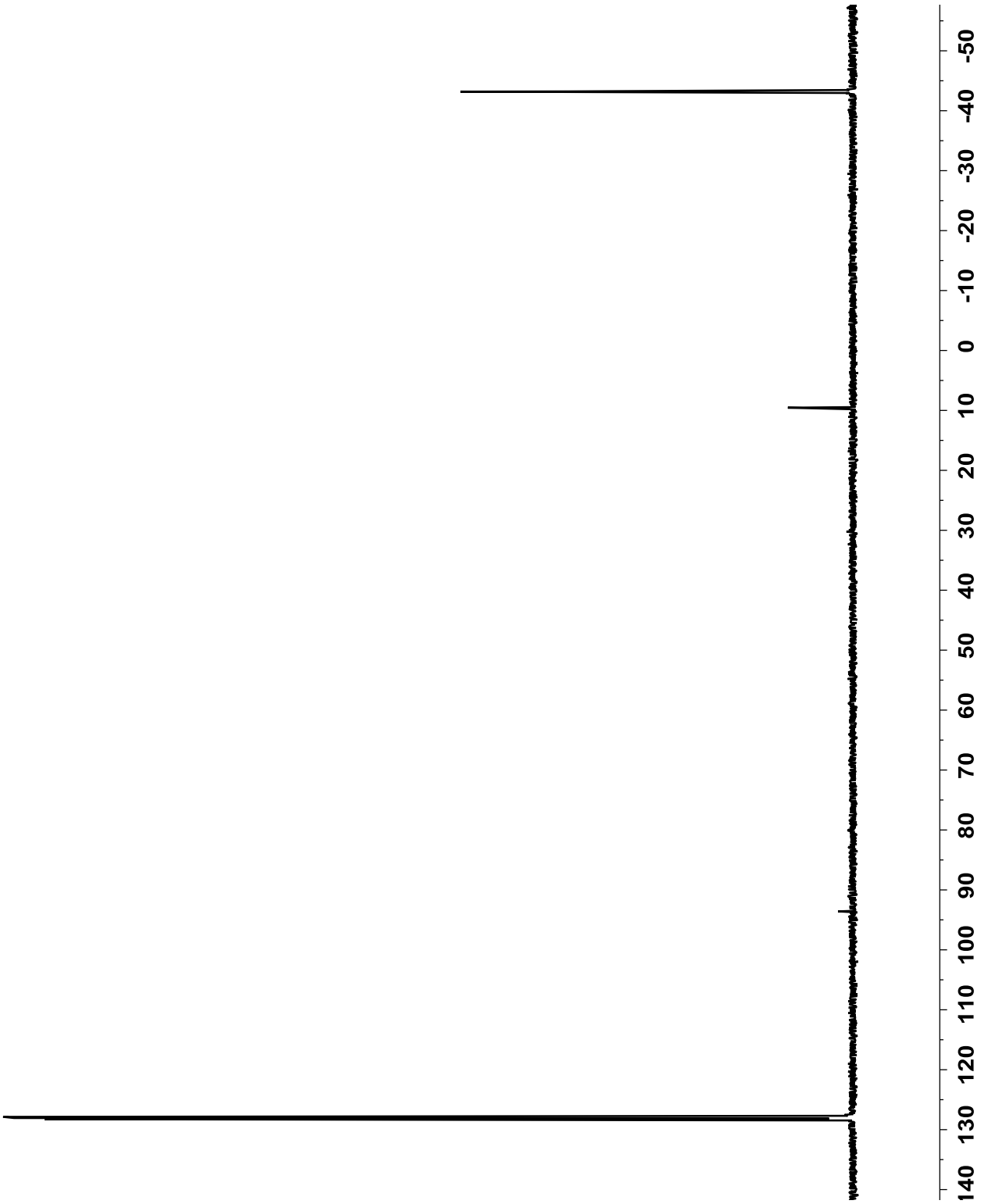

Figure B.15. ^{13}C NMR spectrum of Cp*Os(dfmpm)$^{13}CH_3$ in C_6D_6.

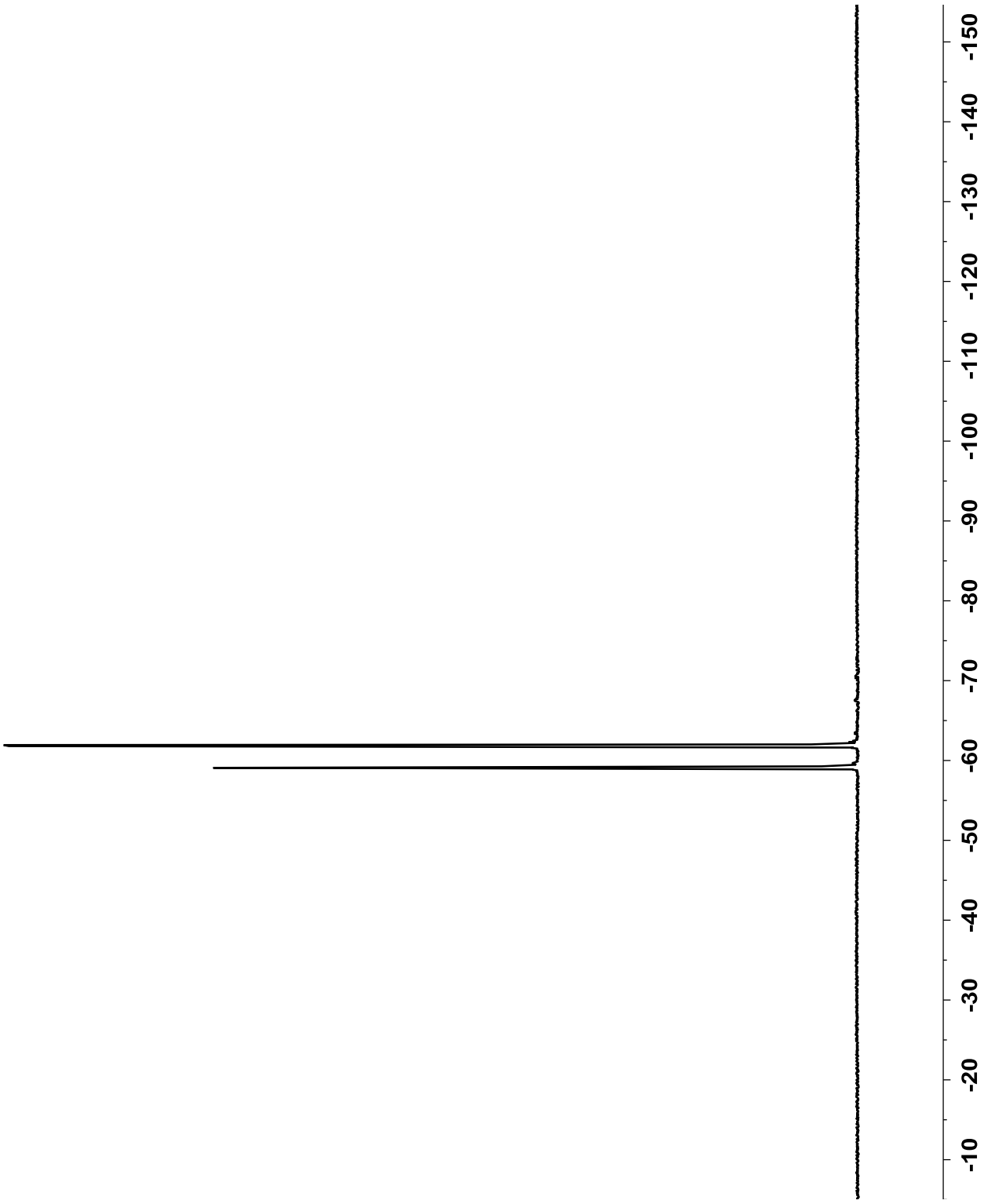

Figure B.16. ^{19}F NMR spectrum of Cp*Os(dfmpm)$^{13}CH_3$ in C_6D_6.

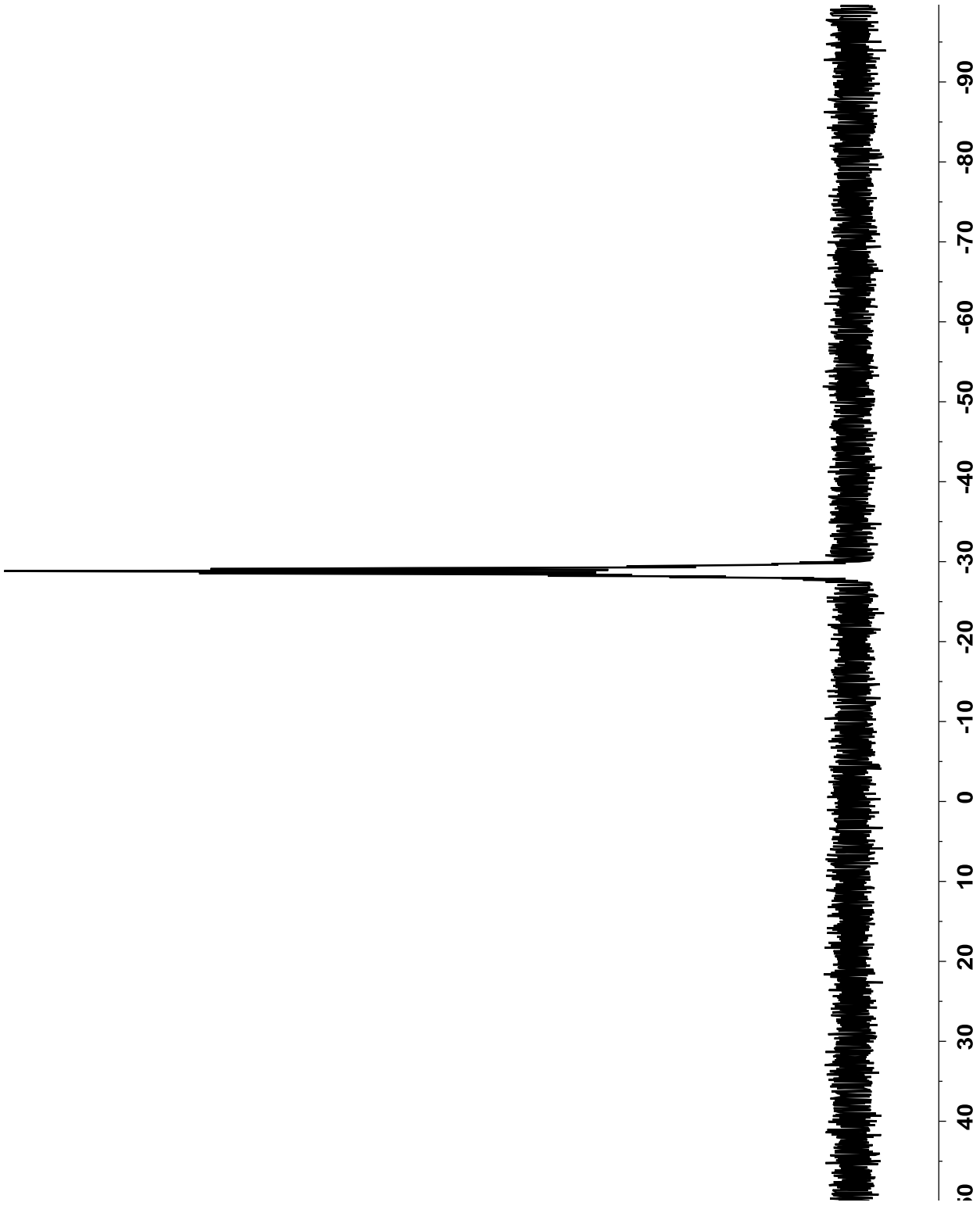

Figure B.17. ^{31}P NMR spectrum of Cp*Os(dfmpm)$^{13}CH_3$ in C_6D_6.

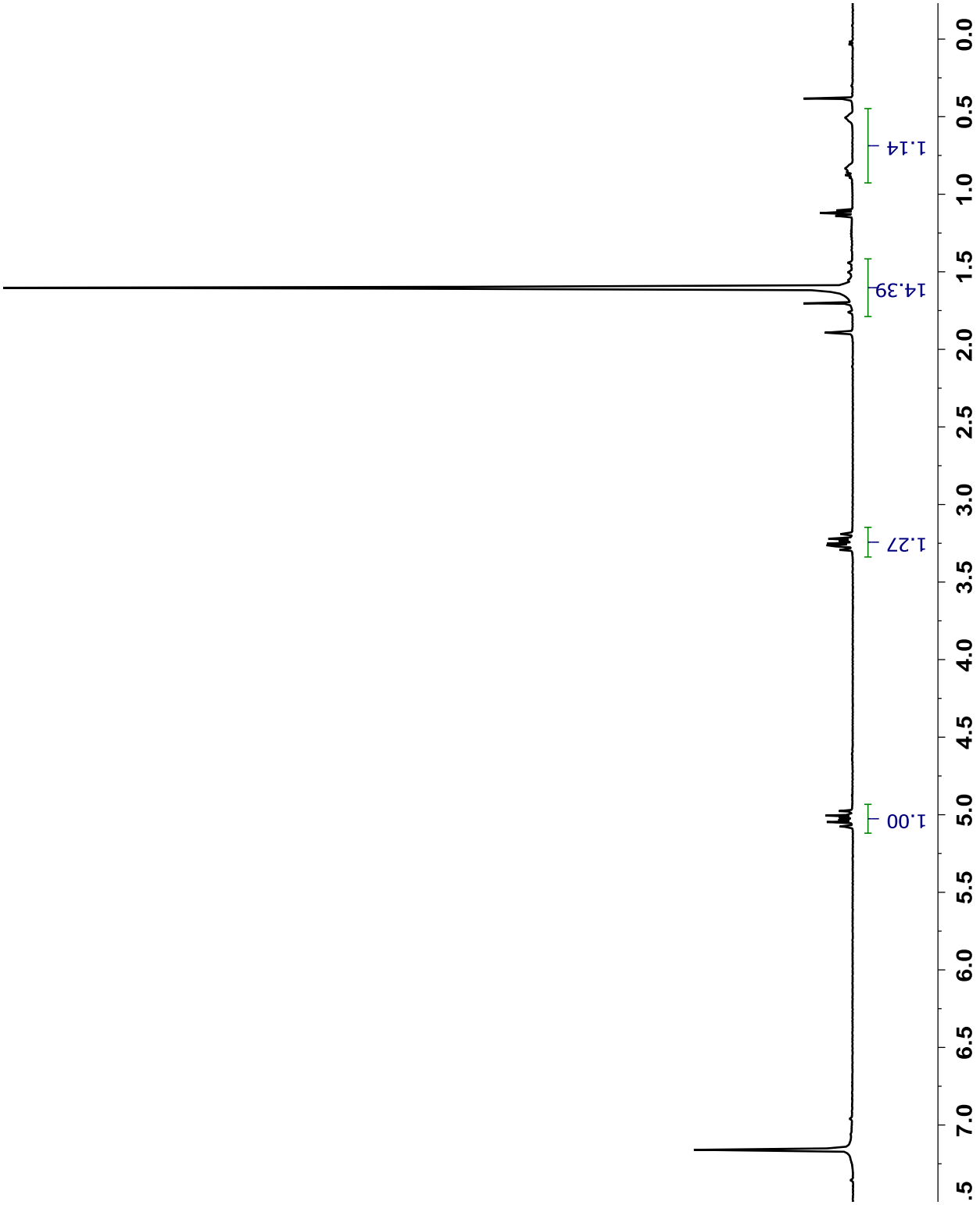

Figure B.18. ^{1}H NMR spectrum of Cp*Os(dfmpm)$^{13}CHD_2$ in C_6D_6. Minor contamination from water and diethyl ether can be seen.

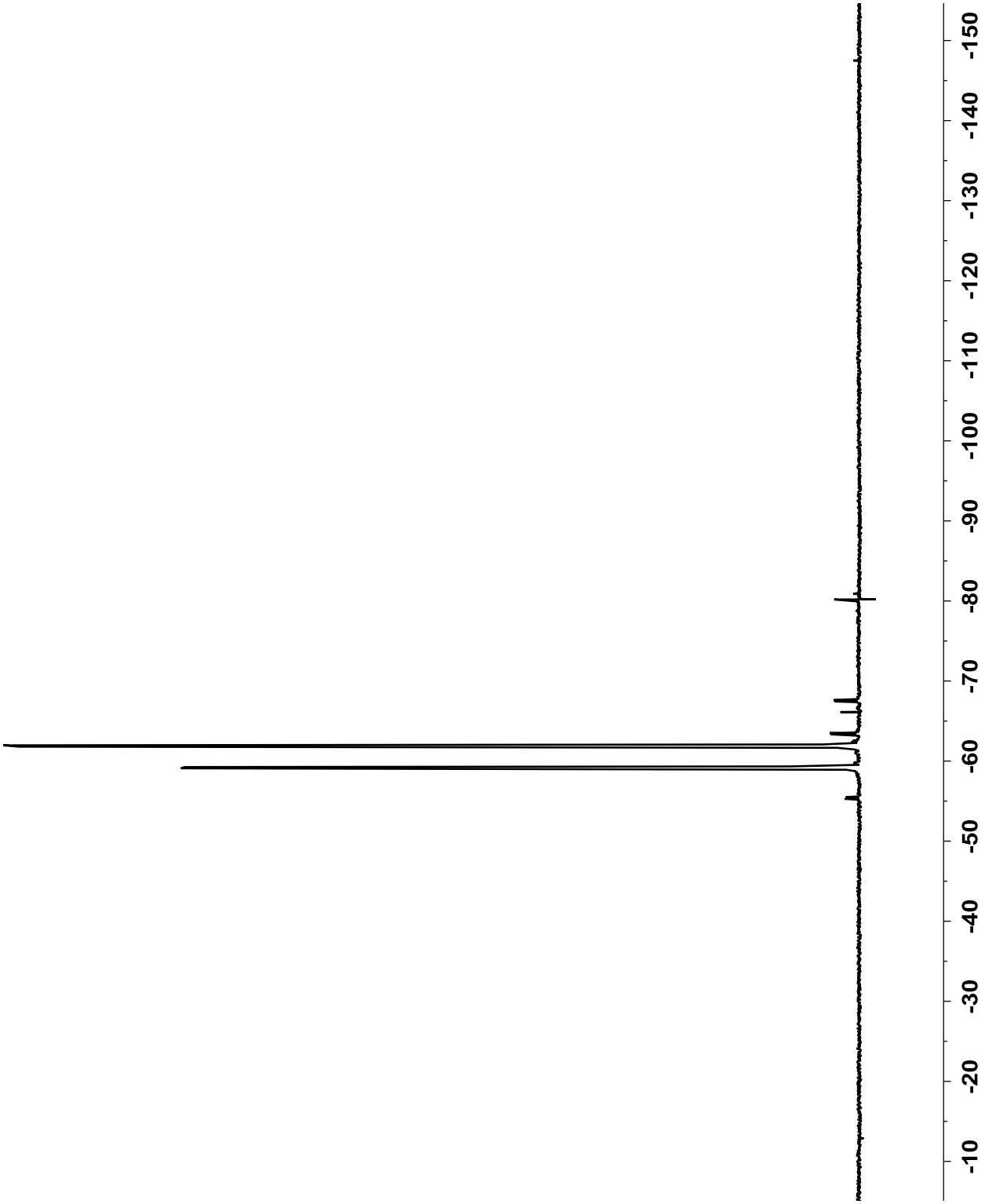

Figure B.19. ^{19}F NMR spectrum of Cp*Os(dfmpm)$^{13}CHD_2$ in C_6D_6.

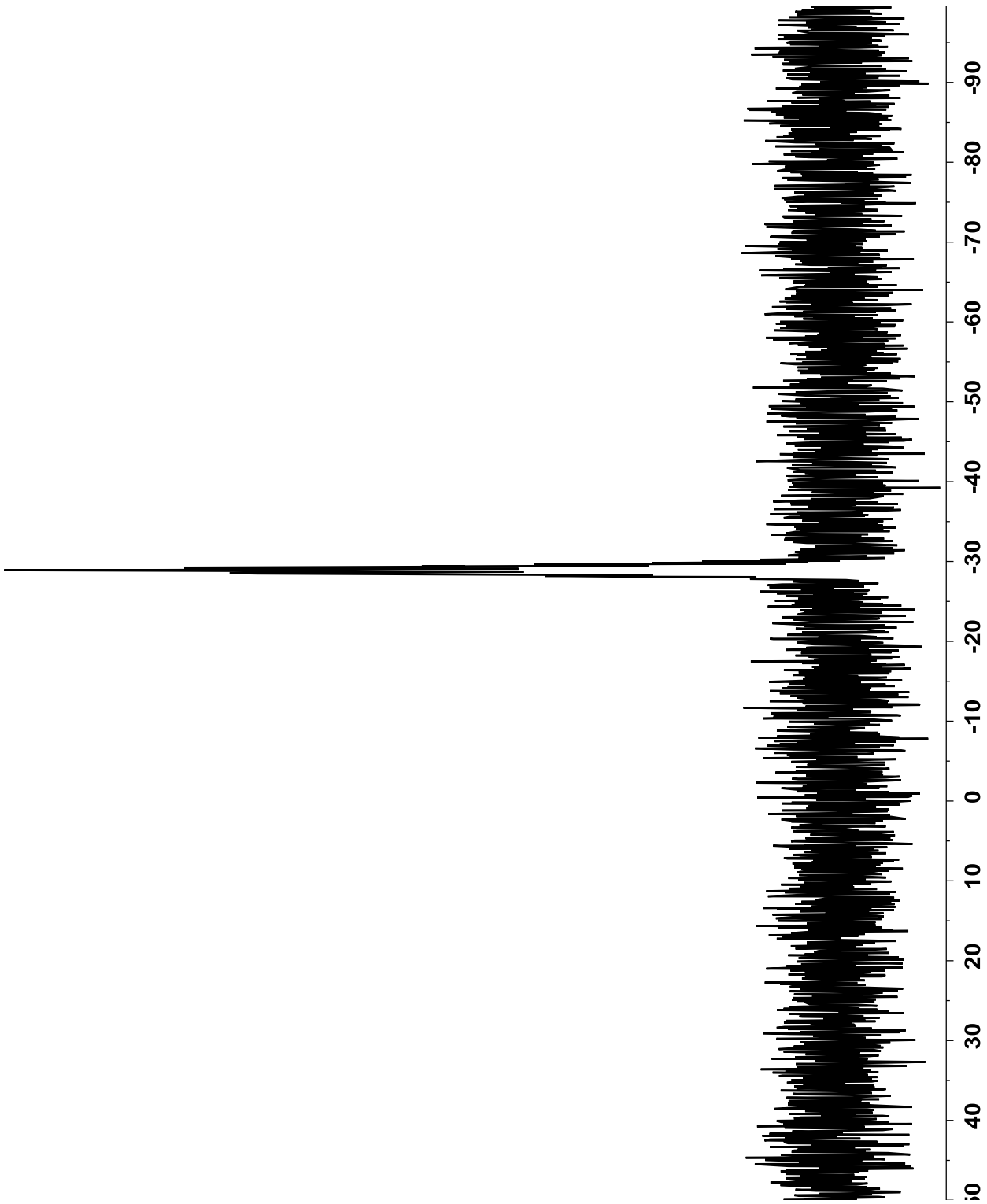

Figure B.20. ^{31}P NMR spectrum of Cp*Os(dfmpm)$^{13}CHD_2$ in C_6D_6.

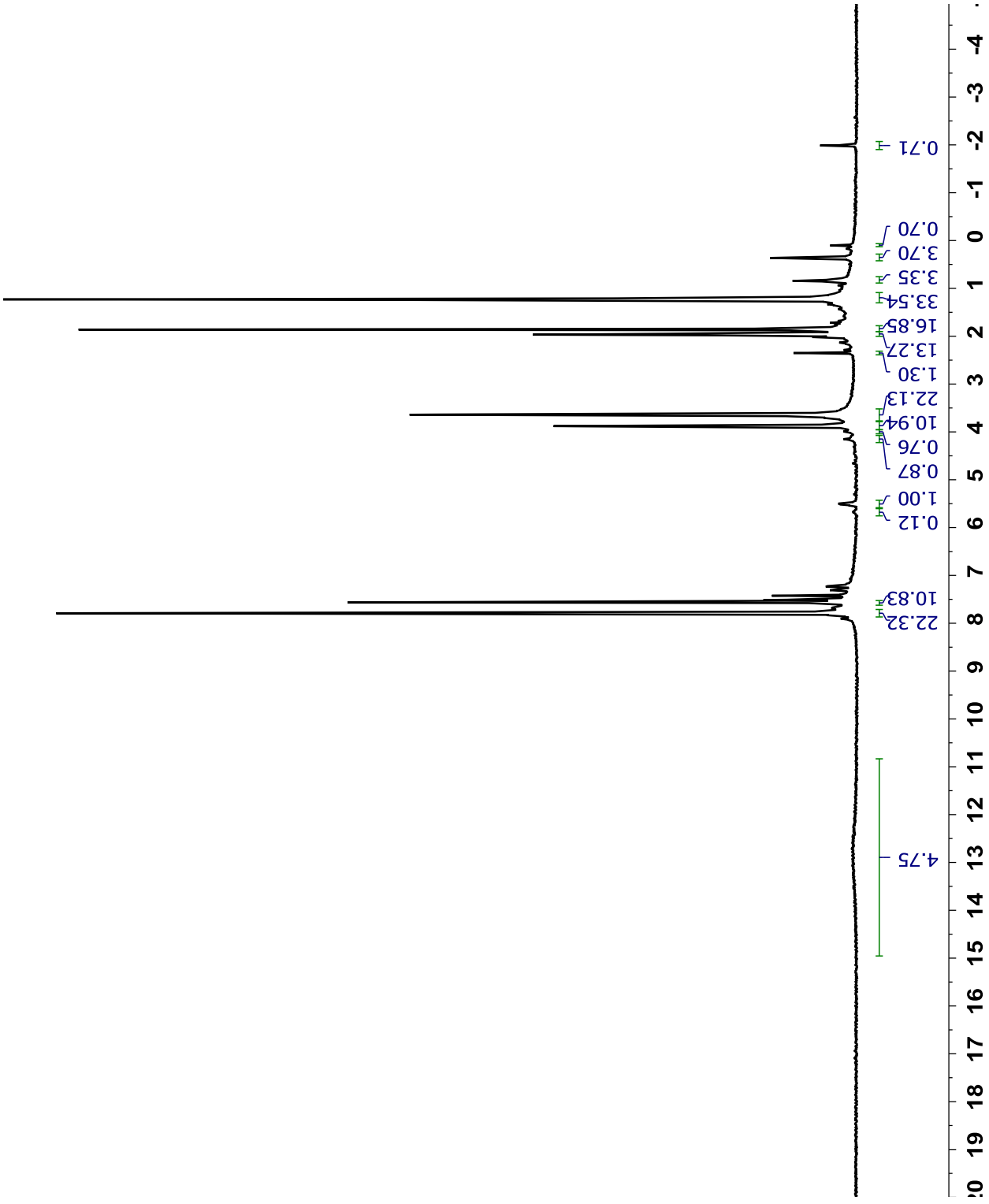

Figure B.21. ^{1}H NMR spectrum of [Cp*Os(dfmpm)CH_4][$B(C_6H_3(CF_3)_2)_4$] at –120 °C in $CDCl_2F$. Minor contamination from silicone grease can be seen, as well as a significant amount of unreacted Cp*Os(dfmpm)Me and $HBAr^F{}_4\cdot(Et_2O)_2$ (the very broad peak around δ 13).

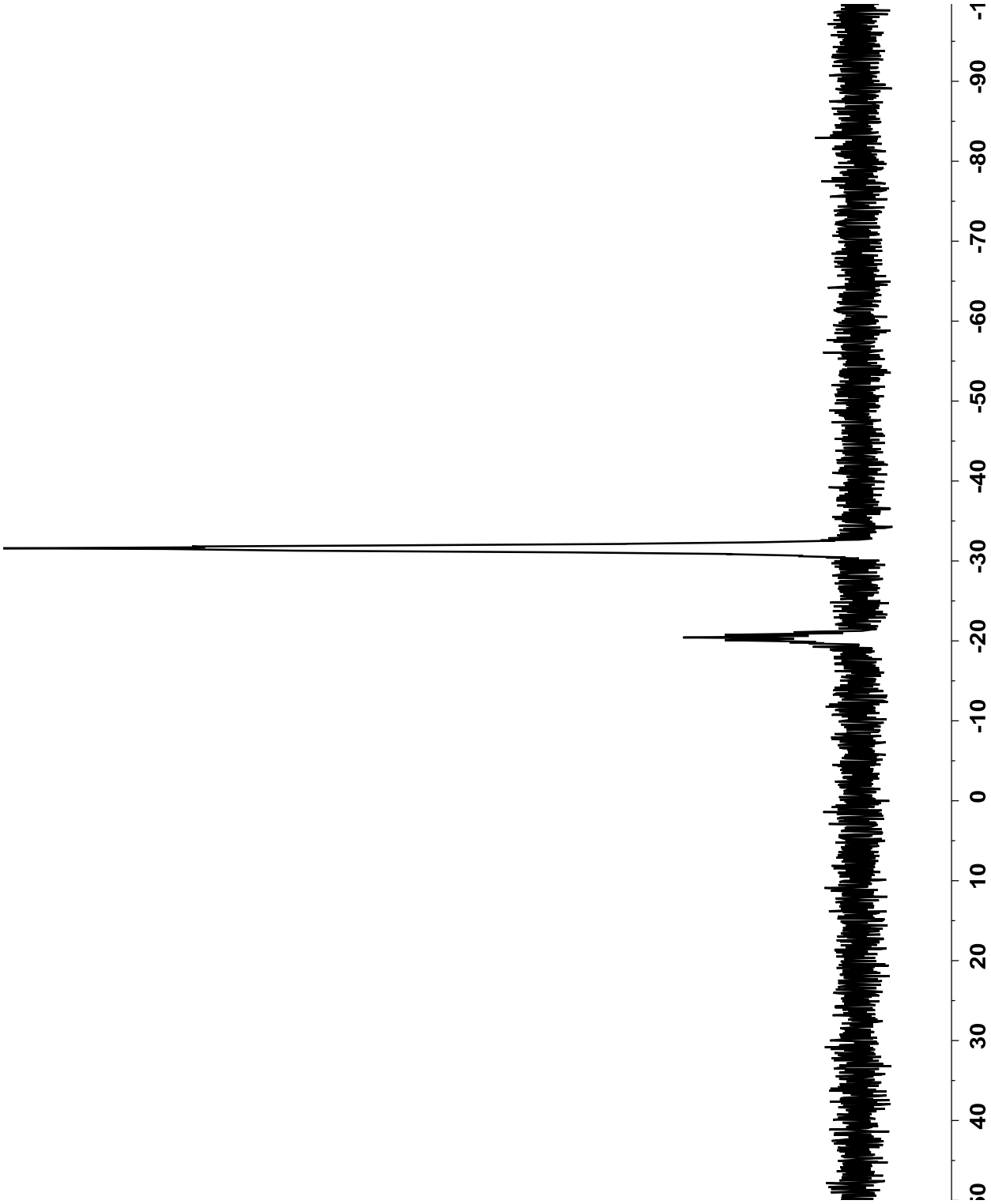

Figure B.22. ^{31}P NMR spectrum of $[Cp^*Os(dfmpm)CH_4][B(C_6H_3(CF_3)_2)_4]$ at –120 °C in $CDCl_2F$.

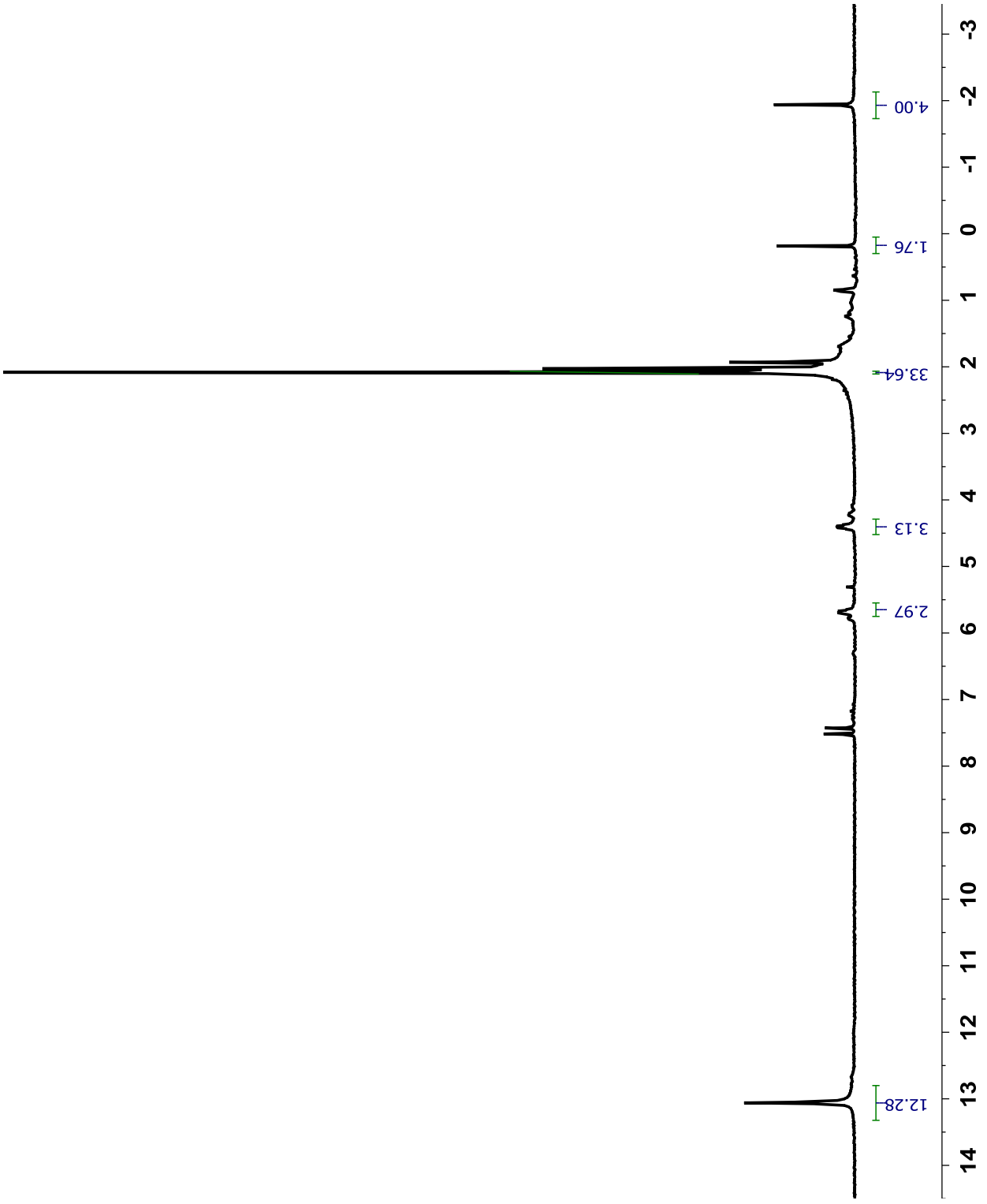

Figure B.23. ^{1}H NMR spectrum of [Cp*Os(dfmpm)CH_4][OSO_2CF_3] at –105 °C in $CDCl_2F$. The peak at δ 13 is due to excess TfOH.

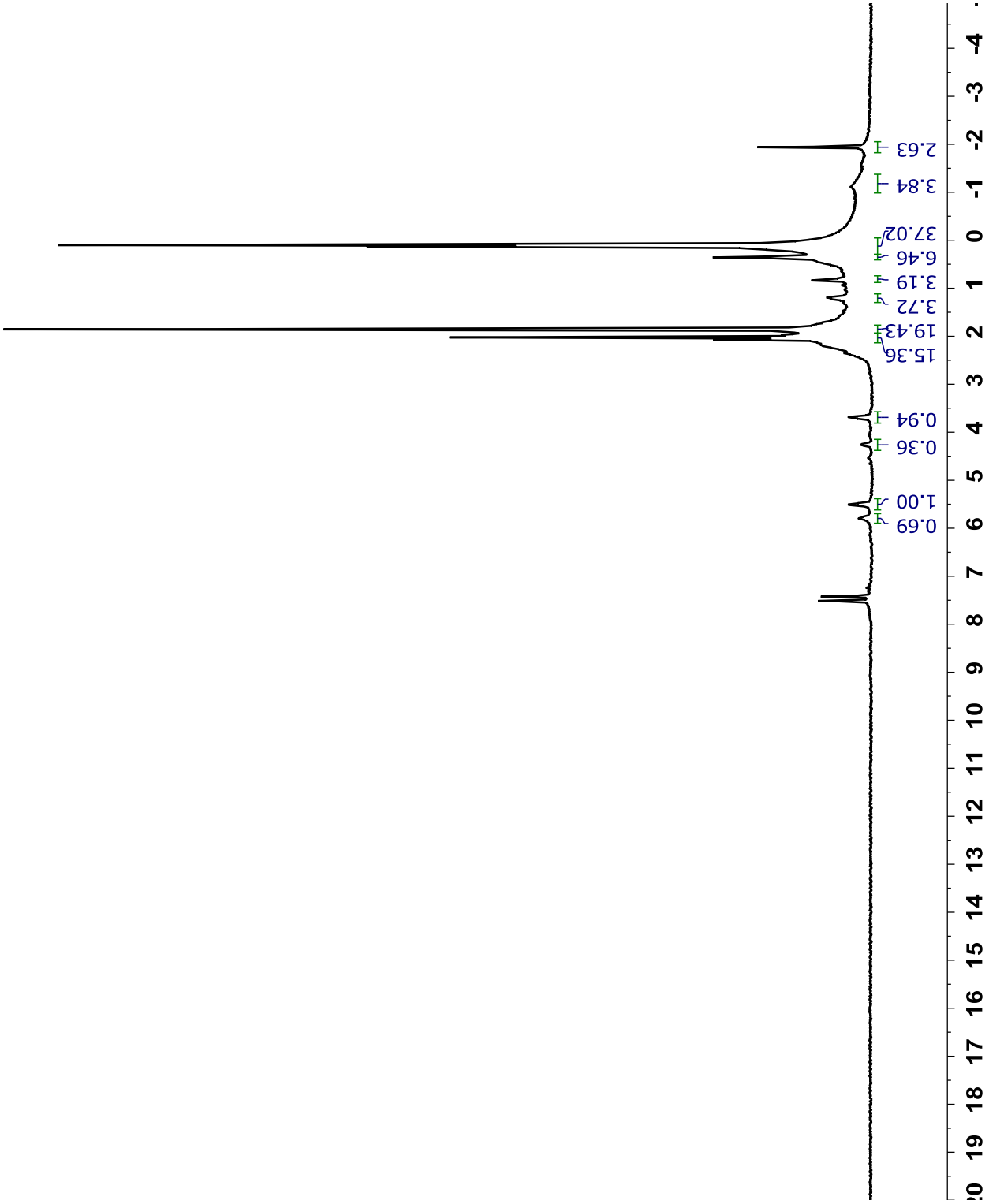

Figure B.24. ^{1}H NMR spectrum of [Cp*Os(dfmpm)CH_4][$N(SO_2CF_3)_2$] at –110 °C in $CDCl_2F$. Major contamination from silicone grease can be seen, as well as a significant amount of unreacted Cp*Os(dfmpm)Me.

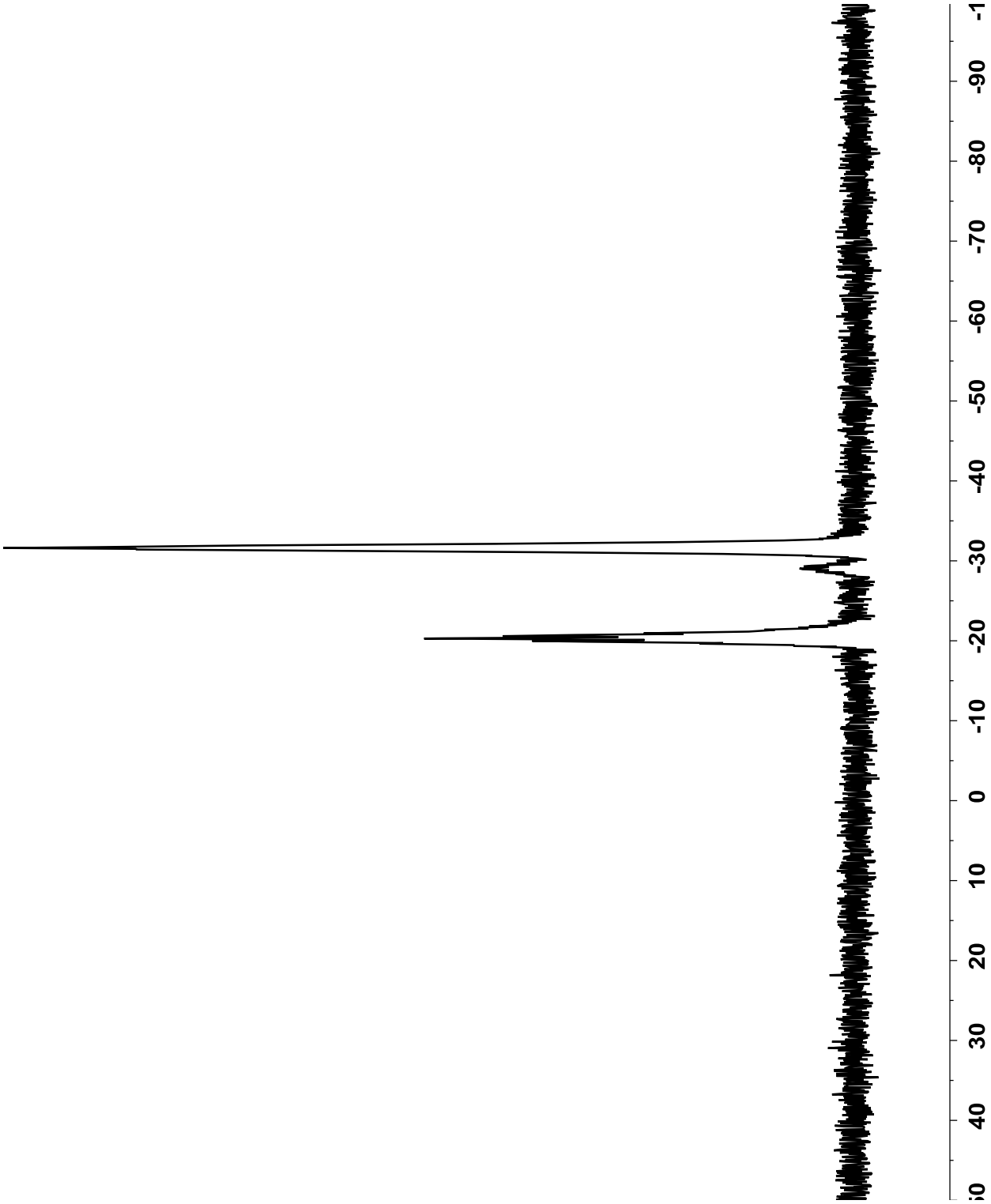

Figure B.25. ^{31}P NMR spectrum of [Cp*Os(dfmpm)CH_4][$N(SO_2CF_3)_2$] at –110 °C in $CDCl_2F$.

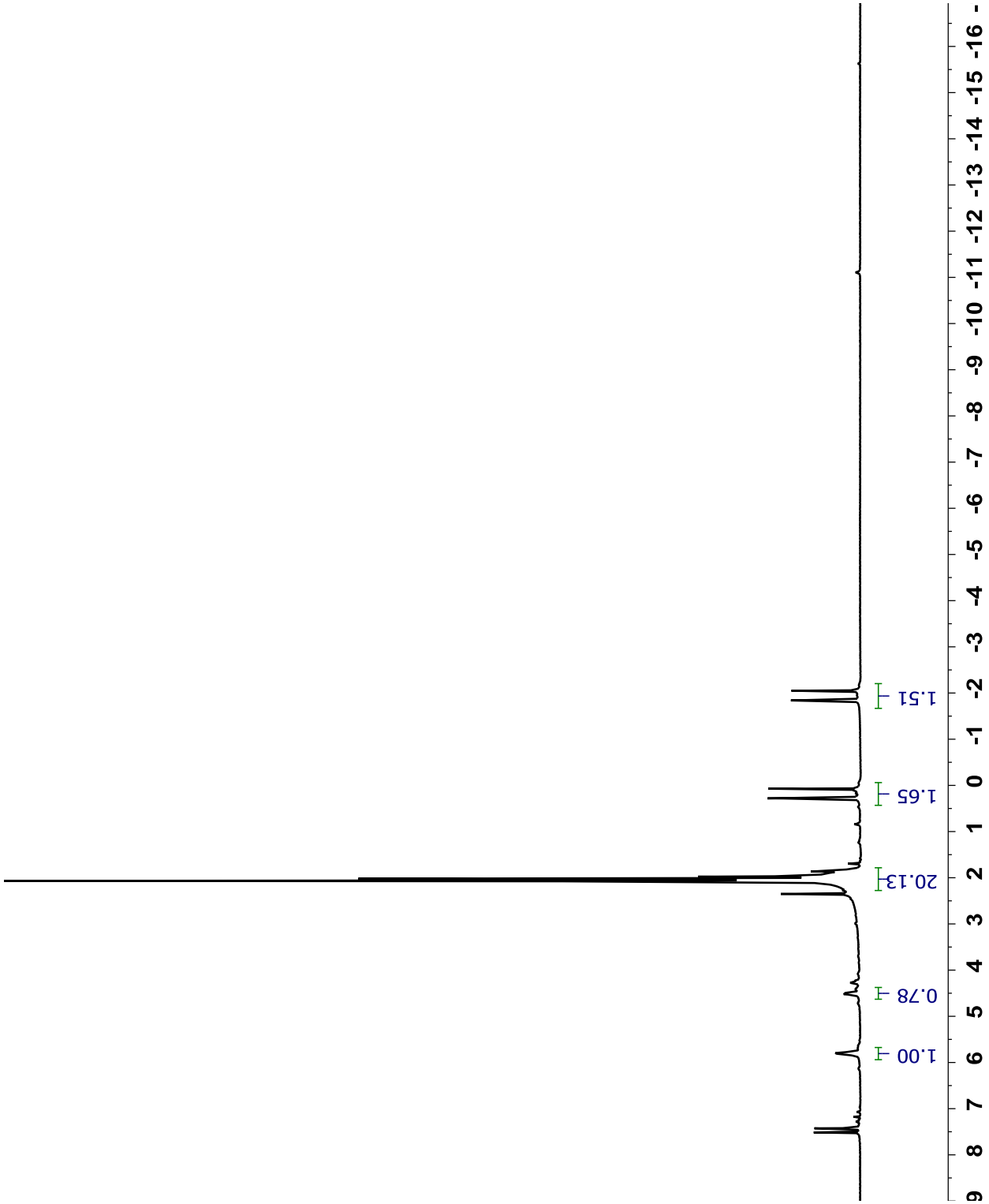

Figure B.26. ^{1}H NMR spectrum of [Cp*Os(dfmpm)^{13}CH$_4$][N(SO$_2$CF$_3$)$_2$] at –110 °C in CDCl$_2$F. The CDCl$_2$F solvent is contaminated with a small amount of CDClF$_2$ (δ 7.17).

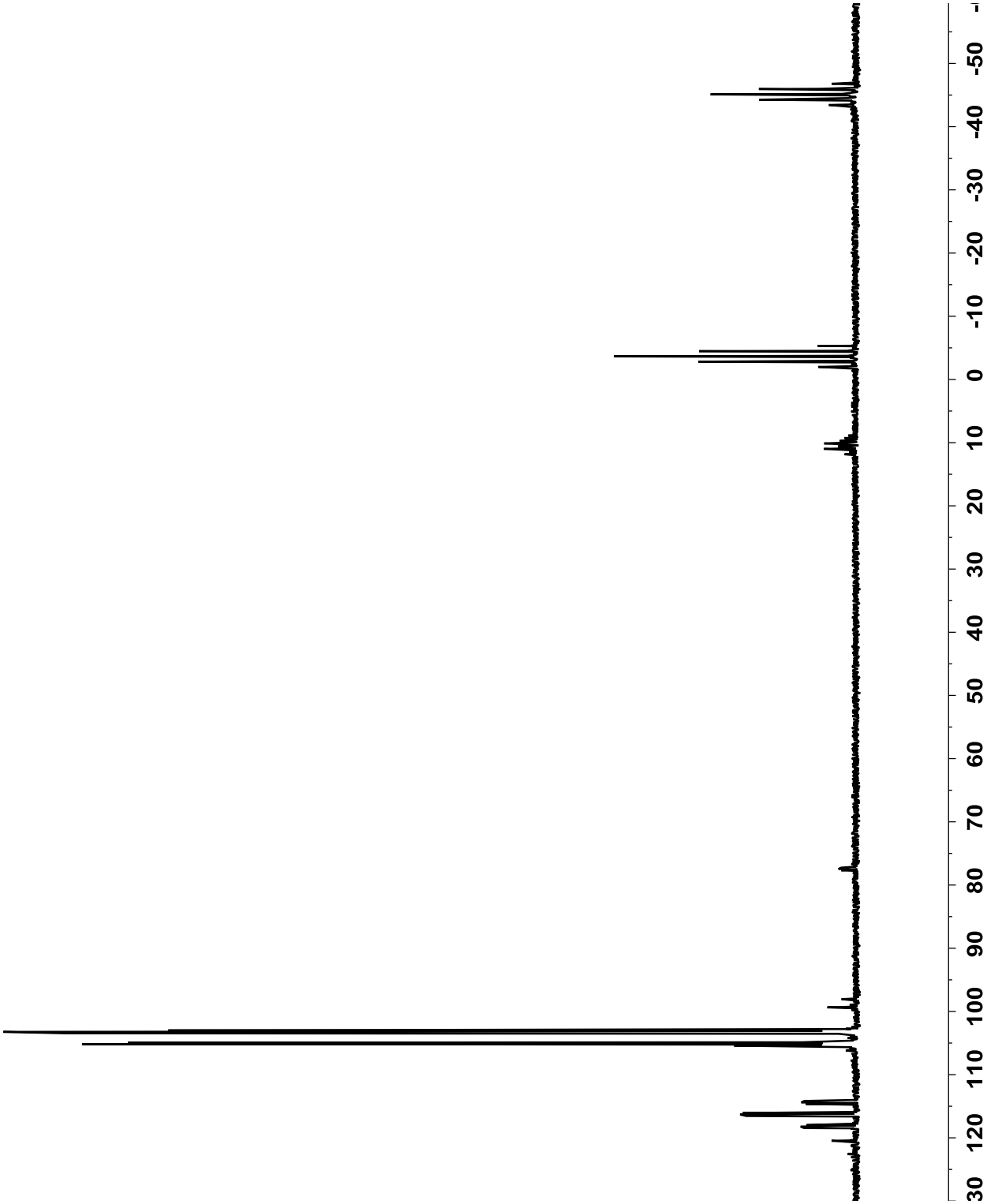

Figure B.27. ^{13}C NMR spectrum of $[Cp^*Os(dfmpm)^{13}CH_4][N(SO_2CF_3)_2]$ at –110 °C in $CDCl_2F$. The $CDCl_2F$ solvent is contaminated with a small amount of $CDClF_2$ (δ 116.3).

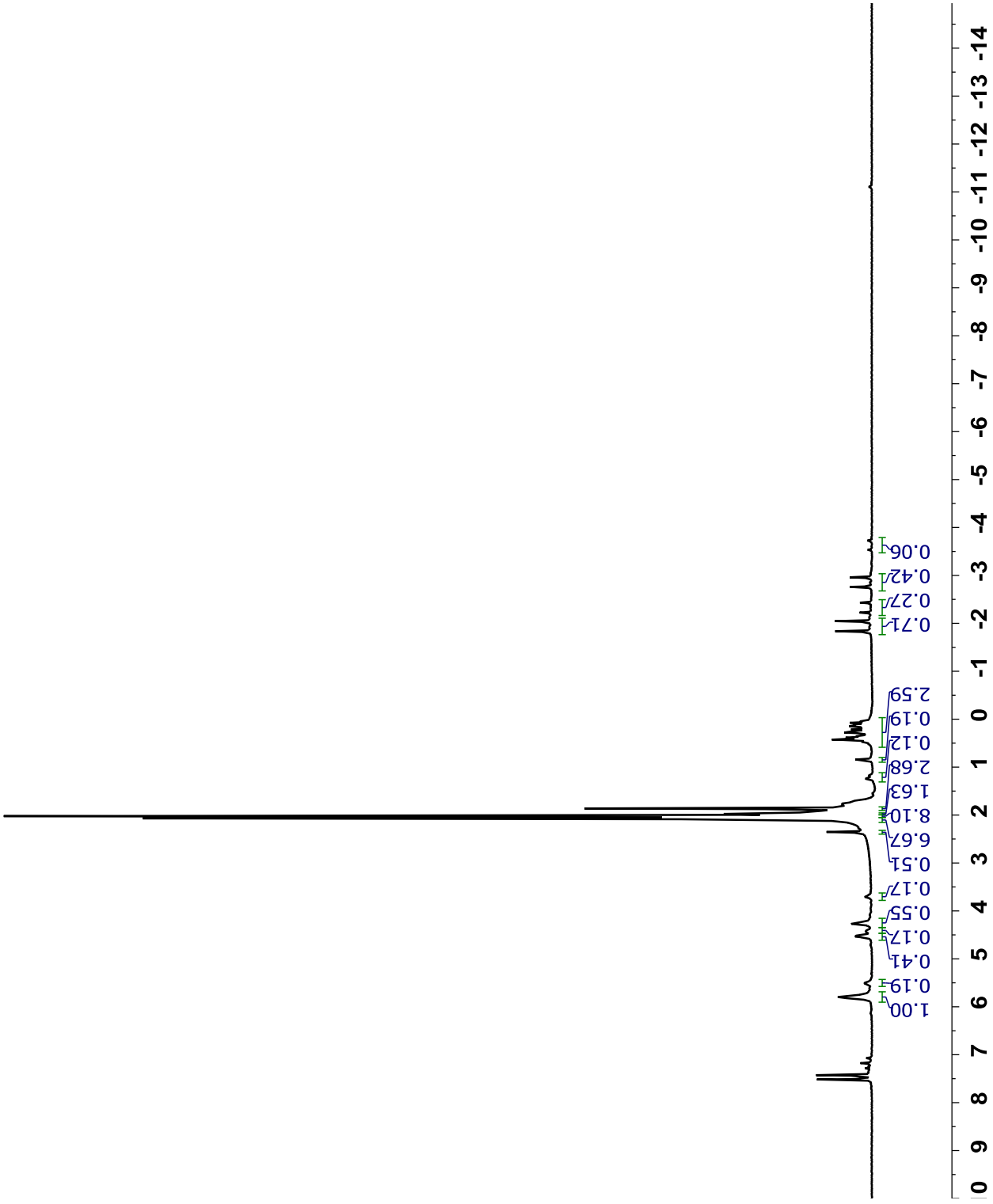

Figure B.28. ^{1}H NMR spectrum of [Cp*Os(dfmpm)^{13}CH$_n$D$_{4-n}$][N(SO$_2$CF$_3$)$_2$], where *n* is 1-4, at –110 °C in $CDCl_2F$.

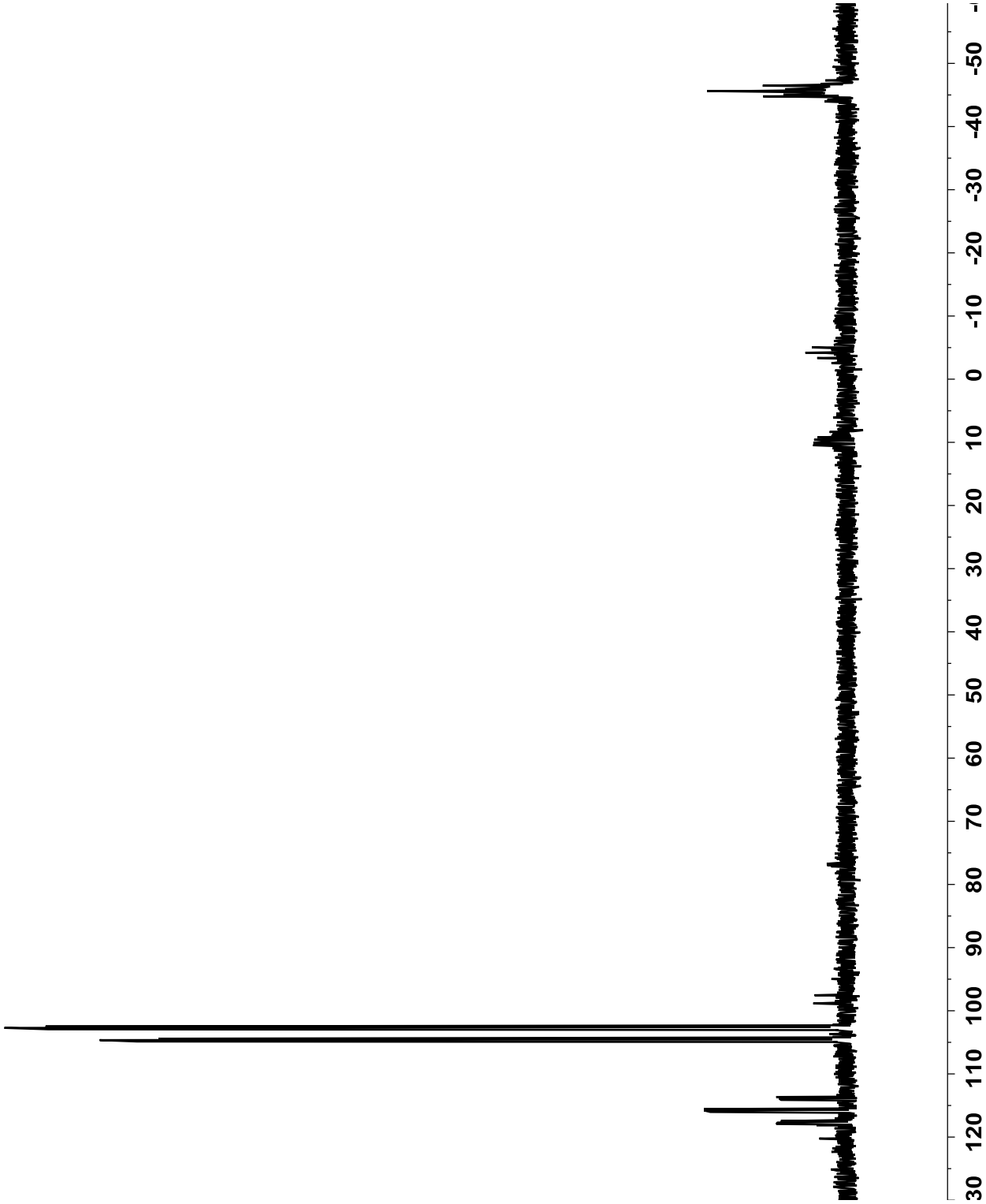

Figure B.29. ^{13}C NMR spectrum of $[Cp^*Os(dfmpm)^{13}CH_nD_{4-n}][N(SO_2CF_3)_2]$, where *n* is 1-4, at –110 °C in $CDCl_2F$.

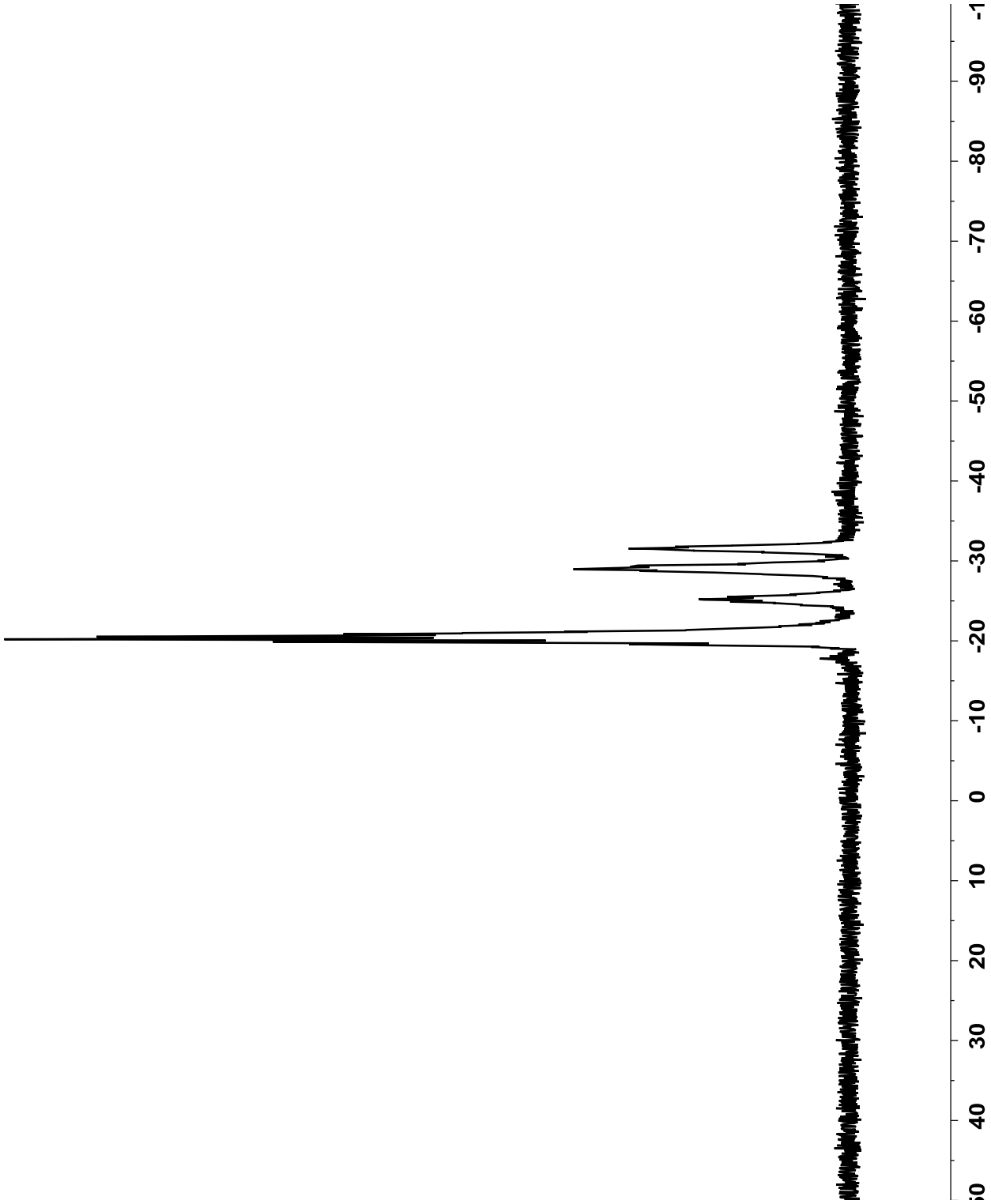

Figure B.30. ^{31}P NMR spectrum of [Cp*Os(dfmpm)^{13}CH$_n$D$_{4-n}$][N(SO$_2$CF$_3$)$_2$], where *n* is 1-4, at –110 °C in $CDCl_2F$.

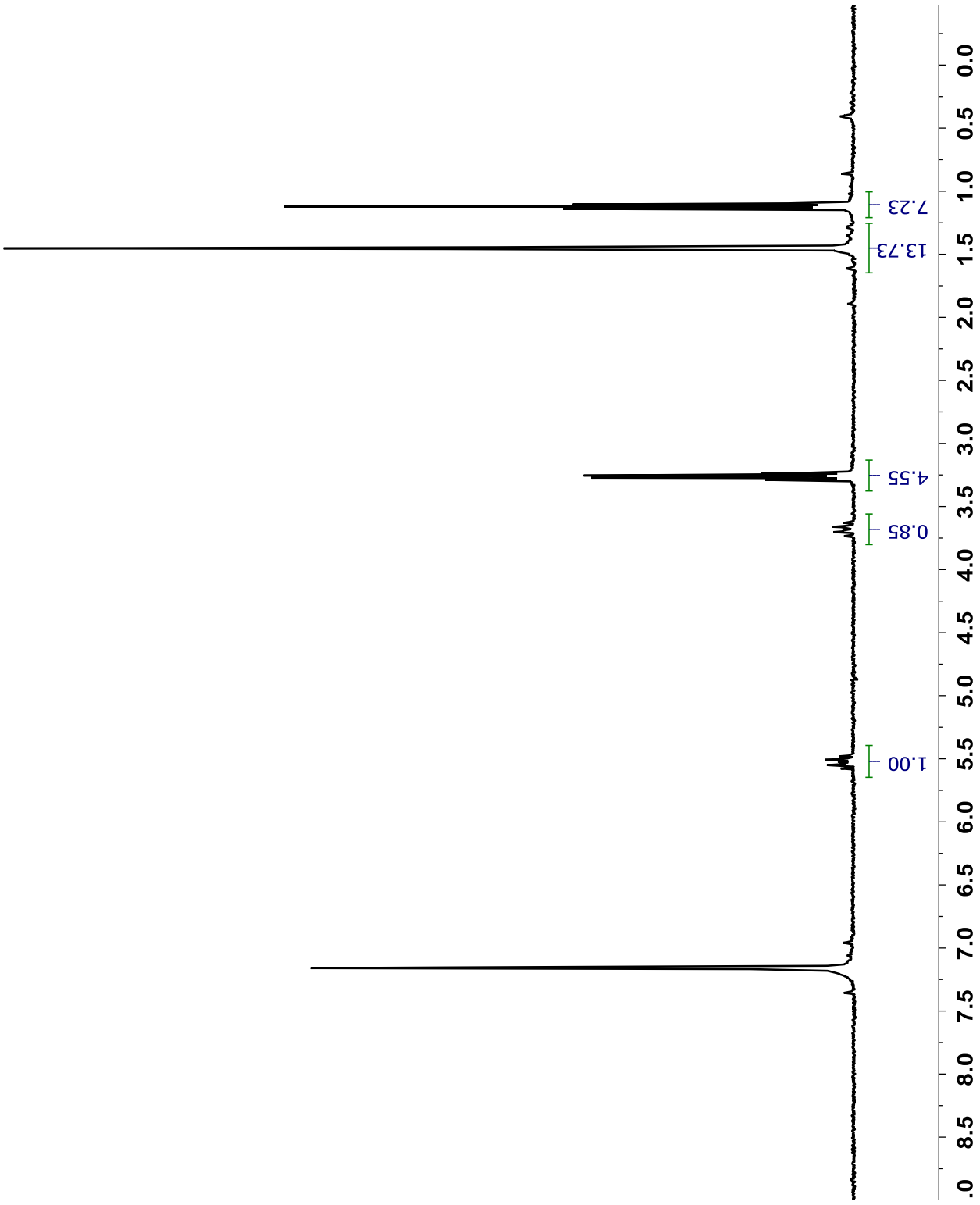

Figure B.31. ^{1}H NMR spectrum of Cp*Os(dfmpm)OTf in C_6D_6. Major contamination from Et_2O can be seen.

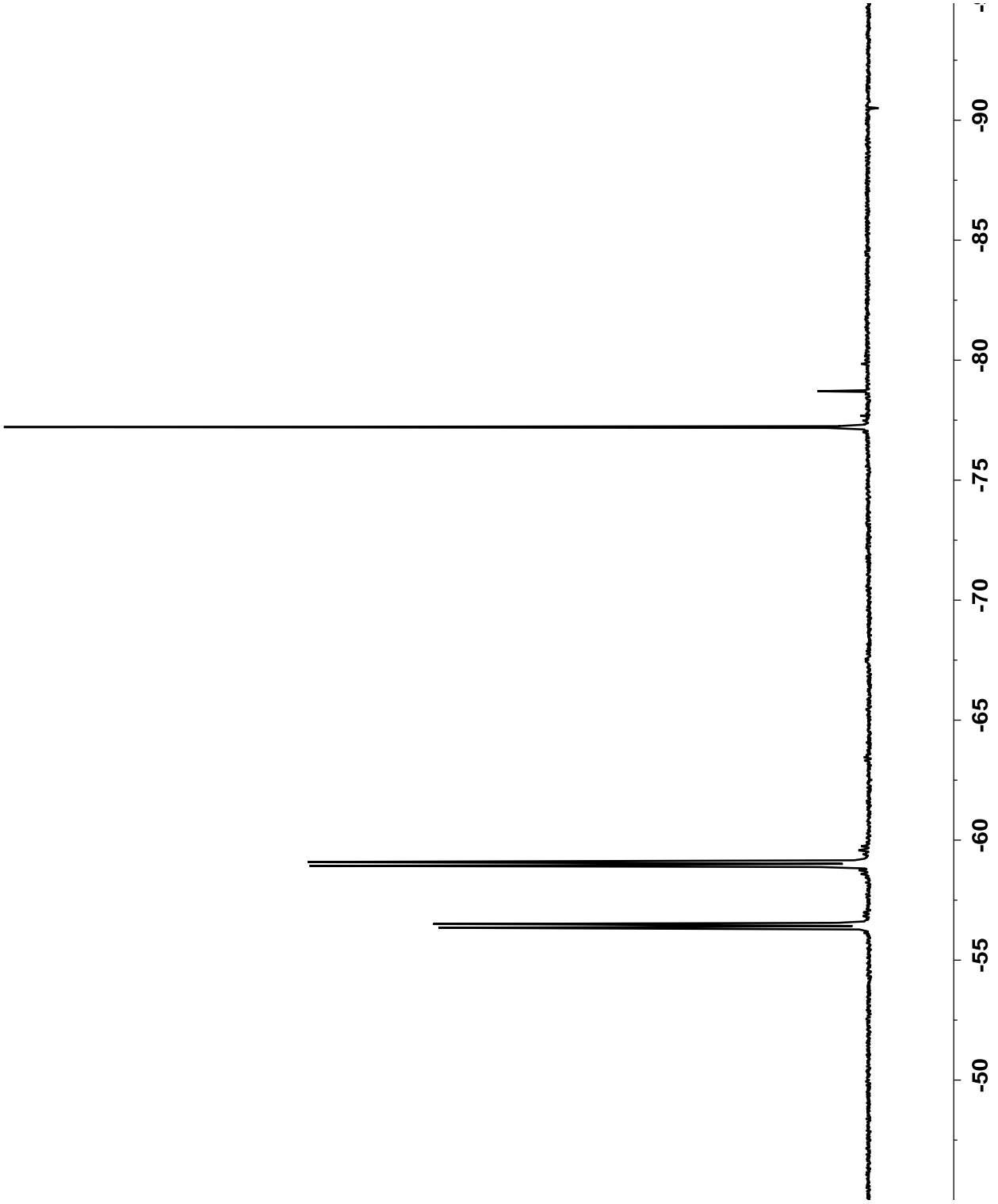

Figure B.32. ^{19}F NMR spectrum of Cp*Os(dfmpm)OTf in C_6D_6.

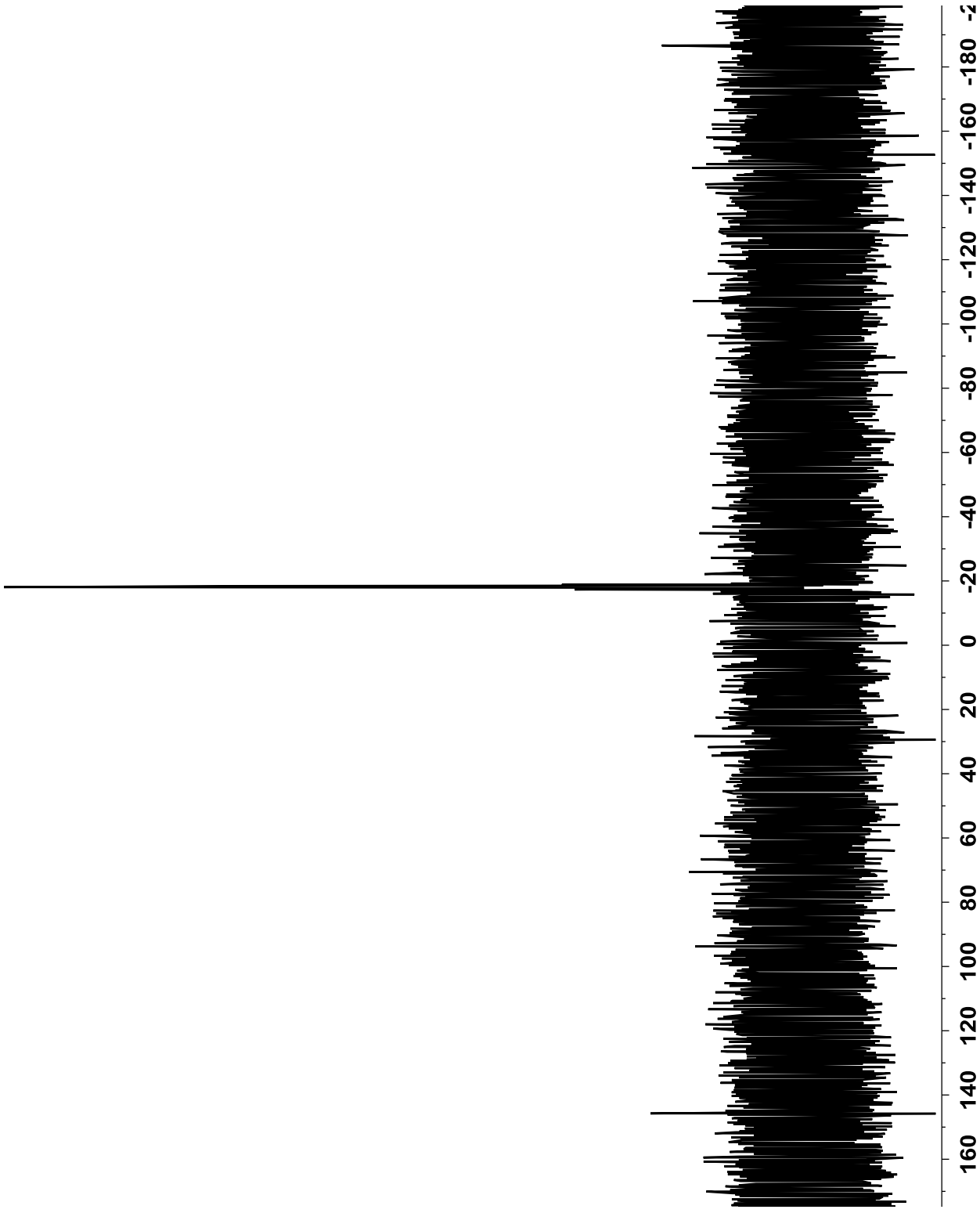

Figure B.33. ^{31}P NMR spectrum of Cp*Os(dfmpm)OTf in C_6D_6.

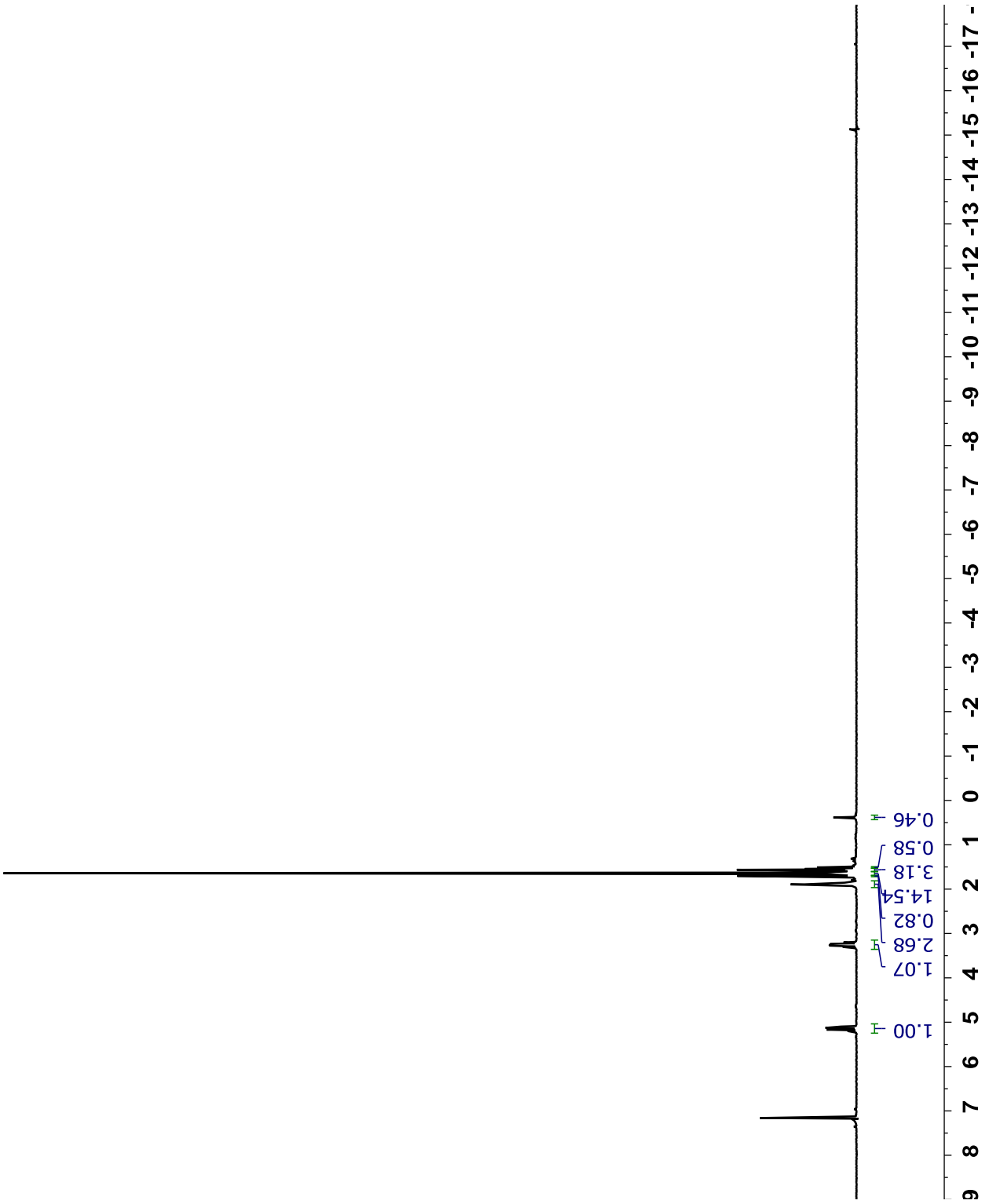

Figure B.34. ^{1}H NMR spectrum of Cp*Os(dfmpm)Et in C_6D_6. Contamination from Cp*Os(κ^1-dfmpm)H and Cp*Os(dfmpm)H can be seen (see chapter 4 for details).

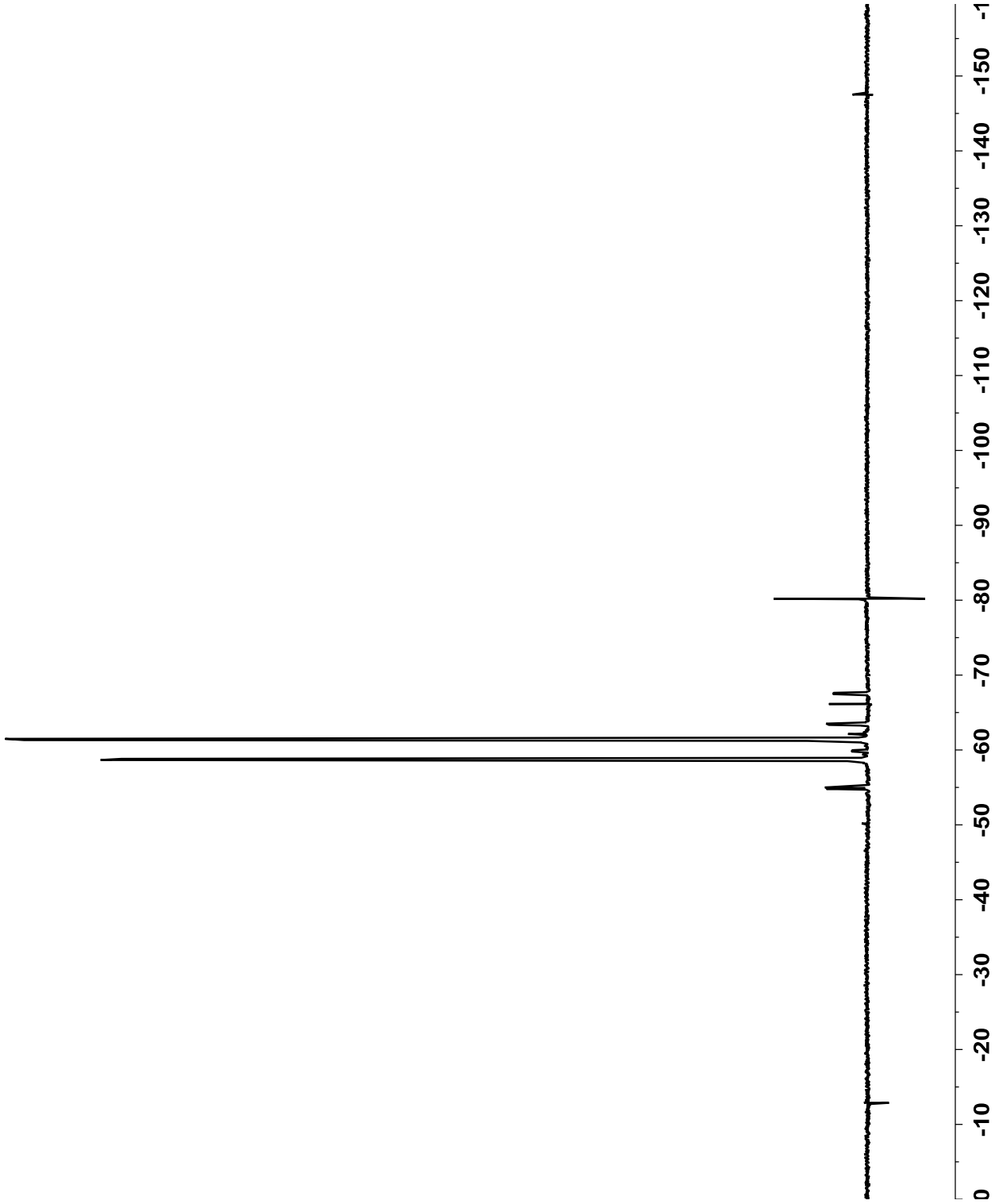

Figure B.35. ^{19}F NMR spectrum of Cp*Os(dfmpm)Et in C_6D_6. Contamination from Cp*Os(κ^1-dfmpm)H and Cp*Os(dfmpm)H can be seen.

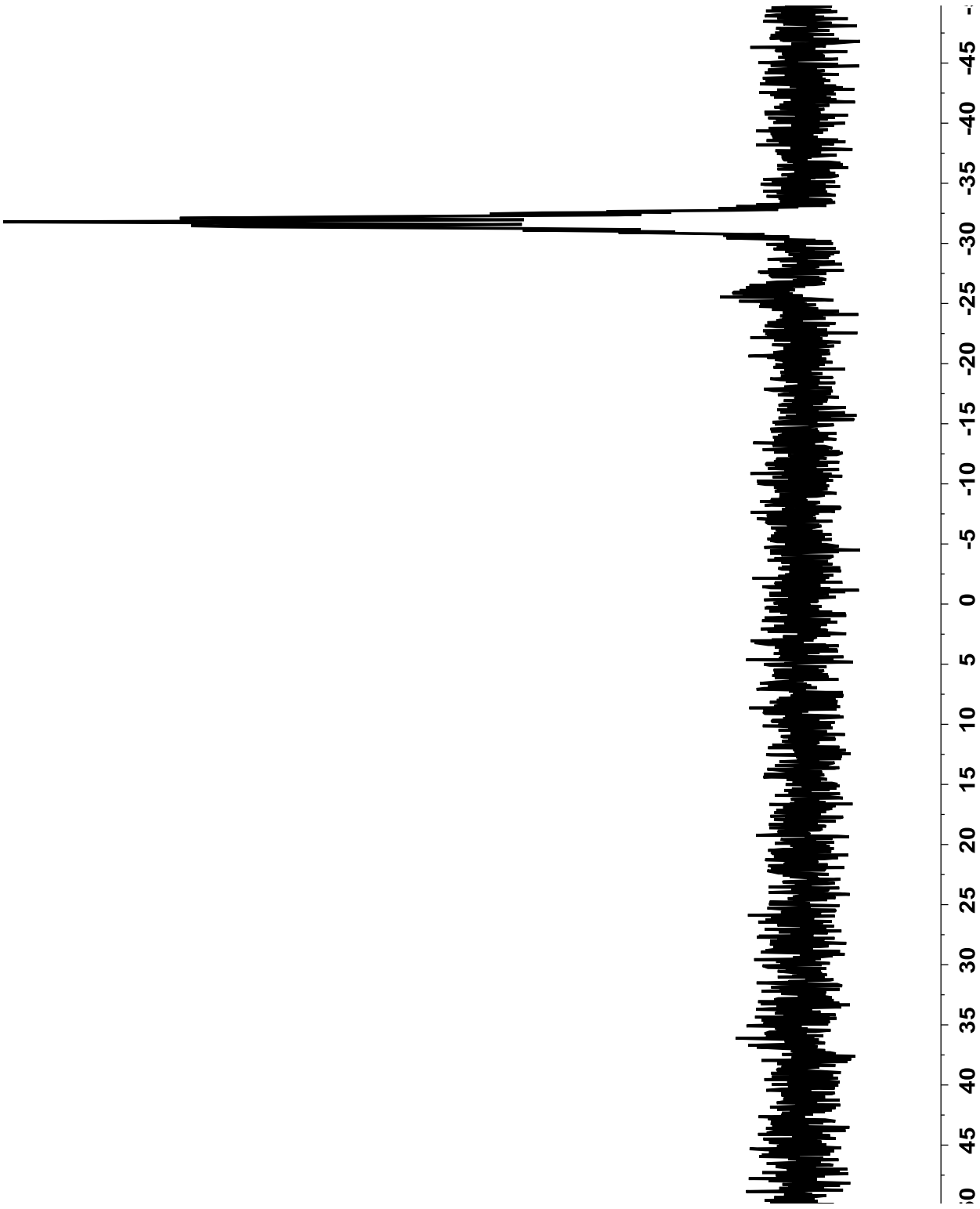

Figure B.36. ^{31}P NMR spectrum of Cp*Os(dfmpm)Et in C_6D_6. Contamination from Cp*Os(κ^1-dfmpm)H and Cp*Os(dfmpm)H can be seen.

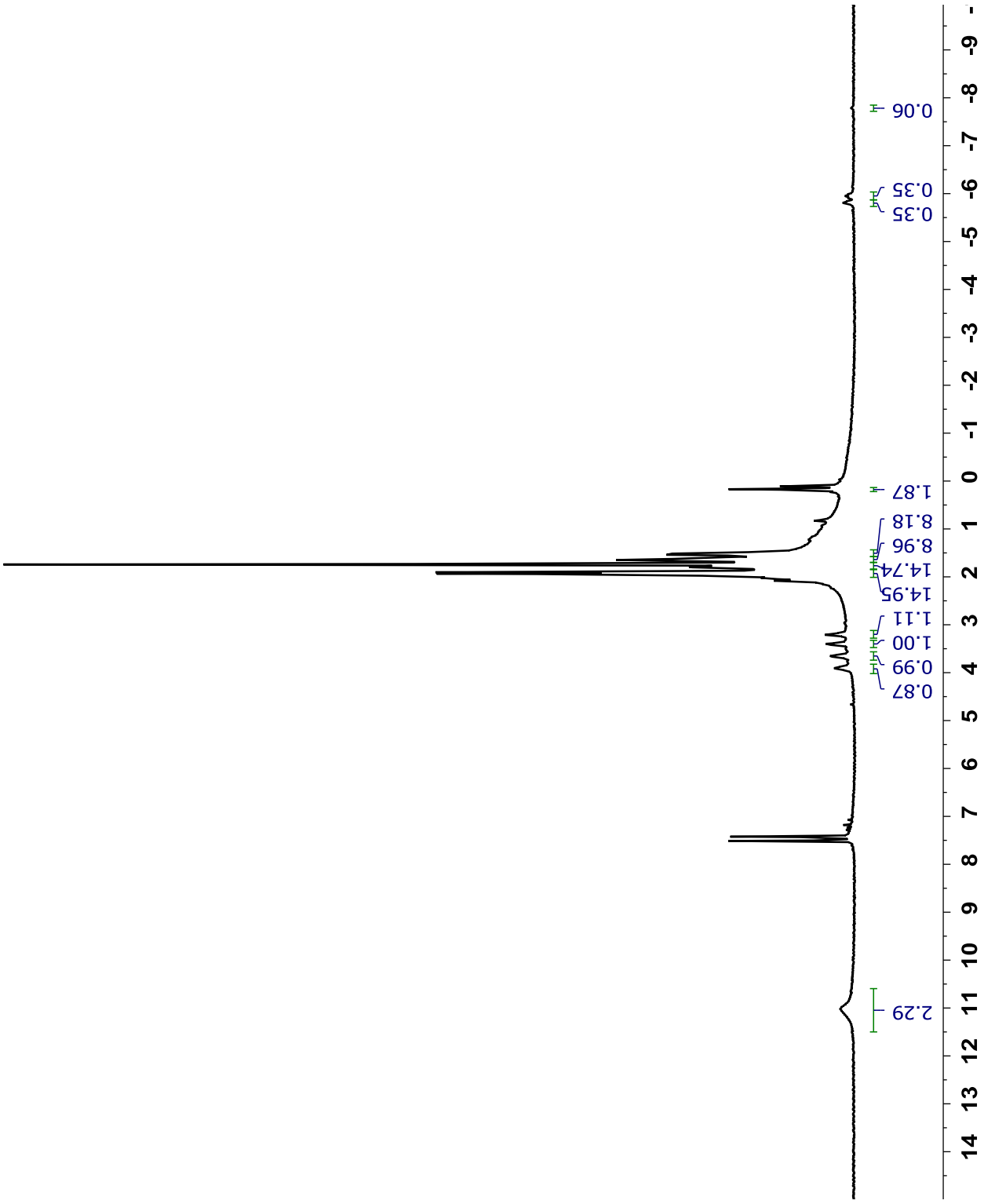

Figure B.37. ^{1}H NMR spectrum of Cp*Ru(dmpm)Me plus $(CF_3SO_2)_2NH$ at –130 °C in $CDCl_2F$.

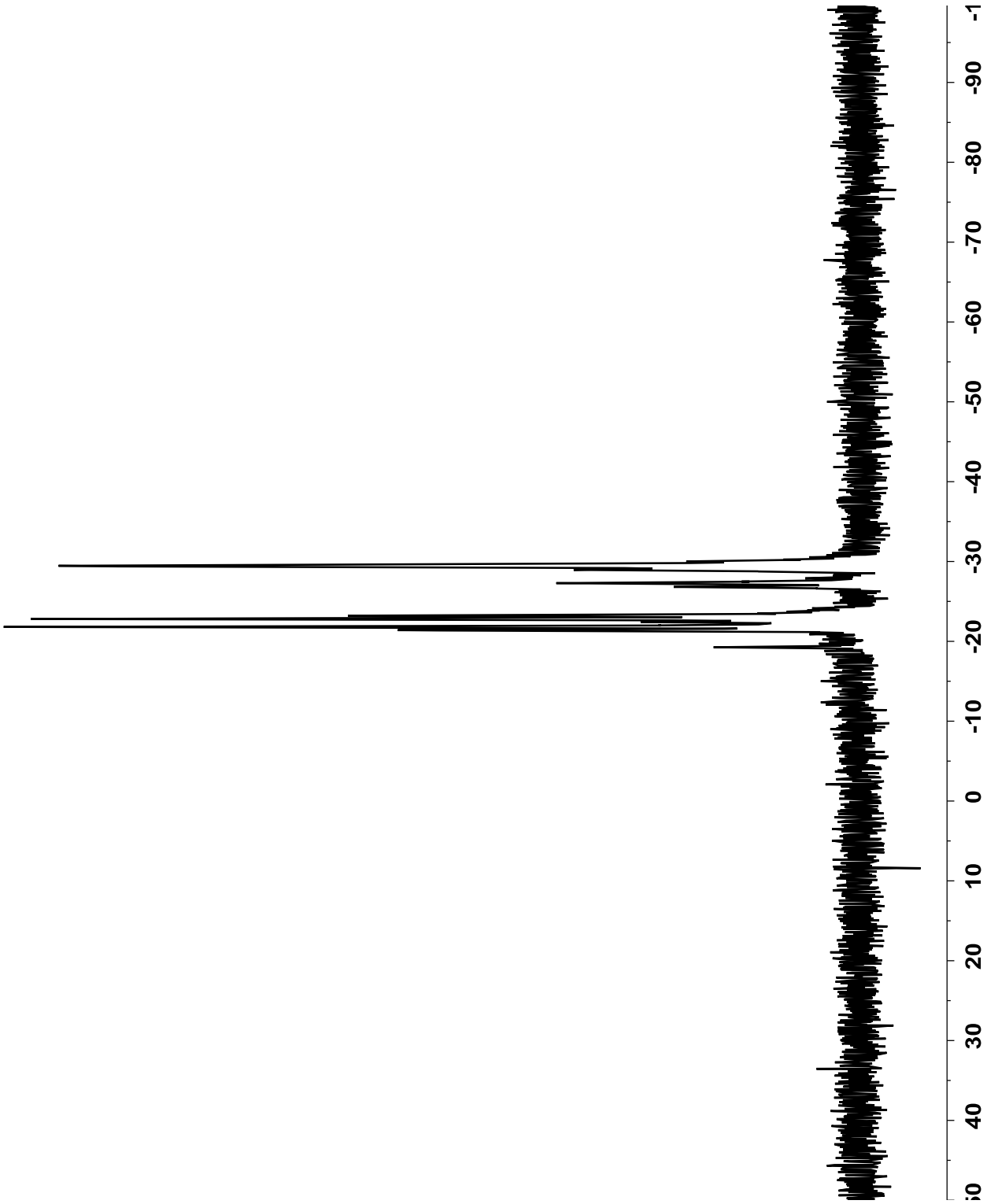

Figure B.38. ^{31}P NMR spectrum of Cp*Ru(dmpm)Me plus $(CF_3SO_2)_2NH$ at –130 °C in $CDCl_2F$.

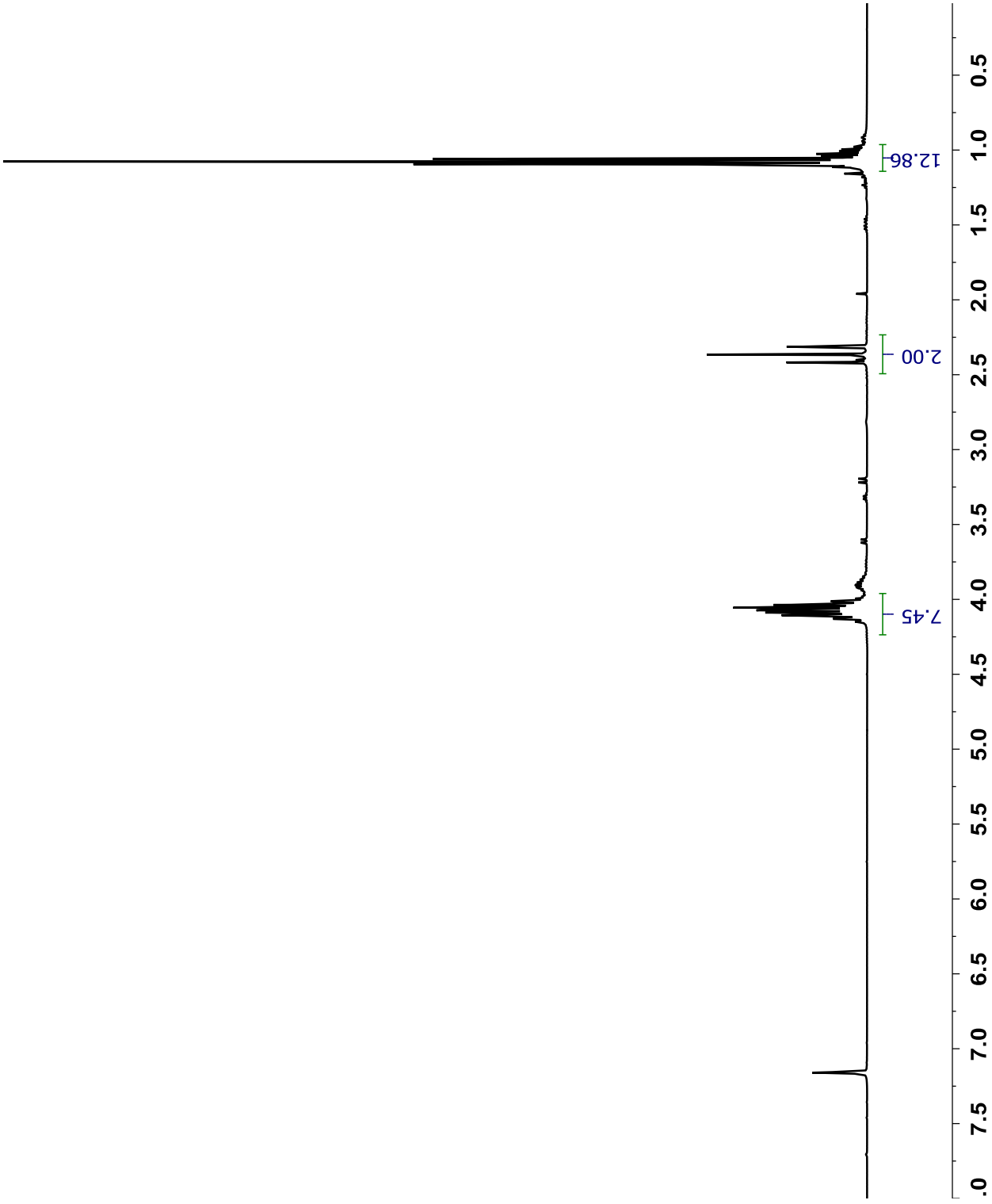

Figure B.39. ^{1}H NMR spectrum of $(EtO)_2P(O)CH_2P(O)(EtO)_2$ in C_6D_6.

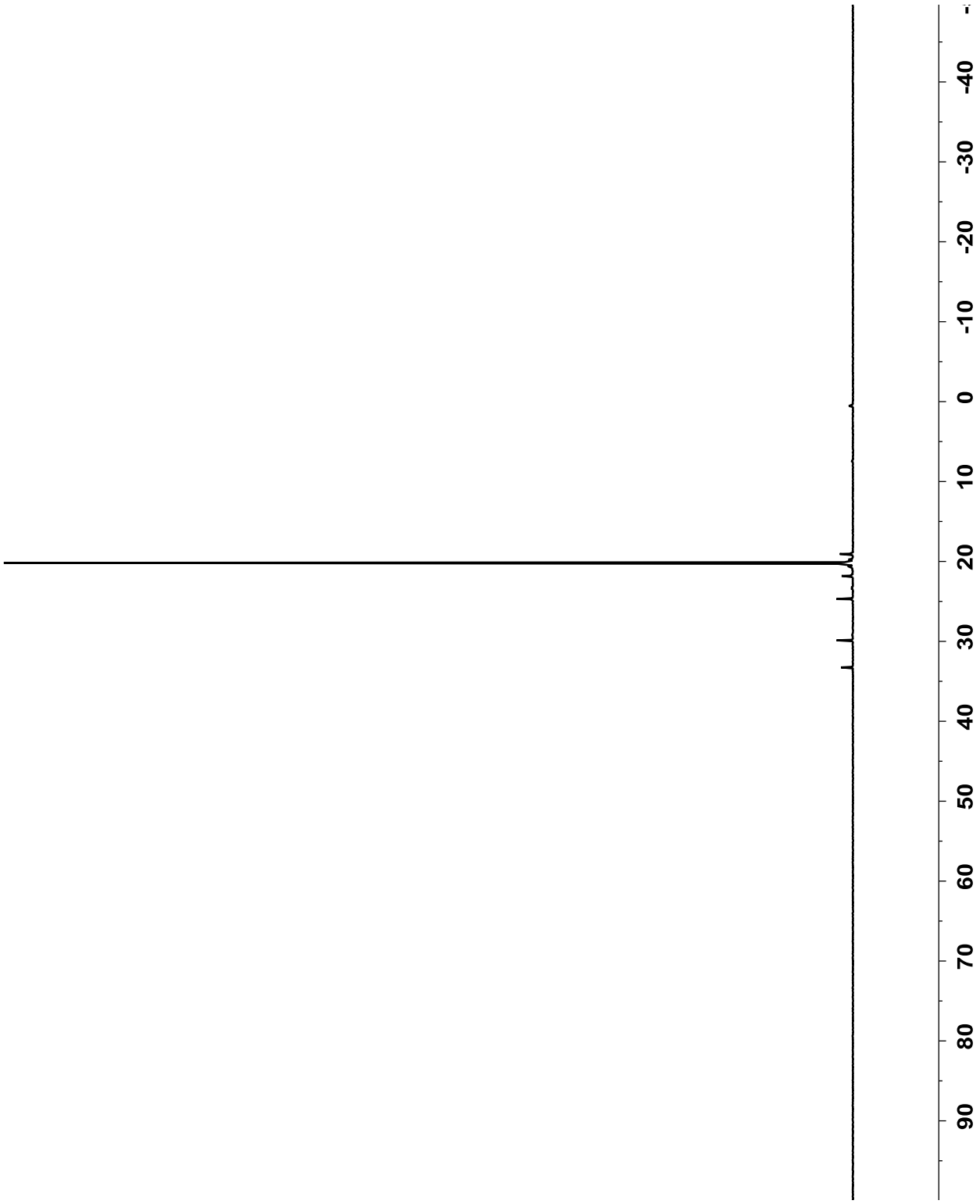

Figure B.40. ^{31}P NMR spectrum of $(EtO)_2P(O)CH_2P(O)(EtO)_2$ in C_6D_6.

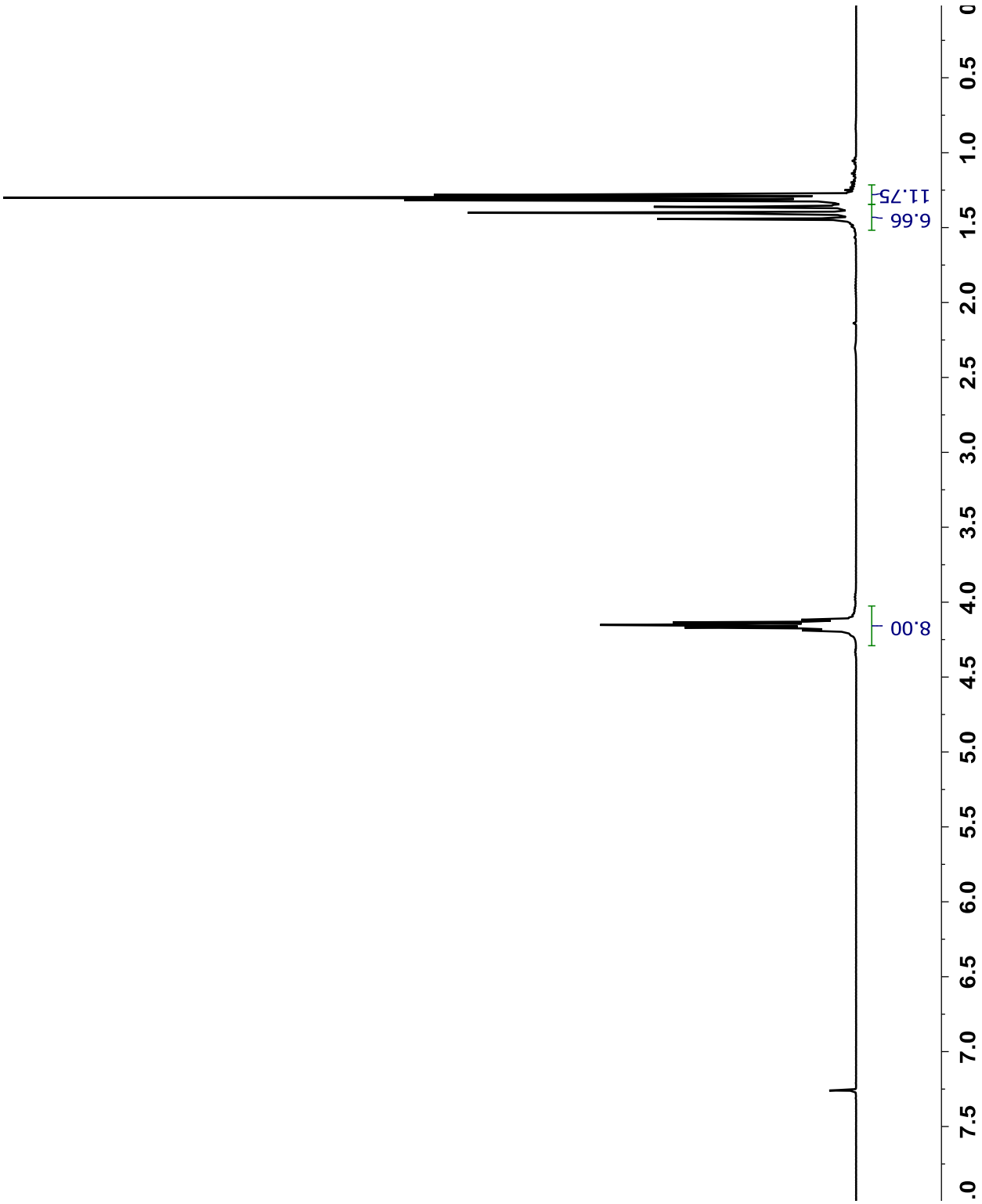

Figure B.41. ^{1}H NMR spectrum of $(EtO)_2P(O)CMe_2P(O)(EtO)_2$ in $CDCl_3$.

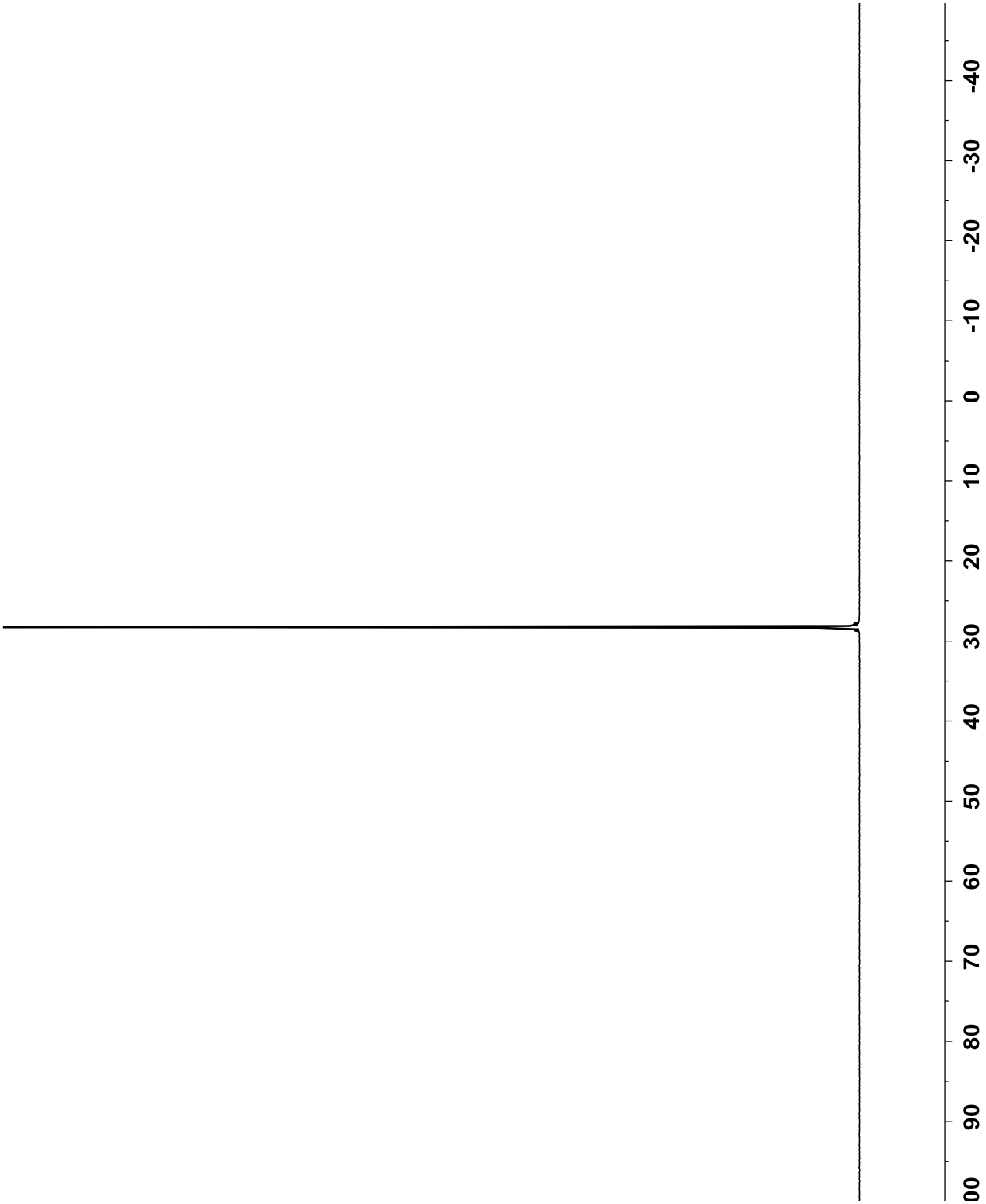

Figure B.42. ^{31}P NMR spectrum of $(EtO)_2P(O)CMe_2P(O)(EtO)_2$ in $CDCl_3$.

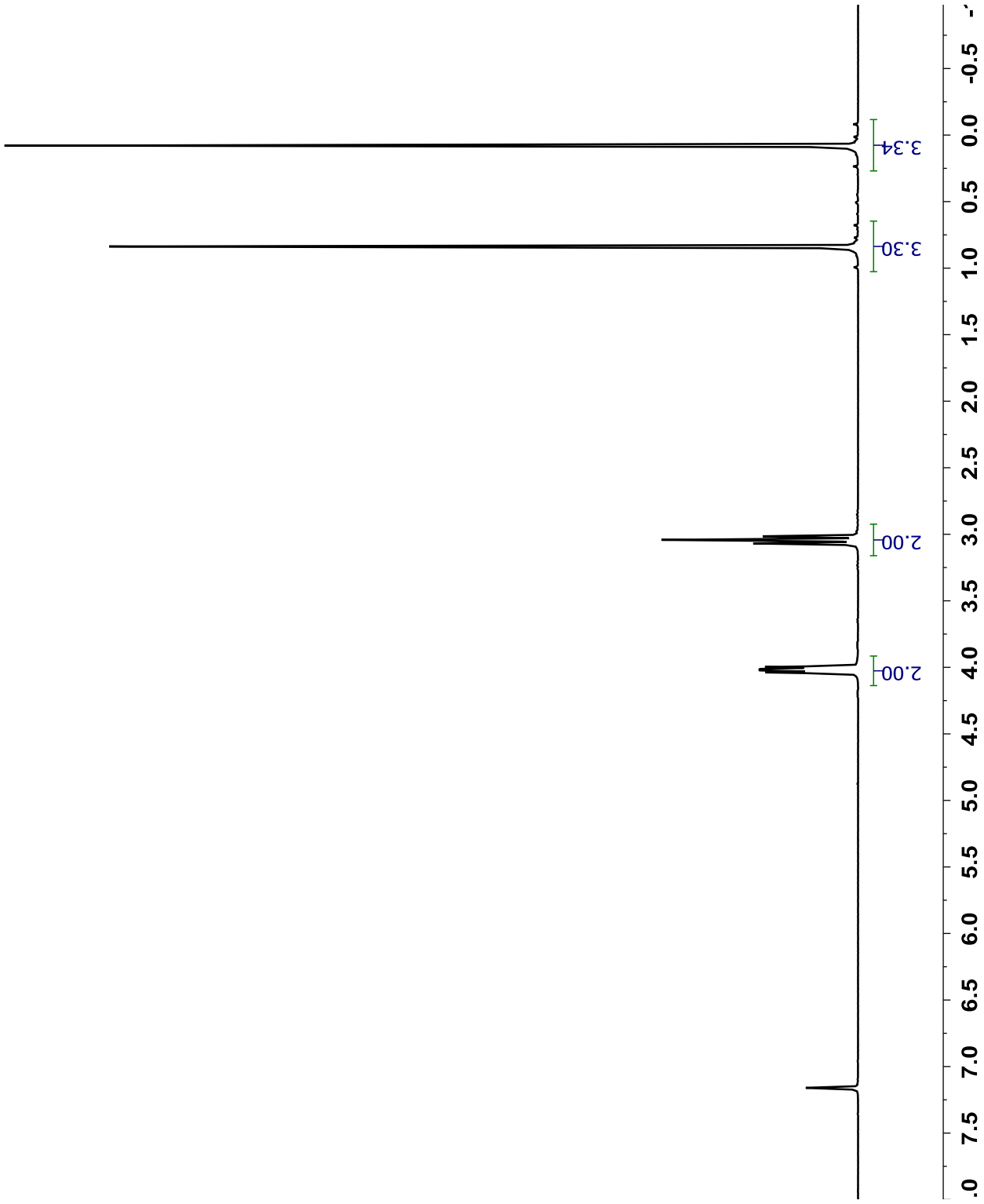

Figure B.43. ^{1}H NMR spectrum of $Me_2C(CH_2O)_2PCl$ in C_6D_6.

Figure B.44. ^{31}P NMR spectrum of $Me_2C(CH_2O)_2PCl$ in C_6D_6.

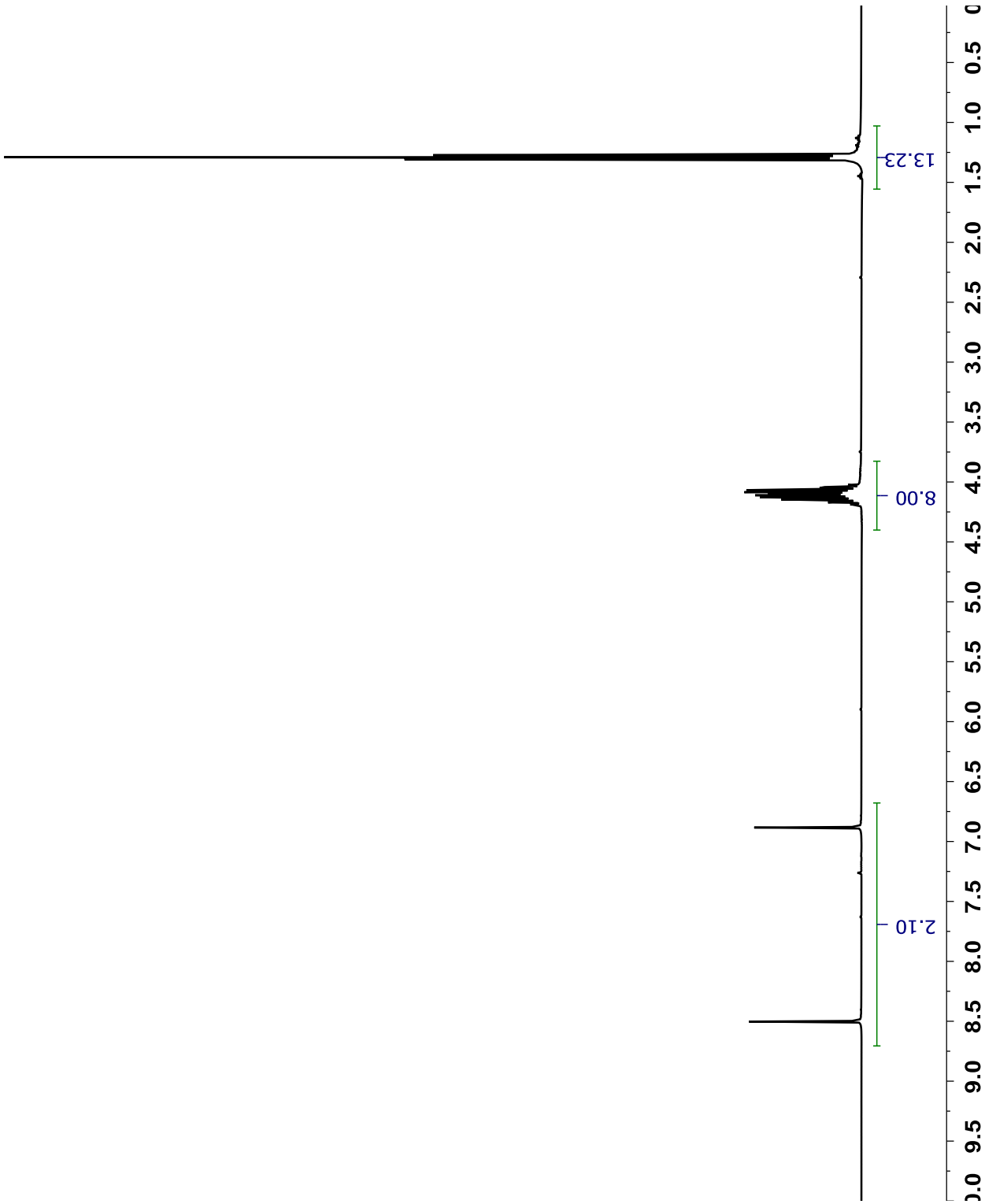

Figure B.45. ^{1}H NMR spectrum of $(EtO)_2P(S)H$ in C_6D_6.

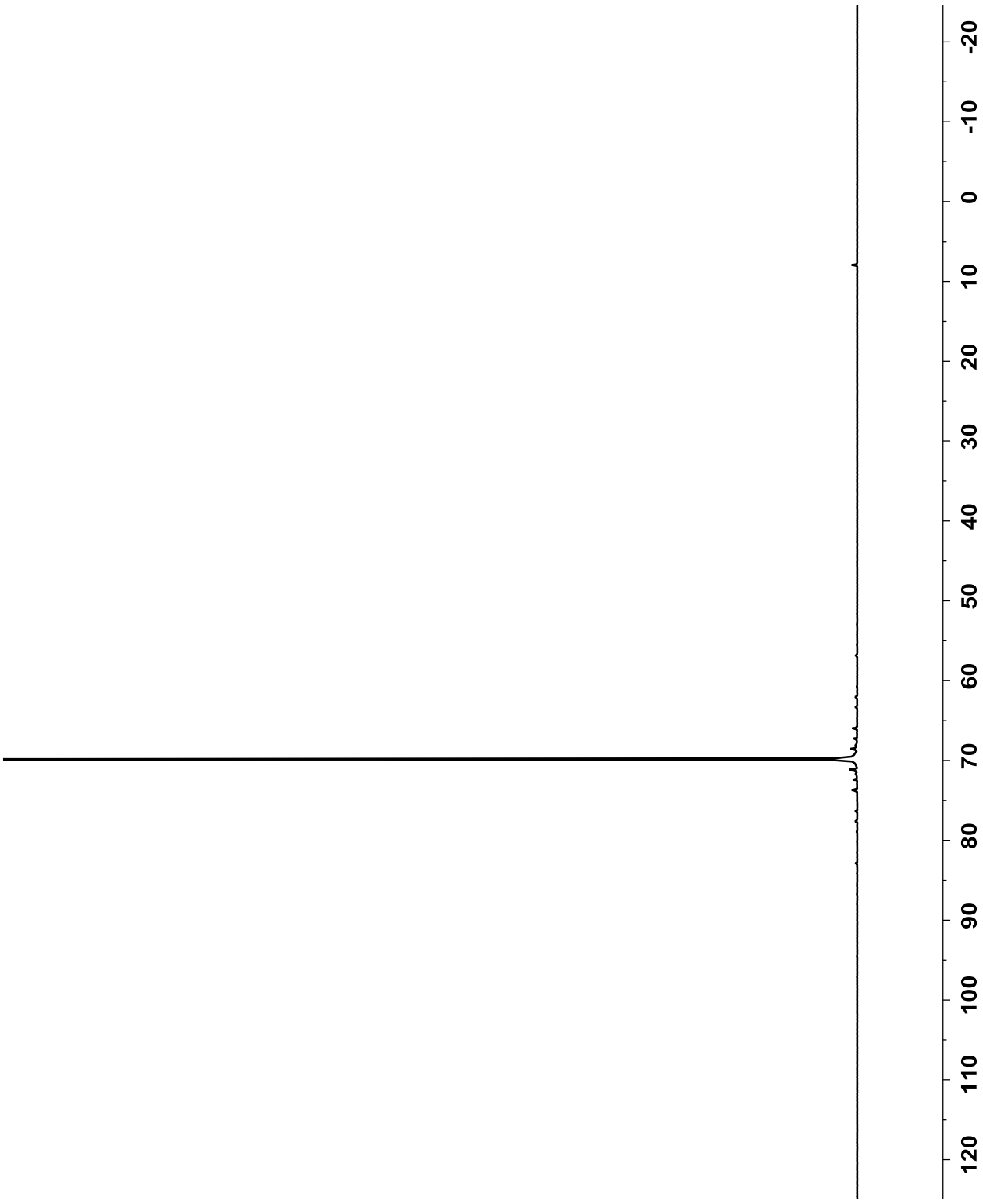

Figure B.46. ^{31}P NMR spectrum of $(EtO)_2P(S)H$ in C_6D_6.

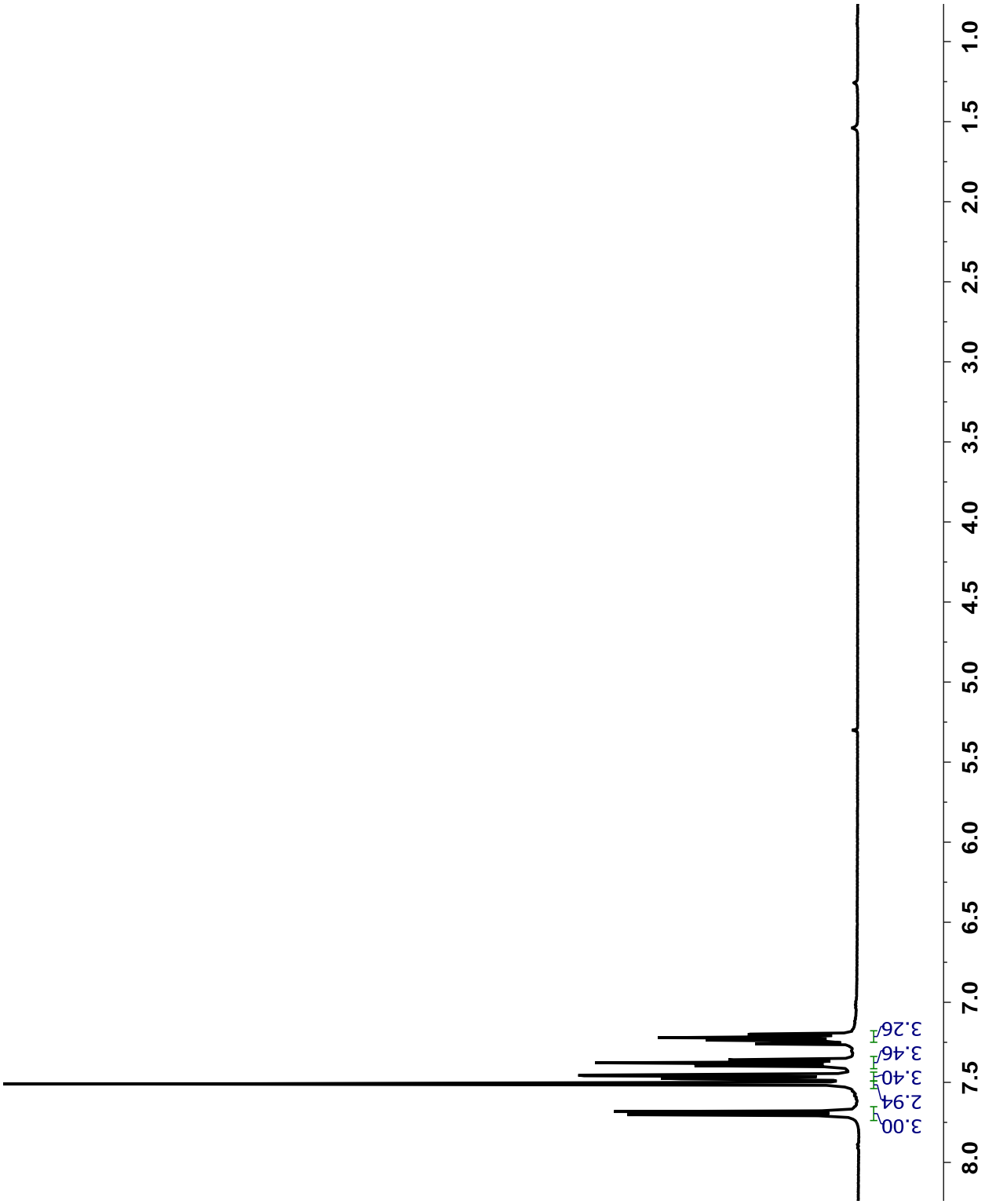

Figure B.47. ^{1}H NMR spectrum of 1,3,5-tris(2-bromophenyl)benzene in $CDCl_3$. Slight contamination from CH_2Cl_2 and hexanes can be seen.

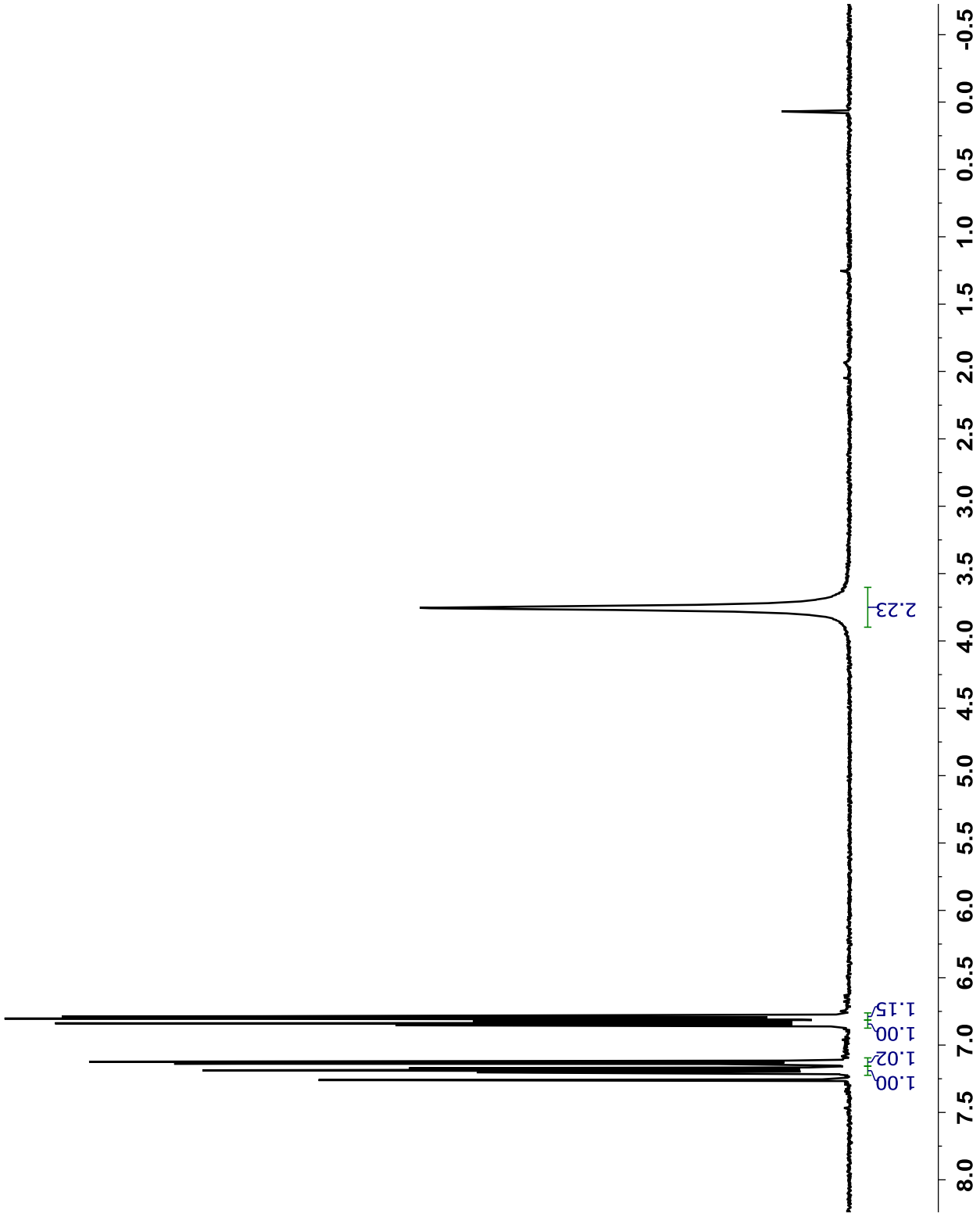

Figure B.48. ^{1}H NMR spectrum of 2,2′-diaminobiphenyl in $CDCl_3$.

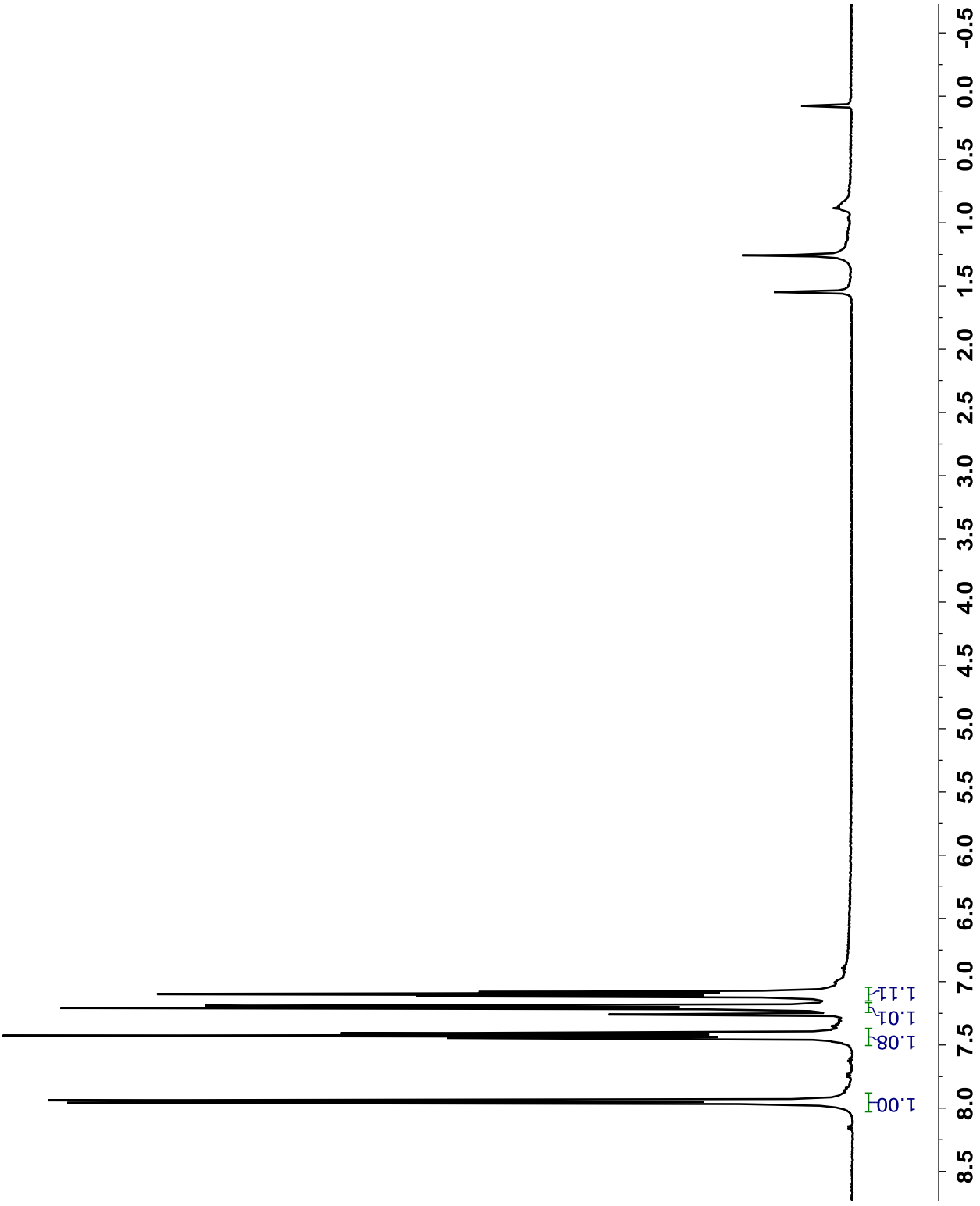

Figure B.49. ^{1}H NMR spectrum of 2,2′-diiodobiphenyl in $CDCl_3$.

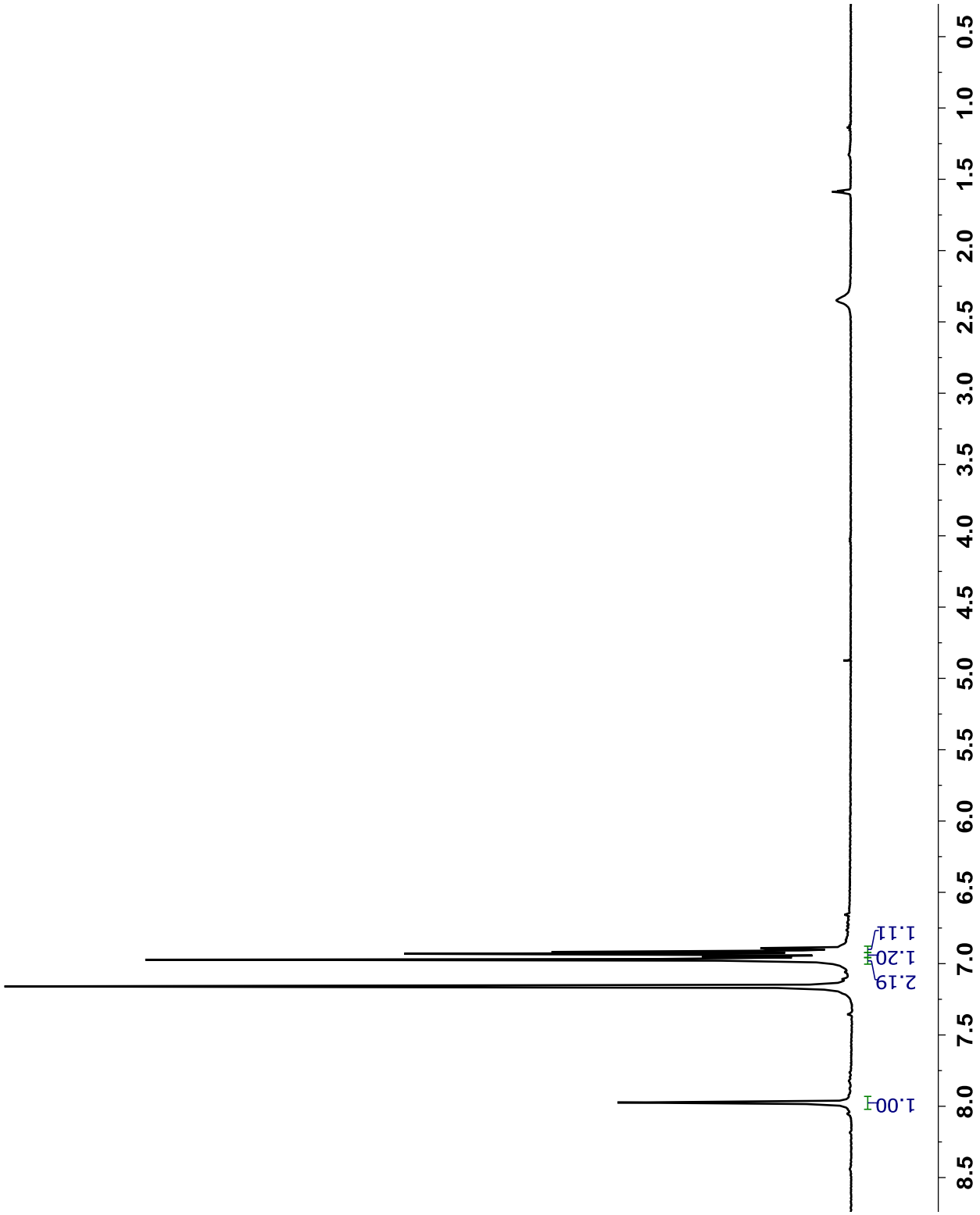

Figure B.50. ^{1}H NMR spectrum of 2,5-dibromophenylboronic acid in C_6D_6. Contamination from acetone and water can be seen.

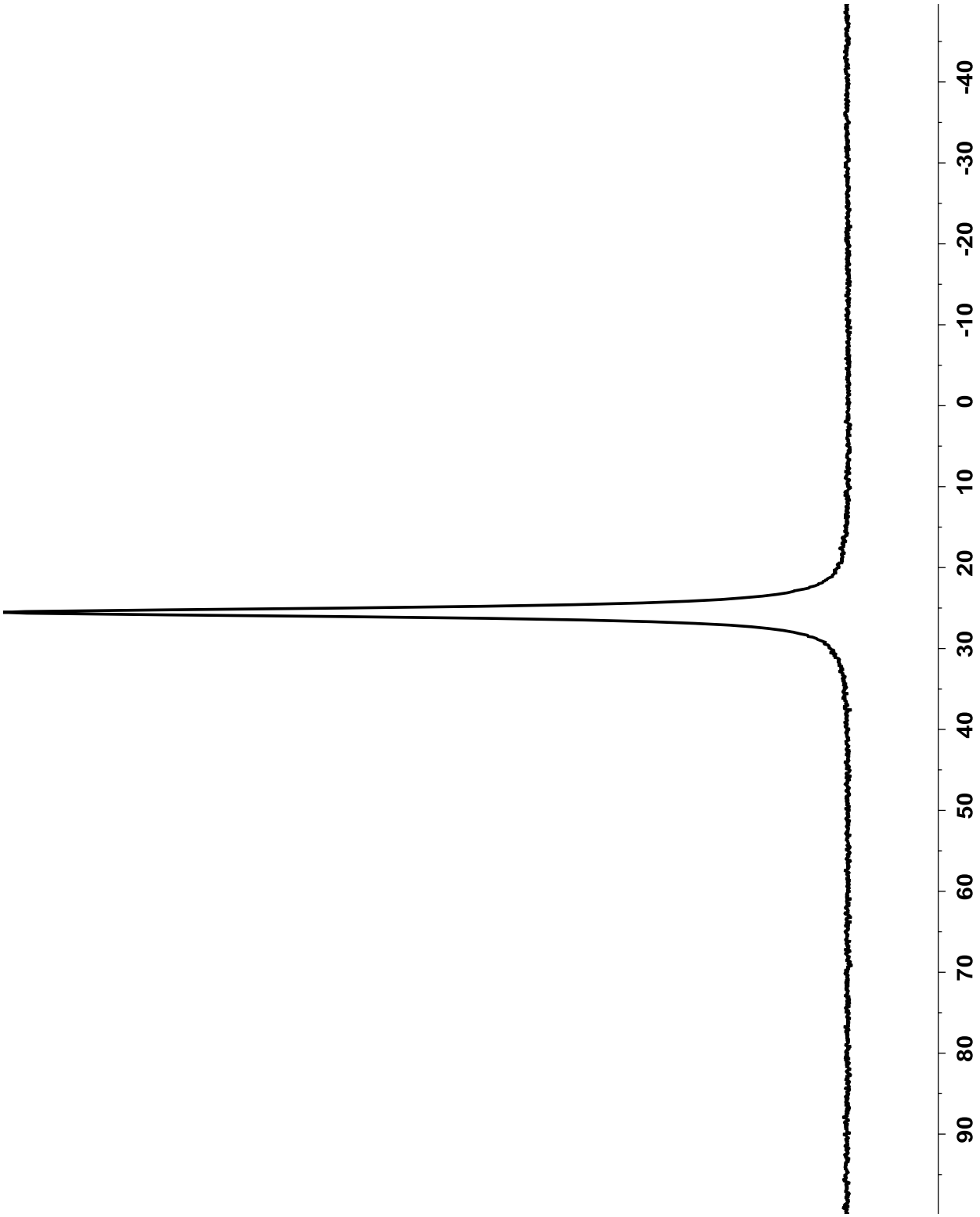

Figure B.51. ^{11}B NMR spectrum of 2,5-dibromophenylboronic acid in C_6D_6.

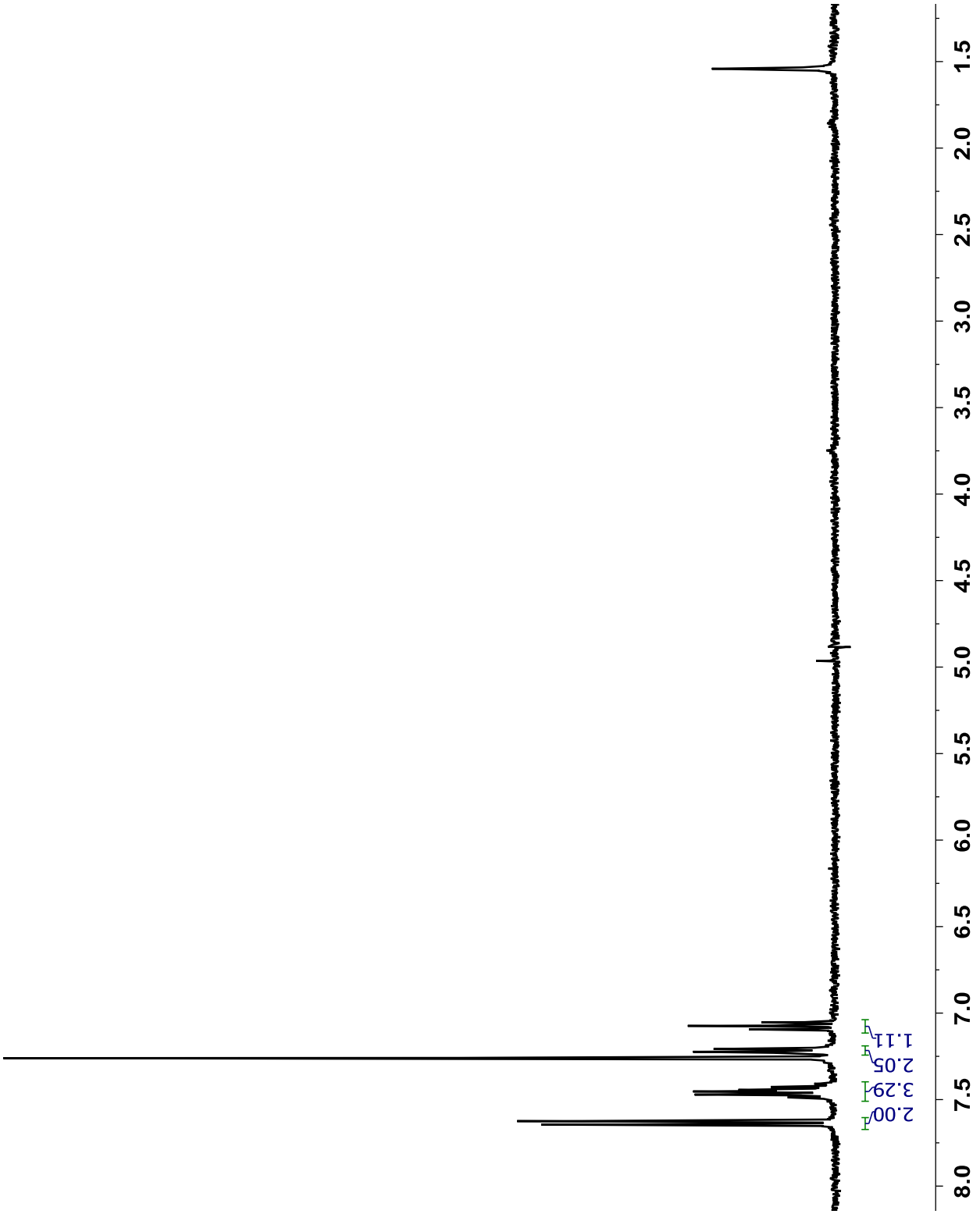

Figure B.52. ^{1}H NMR spectrum of 2,6-dibromobiphenyl in $CDCl_3$. Contamination from water can be seen.

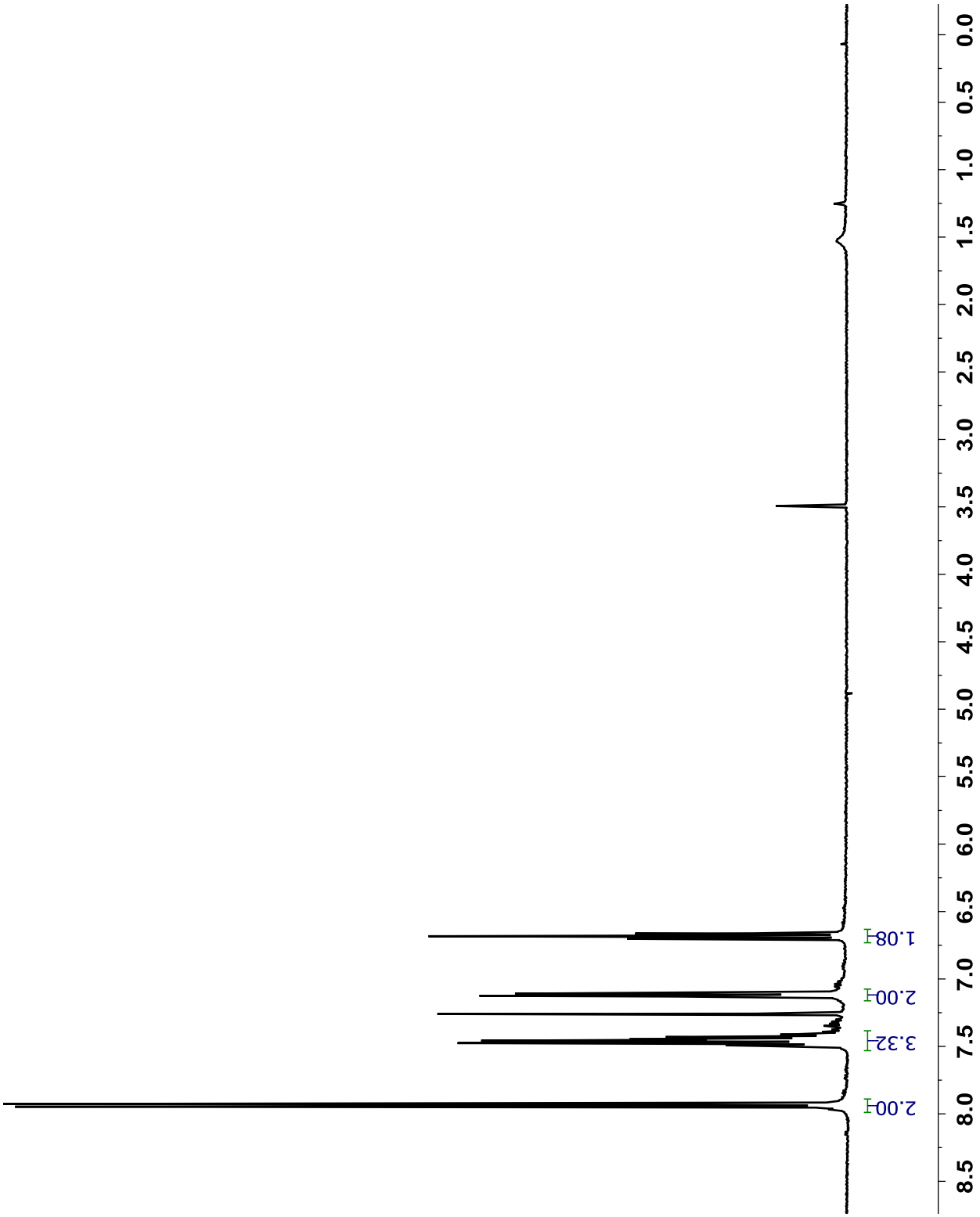

Figure B.53. ^{1}H NMR spectrum of 2,6-diiodobiphenyl in $CDCl_3$. Contamination from methanol and water can be seen.

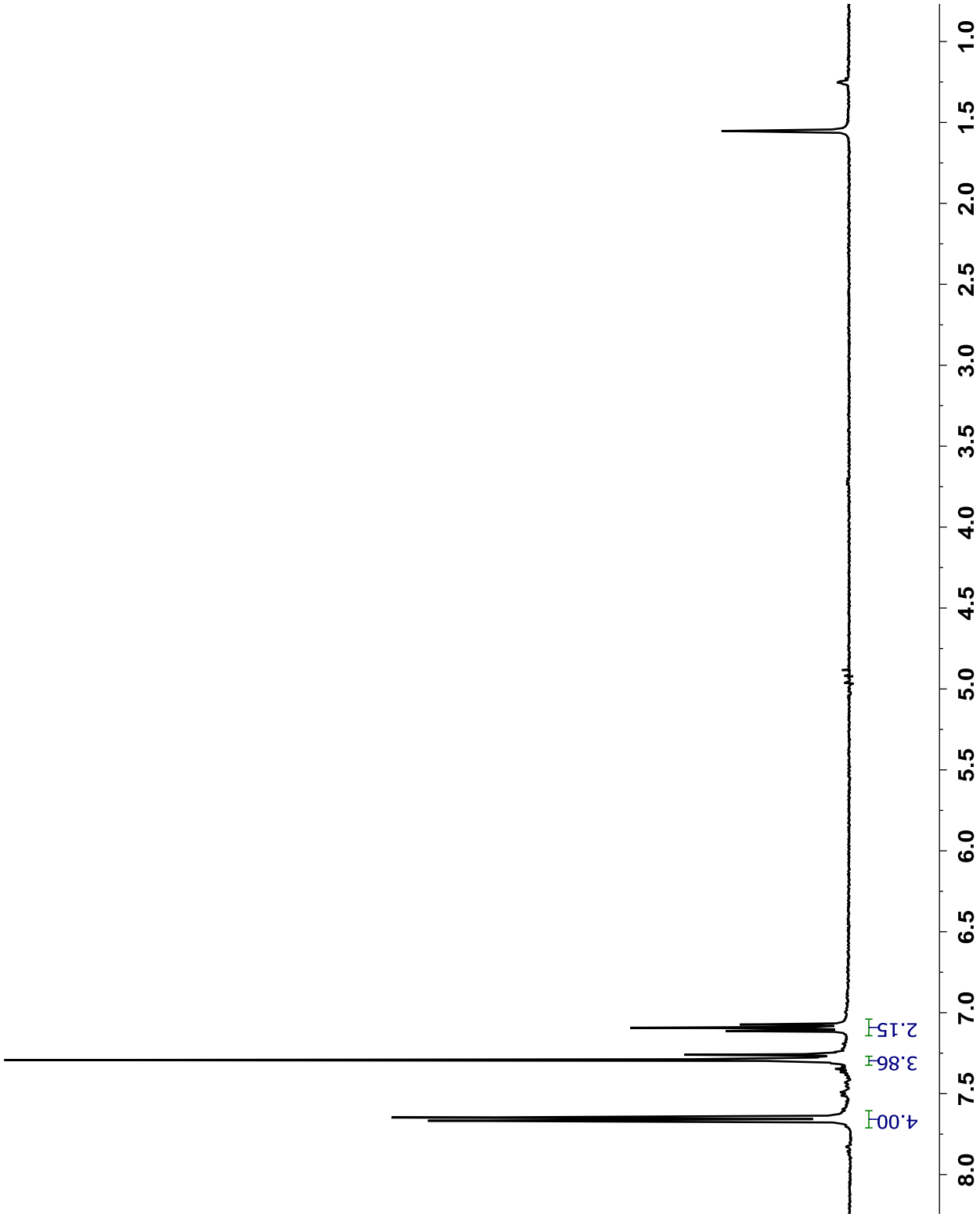

Figure B.54. ^{1}H NMR spectrum of 2,2″,6,6″-tetrabromoterphenyl in $CDCl_3$. Contamination from water can be seen.

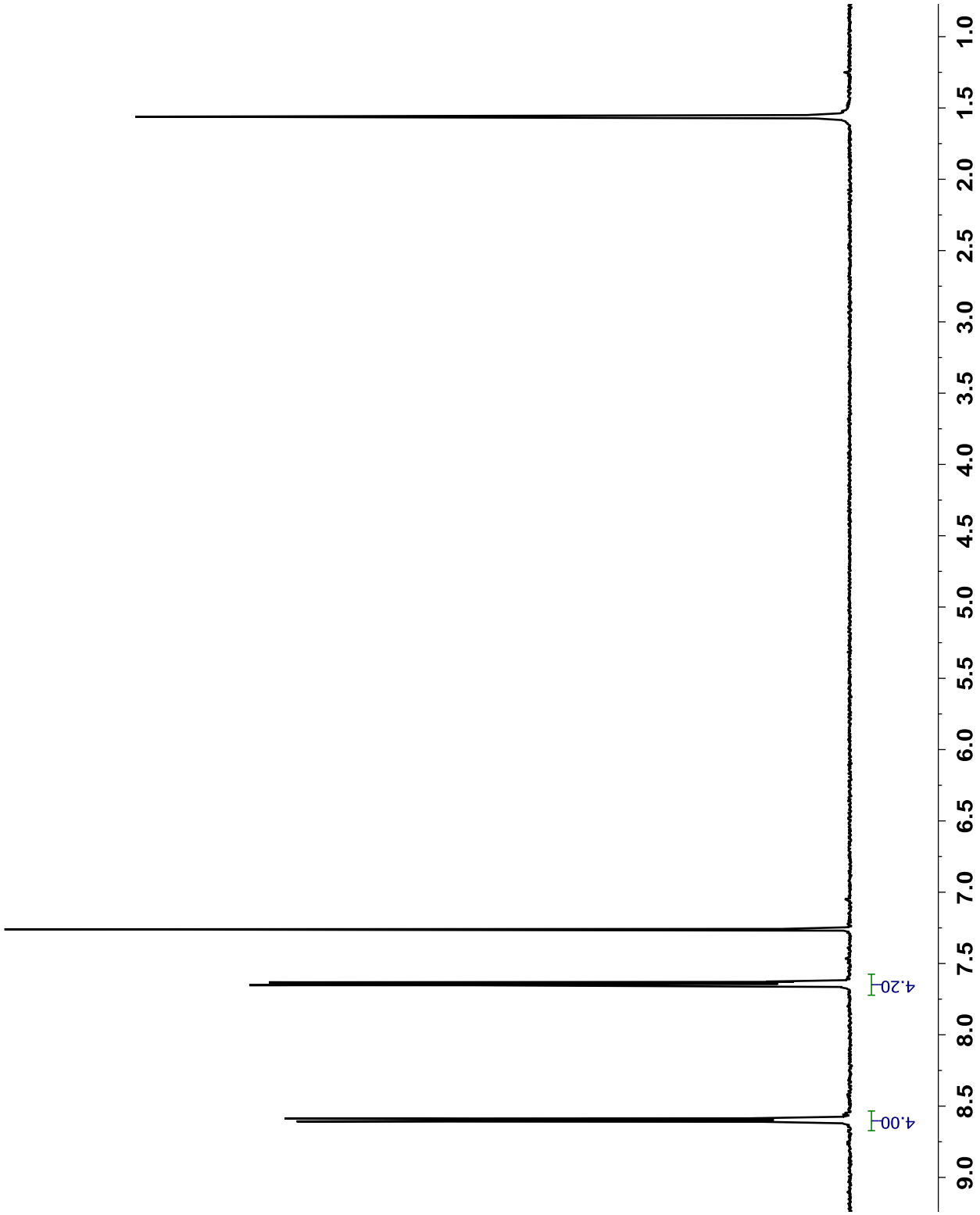

Figure B.55. ^{1}H NMR spectrum of 9-bromo-10-iodoanthracene in $CDCl_3$. Major contamination from water can be seen.